AD-A107 255 AIR FORCE INST OF TECH WRIGHT-PATTERSON AFB OH F/G 11/6
MECHANISMS OF RECOVERING LOW CYCLE FATIGUE DAMAGE IN INCOLOY 90--ETC(U)
1979 R E SCHAFRIK
UNCLASSIFIED AFIT-CI-79-212D NL

1 of 3
AD
A107255

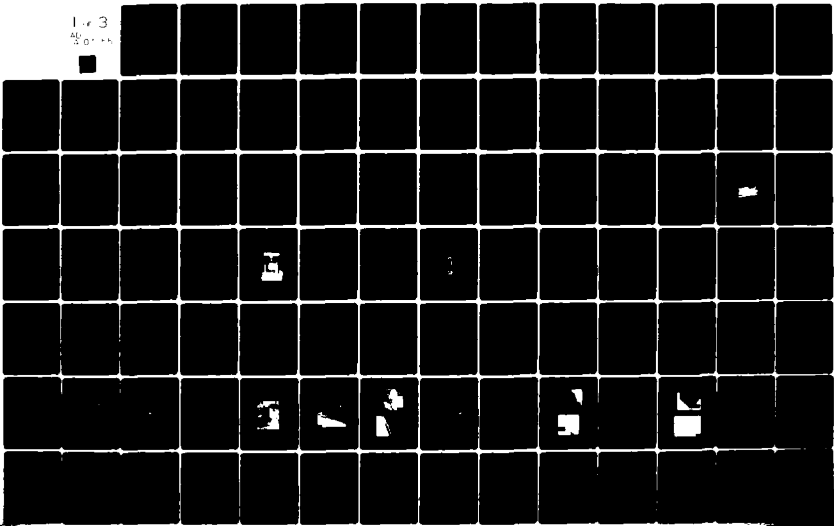

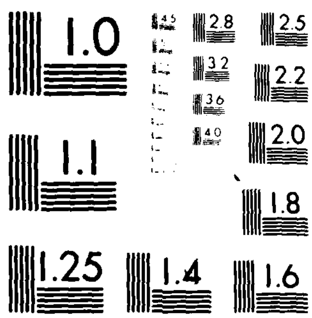

MICROCOPY RESOLUTION TEST CHART

UNCLASS

SECURITY CLASSIFICATION OF THIS PAGE (When Data Entered)

REPORT DOCUMENTATION PAGE

READ INSTRUCTIONS BEFORE COMPLETING FORM

1. REPORT NUMBER 79-212D	2. GOVT ACCESSION NO. AD-A107	3. RECIPIENT'S CATALOG NUMBER 255
4. TITLE (and Subtitle) Mechanisms of Recovering Low Cycle Fatigue Damage in Incoloy 901		5. TYPE OF REPORT & PERIOD COVERED ~~THESIS~~/DISSERTATION
		6. PERFORMING ORG. REPORT NUMBER
7. AUTHOR(s) Capt Robert E. Schafrik		8. CONTRACT OR GRANT NUMBER(s)
9. PERFORMING ORGANIZATION NAME AND ADDRESS AFIT STUDENT AT: The Ohio State University		10. PROGRAM ELEMENT, PROJECT, TASK AREA & WORK UNIT NUMBERS
11. CONTROLLING OFFICE NAME AND ADDRESS AFIT/NR WPAFB OH 45433		12. REPORT DATE 1979
		13. NUMBER OF PAGES 239
14. MONITORING AGENCY NAME & ADDRESS (if different from Controlling Office) LEVEL II		15. SECURITY CLASS. (of this report) UNCLASS
		15a. DECLASSIFICATION/DOWNGRADING SCHEDULE

16. DISTRIBUTION STATEMENT (of this Report)

APPROVED FOR PUBLIC RELEASE; DISTRIBUTION UNLIMITED

DTIC NOV 13 1981 H

17. DISTRIBUTION STATEMENT (of the abstract entered in Block 20, if different from Report)

22 OCT 1981

FREDRIC C. LYNCH, Major, USAF
Director of Public Affairs
Air Force Institute of Technology (ATC)
Wright-Patterson AFB, OH 45433

18. SUPPLEMENTARY NOTES

APPROVED FOR PUBLIC RELEASE: IAW AFR 190-17

19. KEY WORDS (Continue on reverse side if necessary and identify by block number)

20. ABSTRACT (Continue on reverse side if necessary and identify by block number)

ATTACHED

81 10 30 051

DD FORM 1 JAN 73 1473 EDITION OF 1 NOV 65 IS OBSOLETE UNCLASS

SECURITY CLASSIFICATION OF THIS PAGE (When Data Entered)

AD A107255

DTIC FILE COPY

MECHANISMS OF RECOVERING LOW CYCLE FATIGUE DAMAGE
IN INCOLOY 901
BY

Robert E. Schafrik, Capt. USAF (Ph.D.)
The Ohio State University, 1979
Professor James A. Begley, Adviser

ABSTRACT

The effect of thermal treatment and hot isostatic pressing (HIP) on eliminating low cycle fatigue (LCF) damage in the iron-nickel superalloy, Incoloy 901, was investigated. Testing was done in air at 500°F at a total strain range of 0.75%. The mechanisms of crack initiation and crack propagation in baseline specimens were determined and used as the basis of comparison for the rejuvenated specimens.

Crack initiation in the baseline specimens was due to decohering of blocky grain boundary carbides. Pre-crack initiation damage consisted of extrusions and intrusions formed at persistent slip bands and partially decohered grain boundary carbides.

A pre-rejuvenation damage level of 800 cycles (60% of crack initiation) was selected. Some specimens to be HIP processed were ceramic coated; the rest were left uncoated. Post-HIP testing revealed that LCF properties were adversely affected by surface microstructural damage caused by the HIP processing.

Thermal rejuvenation, consisting of a standard solution treatment and double aging, was partially successful in recovering fatigue properties with a pre-rejuvenation damage level of 800 cycles. Initiation life was extended by 400 cycles and cycles to failure was extended by 600 cycles. This behavior is explained in terms of microstructural damage which is resistant to thermal treatment.

Total Pages - 259

Selected Bibliography

1. M.N. Menon and W.H. Reiman, "Low Cycle Fatigue Crack Initiation Study in René 95", J. Mater. Sci. 10, 1571-1581 (1975).

2. B. Leis and A. Clauer, Investigation of Rejuvenation of Fatigue Damage in IN-718, AFML TR-78-90, Wright-Patterson AFB, OH.

3. H.F. Merrick, "The Low Cycle Fatigue of Three Wrought Nickel-Base Alloys", Met Trans 5, 891-897 (1976).

4. C. Laird, Mechanisms and Theories of Fatigue, presented at the Materials Science Seminar, ASM, St. Louis Mo. (1978).

MECHANISMS OF RECOVERING LOW CYCLE FATIGUE DAMAGE IN INCOLOY 901

DISSERTATION

Presented in Partial Fulfillment of the Requirements for the Degree Doctor of Philosophy in the Graduate School of The Ohio State University

By

Robert E. Schafrik, B.S.Met., M.S.

* * * * *

The Ohio State University

1979

Reading Committee:

Dr. G. W. Powell

Dr. J. P. Hirth

Dr. J. A. Begley

Approved By

Adviser
Department of Metallurgical Engineering

DEDICATION

To my wife, Mary; and to my children: Catherine, Frances, Robert Jr., and Steven.

ACKNOWLEDGEMENTS

The author wishes to express his sincere appreciation to Dr. J. A. Begley of The Ohio State University for his guidance and encouragement throughout this project. The author is thankful for the constructive comments of the following individuals in the early stages of this effort: Dr. B. Wilshire of University College, University of Wales; A. Adair, Dr. W. Reimann, and Dr. H. A. Lipsitt of the Air Force Materials Laboratory, Wright-Patterson Air Force Base; Drs. A. Clauer and B. Leis, Battelle-Columbus Laboratories; and Dr. J. C. Williams, Carnegie-Mellon University. Also, the author is grateful for the excellent training in practical aspects of transmission electron microscopy provided by Dr. J. C. Williams.

Appreciation is due to Captain P. Martin and R. Kerans of the Air Force Materials Laboratory for helpful advice, instruction, and troubleshooting assistance in using the many different pieces of laboratory equipment required to complete this dissertation; and for helpful discussions on the research work throughout the project. Also, appreciation is due to Mr. Dwelle Butts of the Air Force Materials Laboratory for his efforts in obtaining necessary supplies.

I wish to thank my wife, Mary, and our four children for their support and extreme patience throughout my graduate education.

The author is obliged to the following for supplying materials: M. M. Allen, Government Products Division, Pratt-Whitney Aircraft Co., for providing a section of a compressor shaft forging; P. Bailey, Aircraft Engine Group, General Electric Co., for providing ceramic coating for some specimens; and D. Weaver, Kelsey-Hayes, Detroit, for a piggybacked hot-isostatic-pressing run.

I would like to recognize the cooperation and help of the following: S. Leffler, J. Henry, M. Henry, G. Cornish, and J. Barlowe. Many thanks are due to Ms. S. Ehlers for typing this manuscript.

Able assistance in transferring my fatigue data from paper punch tape format to computer disk file was provided by Captain D. Summer and Ms. C. Johnson of the Air Force Materials Laboratory.

This research was performed under the auspices of the Air Force Materials Laboratory. I am appreciative of the moral and financial support provided by Dr. H. A. Lipsitt, and for his helpful advice during various stages in this project. I am likewise appreciative of the encouragement given me by Dr. H. Burte and L. Hjelm of the Air Force Materials Laboratory.

Finally, I wish to thank the Air Force Institute of Technology and the U. S. Air Force for the opportunity to complete my graduate education. I would like to acknowledge the administrative assistance provided by my Program Managers, Captains S. Brown and D. Cain.

VITA

February 6, 1946	Born - Cleveland, Ohio
1963-1967	B.S.Met., Case-Western Reserve University, Cleveland, Ohio
1967-1968	Applications Engineer, American Air Filter Co., Louisville, KY
1968	Commissioned and entered U. S. Air Force
1968-1972	Base Civil Engineer, Hanscom Air Force Base, Bedford, MA
1972-1974	M.S., Aerospace Engineering, Air Force Institute of Technology, Wright-Patterson Air Force Base, Ohio
1974-1975	Materials Development Engineer, Metallurgy and Ceramics Laboratory, Aerospace Research Laboratories, Wright-Patterson Air Force Base, Ohio
1975-1977	Assistant Branch Chief, Metals Branch, Manufacturing Technology, Air Force Materials Laboratory, Wright-Patterson Air Force Base, Ohio

PUBLICATIONS

"Determination of Texture Pole Figures Using Picker FACS-1 Apparatus," with L. A. Jacobson, ARL TR 75-0190, Aerospace Research Laboratories, Wright-Patterson Air Force Base, Ohio (1975).

"The Deformation and Fracture of TiAl at Elevated Temperatures," with H. A. Lipsitt and D. S. Schechtman, Met. Trans. A 6A, 1991-1996 (1975).

"Dynamic Elastic Moduli of the Titanium Aluminides," Met. Trans. A 8A, 1003-1006 (1977).

"Manufacture of TiAl by Extrusion of Blended Elemental Powders," Met. Trans. B 7B, 713-716 (1976).

"Manufacture of TiAl by Extrusion of Blended Elemental Powders," DDC Report AD-780630, Defence Documentation Center, Arlington, VA (1974).

TABLE OF CONTENTS

TABLE OF CONTENTS (CONT'D)

TABLE OF CONTENTS (CONT'D)

LIST OF TABLES

LIST OF FIGURES

LIST OF FIGURES (CONT'D)

LIST OF FIGURES (CONT'D)

LIST OF FIGURES (CONT'D)

LIST OF FIGURES (CONT'D)

Chapter 1

INTRODUCTION

The modern gas turbine engine demands the ultimate in performance from materials. Typical material requirements include high strength and stiffness at operating temperatures, good oxidation resistance, low creep rates and high stress rupture values, and good low-cycle and high-cycle fatigue resistance. Since the results of component failure, especially of rotating components, usually are catastrophic, design approaches and material specifications tend to be conservative (1,3,4,61).

A turbine disk is that component which transmits the work done by hot, expanding gases on the turbine blades to the power shaft of the engine. Experience has indicated that turbine disks can fail either by stress rupture at the rim where the blades are attached with dovetail slots; or, as is usually the case, by low-cycle fatigue at cross-sectional changes or at bolt holes (10). The low-cycle fatigue results from vibration, changing engine operating speeds and thermal gradients (3,12). When a turbine disk is limited by low-cycle fatigue (LCF) life, the design approach is to establish a probability of failure of 0.5%, with failure defined as extension of a detectable crack and not component disintegration. Therefore, most turbine disks reach their LCF life with a high probability of additional life remaining (1). Since these disks are quite expensive, there is a great deal of interest in processing the disks in some manner (i.e., rejuvenating the disks) to remove the microstructural damage which leads to LCF failure, so that the disks can be returned to service safely and reliably at low cost (2).

This investigation was undertaken to determine how the LCF process causes crack initiation in Incoloy 901, and to find which rejuvenation treatments can lead to recovery of the initiation life. Incoloy 901 was selected for study because it is a commonly used superalloy and, thus, there are many disks which potentially can be returned to service after rejuvenation.

Subsequent portions of this introduction will briefly review LCF crack initiation and propagation in superalloys, the physical metallurgy of Incoloy 901, and rejuvenation.

I. CRACK INITIATION

Dieter divides the fatigue process into four steps: crack initiation, Stage I crack growth, Stage II crack growth, and ultimate ductile failure (14). This classification will be used in the following discussion.

The mechanisms for LCF crack initiation generally involve the interaction between the deformation processes and the alloy microstructures (1,4,5,6,7,8,9,11,46,64,67,68). The mode of crack nucleation depends on such factors as the amount of deformation, the degree of slip dispersal, test temperature and environment, and the amount and type of microstructural defects (carbo-nitrides, borides, porosity, brittle second phases, etc.). Kim and Laird point out that in pure metals, crack initiation occurs at persistent slip bands at low stress ranges and at grain boundaries at high stress ranges exclusive of severe environmental effects (47). In lower temperature regimes (less than about 700°F or 370°C), superalloys deform by planar slip which is heterogeneous in nature (4). Kuhlmann-Wilsdorf and Laird have developed a dislocation model to explain how persistent slip bands can lead to the formation of instrusions and extrusions on the specimen surface which in turn lead to crack initiation (49,46). This model presents the rationale for the simple stress-raiser mechanism proposed by Wood 20 years ago (50).

At high cyclic ranges, cracks generally initiate at the grain boundaries. Recent work by Kim and Laird (47,48) have developed three criteria for crack initiation in pure metals at grain boundaries: (a) The grain boundaries must have a high degree of lattice mismatch; (b) The slip on the active slip system in either one or both of the adjacent grains should be directed at the intersection of the boundary with the specimen surface; and (c) The trace of the boundary at the free surface should lie at an angle of 30-90° with respect to the stress axis. Kim and Laird also observed grain boundary sliding in their LCF experiments on pure copper (47). The cracks were observed to have initiated at grain boundary steps.

Superalloys contain a substantial amount of carbides, carbo-nitrides, and borides intentionally added to control the grain size, improve creep resistance, increase grain boundary strength, and to vitiate the adverse effects of trace elements (17). Unfortunately, it has been found that these nonmetallic inclusions serve as favorable sites for crack initiation. In a study by Gell and Leverant on the LCF behavior of Mar-M200, it was found that metal carbides played a key role in determining the crack initiation life (8). The carbides can be pre-cracked due to differential contraction during the solidification process or during the various metalworking processes. Also, the carbides can de-cohere from the matrix, especially at the surface, leading to a localized strain concentration region. As recently shown by Reimann and Menon, carbides provide a preferential path for developing LCF cracks in René 95 and seem to be associated with initiation of the cracks themselves (1).

Many investigators have found coherent twin boundaries to be significant sites for crack initiation at lower stress ranges (4).

II. STAGE I CRACK PROPAGATION

There is some disagreement in the literature about a definition of Stage I cracking. Coffin suggests that Stage I is early growth of a crack to some detectable limit and then propagation through a plastic regime (12). A more accepted definition is that Stage I cracking is that stage where cracks propagate along specific crystallographic planes which are oriented near 45° to the applied stress axis (46). But Laird points out that this definition is not strictly applicable to LCF where crack nucleation and growth may occur along sections which are not crystallographic (47).

Since persistent slip bands develop on the most active slip plane, cracks initiated at them generally continue to propagate along them (46). Thus, a persistent slip band can lead to the development of intrusions/extrusions, to a crack nucleus, and finally to crack propagation.

Similarly, cracks nucleated at grain boundaries tend to grow along the boundary both on the surface and into the bulk (47). Thus, the crack front develops a thumbnail shape. Also, Kim and Laird predicted and observed a crack path which is asymmetric with respect to the boundary, with the crack occurring in that grain with the most favorably oriented active slip system (48).

III. STAGE II CRACK PROPAGATION

Coffin proposes that Stage I cracking leads to Stage II cracking when the crack overcomes the plastic zone which envelops it during its early stages, and thus it begins to grow elastically (12).

Usually, however, Stage II is denoted as the transition of the crack from growing along the maximum shear direction to growing normal to the applied stress direction. At high stress ranges, the crack will almost immediately propagate by Stage II processes (46).

It is during Stage II crack growth that fatigue striations are generated, although not all materials develop a striation pattern. Striations are usually observed in superalloys (53). It is generally accepted that each striation represents the propagation distance of a fatigue crack during each cycle. A crack plastic blunting process proposed by Laird requiring two slip systems (51) is a very reasonable explanation for the formation of striations (52).

Stage II continues until the crack becomes long enough to cause the final instability. In brittle materials, the crack begins to propagate unstably after a critical length is reached. In ductile materials, the crack grows until a tensile overload occurs, at which time fracture occurs by shear rupture on planes inclined 45° to the tensile axis (52).

IV. PHYSICAL METALLURGY OF INCOLOY 901

Incoloy 901 is an iron-nickel superalloy widely used as a turbine disk material since the early 1960's (17). Its nominal composition is (in weight percent): Ni-42.5, Fe-36.0, Cr-12.5, Mo-5.7, Ti-2.8, Al-0.2, C-0.05, and B-0.015. Since it is fairly strong and ductile at intermediate temperatures (up to 1000°F/540°C) and contains substantial iron and relatively low chromium, it is widely used due to its comparatively low cost. It also possesses the advantage of being in that group of superalloys which can be forged and machined fairly conventionally (19).

Incoloy 901 has an austenitic (γ-f.c.c.) iron-nickel-chromium matrix. Molybdenum, titanium, carbon, and boron are the other principal substitutional solid-solution strengtheners of the matrix (17). The stacking fault energy is not known, but from data presented by Decker and Floreen, it can be estimated to be greater than 60 ergs/cm^2 (18).

The primary precipitate is γ', an intermetallic compound of the type Cu_3Au, possessing a Strukturbericht structure type $L1_2$. Its stoichiometric composition is Ni_3Al with a lattice parameter of 3.60 Å. In actual fact, γ' contains some iron on the nickel lattice sites, and some titanium on the aluminum lattice sites, so that γ' is usually denoted as $(Ni,Fe)_3(Al,Ti)$. The lattice mismatch between γ' and the γ matrix is low, so that the γ' nucleates homogeneously. The γ' grows in a spherical morphology which indicates that the lattice misfit is less than 0.5% (17,20). The solvus temperature is 1725°F (940°C) (17).

Actually, in Incoloy 901, γ' is a metastable precipitate (18). The equilibrium precipitate is η, an h.c.p.-ordered intermetallic compound with a Strukturbericht structure type DO_{24}. It has the stoichiometric composition Ni_3Ti. Unlike γ', it does not dissolve substantial amounts of other elements (20). The precipitation of η may occur in two forms: at the grain boundaries in a cellular morphology or intergranularly as plates (22,20). The cellular precipitation nucleates at a lower temperature than the plate-shaped precipitates. The solvus temperature for η is 1825°F (996°C)(17). Significant precipitation occurs in the temperature range 1500-1750°F (816-954°C), with the most rapid precipitation rate in the temperature region 1600-1650°F (871-899°C) (25).

The cellar precipitation reaction consi-ts of alternating lamellae of γ and η. These cells have a random orientation with respect to the grain into which they are growing. But the close-packed planes and directions of the h.c.p. η and the f.c.c. γ are parallel to one another (20). These orientation relationships are also true for the plate morphology which are thought to nucleate on stacking faults in γ' (18). The interface between γ and η is semi-coherent, with a lattice mismatch of 0.65% (19). The η phase is associated with severe degradation in mechanical properties. Not only is the phase itself brittle, but also it grows at the expense of the γ'. However, η has successfully been used to control the grain size of Incoloy 901 during forging by the utilization of special thermomechanical processing (25).

Carbides play a key role in superalloys. They help to control grain size since some carbide types are stable nearly to the melting point of the alloys. Also, the carbides which precipitate in the grain boundary greatly increase stress rupture strength at elevated temperatures. And, carbides can increase the chemical stability of the matrix by removing reacting elements (26). MC carbides form shortly after freezing and, hence, they occur as discrete particles distributed homogeneously throughout the alloy. In Incoloy 901, these MC carbides have the composition TiC with an f.c.c. structure. Some molybdenum can substitute on the titanium lattice sites, so that a carbide of the type (Ti,Mo)C is possible (26,70).

Although carbides of the type $M_{23}C_6$ usually form in superalloys during low-temperature heat treatment and service in the temperature range 1400-1800°F (760-980°C), they are not found in Incoloy 901. Instead, MC carbides of the type (Ti,Mo)C precipitate at the grain boundaries during the stabilization portion of the heat treatment (70). The morphology of these grain boundary carbides is similar to that for a Laves phase and they have been incorrectly identified as Laves phases (24).

The formation of carbo-nitrides and titanium nitrides has been reported (24). Cubic TiN is as thermally inert in the superalloy as is TiC.

The boron which is added to improve creep properties results in the precipitation of hard, refractory M_3B_2 borides (26). Typical composition of these borides is: $(Mo,Ti,Al,Cr,Fe,Ni,Si)_3B_2$ (24,69).

In addition to the intentional precipitates, various topologically close-packed (t.c.p.) intermetallic compounds form in superalloys due to solid-state bonding phenomena (t.c.p. phases are also referred to as "Hume-Rothery compounds" and "electron compounds"). A hexagonal Laves phase of the type $(Fe,Cr,Mn,Si)_2(Mo,Ti,Cb)$ has been found in Incoloy 901 after aging for long times in the temperature range 1200-2000°F (649-1093°C). The morphology varies from general intergranular to grain boundary precipitation (24,23,18). The trigonal μ phase has been observed in Incoloy 901 with high boron additions (0.1 weight percent) (24). This phase has a close structural relationship to the M_6C carbides and, thus, it may be that M_6C can precipitate in this alloy, although it has not been reported. The chemical composition of the μ phase can be quite complex. It is, in general, $(Ti,Mo)_6(Fe,Ni)_7$ (24). The precipitation is intragranular as thin platelets parallel to γ close-packed planes.

V. REJUVENATION

Metallurgical engineers who are responsible for the maintenance of turbine engines have long expressed a desire to be able to restore at least a portion of the design life of expensive engine components through some sort of processing operation. This process has been given the name "rejuvenation." Recent advances made by Wilshire and others have shown that thermal treatments are successful in recovering the creep life of superalloys (28,29). Wilshire found that the onset of tertiary creep is caused either by development and growth of grain boundary cavities or by microstructural changes which cause changes in volume fraction and morphology of the γ' (28). Thus, suitable heat treatments could be devised to sinter out the cavities in the first case, or to restore the original microstructure in the second case in order to recover the creep life.

The success with creep damage has given impetus to finding suitable processing conditions for recovering the low-cycle fatigue (LCF) life of superalloys. The use of hot-isostatic-pressing (HIP) technology to consolidate metal powders has been quite successful (31) and it was inferred that this technology would be useful in heatling LCF damage. The HIP process involves the introduction of high pressure gas into an autoclave at elevated temperature. Thus, some mechanical energy is available as well as thermal energy.

Researchers at the Stellite Division of the Cabot Corporation obtained some preliminary data on turbine blades which indicated that some recovery of creep and fatigue properties was possible with HIP processing (30). An Air Force funded study on HIP rejuvenation in IN-718 concluded that there was no rejuvenation of pre-crack initiated damage, but that there was some rejuvenation of post-crack initiation life due to the closure and bonding of fatigue cracks (2). However, this work was not conclusive because the HIP cycle chosen for the rejuvenation effort substantially changed the baseline properties of the material, and there was relatively little effort devoted to microstructural characterization.

It is the purpose of this dissertation to report the results of the experimental investigation to recover some portion of pre-crack initiated LCF life using thermal and HIP processing. Pertinent aspects of the physical metallurgy of Incoloy 901 are presented. The LCF behavior of Incoloy 901 at various strain ranges is reported. The microstructural mechanisms of LCF damage and the resultant effects of the rejuvenation processes are detailed.

Chapter 2

EXPERIMENTAL PROCEDURE

I. METALLOGRAPHY TECHNIQUES

A. Optical Microscopy

The samples to be examined were mounted in Bakelite, hand polished through 600-grit silicon carbide paper using water as a lubricant, and polished successively with 6-μ, 1-μ, and 1/4-μ diamond paste. Several different etchants were utilized. ASTM Etchant 105 (32) was most generally used to reveal microstructural details. It was freshly mixed each time in these proportions: 92% HCl, 5% H_2SO_4, and 3% HNO_3. Immersion for 5-30 seconds was usually sufficient. Marble's Reagent (ASTM Etchant 25) was effective in highlighting the grain boundaries. It was mixed in these proportions: 10 g $CuSO_4$, 50 ml HCl, and 50 ml water (32). Etchant times were generally 10-30 seconds. Glyceregia (ASTM Etchant 87) was useful in highlighting microstructural details when the other etchants were not adequate. It was freshly mixed each time according to the formula: 10 ml HNO_3, 50 ml HCl, 30 ml glycerin (32). The samples were bathed in hot water prior to immersion in the glyceregia. Etchant times depended on the surface temperature of the specimen. Average times were between 20 seconds and 1 minute. Sometimes the samples were immersed in HF for a few seconds to remove a passive layer prior to etching.

After the samples were satisfactorily etched, they were thoroughly rinsed in water and bathed in a saturated sodium bicarbonate solution placed in an ultrasonic cleaner for several minutes. This step was necessary to prevent etching of the microscope objective piece. The etched surface was then dried using a methanol wash and a blower. The samples were examined and photographed in a Bausch and Lomb Research II Metallograph using a xenon light source.

B. Transmission Electron Microscopy

Thin slices of Incoloy 901, approximately 0.010 inch thick, were cut using a thin abrasive cut-off wheel. These slices were then ground flat on 240- and 320-grit silicon carbide paper using water as a lubricant. The slices were attached to the bottom of a stainless steel mount using balsam wax. The slice was further ground down to a thickness of 5-6 mils on 320- and 400-grit silicon carbide paper using a water lubricant. The thin slices were then dismounted and the residual balsam was removed by slight grinding on the 400-grit paper. A punch-out die, with a 3-mm opening, was used to cut out the disks. In the case of the fatigue specimens where the disks were taken normal to the longitudinal axis, the above procedure was simplified somewhat since the fatigue specimens had a nominal 3-mm diameter.

Electropolishing was done with a dual-jet Tenupol. The electrolyte had the following composition: 600 ml methanol, 250 ml butanol, and 60 ml perchloric acid (70%). The electrolyte was maintained at a temperature of about -60°C by constantly adding liquid nitrogen to a methanol bath surrounding the electrolyte.

The controls on the polisher were set for minimum flow rate and maximum sensitivity of the photocell detector which turned off the electrolyte pump after perforation of the disk. A two-step polishing sequence worked best. Electropolishing for 15-30 minutes at 30 volts followed by final polishing at 16-20 volts produced dished disks with holes close to the center. After electropolishing, the disks were washed in methanol. Great care was taken in handling to prevent inducing artifact dislocations into the structure.

C. Scanning Electron Microscopy (SEM)

An AMR Model 1000 Scanning Electron Microscope was used in this investigation. An Energy Dispersive Analysis of X-Rays (EDAX) attachment to the SEM was used to identify chemical elements. Sample preparation involved cutting the LCF specimen just below the extensometer flange, and mounting it on an aluminum stud using a silver paste.

D. Surface Replication

Acetyl cellulose replicating film was used to replicate the surface in the gauge section of the low-cycle fatigue specimen. The replication was done on loose specimens and while the specimens were mounted in the Instron Hydraulic Testing Machine (37). The replicating film, 0.034 mm thick (1.34 mils), was cut into strips 0.30 in. wide (the approximate length of the gauge section). The strips were cut into lengths 0.25-0.30 in. long. Strips of this length covered about 75% of the gauge length area. A reference line was made on the LCF specimen above the extensometer flange so that the location of each replica could be noted. At least six replicas were made for each gauge length, with adequate overlap of areas between adjacent replicas. Thus, the gauge section was completely replicated about three times. This provided insurance against an artifact in the replica obscuring a vital surface detail.

The replicating film was prepared for use by submerging it in acetone for 8-10 seconds, holding a corner with tweezers. The film was removed from the acetone and quickly applied to the surface. The film "grabbed" onto the surface almost immediately. The film dried on the surface for 5-10 minutes, and then was stripped off with tweezers. It was placed on a piece of double-sided sticky tape mounted on a glass slide. The position of the reference mark on the LCF specimen with respect to the replica was scribed into the sticky tape at the appropriate position. A piece of masking tape on the reverse of the glass contained the identification data. Two glass slides at a time were then placed in a vacuum evaporator, and the belljar evacuated to 2×10^{-5} torr. The slides were rotated and a uniform thin coating of 99.99% purity aluminum was applied. The replicas were then examined using a light microscope or a scanning electron microscope.

II. AGING RESPONSE OF INCOLOY 901

A. Material Specification

The Incoloy 901 was received in the form of a segment of a partially finished compressor shaft. The shaft had been cast, forged, and pierced. A chemical analysis is presented in Table 1. A band saw with a bi-metal blade was used to cut pieces of material for study. The material was received in solution-treated and double-aged condition. The commercial heat treatment specification is shown in Table 2 (34).

B. Thermal Treatments

Heat treating studies were conducted in two different furnaces. A vertical tube drop Marshall furnace was used when rapid quenching

TABLE 1

CHEMICAL ANALYSIS OF BILLET

Element	Weight Percent	Atomic Percent
C	0.034	0.162
Mn	0.10	0.104
P	0.019	0.035
S	0.005	0.009
Si	0.10	0.203
Cr	12.41	13.63
Ni	41.33	40.21
Mo	5.31	3.16
Ti	2.99	3.57
Al	0.29	0.61
Cu	0.09	0.08
Co	0.29	0.28
Bi	0.00005	0.00001
Pb	0.0003	0.00008
B	0.015	0.079
Fe	Balance (37.02)	37.86

TABLE 2

COMMERCIAL HEAT TREATMENT SPECIFICATION
FOR INCOLOY 901

SOLUTION	Heat to 1975-2025 F Hold within ±25 F for 2 hours Cool at rate equivalent to air cool or faster
STABILIZATION	Heat to 1400-1475 F Hold within ±15 F for 2-4 hours Cool in air or quench in water
PRECIPITATION	Heat to 1300-1375 F Hold within ±15 F for 24 hours Cool in air

Reference: Pratt & Whitney Aircraft Specification 1003H, 20 Nov. 1973.

of the specimen was desired. A thin piece of alumel wire was used to suspend a tantalum specimen basket in the furnace hot zone. The alumel wire was formed into a loop and each end was connected to a metal post in a cap at the top of the furnace. Heavy gauge nichrome wire, bent at each end in the form of a "U", was used to connect the basket to the alumel wire. Helium gas was passed through a gas train to remove impurities and then introduced into the top cap of the tube. The bottom tube opening was covered with a thin sheet of plastic held in place by a rubber band wrapped around the tube. Tygon tubing, connected to a side tap in the tube, near the bottom, directed the helium gas into a beaker of vacuum pump oil. Minimal pressure and flow rate of the gas was maintained, i.e., only sufficient pressure to generate a bubble every few seconds in the oil was used. A chromel-alumel thermocouple placed at the same height in the tube as the basket was used to monitor temperature. When the heat treatment was completed, the thin alumel wire loop was broken by passing a 110-volt line current through it. The basket, with the specimen in it, fell out the bottom of the tube, easily penetrating the plastic membrane on the bottom. A pail of water was placed under the tube to serve as the quenching medium.

A Brew High Vacuum Furnace was also used for heat treatment studies. Vacuums on the order of 10^{-6} torr were easily obtainable at the temperatures used in this study. A platinum/platinum-10% rhodium thermocouple was used to monitor temperature. The hot zone of the furnace was 6 inches in diameter by 14 inches high. Tantalum heating elements and shields were used. The furnace design was of the cold wall type. Temperature was controlled within ± 5°F. The specimens were either cooled *in vacuo* or by backfilling the furnace chamber with helium gas, which passed through the gas train, to a partial pressure of 640 torr (about 0.83 atmosphere). The cooling rates, as measured by a thermocouple, for the vacuum cool and the helium quench, are presented in Table 3.

III. LOW-CYCLE FATIGUE

A. LCF Specimen Design and Manufacture

The specimen design is shown in Figure 1. The outstanding feature of the specimen is the extensometer ridges located on either side of the gauge section. This allows accurate measurement of displacement and the ability to maintain constant, uniform temperature in the gauge section using a clamshell furnace. The disadvantages of the system are the long times required for the entire system to reach equilibrium (typically 2-3 hours) and the fact that the calculation of strain necessarily involves the application of effective gauge lengths. The details of the load train, the strain measuring system, and the equations required to convert displacement to strain are discussed in following sections.

The specimens were manufactured by Metcut Research Associates from blanks sawed from a portion of a forged shaft. Figure 2(a) shows a photograph of the shaft segment. Specimen blanks were sawed from this segment parallel to the shaft axis. A typical cutout configuration is depicted in Figure 2(b). The blanks were then rounded by straight wheel grinding, and rough machined to ~ 0.020 in. oversize in the gauge section. The specimens were given a standard heat treatment, designated as STA 3A

TABLE 3

FURNACE COOLING RATES

Vacuum Cool

A. Heat Treatment Temperature: 1975 F

Temperature (°F)	Average Cooling Rate (°F/min.)
1400	192.0
1299	97.6
1072	72.2
893	55.8
709	47.8
509	27.1

B. Heat Treatment Temperature: 1400 F

1299	100.0
1072	50.5
893	40.2
709	28.2
509	15.1

C. Heat Treatment Temperature: 1300 F

1072	46.5
893	35.4
709	25.1
509	33.7

TABLE 3 (CONT'D)

Helium Gas Quench (640 torr)

A. Heat Treatment Temperature: 1975 F

Temperature (°F)	Average Cooling Rate (°F/min.)
1400	243.4
1299	214.6
1072	166.2
893	137.4
709	120.0
509	116.4

B. Heat Treatment Temperature: 1400 F

Temperature (°F)	Average Cooling Rate (°F/min.)
1299	85.5
1072	104.1
893	92.0
709	83.6
509	75.4

C. Heat Treatment Temperature: 1300 F

Temperature (°F)	Average Cooling Rate (°F/min.)
1072	82.7
893	86.1
709	75.1
509	67.0

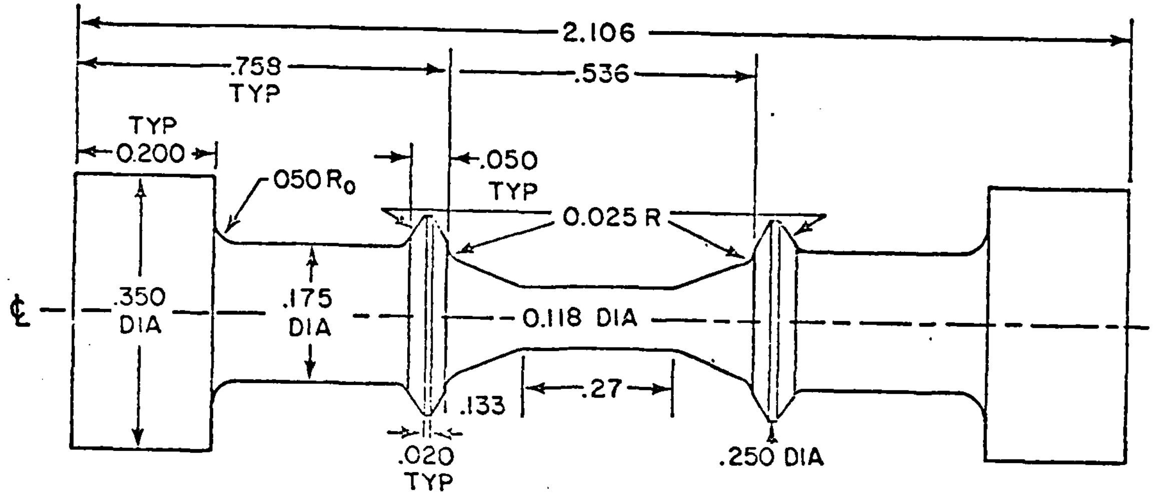

SCALE:

ALL DIMENSIONS IN INCHES

Figure 1. Low-Cycle Fatigue Specimen Design

Figure 2a. Incoloy 901 Shaft Forging Photograph

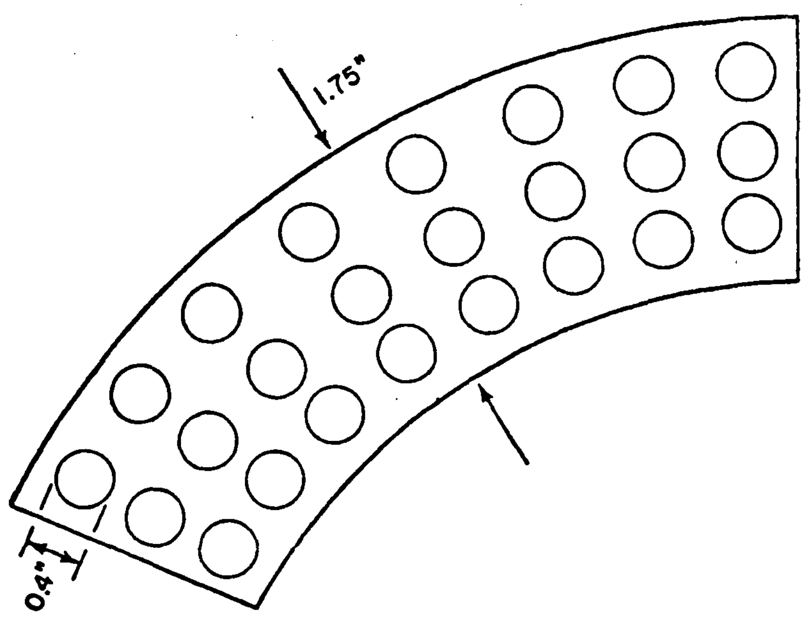

Figure 2b. Incoloy 901 Shaft Forging Segment Indicating Cut-Out Pattern for LCF Test Specimens

prior to final machining. The heat treatment parameters for STA 3A are contained in Table 4. The specimens, in groups of nine, were heat treated in a Brew High Vacuum Furnace. The fixture used to support the specimens in the furnace chamber is described in Section V of this chapter.

Final machining of the gauge section was done using a low-stress grinding approach (35). The machining parameters are summarized in Table 5. Final polishing of the gauge section was done with 400-grit silicon carbide paper using water as a lubricant, followed by 3/0 and 4/0 Emery polishing paper using Buehler Isocut Fluid as a lubricant. The paper was cut into strips approximately 0.20 inches wide, and polishing was done axially with the specimen chucked in a jeweler's lathe.

B. Ceramic Coating Procedure

A gas-tight ceramic coating, Solaramic 5210, was applied to the gauge sections of some specimens at General Electric's Materials and Processing Laboratory in Evendale, Ohio. Before the coating was applied, the gauge section was vapor blasted; this procedure entailed impinging fine alumina powder (Novacite 1250/150, supplied by Malvern Minerals) in a water stream at 0.31 MPa at the specimen surface. The specimen-to-surface distance was kept at about 5 cm, and total honing time was approximately 1 minute. The surface had a bright matte finish after the vapor blasting.

The ceramic coating was then applied, and baked in air at 1750°F for 20 minutes, and air cooled. The gauge section was inspected for spallation of the coating.

TABLE 4

STANDARD HEAT TREATMENT STA 3A
FOR INCOLOY 901

SOLUTION	Heat to 1975°F in vacuum Hold within ±4 F for 2 hours Backfill furnace with helium gas to a partial pressure of 640 torr
STABILIZATION	Heat to 1400°F in vacuum Hold within ±4 F for 2 hours Backfill furnace with helium gas to a partial pressure of 640 torr
PRECIPITATION	Heat to 1300°F in vacuum Hold within ±4 F for 24 hours Backfill furnace with helium gas to a partial pressure of 640 torr

TABLE 5

LOW STRESS GRINDING PARAMETERS

SPEEDS	Work surface: 8-26 ft/min.
	Table speed: 7 in./min.
	Wheel speed for traverse grinding: 2800-3250 ft/min.
FEEDS	Traverse grinding
	Roughing: 0.001 in./pass
	Finishing: Last 0.010 in. (250 μm)
	First 0.0080 in.: 0.0005 in./pass
	Next 0.0008 in. : 0.0004 in./pass
	Final 0.0012 in.: 0.0002 in./pass
	Plung grinding: 0.00002 to 0.00008 in./rev.

C. Specimen Preparation after Rejuvenation

After the specimens were thermally rejuvenated (see Section V-A), the gauge section was axially repolished with 3/0 and 4/0 emery polishing paper as described above in Section III-A. This provided a good quality surface for replication; an oxided surface could not be replicated without loss of detail.

After the specimens were HIP rejuvenated (see Section V-B), those specimens which were ceramic coated were mechanically polished with 240-grit polishing paper to remove the coating. The specimens were given the standard STA 3A (Table 5) to restore the morphology of the precipitates in the matrix. The gauge length was then lightly polished through 4/0 emery polishing paper as previously described.

D. Load Train Configuration

A photograph of the load train is shown in Figure 3(a). Note that a resistance-wound clamshell furnace was used for heating. A sketch of the load train with the various components labelled is illustrated in Figure 3(b). The grip design is contained in Figure 4. A molybdenum di-sulfide lubricant was effective in preventing binding in the grips.

E. Strain Measuring System

Although commonly referred to as a strain measuring system, the system employed actually measured displacement which must then be converted to strain. The necessary equations to accomplish this are described in Sections III-F and IV-C. Figure 5 is a photograph of the extensometer system used in this investigation. The system features a Satek PSH-8MS High Temperature Extensometer with a Microformer (Linear

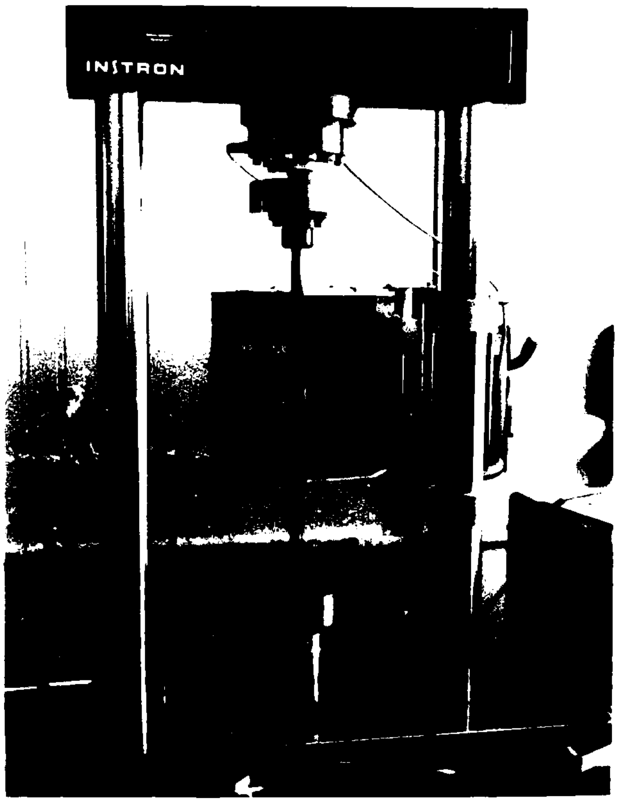

Figure 3a. Photograph of Load Train

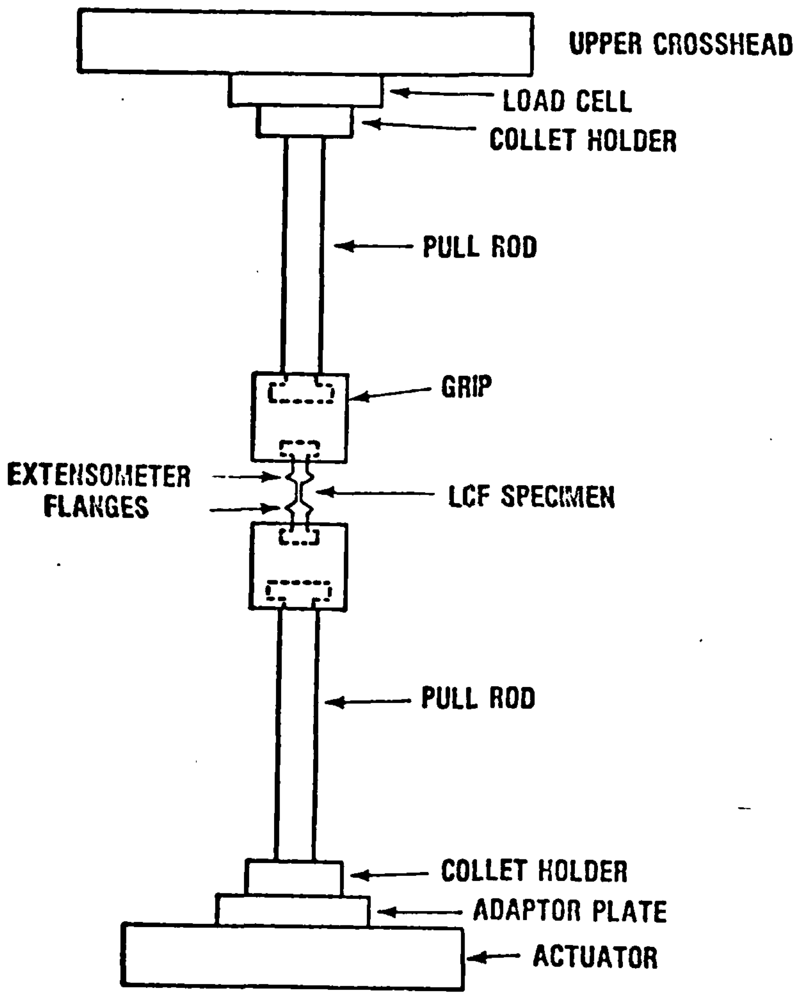

Figure 3b. Sketch of Load Train

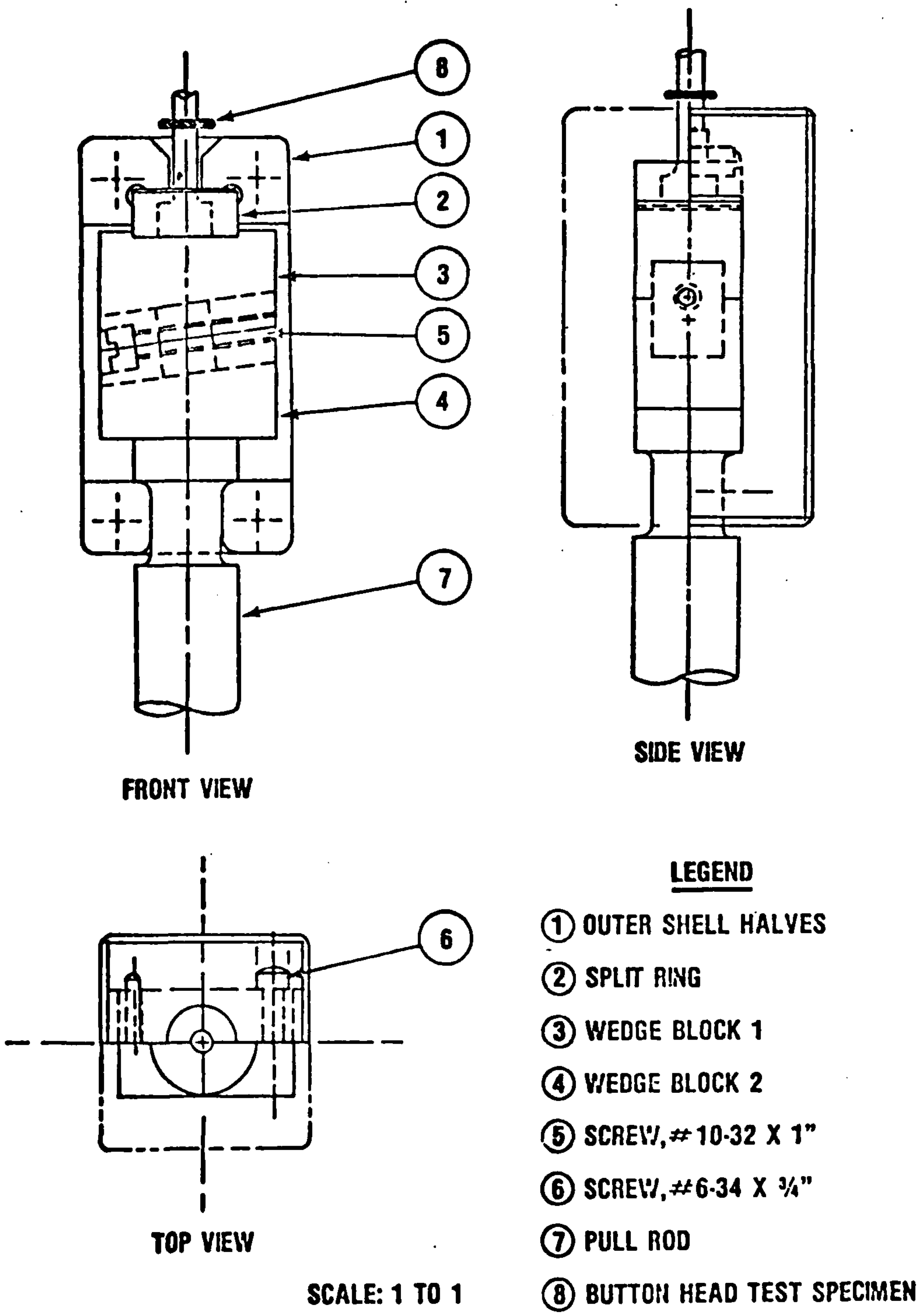

Figure 4. LCF Specimen Grip Design

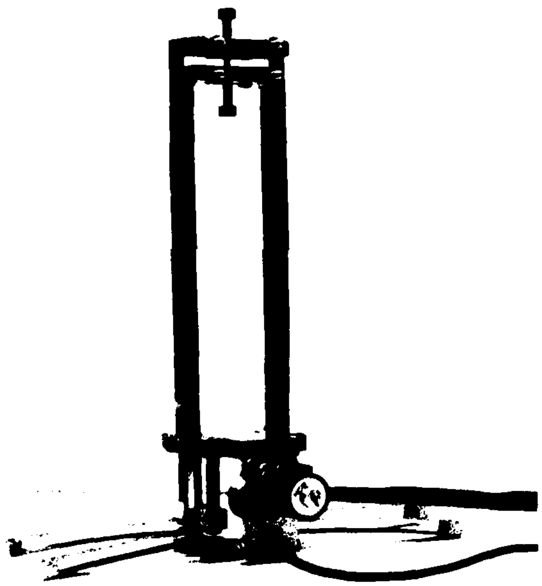

Figure 5. Photograph of Strain Measuring System

Variable Differential Transducer or "LVDT") to measure displacement. The suspension arms, which lock into the extensometer fixture, bolt around the flanges on the LCF specimen and effectively transmit the displacement of the specimen to the LVDT located beneath the furnace. The length of the suspension arms was governed by two criteria: (a) adequate length to allow the center of the specimen gauge length to be located in the center of the furnace hot zone with a one-inch clearance between the top of the extensometer fixture and the bottom of the furnace; and (b) proper difference in length between the top and bottom arms so that they would lock into the fixture for the particular flange separation distance used for the LCF specimen.

Calibration of the strain measuring system was accomplished as follows: The extensometer system was mounted in a Boeckeler Instrument Calibration Fixture. The top extension arm remained fixed and the bottom arm was movable using a dial calibrated in increments of 0.0001 inch. The LVDT was connected to an Instron Model 602A Stroke Controller. A Resistance-Capacitance (R-C) balancing network was adjusted to compensate for the resistive and capacitive characteristics of the system.

The zero suppression control was used to give a zero voltage when the LVDT core was in the center position of the LVDT. Output was read as a voltage on a digital voltmeter. Voltage readings were then taken as the dial was advanced in increments of a thousandths of an inch from 0 mils to 10 mils to -10 mils, and back to 0 mils. These 41 data points were then used to compute a linear least-square error line of the form $y - mx + b$ (36) where y is the displacement in volts, x is the displacement in mils, m is the slope of the line in volts/mil, and b is the y-intercept value. Table 6 contains typical data obtained from a

TABLE 6

TYPICAL LVDT CALIBRATION CURVE DATA

Inches × 10^3	Output Voltage	Inches × 10^3	Output Voltage
0.0	0.003	-1.0	-0.687
1.0	0.723	-2.0	-1.397
2.0	1.429	-3.0	-2.120
3.0	2.129	-4.0	-2.835
4.0	2.828	-5.0	-3.552
5.0	3.534	-6.0	-4.269
6.0	4.230	-7.0	-4.991
7.0	4.927	-8.0	-5.707
8.0	5.622	-9.0	-6.428
9.0	6.320	-10.0	-7.153
10.0	6.994	-9.0	-6.421
9.0	6.324	-8.0	-5.700
8.0	5.630	-7.0	-4.980
7.0	4.926	-6.0	-4.258
6.0	4.243	-5.0	-3.538
5.0	3.553	-4.0	-2.821
4.0	2.848	-3.0	-2.110
3.0	2.130	-2.0	-1.396
2.0	1.421	-1.0	-0.678
1.0	0.721	0.0	0.023
0.0	0.007		

calibration run. The data is plotted in Figure 6. Note that it is very linear. The inverse slope of this graph, or 1/m, is the desired calibration factor, λ, in volts per mil. These calibration runs were typically done before and after each LCF test.

F. Low Cycle Fatigue Testing

All LCF testing was performed on an Instron Dynamic Materials Testing System. The testing was done using a saw-tooth wave form at a frequency of 0.4 Hz under strain control (actually displacement control, as explained above) with zero mean level (i.e., fully reversed). The signal cable connecting the actuator LVDT with the Stroke Controller was disconnected and attached to the extensometer LVDT by means of an adapter cable. Specimen displacement thus served as the feedback to the controller. Command signals to the servovalve were generated by two different techniques: (a) Instron Model 860 Function Generator (i.e., an analog computer), and (b) Instron Series 900 Computer System, utilizing a Computer Automation Alpha 16 Minicomputer. Load-displacement hysteresis loops were plotted on a Hewlett Packard Model 7004B X-Y Plotter.

The load train alignment was checked and the load cell calibrated prior to each test. To begin the actual testing, the specimen was loaded into the grips, the extension arms were attached, and a chromel-alumel thermocouple was placed in close proximity to the LCF specimen surface in the center of the gauge length. Then the clamshell furnace was placed around the assembly. All testing was done at 500°F. Temperature was controlled using a West Guardsman Controller. The specimen was heated under load control at a tensile stress of ~ 3 ksi.

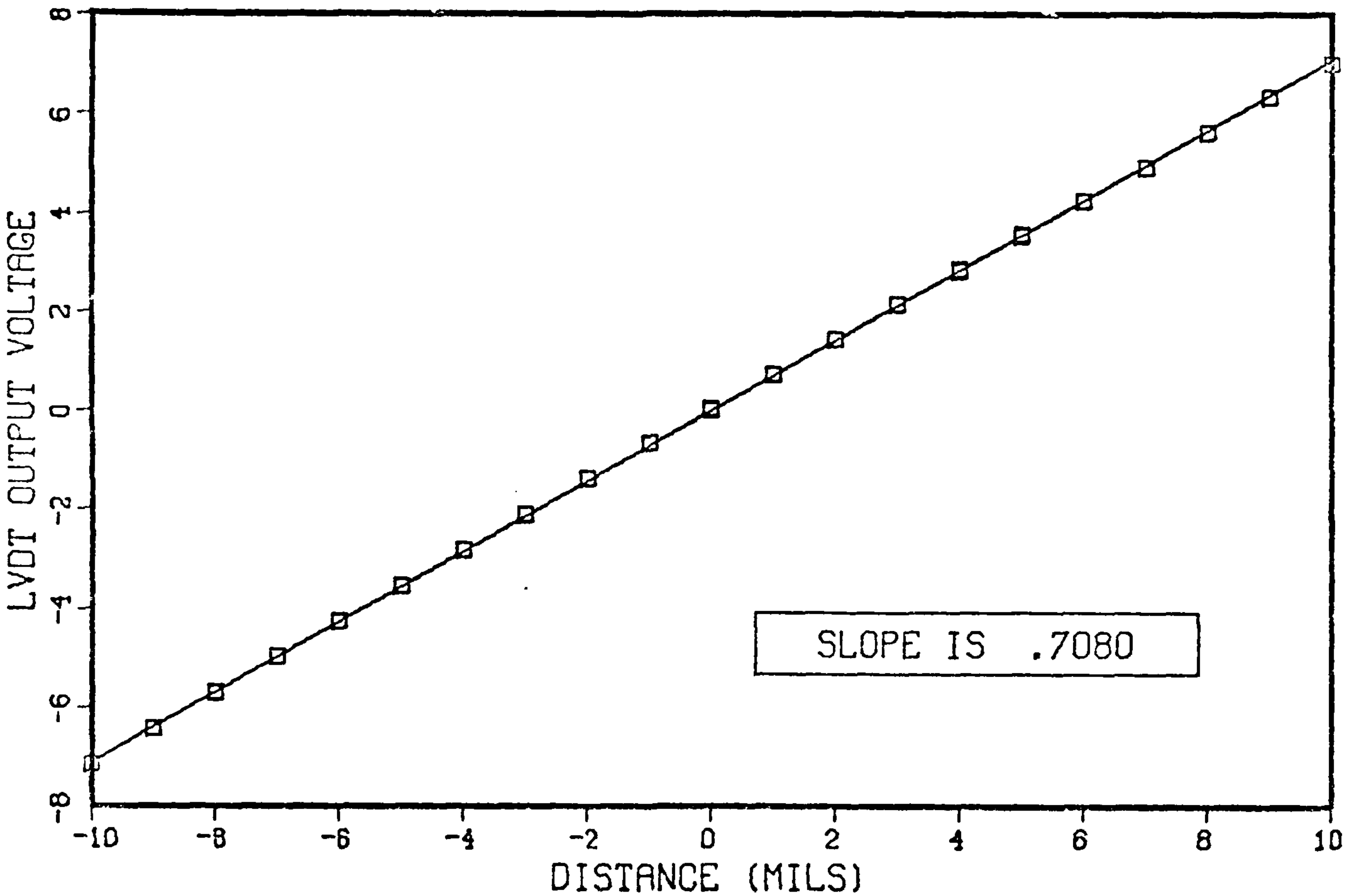

Figure 6. LVDT Calibration Curve

Once the temperature and the indicated specimen displacement readings had equilibrated, the Stroke Zero Suppression control was used to obtain zero voltage output of the LVDT at zero load.

The operation of the Function Generator was fairly straightforward. The proper amplitude setting to provide the desired strain range was empirically determined, using several specimens.

Testing under computer control required the use of a computer program. Instron's Low Cycle Fatigue Application Program APP-900-A3A8 (1974) was modified to provide more frequent and better formatted data output. The Appendix contains the source listing of the modified program. The address locations are in hexadecimal notation. The program was assembled using an Alpha 16 Assembler. Program parameters were entered via a teletype keyboard. Output was accomplished by teletype printer and punched paper tape. The frequency of data output was governed only by the speed of the paper tape punch. The fastest rate that data could be recorded was every three cycles at the test strain rate. The data on paper tape was processed by another program, written in Fortran, on a CDC 6600 computer. This program provided data, typically every five cycles, in tabular format for the following parameters: total displacement, plastic displacement, maximum elongation, minimum elongation, stress range, maximum stress, minimum stress, the ratio of maximum stress to minimum stress, elastic strain range, plastic strain range, and total strain range. Also, the program generated plots of stress range versus cycles, ratio of maximum stress to minimum stress versus cycles, and strain range versus cycles. A source listing of the computer program is contained in the Appendix.

The Instron computer program required a specification of strain rate, rather than frequency. Equation 1 is the appropriate expression relating frequency to strain rate:

$$\dot{u} = 2\nu \, \Delta u \tag{1}$$

where $\dot{u}$ is "strain" rate (actually displacement rate) in mils per second, ν is frequency in hertz (cycles per second), and Δu is displacement in mils.

The instron was capable of controlling displacements to ±0.00004 in. A typical plot of displacement versus cycles is shown in Figure 7.

G. Computation of Strain Range and Stress Range

As previously explained, the strain measuring system actually measured displacement. Since the cross-section of the LCF specimen between the extensometer flanges was not uniform, as is apparent from Figure 1, the computation of strain involved consideration of an effective gauge length. An effective gauge length is defined as that gauge length of uniform cross-sectional area which produces the same displacement under the application of a given load as does the gauge section of variable geometry. Use of the effective gauge length concept is made in the following equation which allows the computation of strain from displacement data:

$$\Delta\varepsilon_t = \Delta\varepsilon_e + \Delta\varepsilon_p = \frac{u_t - u_p}{L^e_{eff}} + \frac{u_p}{L^p_{eff}} \tag{2}$$

where $\Delta\varepsilon_t$ is the total strain range, $\Delta\varepsilon_e$ is the elastic strain range, $\Delta\varepsilon_p$ is the plastic strain range, u_t is the total specimen displacement (in inches), u_p is the plastic displacement (in inches), L^e_{eff} is the effective gauge length in the elastic regime (in inches), and L^p_{eff} is

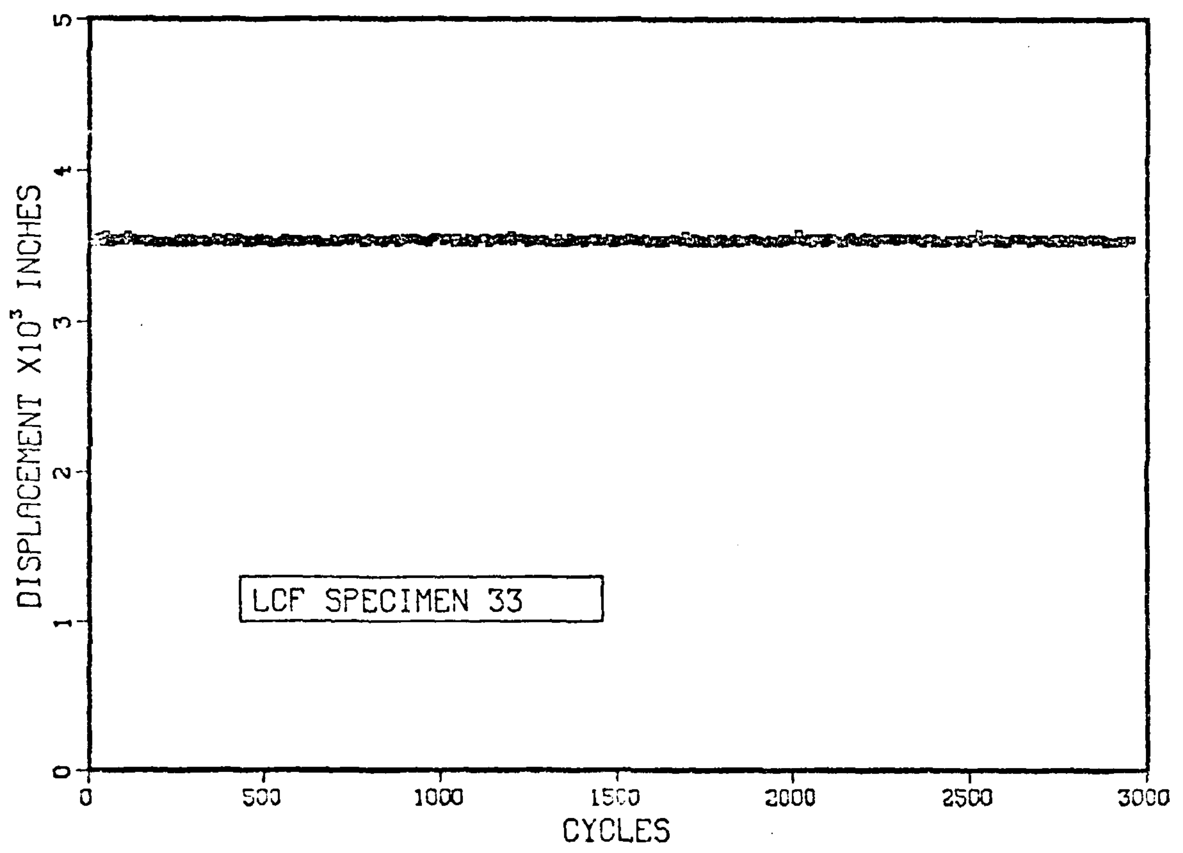

Figure 7. Plot of Displacement vs Cycles

the effective gauge length in the plastic regime (in inches). Now, u_t and u_p can be measured directly from the hysteresis loop plots or can be obtained from the computer data.

Equation 3 was used to compute displacement in thousandths of an inch when displacement distances were measured from hysteresis loop plots:

$$u = \lambda \cdot s \cdot \ell_D \tag{3}$$

where u is displacement (in mils), λ is the LVDT calibration factor, m^{-1} (in mils/volt), s is the plotter chart scale factor (in volts/inch of chart), and ℓ_D is the measured chart distance along the displacement axis of the hysteresis loop plot (in inches).

The plastic effective gauge length, L^p_{eff}, was assumed to be the straight portion of gauge length. This straight segment was measured for each specimen using a traveling microscope. Measurements were made along the top and bottom surfaces of a specimen supported horizontally; these were then averaged and rounded off to two significant figures.

The experimental determination of the elastic effective gauge length, L^e_{eff}, involved comparing the slope of a stress-displacement curve to a known elastic modulus value. The equation of interest was:

$$L^e_{eff} = \frac{E_{ACT}}{\Delta\sigma/\Delta u} \tag{4}$$

where L^e_{eff} is the effective elastic gauge length (in inches), E_{ACT} is the known Young's Modulus (in psi), Δσ is the stress range (in psi), and Δu is the displacement range (in inches).

The calculation of stress, using distances measured along the load axis on the fatigue hysteresis loop, was done by applying Equation 5:

$$\sigma = k \cdot (1/d_o^2) \cdot t \cdot \ell_L \qquad (5)$$

where σ is stress (in psi), k is a constant = 6.367×10^2 when the full scale load is 5000 lbs, d_o is the specimen diameter (in inches), t is the plotter chart scale factor (in volts/inch of chart), and ℓ_L is the measured chart distance (in inches) along the load axis of the hysteresis loop plot.

H. In Situ Surface Replication

When it was necessary to interrupt a fatigue test in order to replicate the gauge length of the specimen, the specimen was not removed from the load train but rather replicated in place in order to maintain the same alignment (37). The procedure is detailed below.

After the LCF test was halted, while the specimen was going into compression, the system was placed in Load Control with a mean level of zero. Then the stroke value was recorded. A mean tensile stress of about 3 ksi was then imposed on the specimen. The furnace was removed and a small fan was used to speed the cooling of the load train. After the system was at room temperature, the actuator was turned off, the thermocouple pulled back, and the extensometer removed. These procedures exposed the gauge section. The gauge section was cleaned with acetone and the replication was accomplished as explained in Section I-D.

In order to restart the test, the extensometer was reattached and the thermocouple placed back in position. The actuator was turned on, and a mean tensile stress of about 3 ksi was imposed. The furnace was placed back around the load train. When the system was equilibrated, both with respect to temperature and dimensions, a zero mean level was imposed and the Stroke Zero Suppression Control was used to set the same stroke value which was recorded when test was initially stopped. Then the test was restarted.

IV. TENSILE TESTING

A. Specimen Configuration

The same specimen design, shown in Figure 1 for LCF testing, was used for tensile testing. Specimen manufacture was also done in the same way.

B. Machine Description

Mechanical testing was performed on an Instron Tensile Testing Machine, Model TT-C. The cross-head was moved at a constant speed utilizing an amplidyne drive and selsyn control elements. A Leeds and Northrup chart recorder (1.5 seconds full scale response time) was driven by the output from the extensometer LVDT. Load was measured by an Instron Load Cell. The chart was operated at 100 lbs full scale to provide good sensitivity of the load-displacement curve. The load cell and the LVDT gain control were calibrated prior to each test. The load train and furnace assembly were essentially the same as shown in Figure 3 for the LCF testing.

C. Computation of Stress and Strain

Stress was simply computed by dividing the load by the cross-sectional area of the specimen. The strain was computed in an analogous manner to that for the LCF data. Thus, a relationship was required to convert displacement to strain. It is certainly true that

$$\varepsilon_t = \varepsilon_e + \varepsilon_p \tag{6}$$

where ε_t is total strain, ε_e is elastic strain, and ε_p is plastic strain. But

$$\varepsilon_e = \frac{\sigma}{E} = \frac{u_e}{L^e_{eff}} \tag{7a}$$

and

$$\varepsilon_p = \frac{u_p}{L^p_{eff}} = \frac{u_t - u_e}{L^p_{eff}} \tag{7b}$$

where σ is the stress (in psi), E is Young's Modulus (in ksi), u_p is the plastic displacement of the gauge section (in inches), u_t is the total displacement of the gauge section (in inches), u_e is the elastic displacement of the gauge section (in inches), L^e_{eff} is the effective gauge length in the elastic regime (in inches), and L^p_{eff} is the effective gauge length in the plastic regime (in inches). Thus, it is apparent that:

$$\varepsilon_t = \frac{\sigma}{E} + \frac{u_t - \dfrac{\sigma \cdot L^e_{eff}}{E}}{L^p_{eff}} \tag{8}$$

So, Equation 8 is the desired relationship.

V. REJUVENATION TREATMENTS

A. Thermal Treatments

The only thermal rejuvenation treatment which was investigated was STA 3A which is defined in Table 4. It was necessary to suspend the specimen vertically in the furnace in order to minimize creep effects which could warp the specimen. A heat treating fixture, shown in Figure 8(a) and Figure 8(b), was designed to support the specimens in the center of the furnace hot zone. This fixture minimized the

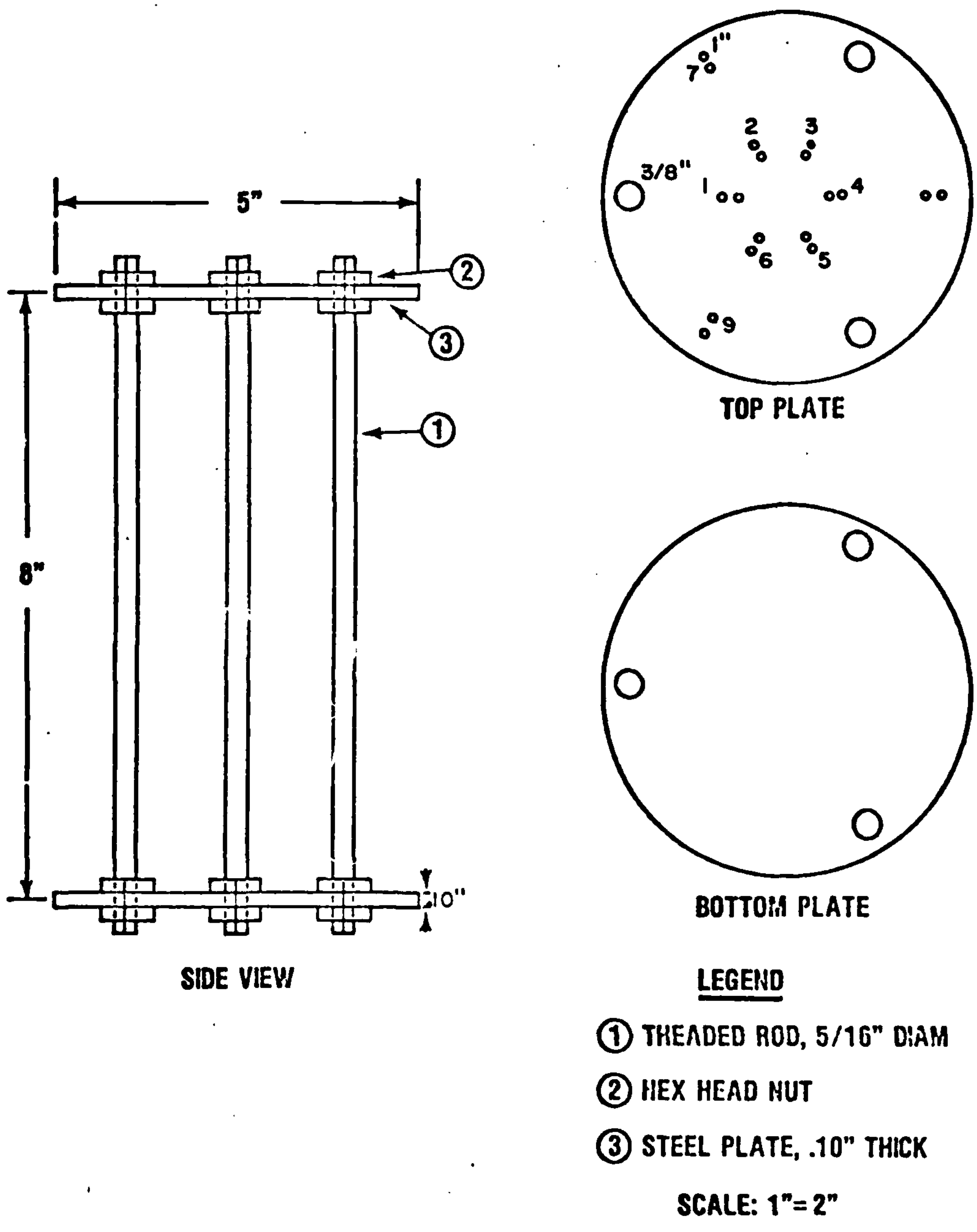

Figure 8a. Heat Treatment Fixture Design

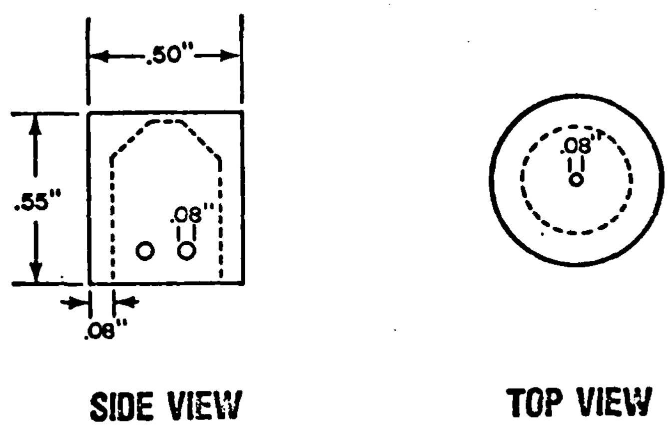

Figure 8b. Button Head Cap Design

possibility of specimen distortion, did not adversely affect critical machined surfaces, and was fairly simple to use. It held nine specimens. The cap, depicted in Figure 8(b), fit over the LCF specimen button head. Fine Nichrome wire was threaded into the two holes on each side of the cap, and thus the specimen was supported on the surface under the button head. Chromel wire, with a bead on one end, was threaded through the hole at the top of the cap. This wire was then pulled through a hole on the top plate of the fixture shown in Figure 8(a). The material used to manufacture the fixture and cap was AISI 1020 steel.

B. Hot Isostatic Pressing (HIP) Treatments

The HIP processing was conducted in a small, high-pressure, 7-in. i.d. × 14-in. long, HIP unit at Kelsey-Hayes, Detroit, Michigan. The chamber was designed by Autoclave Engineering, Erie, Pennsylvania. The heating elements were Kanthal wound, supplied by Conway Pressure Systems, Columbus, Ohio.

The fatigue specimens were vertically supported in a special fixture, shown in Figure 9. The same button head cap design, depicted in Figure 8(b) was used.

The temperature and pressure profiles for the HIP run are shown in Figures 10 and 11. The autoclave gas used was commercially pure argon.

A summary of the HIP run is as follows: The specimens mounted in the fixture were loaded into the HIP chamber, The system was flushed with argon gas until the atmosphere was primarily argon, The unit was slowly heated to 2050^{o}F and the pressure was raied to 15 ksi. The 2050^{o}F temperature was maintained for one hour, then the temperature

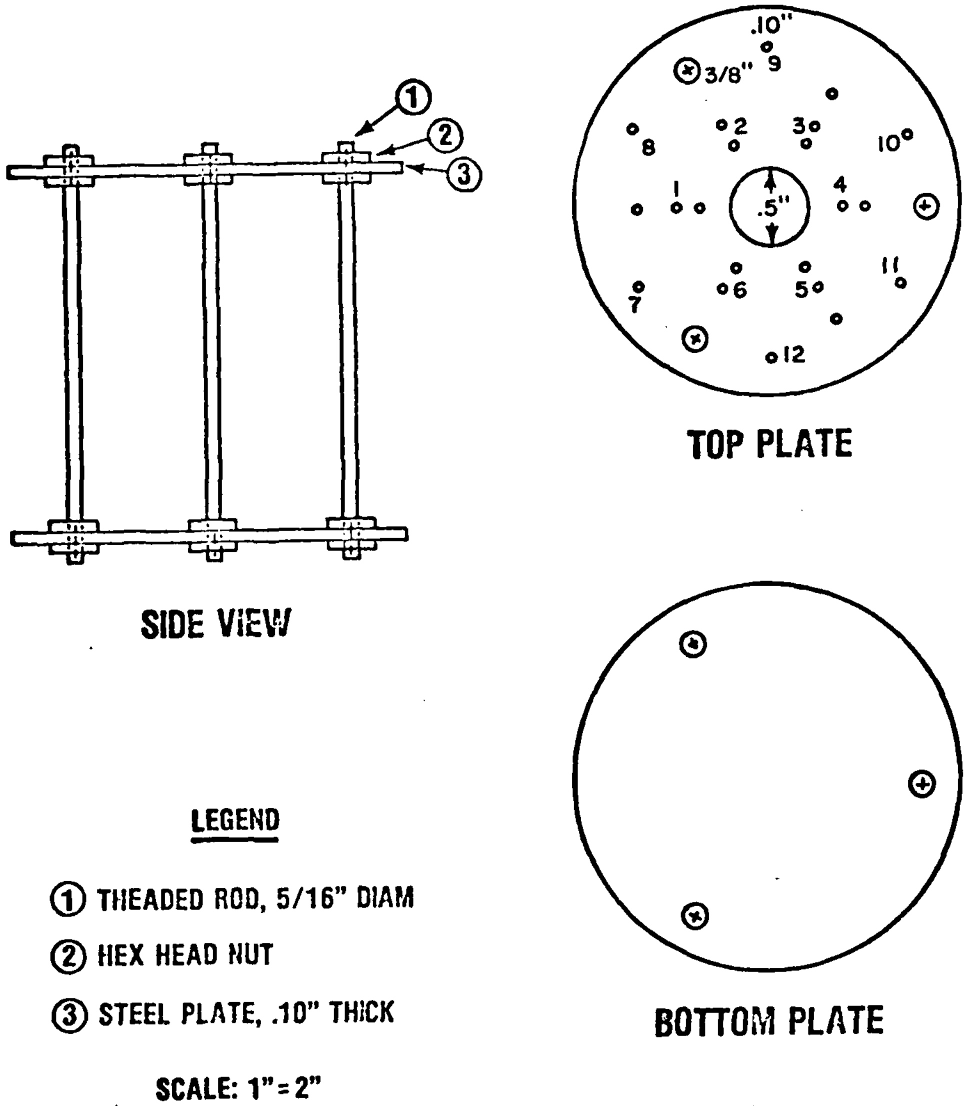

Figure 9. HIP Fixture Design

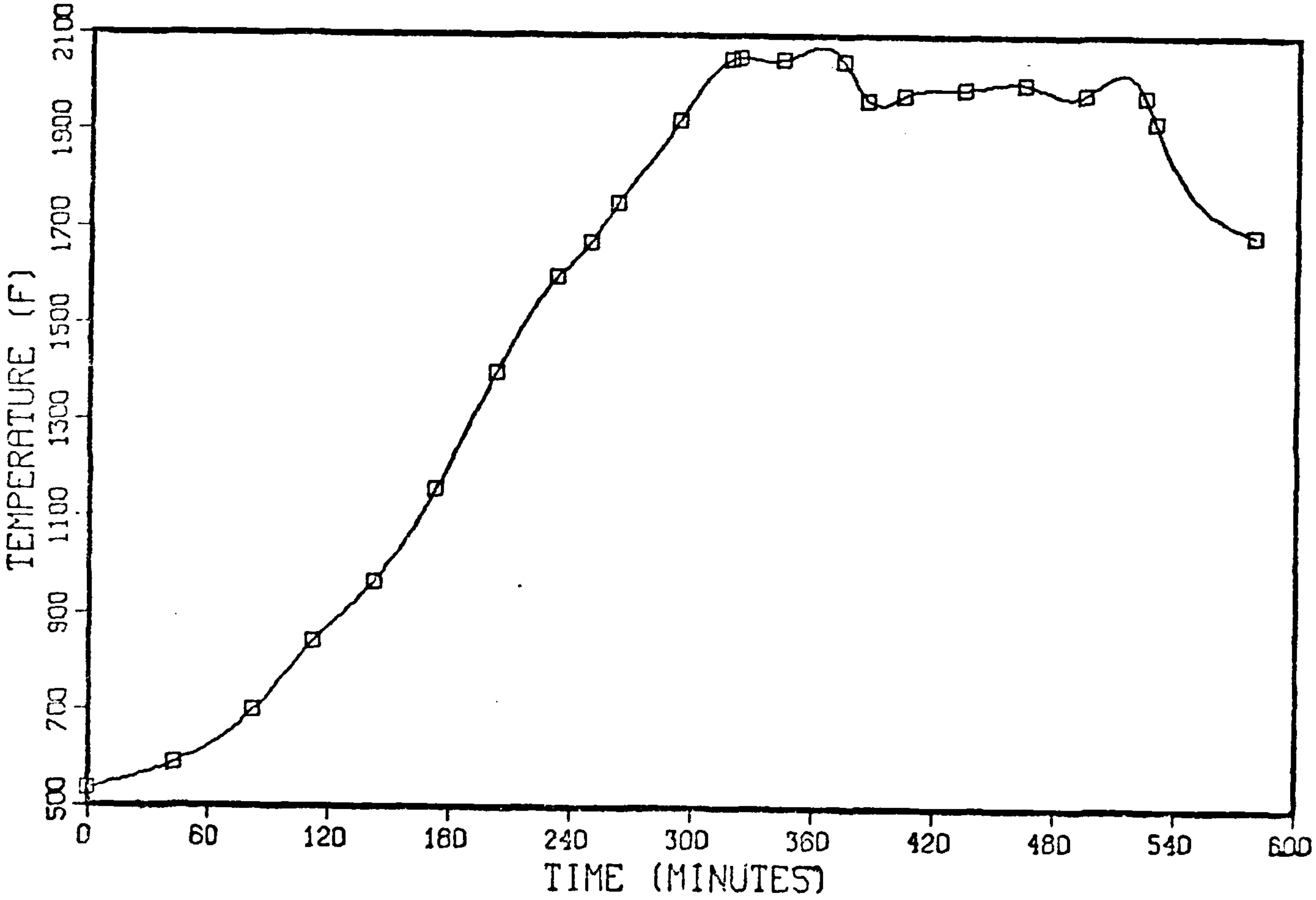

Figure 10. Plot of Temperature vs Time for HIP Run

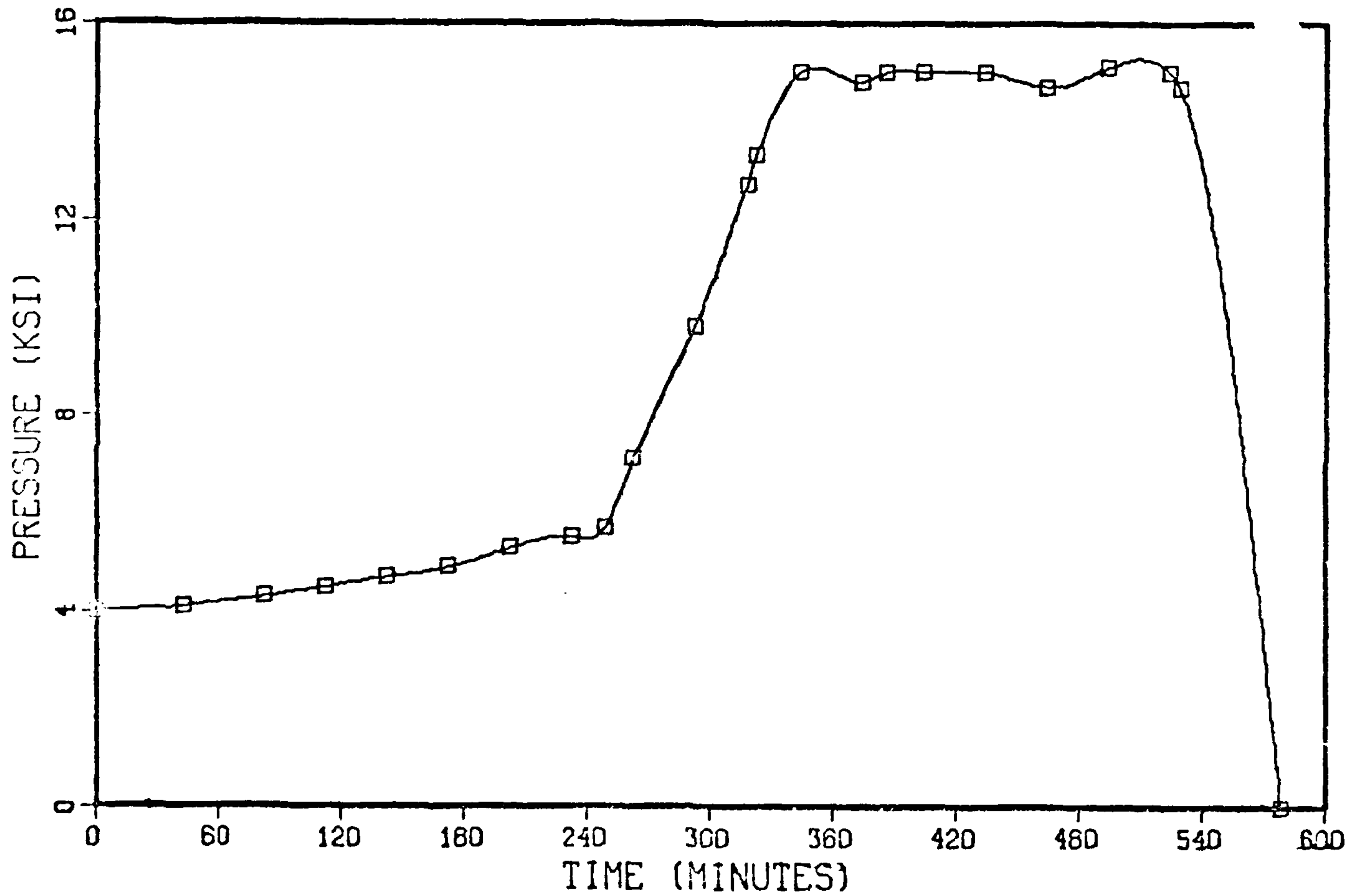

Figure 11. Plot of Pressure vs Time for HIP Run

was lowered to 1975°F while maintaining 15 ksi. After two hours at 1975°F, the pressure was released and the heating elements were turned off. When the chamber temperature reached 1700°F, the unit was opened, and the fixture removed. It was then placed in an argon gas stream until it reached ambient temperature.

VI. SONIC MODULUS TESTING

Moduli of elasticity were measured at room temperature using a Magnaflux FM-500 Elastomat. A right cylindrical rod was centerless ground to a uniform diameter of 0,4983 inches. The rod was 4.483 inches long and weighed 117.625 g.

The test rod was suspended at its nodal points by adjustable cross wires. Mechanical vibration was transmitted to the sample by a piezoelectric transducer by means of a 0.004-inch Nichrome wire spot wleded to the rod about 0.010 inch from the circumference. Another transducer, similarly connected on the other side of the rod, received the mechanical vibration from the specimen. The rod was excited by means of a variable frequency oscillator which contained a digital counter. The resonant frequency was determined by the appearance of a circular Lissajou figure on an oscilloscope. The oscilloscope had the voltage output of one transducer connected to the x-axis and the voltage output of the other transducer connected to the y-axis. In such a manner, the resonant frequencies for the longitudinal (Young's) modulus, transverse modulus, and shear modulus were measured. The following equations were then used to compute the moduli:

Longitudinal (Young's) Modulus (39):

$$E = \frac{4.00 \times 10^{-4}\ \rho\ \ell^2\ f_L^2}{6.895} \tag{9}$$

Shear Modulus (39):

$$G = \frac{4.00 \times 10^{-4}\ \rho\ \ell^2\ f_G^2}{6.895} \tag{10}$$

Transverse Modulus (40):

$$E_T = \frac{1.261886 \times 10^{-4}}{6.895}\ \frac{\rho\ \ell^2\ f_T^2\ T_1}{d^2} \tag{11}$$

Shape Correction Factor, T_1 (41):

$$T_1 = 1 + 4.88669 \left[\frac{1 + 1.26225\ \nu + 0.2098\ \nu^2}{1 + \nu}\right] \left(\frac{d}{\ell}\right)^2 \tag{12}$$

where ρ is density (in g/cc); ℓ is length (in cm); d is diameter (in cm); f_L, f_G, and f_T are the resonant frequencies; E, G, and E_T are the elastic modulii (in psi); and ν is Poisson's ratio.

Chapter 3

RESULTS AND DISCUSSION

I. AGING RESPONSE OF INCOLOY 901

A. Characterization of As-Received Microstructure

The microstructure of the Incoloy 901 forging was examined using a metallograph, a transmission electron microscope, and an electron microprobe.

Figure 12 shows a typical microstructure. Using the ASTM Linear Intercept Method to measure grain size (42), the grain size was determined to be 90 μm or ASTM Equivalent Grain Size 3.5. Particularly evident in Figure 12(a) are the inclusion stringers which parallel the forging direction. Figures 12(b) and 12(c) are higher magnification photographs of these inclusions. It is evident that these particles act as obstacles to grain boundary migration and thus assist in controlling the grain size during processing and thermal treatment. Figures 12(a) and 12(c) contain several annealing twins. These twins were commonly observed in the as-received material. Also evident in Figures 12(b) and 12(c) are much smaller particles.

Figure 13 is an electron image produced in a microprobe of a lightly etched sample. This clearly shows that there are two different particle morphologies.

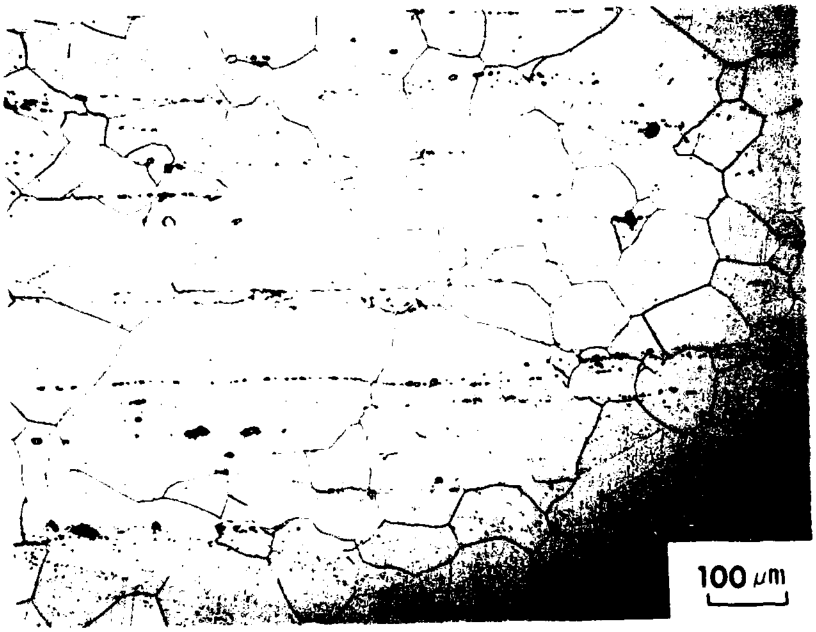

a. General Microstructure

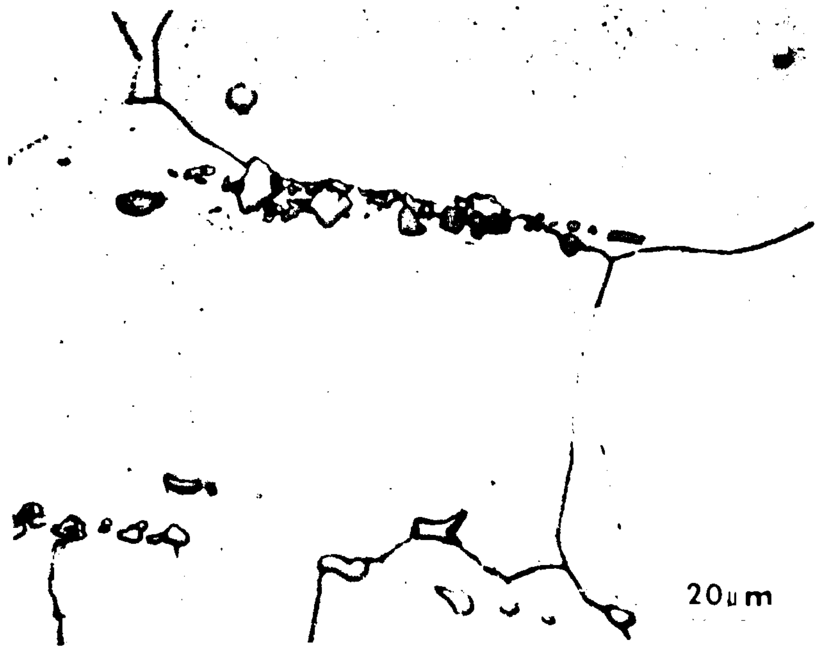

b. Inclusion Stringers

Figure 12. Micrograph of As-Received Material

Figure 12 (continued)

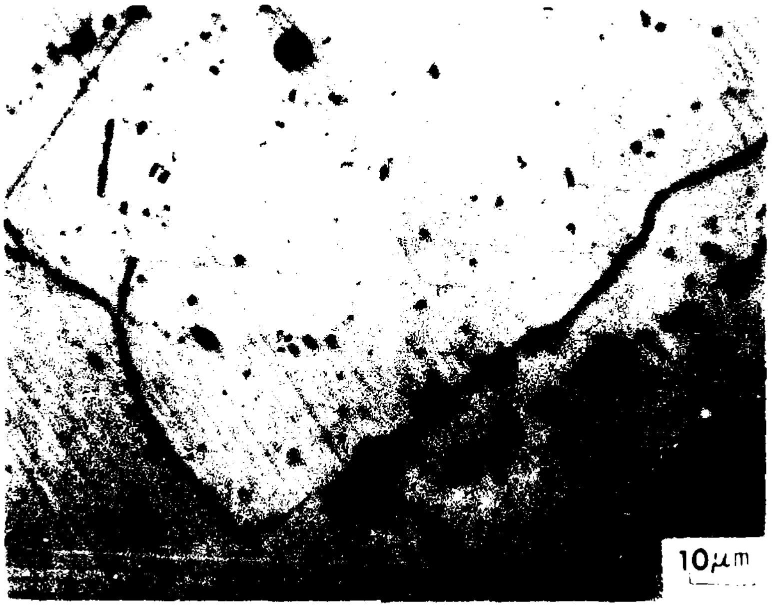

c. Inclusion Stringers

Figure 13. Electron Micrograph of Inclusion

Qualitative electron probe analysis, shown in Figure 14, clearly identifies the large, blocky phase as a titanium/molybdenum carbide. Quantitative analysis indicates that these are MC-type carbides with slightly varying proportions of titanium and molybdenum. A typical carbide had the composition $Ti_{0.8}Mo_{0.2}C$. The sizes of these primary carbides typically ranged from 2-15 μm.

The small symmetrical particles in Figures 13 and 14 were approximately 1 μm in size and thus were difficult to quantitatively analyze. However, the results from an electron microprobe quantitative analysis indicated the following composition in weight percent: Ti-9.88, Co-13.52, Fe-8.55, Ni-3.42, Mo-52.23; difference from 100% is 12.40. Although boron could not be analyzed for in the microprobe, this analysis is consistent with the hypothesis that these particles are M_3B_2 borides. Furthermore, Beattie electrolytically extracted similar particles from Incoloy 901 and analyzed them chemically and by x-ray diffraction (69). His conclusion was that these particles were M_3B_2 borides.

Transmission electron microscopy was used to characterize the small γ' precipitates and the grain boundary precipitates. Figure 15 shows γ' in dark field. The particles have a spherical morphology and an average diameter of 300 Å units. Figure 16 shows the grain boundary precipitates. These are MC carbides of the type (Ti,Mo)C rather than $M_{23}C_6$ carbides (70). It should be noted that some grain boundaries, as indicated in Figure 17, were relatively free of precipitates.

B. Development of Standard Solution and Double-Aged Treatment

Since the LCF test specimens were cut from different portions of a shaft forging, it was desired to subject them all to a standard,

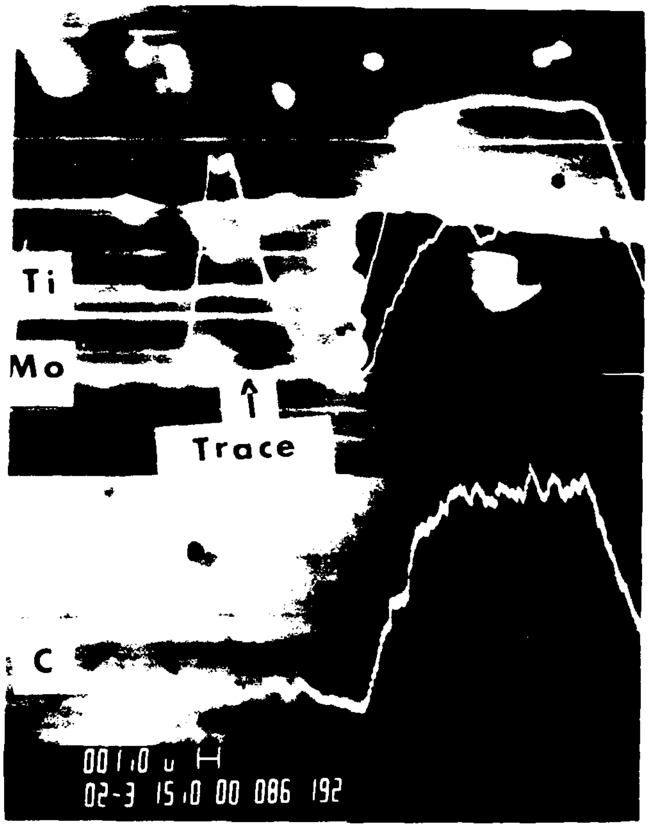

Figure 14. Electron Microprobe Image of Carbide Inclusion

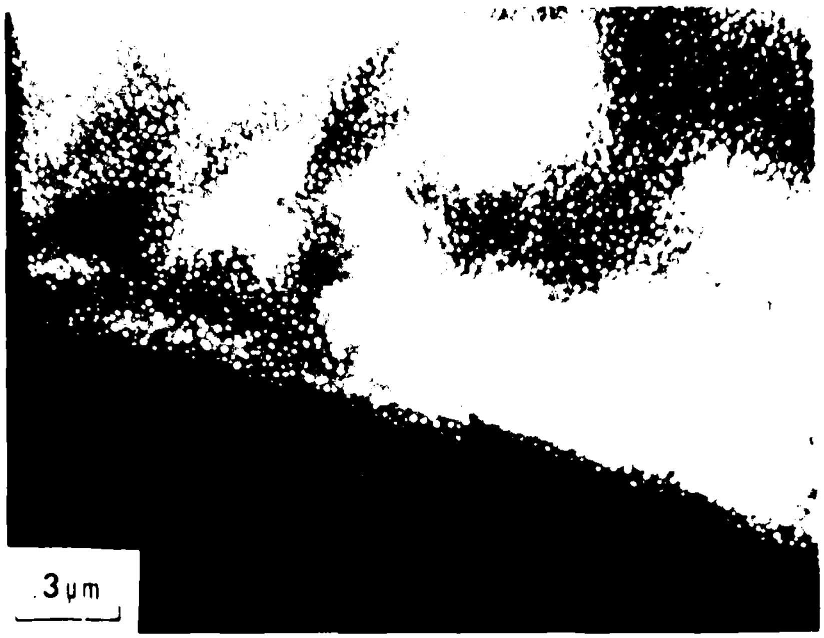

Figure 15. TEM Micrograph of γ'

a. Typical Grain Boundary MC Precipitates

b. Typical Grain Boundary MC Precipitates

Figure 16. TEM Micrograph of Grain Boundary MC Carbides

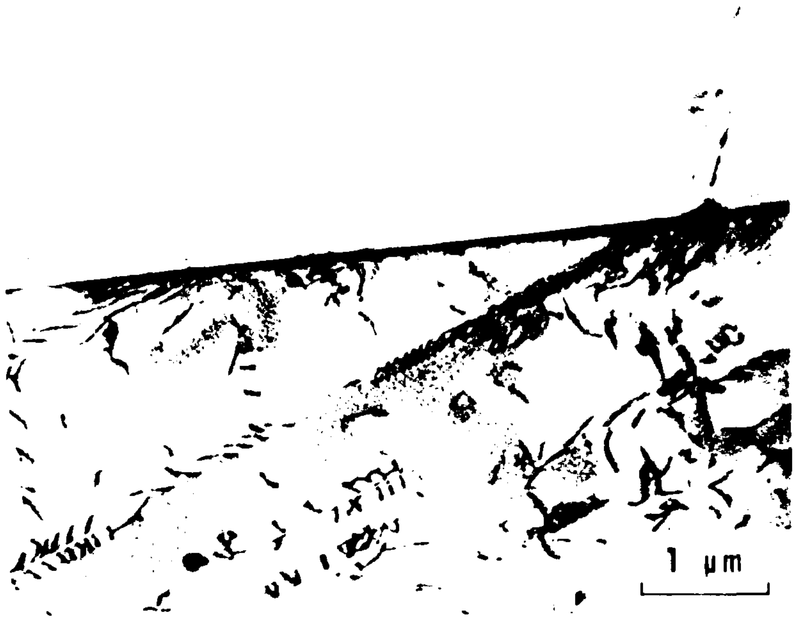

Figure 17. TEM Micrograph of Precipitate-Free Grain Boundary

known heat treatment prior to testing. Also, this standard heat treatment could be used for thermal rejuvenation and to restore the microstructure of hot isostatically pressed specimens. Table 2 contains the specification for the commercial heat treatment. Since the minimization of grain growth was an important consideration in developing the standard heat treatment, the lowest portion of the time and temperature ranges were selected for the solutioning treatment. The drop furnace was used to rapidly quench a piece of material which was subsequently examined by transmission electron microscopy. It was determined that 2 hours at 1975°F was sufficient to dissolve all phases except for the primary MC carbides.

All heat treatments were done in a vacuum furnace to minimize surface contamination. However, it was necessary to backfill the furnace with helium gas in order to obtain a high enough cooling rate to prevent the nucleation and growth of undesirable precipitates and precipitate morphologies. Such undesirable grain boundary morphologies are shown in Figure 18. Figure 18(a) shows needles of a η phase growing out from a grain boundary MC precipitate in a platelet morphology, and Figure 18(b) is a dark field view of the MC platelets growing out from a grain boundary. These precipitates were formed during vacuum cooling from the solutioning temperature because the cooling rate was too slow. It was found that backfilling the furnace to 640 torr of helium gas produced the proper grain boundary morphology. The standard heat treatment, designated as STA 3A, is presented in Table 4.

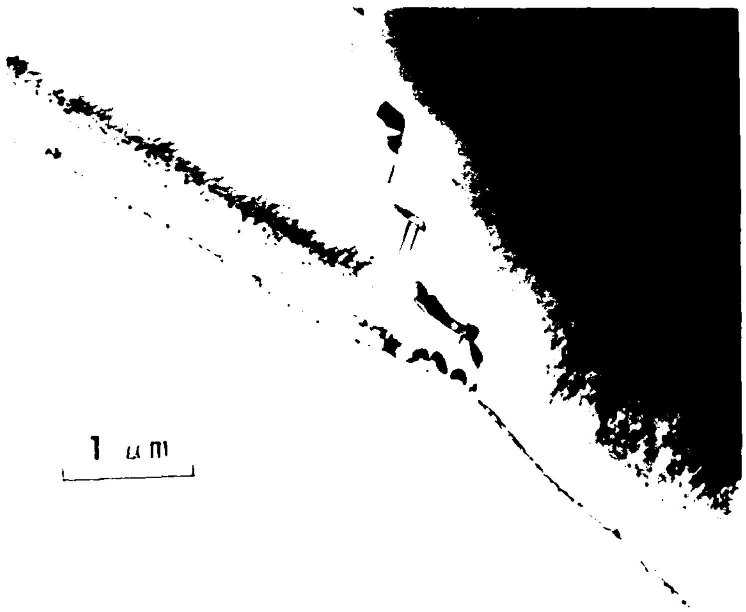

a. Needle-Shaped η Phase and MC Platelets

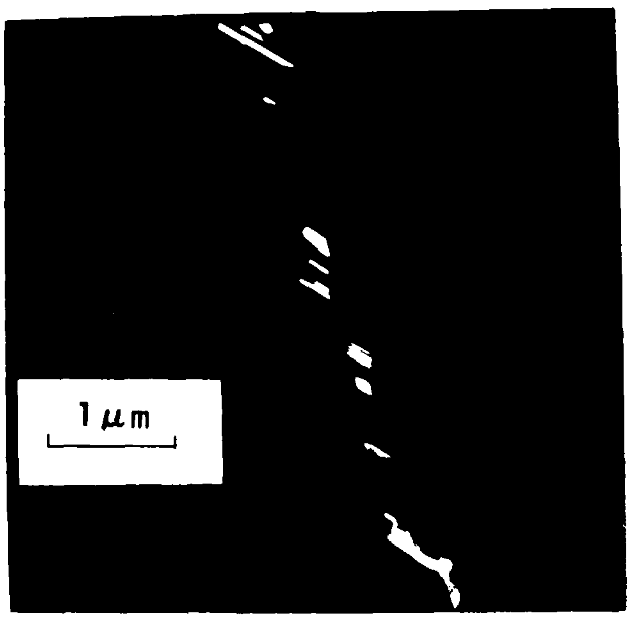

b. MC Platelets (Dark Field)

Figure 18. TEM Micrograph of Undesirable Grain Boundary Precipitate Morphology

The effect of STA 3A on grain size was measured. The average grain size was increased to 120 μm (ASTM Equivalent Grain Size 3), but remained fairly stable at this size with subsequent heat treatments. The matrix was not dislocation-free, but the dislocations were randomly oriented.

C. Microstructure Response at Elevated Temperatures

In order to better understand the physical metallurgy of Incoloy 901, the microstructure which developed at 1500°F and 1700°F was studied using a drop furnace. After 6 hours at 1500°F, no change in the grain size occurred. The fine γ' coarsened appreciably, approximately doubling in size to 600 Å units. The grain boundary carbides developed a blocky morphology.

After 6 hours at 1700°F, no change in the grain size occurred. The change in precipitates was dramatic. No γ' was seen, although the solvus temperature is assumed to be 1725°F (17). The platelet morphology of the η phase is evident from the transmission electron micrographs in Figure 19. Figure 20 shows these η platelets at lower magnification as seen in a metallograph.

D. Microstructure Resulting from Hot Isostatic Pressing (HIP)

Hot isostatic pressing of superalloys is normally accomplished at very high temperatures; i.e., above the 1975°F solutioning temperature of Incoloy 901. In an attempt to measure the effect on grain growth of these high HIP temperatures, one piece of material was heated in a vacuum furnace to 2100°F for five hours and another piece was heated to 2050°F for three hours. The average grain size after the 2100°F

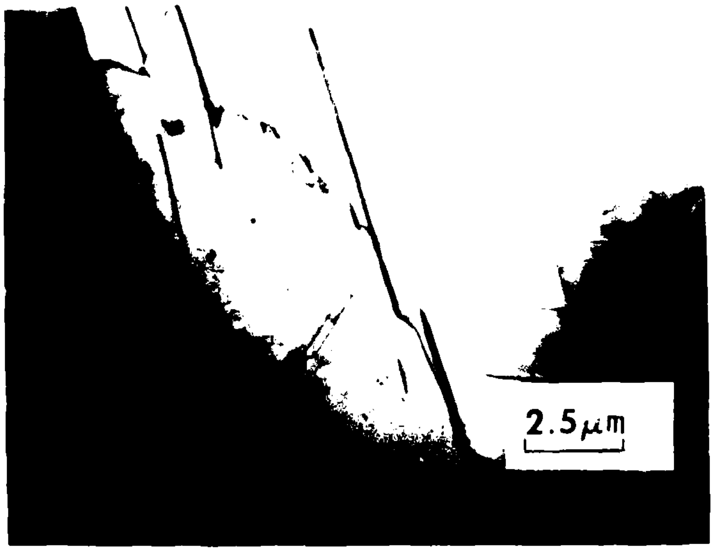

a. Nucleation of η at Grain Boundary

b. Matrix Nucleation of η

Figure 19. TEM Micrograph of η Platelets

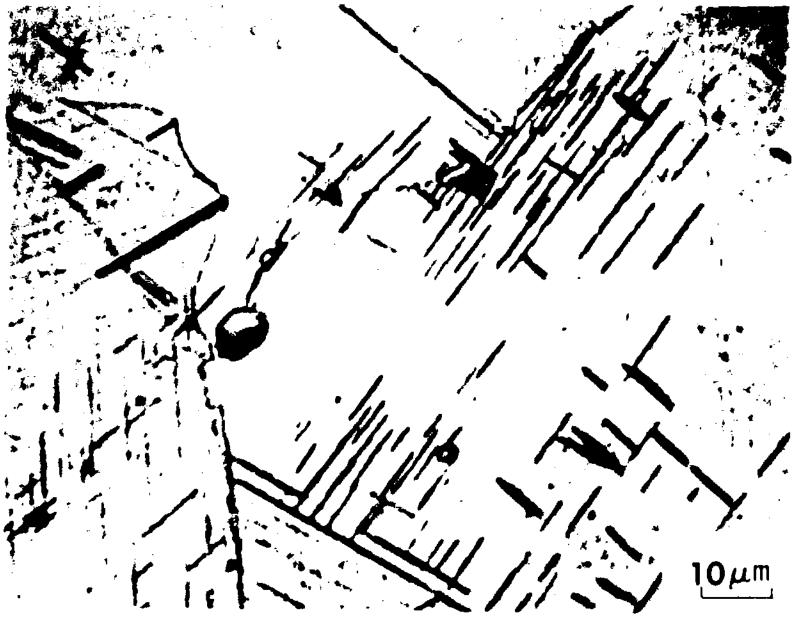

a. Typical η Platelets

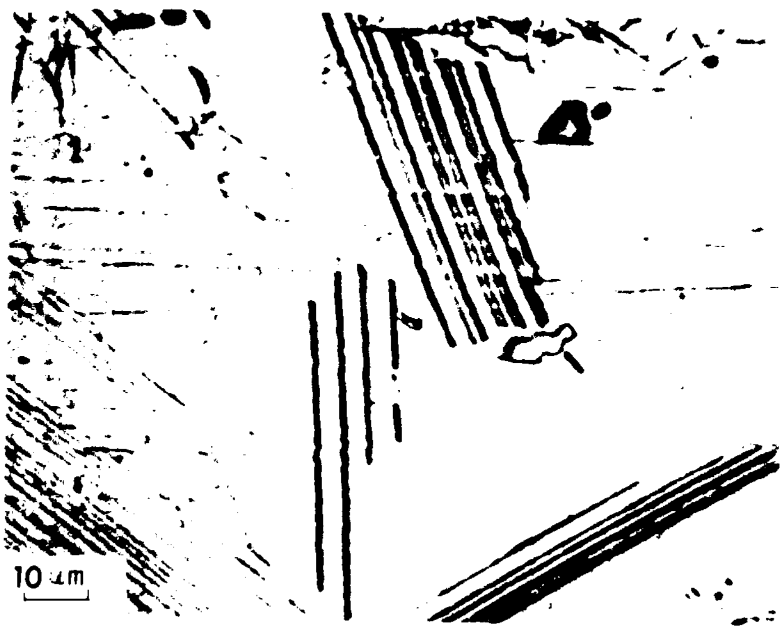

b. Typical η Platelets

Figure 20. Micrographs of η Platelets

heat treatment was 237 μm (ASTM Equivalent Grain Size 1). The average grain size which resulted from the 2050°F heat treatment was 181 μm (ASTM Equivalent Grain Size 1.5).

Figure 21 shows photomicrographs of as-HIPed material (15 ksi pressure, 1 hour at 2050°F, 2 hours at 1975°F). Note that the primary carbides helped to control grain growth. There also appears to be some η-phase precipitation which occurred during cooling. Except for the primary carbides and η platelets, transmission electron microscopy did not reveal any other precipitates. The grain size was about 150 μm, or ASTM Equivalent Grain Size 2.

When the as-HIPed material was given the standard STA 3A heat treatment, the desirable morphology and distribution of precipitates was restored.

II. MECHANICAL PROPERTIES

A. Tensile Properties

The measured tensile properties of the Incoloy 901 test specimens, after STA 3A, are summarized in Table 7. These properties (at room temperature) are well above the specified minimums of 100 ksi yield strength and 150 ksi ultimate tensile strength (43).

B. Elastic Constants

The elastic moduli were measured at room temperature using an Elastomat Sonic Modulus Tester. Young's Modulus was determined to be 30.2×10^6 psi; the corrected transverse modulus was 30.3×10^6 psi; the shear modulus was 11.2×10^6 psi; and Poisson's ratio was 0.35. Young's Modulus of 29.9×10^6 psi at room temperature and 27.51×10^6 psi at 500°F have been reported from mechanical test data (44).

TABLE 7

INCOLOY 901 TENSILE DATA

Specimen	Test Temperature (°F)	Yield Stress (ksi)	Tensile Stress (ksi)	Fracture Stress (ksi)	Reduction in Area (%)	Strain Rate (in./in./min.)
B2	70	135.3	178.3	207.6	14.3	2×10^{-2}
B1	500	119.4	155.4	175.4	12.6	2×10^{-2}
B3	500	123.3	165.7	194.3	14.9	2×10^{-2}
B4	500	123.7	161.3	189.0	15.1	2×10^{-3}

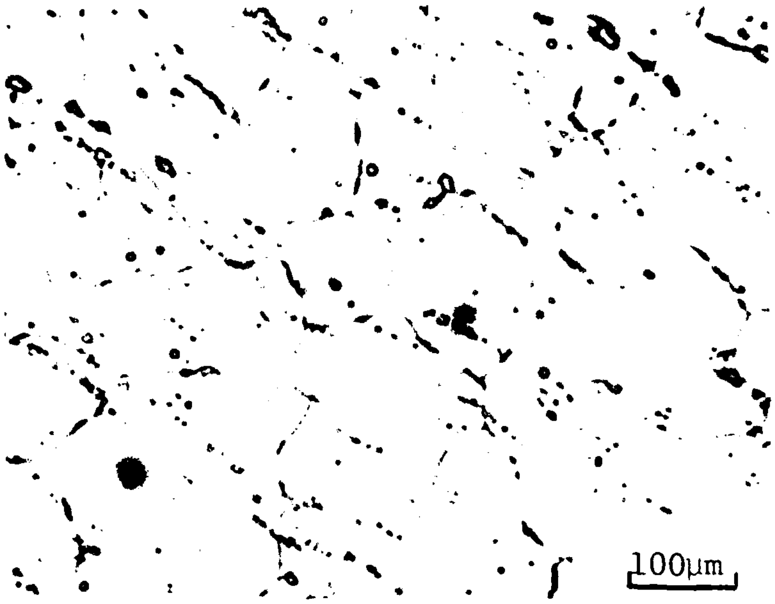

a. Typical Microstructure

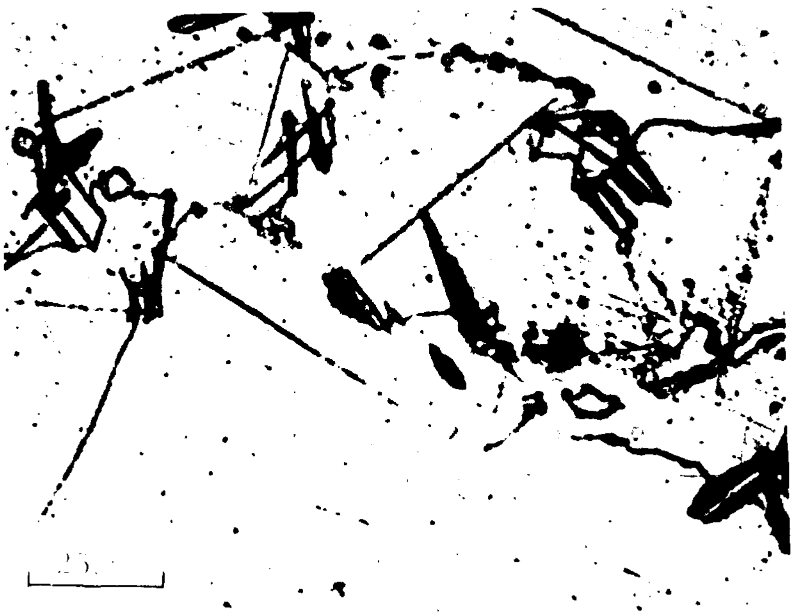

b. Grain Boundary Region

Figure 21. Micrographs of As-HIP'd Material

III. LOW-CYCLE FATIGUE BASELINE TESTING

A. Determination of Effective Gauge Length

The low-cycle fatigue specimen design (Figure 1) requires the use of an effective gauge length in order to compute a strain from the measured displacement between the flanges. A plot of Stress vs Displacement at room temperature is shown in Figure 22, and Figure 23 shows Stress vs Displacement at 500°F. The slope of the linear portions of these curves is an effective modulus, $\Delta\sigma/\Delta u$ (recall Equation 4). Thus, Equation 4 allows computation of the effective elastic gauge length, L^e_{eff}, once the effective modulus, $\Delta\sigma/\Delta u$, is known. Using a linear least square error curve fit to the linear portion of the data in Figures 22 and 23, the effective modulus at 70°F was found to be 58.76×10^6 psi/in. with a correlation coefficient of 0.9999. At 500°F, the effective modulus was found to be 54.89×10^6 psi/in. with a correlation coefficient of 0.999. The results are summarized in Table 8. Strain was then computed using Equations 2 and 8.

Table 8

EFFECTIVE ELASTIC GAUGE LENGTH

Temperature (°F)	Young's Modulus ($\times 10^{-6}$ psi)	Effective Modulus ($\times 10^{-6}$ psi/in.)	Effective Elastic Gauge Length (in.)
70	30.2	58.76	0.51
500	27.5	54.89	0.50

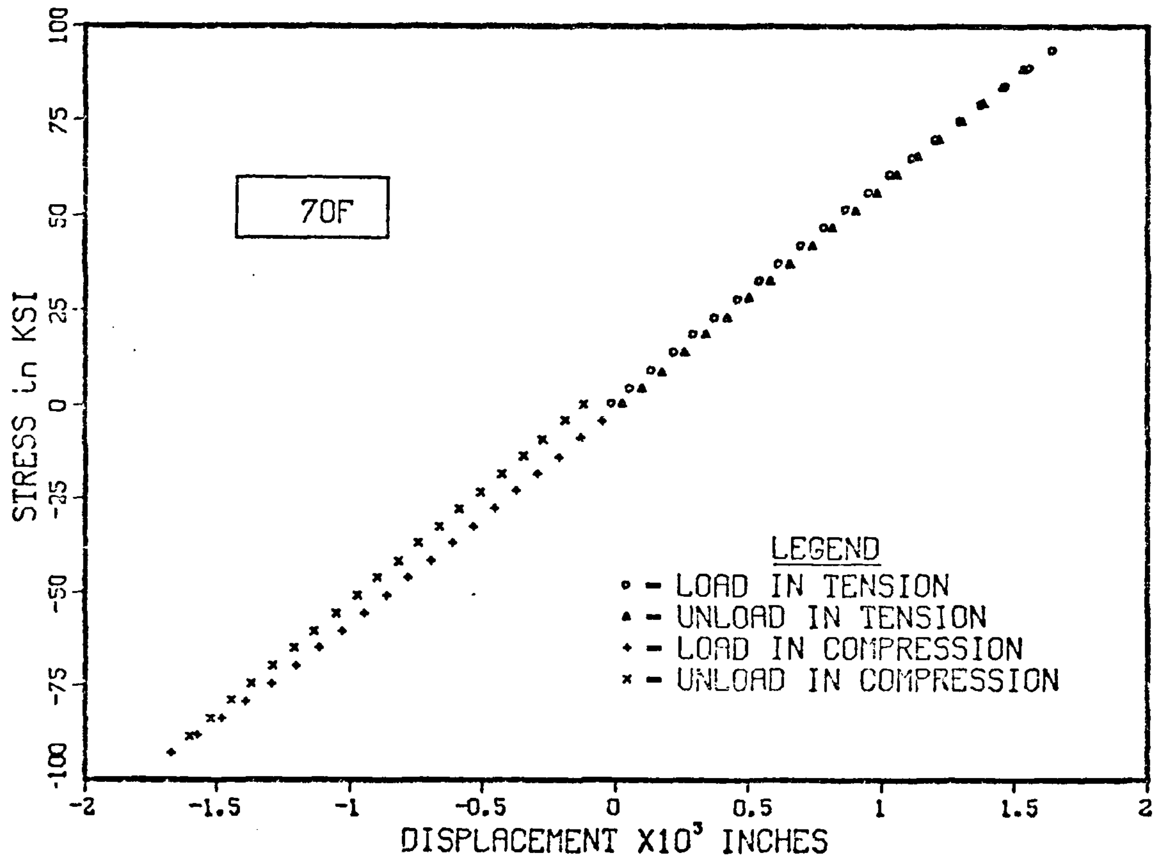

Figure 22. Plot of Stress vs Displacement at 70°F

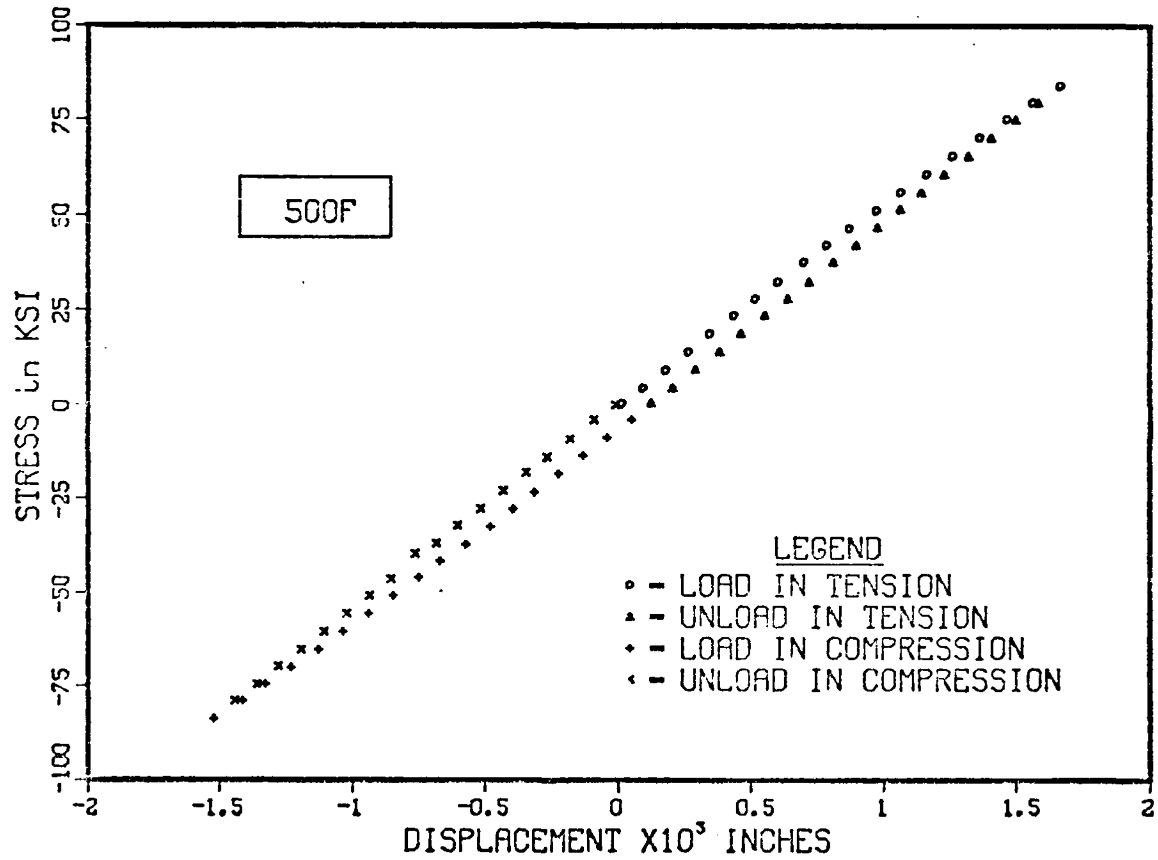

Figure 23. Plot of Stress vs Displacement at 500°F

B. Cyclic Stress-Strain Curve

Using the methodology described by Manson (3), a comparison of a 500°F static stress-strain curve with the 500°F cyclic stress-strain curve was made. For experimental ease, the tensile data used was measured at a strain rate of 2×10^{-2} in./in./min., while the cyclic data was obtained at a higher strain rate of 3.3×10^{-1} in./in./min. The tensile data presented in Table 7 shows that the mechanical properties of this alloy at 500°F are not very sensitive to strain rate within the range studied; thus, this comparison is not expected to be in significant error.

Figure 24 is the cyclic stress-strain curve compared to the static curve. At the lower strain ranges, the alloy cyclically softens; and, at the higher strain ranges, it cyclically hardens. For total strain ranges greater than 2.0%, Merrick observed rapid strain hardening of Incoloy 901 at room temperature and at 1000°F (16). The strain rate was not specified. Hardening peaked at about 10 cycles, then gradual softening occurred. Very rapid strain hardening was observed in this work also. The strain softening which occurred happened very gradually.

Cyclic strain hardening has been explained phenomenologically as being caused by dispersal of slip onto neighboring slip planes, and analogous to unidirectional hardening (4,66,67). The cyclic softening is due to the concentration of cyclic slip in the active slip bands (4,64,65,68). Thus, the shape of the cyclic stress-strain curve can be explained as follows: At the higher strain ranges, strain hardening has occurred but since the lifetimes at these high ranges is short, there was insufficient time for appreciable strain softening to

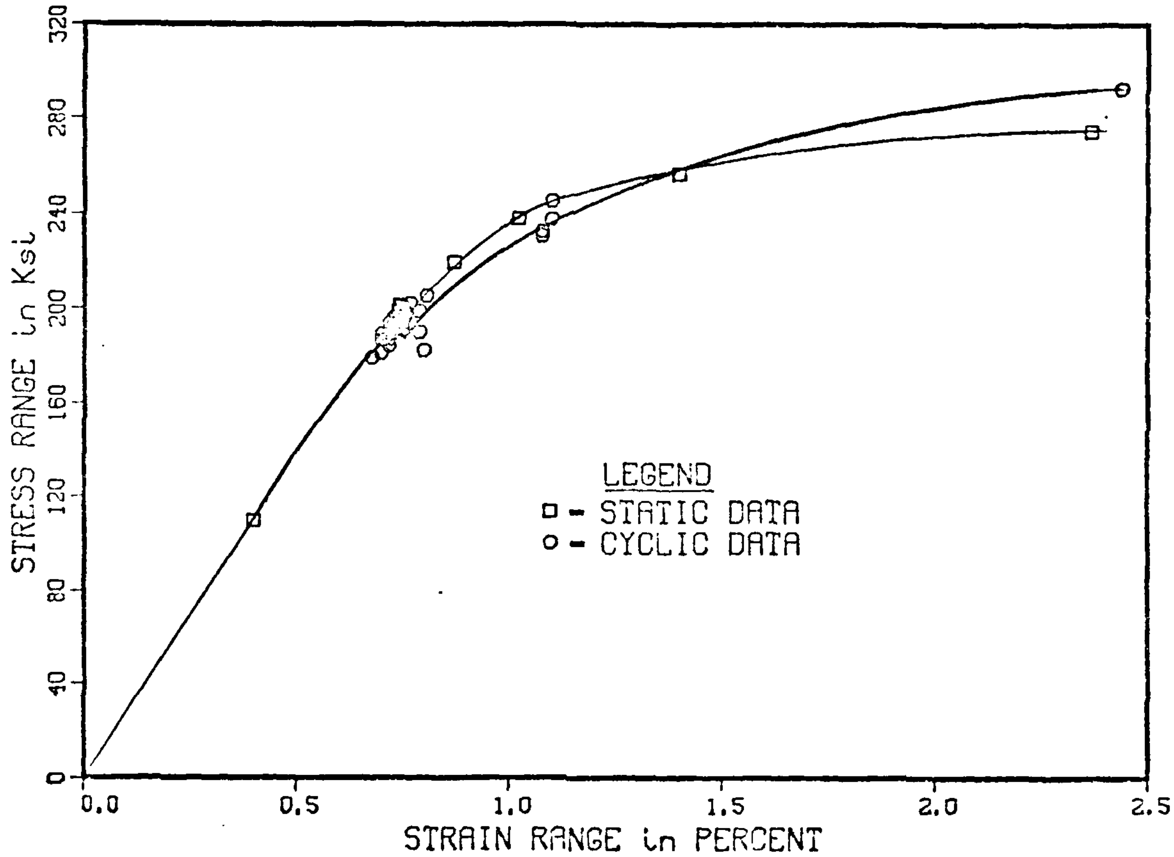

Figure 24. Plot of Cyclic Stress-Strain Curve

occur. At the lower strain ranges, the lifetimes are relatively long and hence there was time for softening to occur.

C. Characterization of Fatigue Damage

1. Baseline Data

A summary of the baseline data is presented in Table 9. The stress range reported is the stabilized range. The initiation cycle, N_i, was determined by extrapolating the asymmetric load drop back to the stable stress range on a plot of expanded Stress Range vs Cycles (2). A typical plot of this type is shown in Figure 25. The transition to the rapid load decrease, N_i', was determined by the point at which the load drop-off was no longer linear. The cycles to failure, N_f, was determined when the maximum tensile stress was 20 ksi. Figure 26 is a log-log plot of Strain Range vs Cycles. Table 10 contains the constants for the linear least square fit lines of Figure 26. Using the data in Table 10, the following Coffin-Manson type equations can be derived:

$$\Delta\varepsilon_t = 8.15\ N^{-0.295} \quad (13a)$$

$$\Delta\varepsilon_e = 1.75\ N^{-0.114} \quad (13b)$$

$$\Delta\varepsilon_p = 71.29\ N^{-0.898} \quad (13c)$$

The data estimated from Merrick (16) was obtained by merely averaging his room temperature and 1000°F data. Figure 27 compares the trend line for Cycles to Initiation with Cycles to Failure.

Plots of Stress Range vs Cycles for the baseline specimens listed in Table 9 are contained in Figures 28-38, respectively. Note that these plots, in general, contain data obtained by measurement of hysteresis loops and by output from the Instron Minicomputer. The computer data

TABLE 9

SUMMARY OF BASELINE LCF PROPERTIES

Specimen	Strain Range (%)			Stress Range (ksi)	Cycles			N_i/N_f	N_i'/N_f
	$\Delta\varepsilon_t$	$\Delta\varepsilon_p$	$\Delta\varepsilon_e$		N_i	N_i'	N_f		
2	1.08	0.25	0.83	232	780	-	1139	0.68	-
3	2.44	1.37	1.07	292	-	-	58	-	-
5	1.10	0.27	0.83	237	480	760	852	0.56	0.89
6	0.71	0.07	0.64	187	1400	2610	3263	0.43	0.80
7	0.72	0.05	0.67	191	1600	3200	3752	0.43	0.85
8	0.72	0.05	0.67	184	1200	3300	3820	0.31	0.82
11	0.70	0.05	0.65	181	2350	3800	4025	0.58	0.94
12	0.79	0.04	0.75	190	1300	2550	3398	0.38	0.75
32	0.70	0.04	0.66	189	1350	2900	4059	0.33	0.71
33	0.76	0.05	0.71	196	1000	2300	2965	0.34	0.78
53*	0.72	0.03	0.69	191	900	2600	3264	0.28	0.80

*Electropolished before test

TABLE 10

LINE CONSTANTS FOR log $\Delta\varepsilon$ vs log N CURVES

	b*	m*
$\Delta\varepsilon_t$	0.911	-0.295
$\Delta\varepsilon_p$	1.853	-0.898
$\Delta\varepsilon_e$	0.242	-0.114

*Equation is of the form:

$$\log \Delta\varepsilon = m \log N + b$$

where $\Delta\varepsilon$ is strain range (%)

N is number of cycles

m is slope of the line

b is the y-intercept

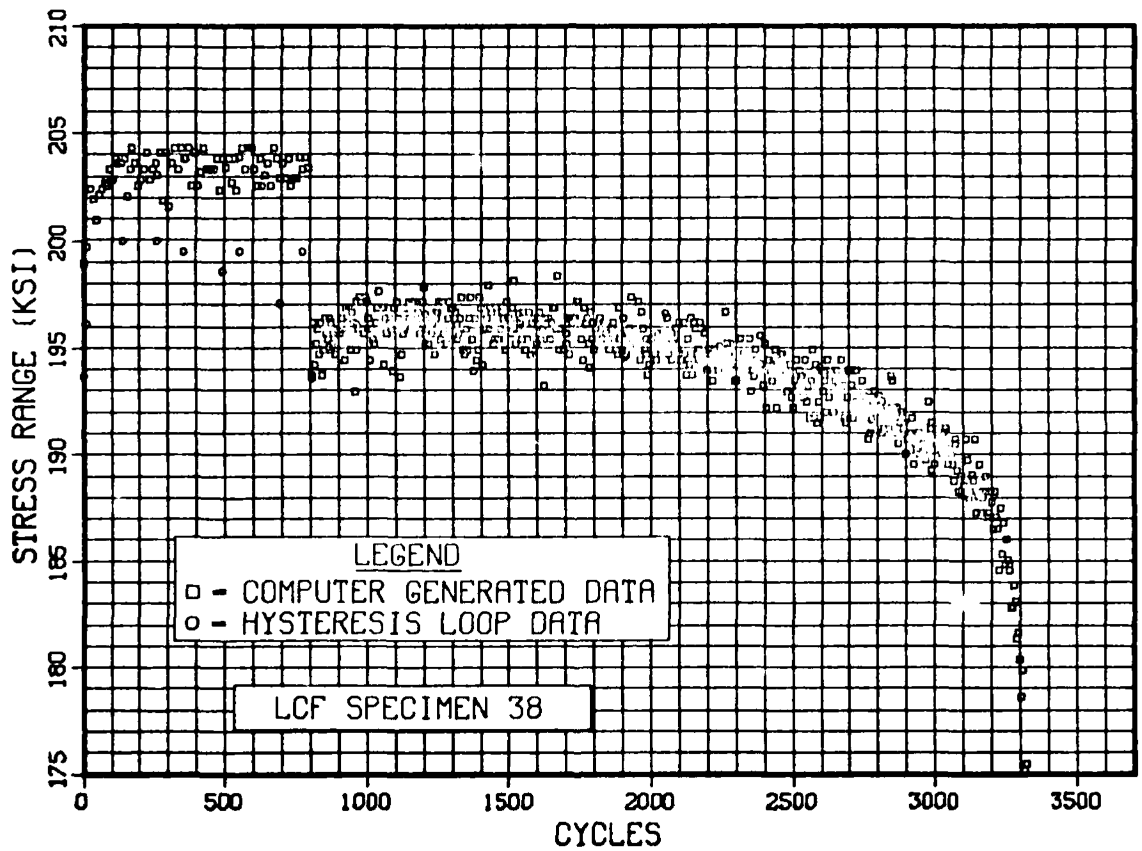

Figure 25. Plot of Stress Range vs Cycles - Expanded Scale

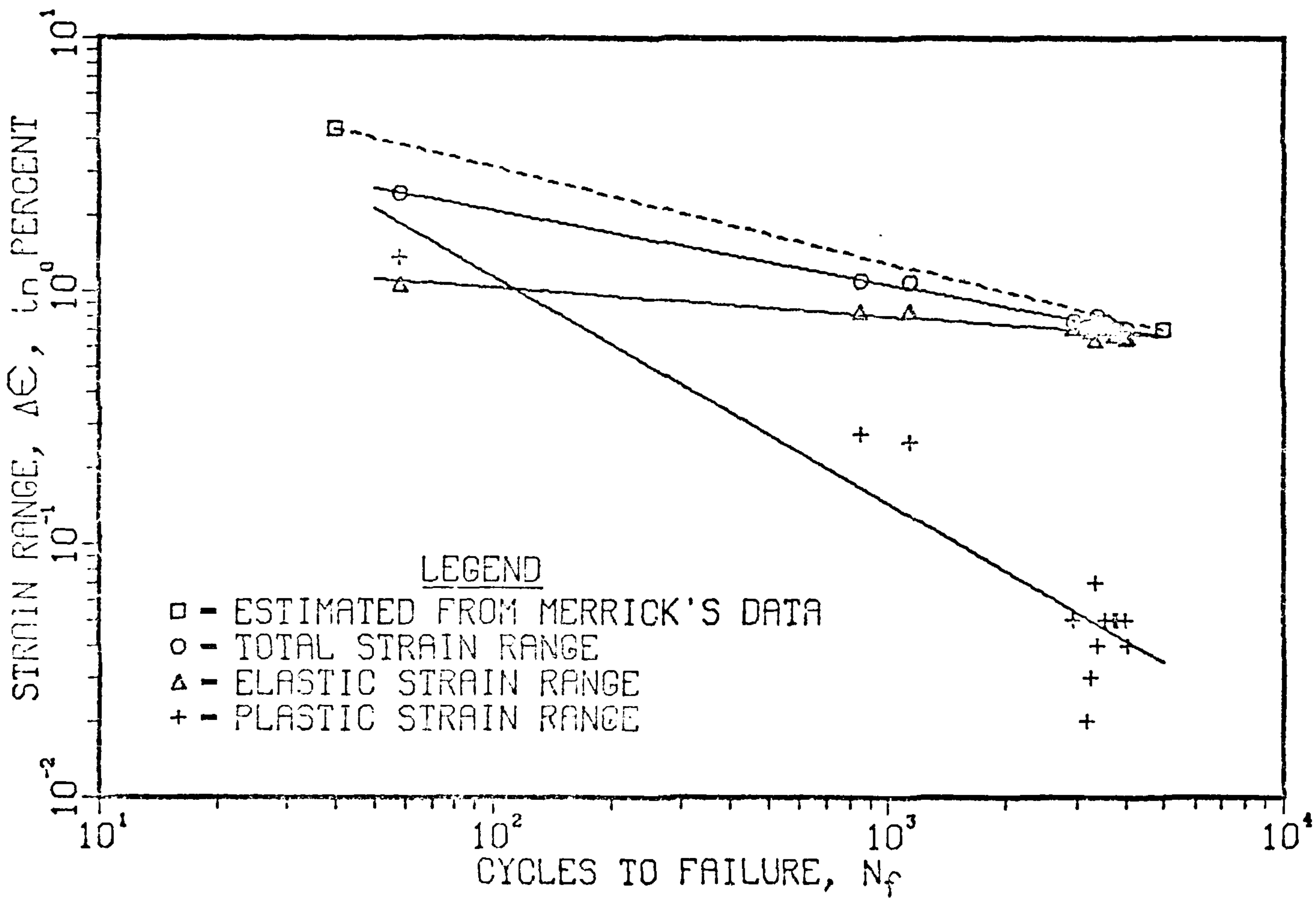

Figure 26. Plot of Baseline Strain Range vs Cycles to Failure

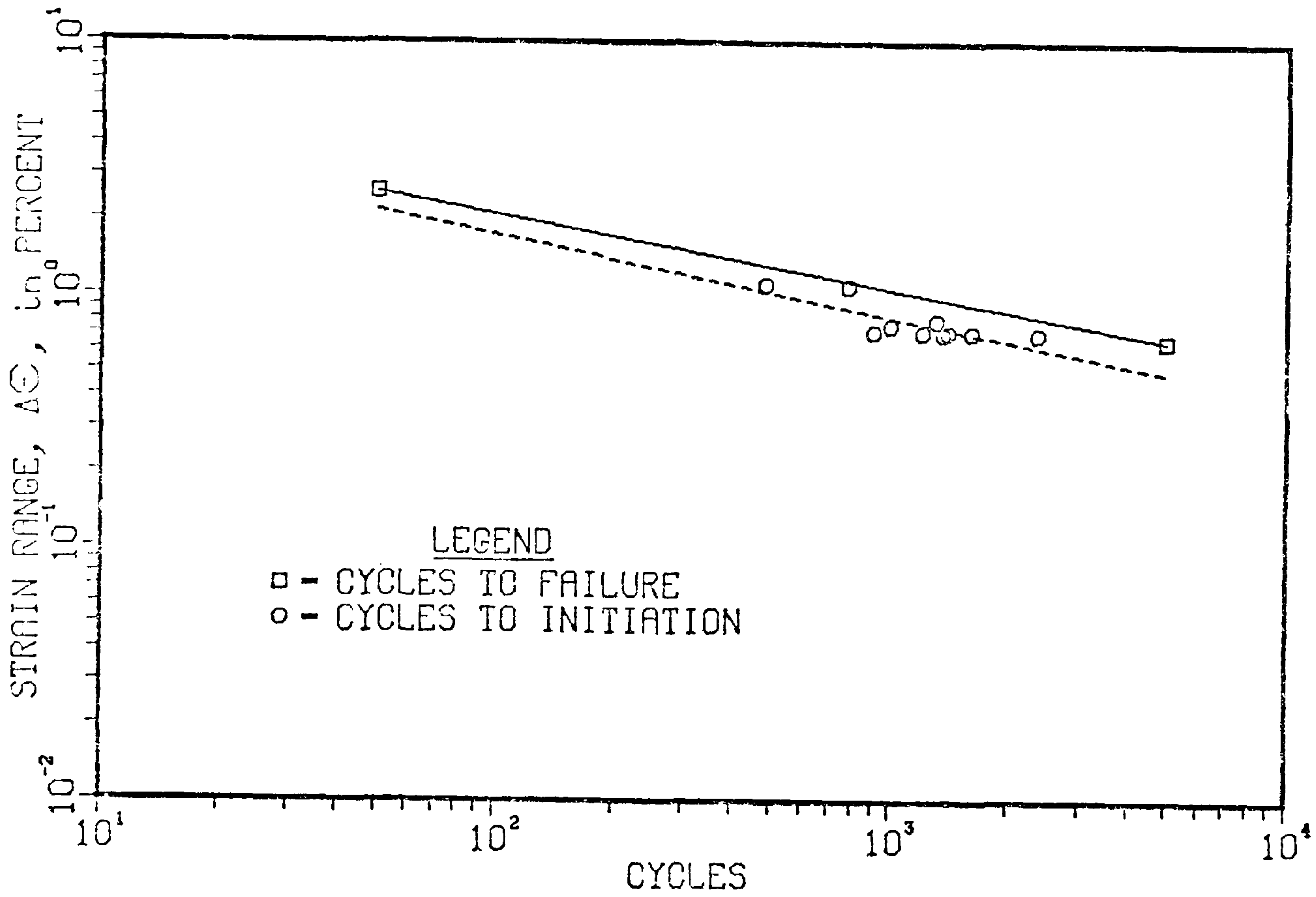

Figure 27. Plot of Baseline Strain Range vs Cycles to Initiation

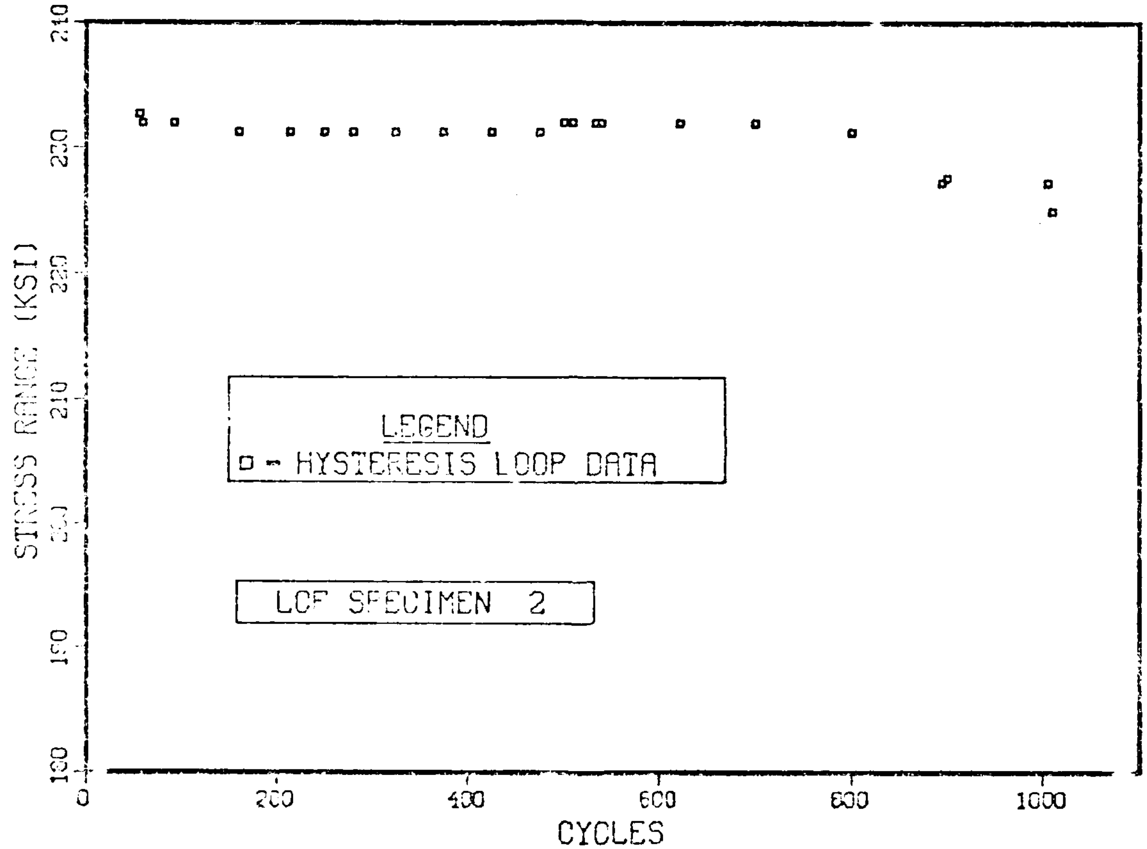

Figure 28. Plot of Stress Range vs Cycles - LCF Specimen 2

AD-A107 255 AIR FORCE INST OF TECH WRIGHT-PATTERSON AFB OH F/G 11/6
MECHANISMS OF RECOVERING LOW CYCLE FATIGUE DAMAGE IN INCOLOY 90--ETC(U)
1979 R E SCHAFRIK
UNCLASSIFIED AFIT-CI-79-212D NL

2 of 3
AD
A107255

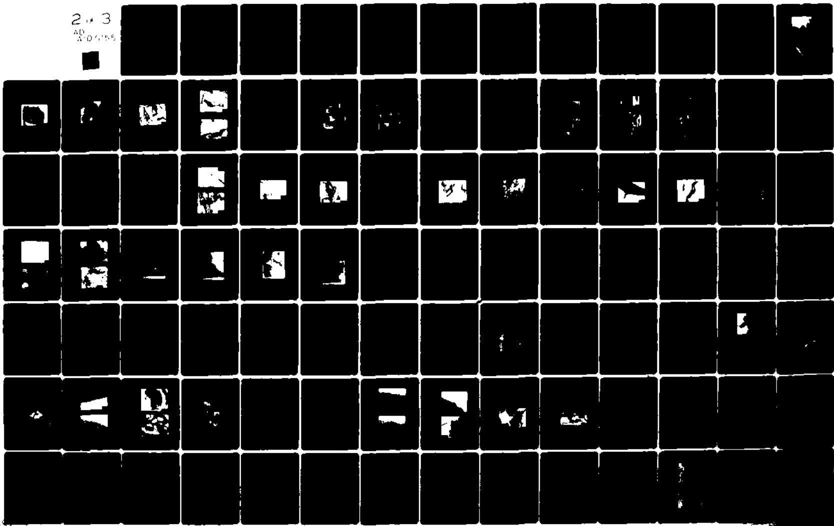

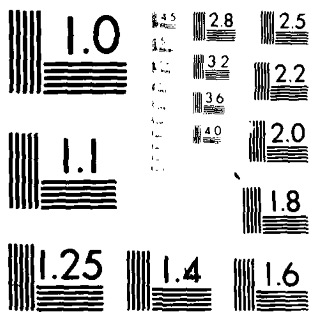

MICROCOPY RESOLUTION TEST CHART

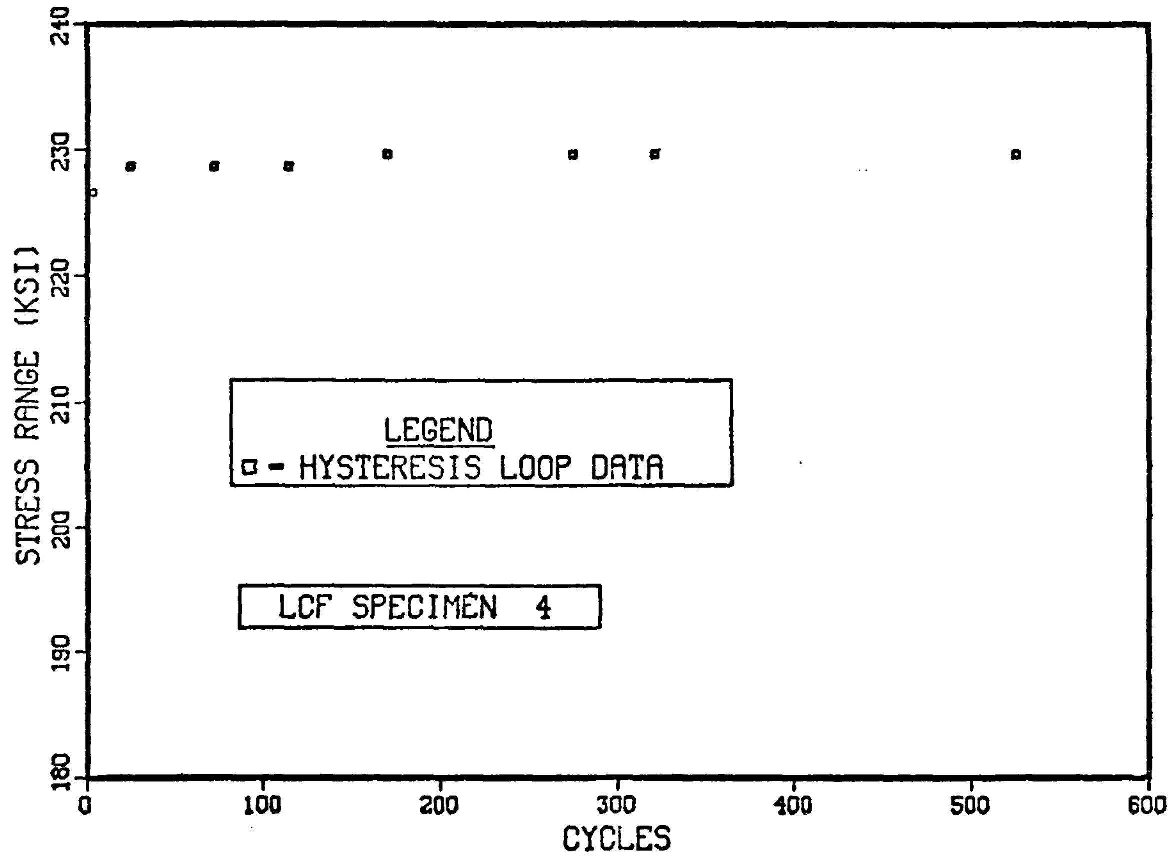

Figure 29. Plot of Stress Range vs Cycles - LCF Specimen 4

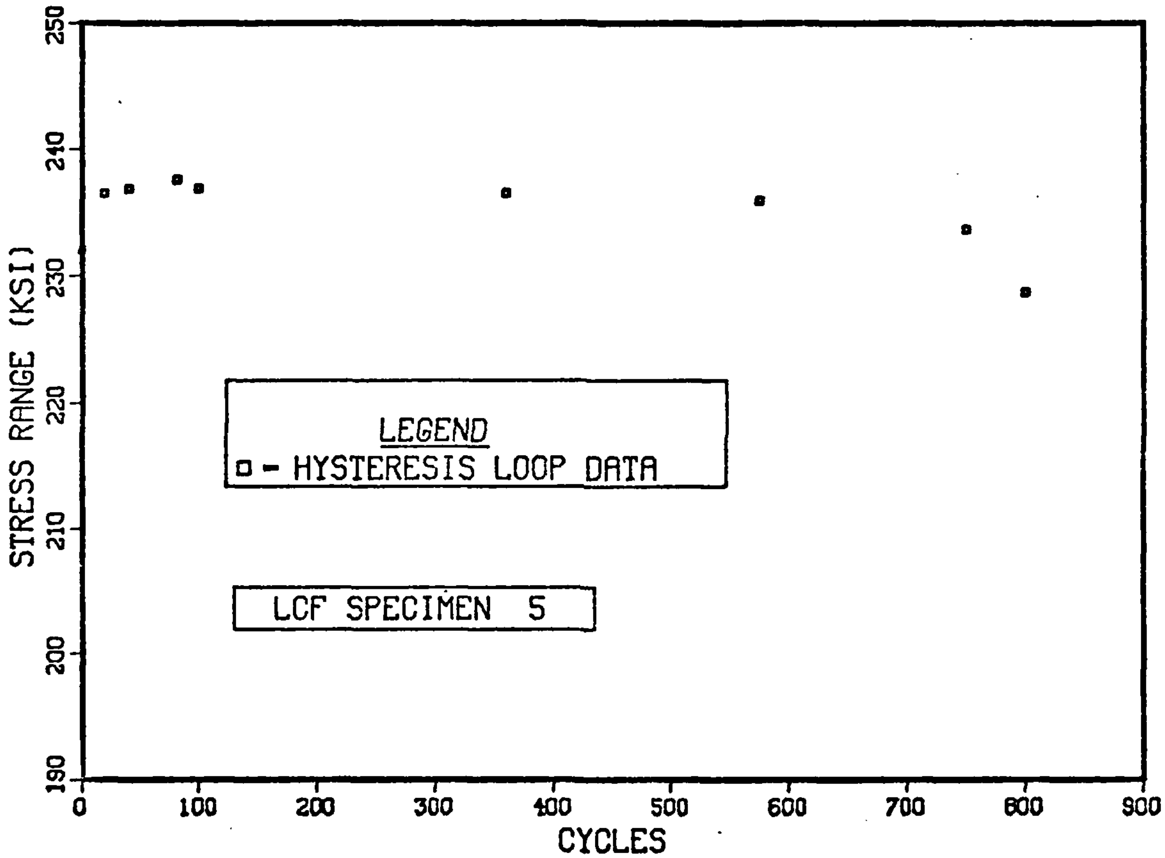

Figure 30. Plot of Stress Range vs Cycles - LCF Specimen 5

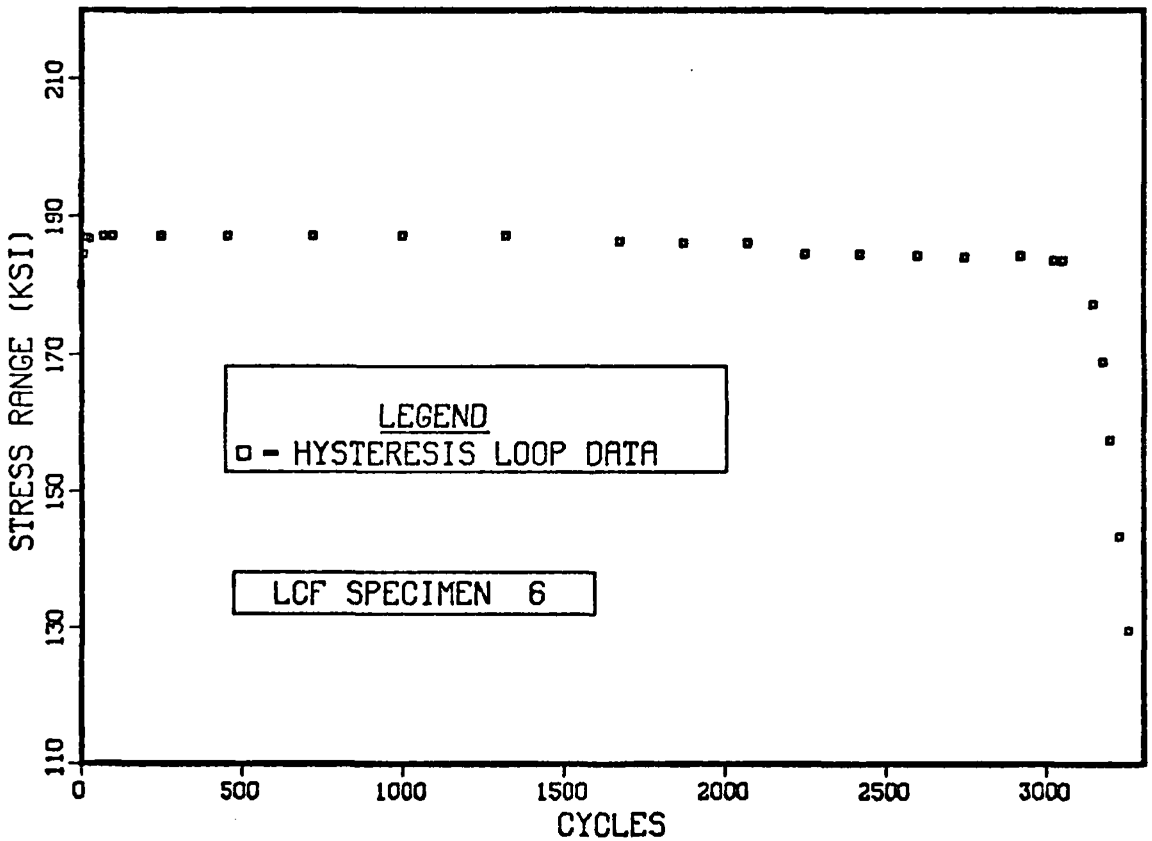

Figure 31. Plot of Stress Range vs Cycles - LCF Specimen 6

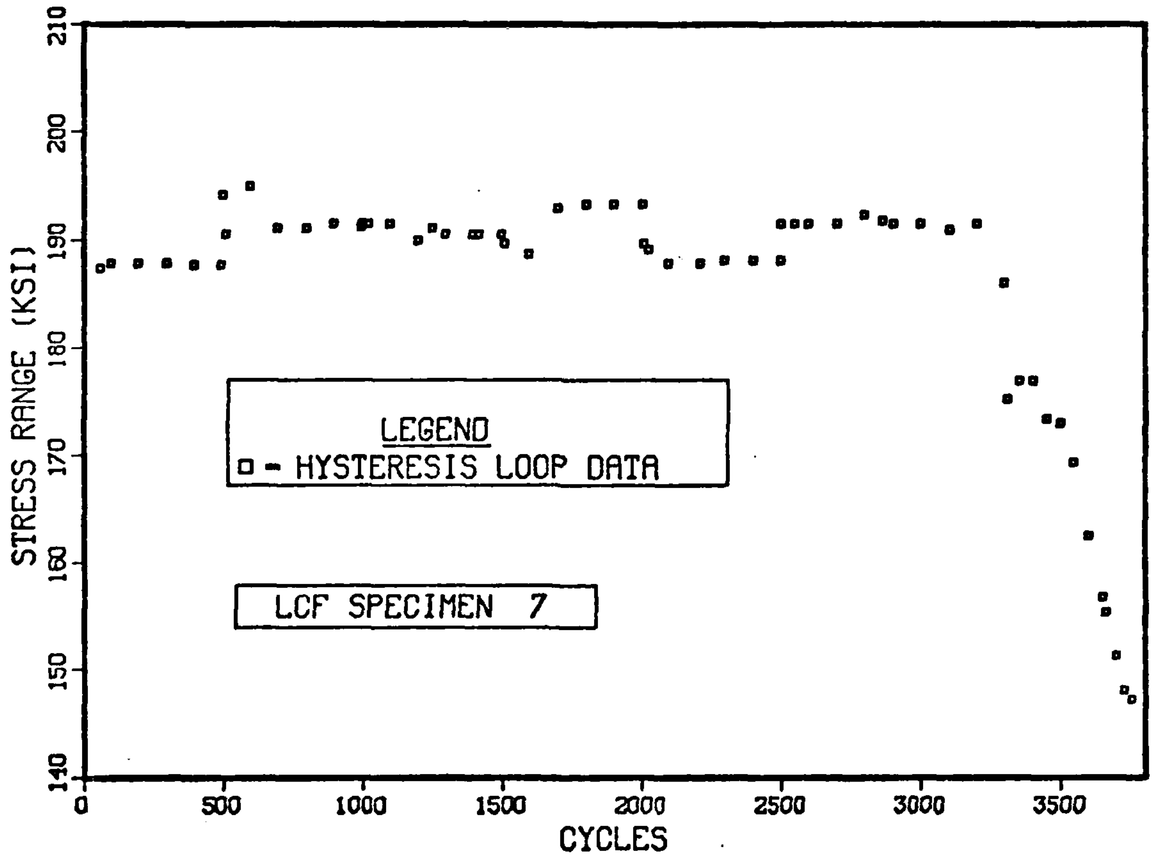

Figure 32. Plot of Stress Range vs Cycles - LCF Specimen 7

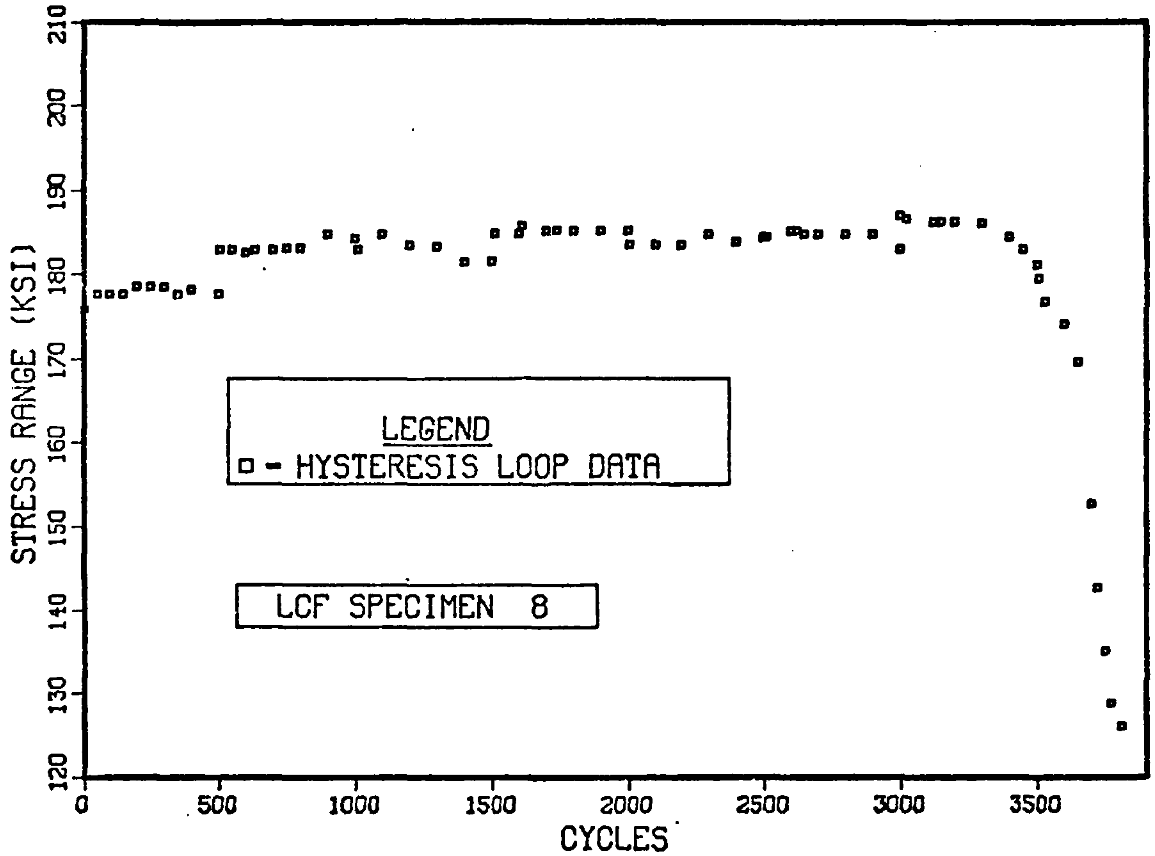

Figure 33. Plot of Stress Range vs Cycles - LCF Specimen 8

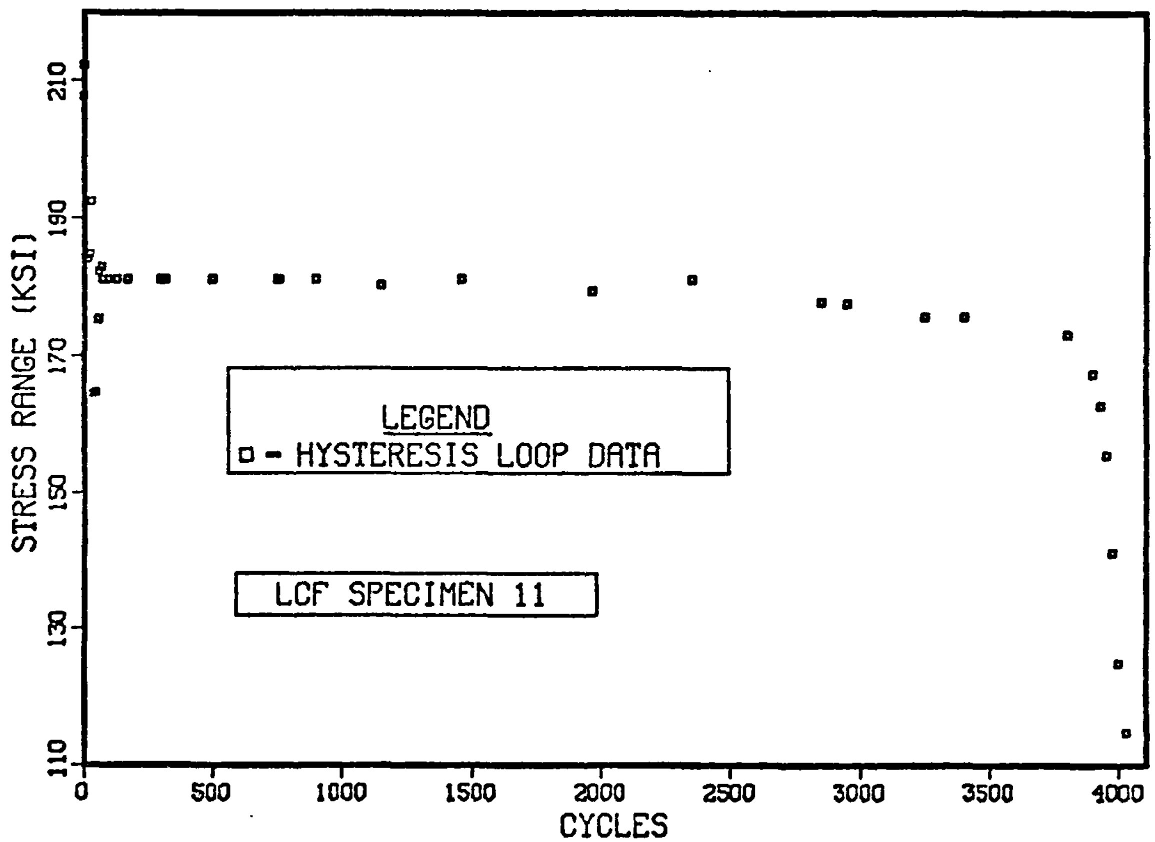

Figure 34. Plot of Stress Range vs Cycles - LCF Specimen 11

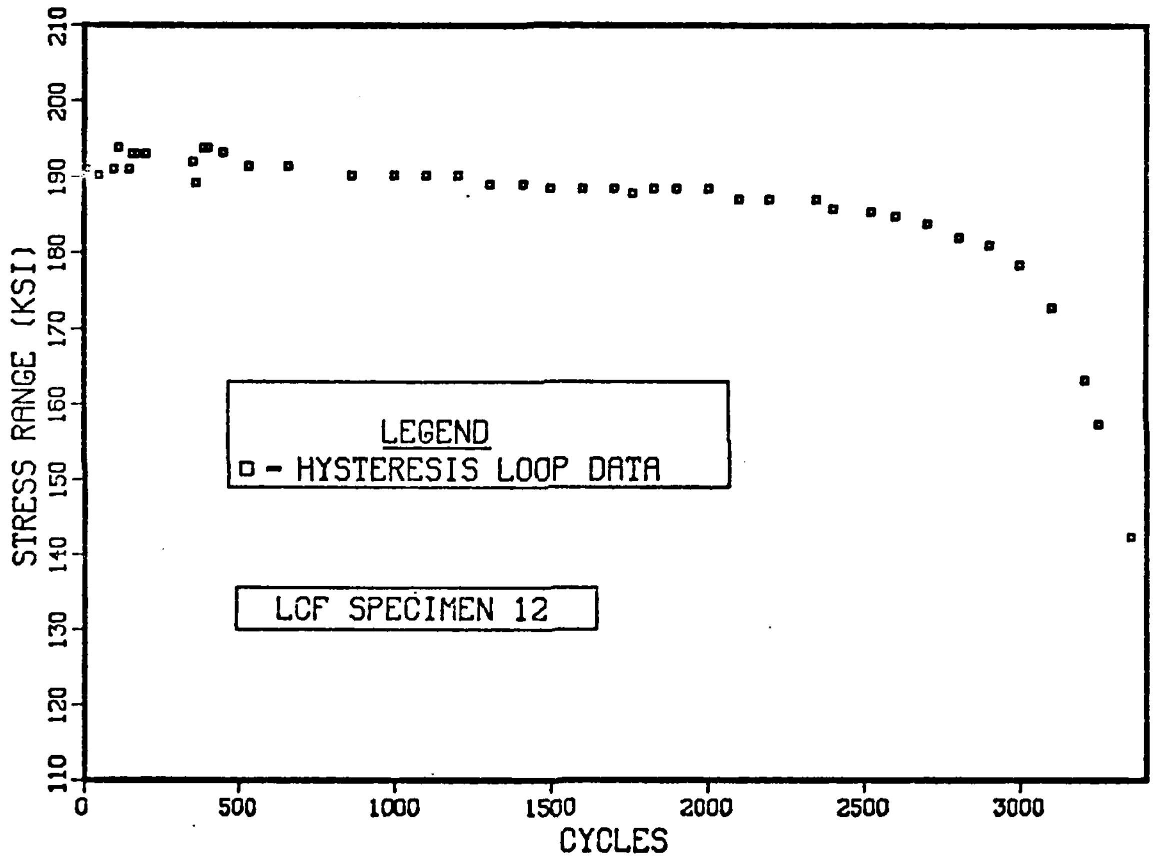

Figure 35. Plot of Stress Range vs Cycles - LCF Specimen 12

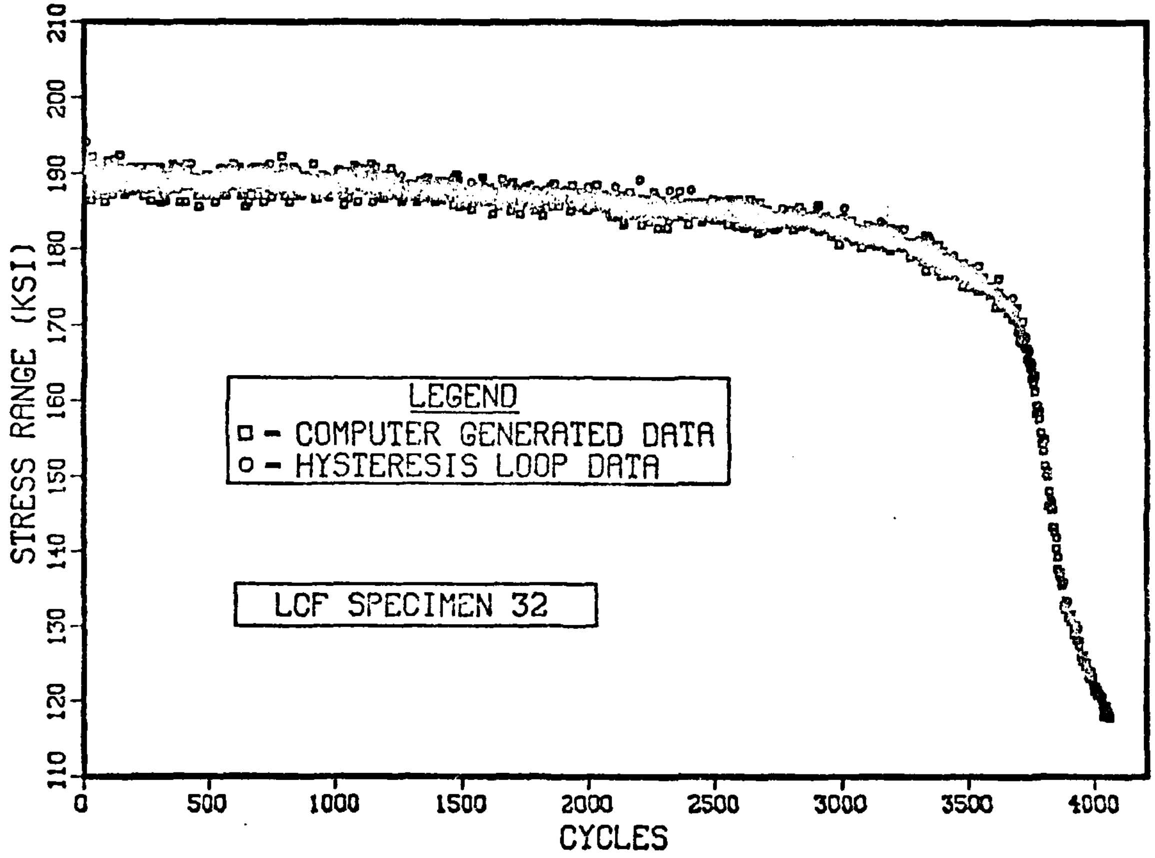

Figure 36. Plot of Stress Range vs Cycles - LCF Specimen 32

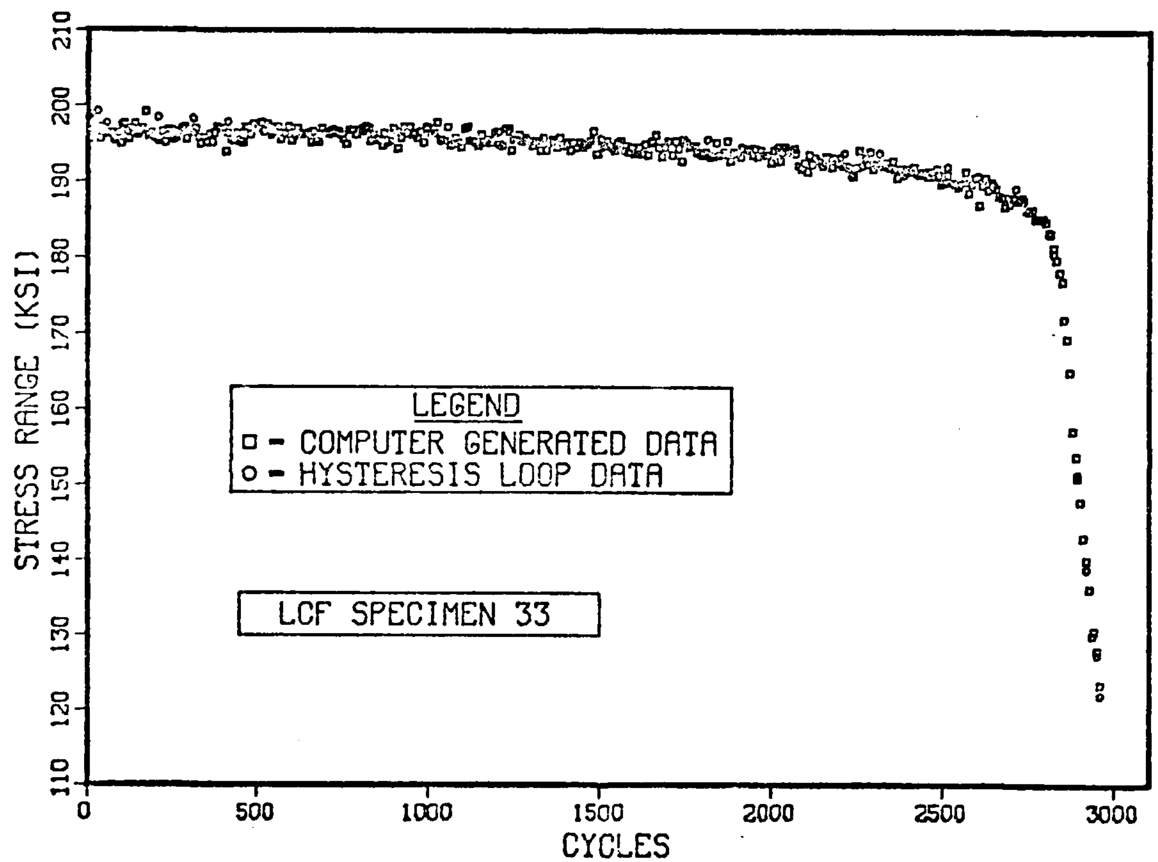

Figure 37. Plot of Stress Range vs Cycles - LCF Specimen 33

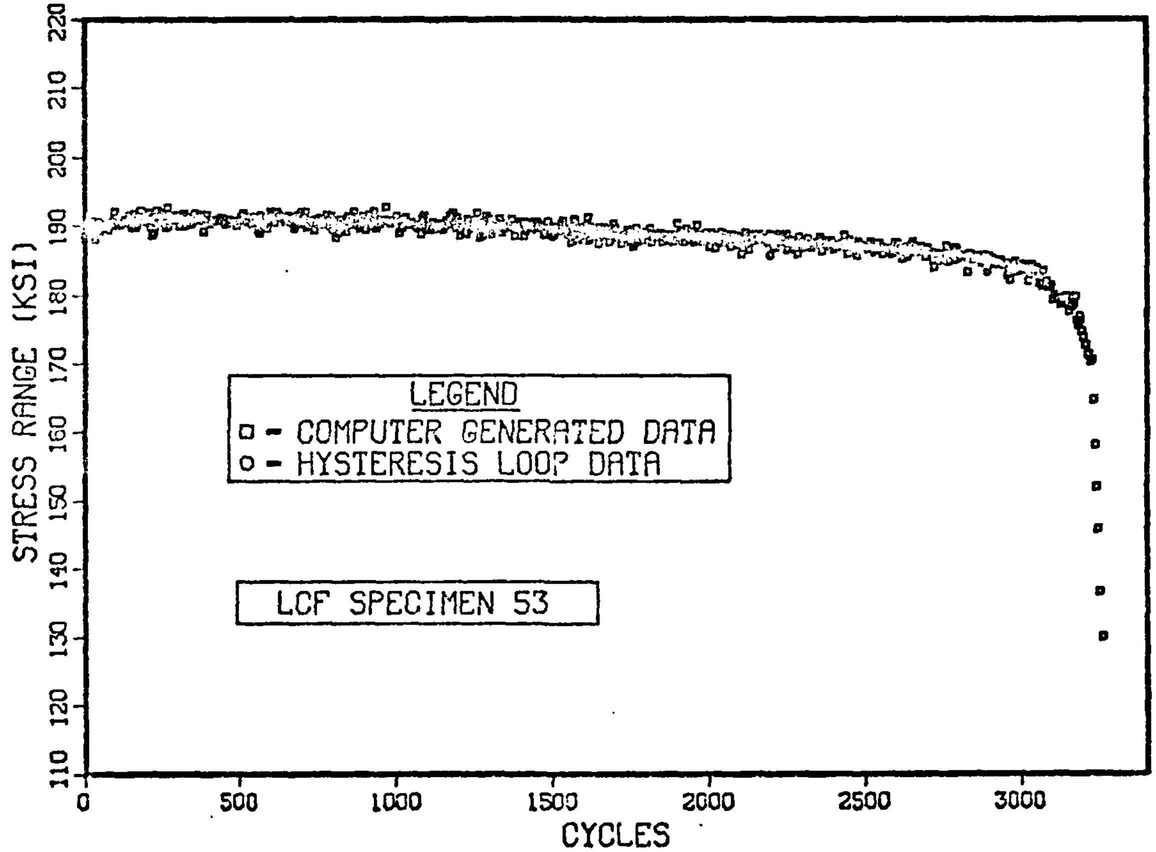

Figure 38. Plot of Stress Range vs Cycles - LCF Specimen 53

was obtained, in general, at every fifth cycle. The hysteresis loop data was usually obtained every 100 cycles. The effect of rejuvenation efforts will be discussed with respect to this baseline data.

ii. Dislocation Substructure

A typical dislocation substructure after a test is shown in Figure 39. The dislocations are aligned in bands, giving rise to the planar slip characteristics of this alloy. The dislocations are bowed around and looped around γ' precipitates, although cutting of the precipitates cannot be ruled out. Stacking fault contrast was observed in some precipitates, leading to the conclusion that they had been sheared. Using surface replication techniques, others have observed sheared γ' on the surface (16). Not every foil showed the concentration of slip bands depicted in Figure 39. Thus, deformation even at these higher strain ranges, is still somewhat localized.

iii. Fractography

Extensive fractography was carried out on samples which were removed unbroken from the fatigue machine and subsequently broken in tension. This procedure preserved the character of the fracture surface. The fractures were mixed mode, with both intergranular and transgranular regions. This behavior has been observed by others (16,45). A typical fractograph for LCF Specimen 33 is shown in Figure 40. Figure 41 is a higher magnification view of a likely crack initiation area. This was determined by following fatigue striations back to the edge. Typical fatigue striations are shown in Figure 42. Striations were seen close to the edge. Figures 43(a) and 43(b) demonstrate the cracking of carbides which lie on the fracture surface. The morphology of the

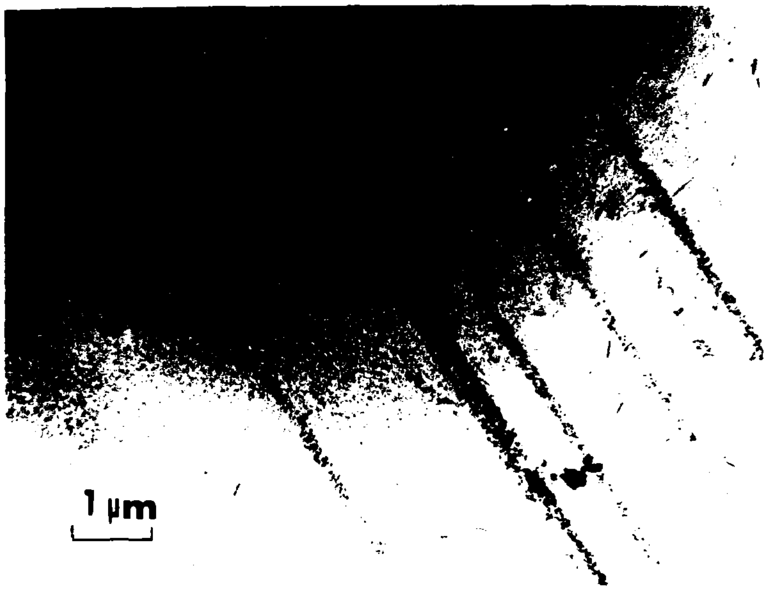

a. Planar Dislocations

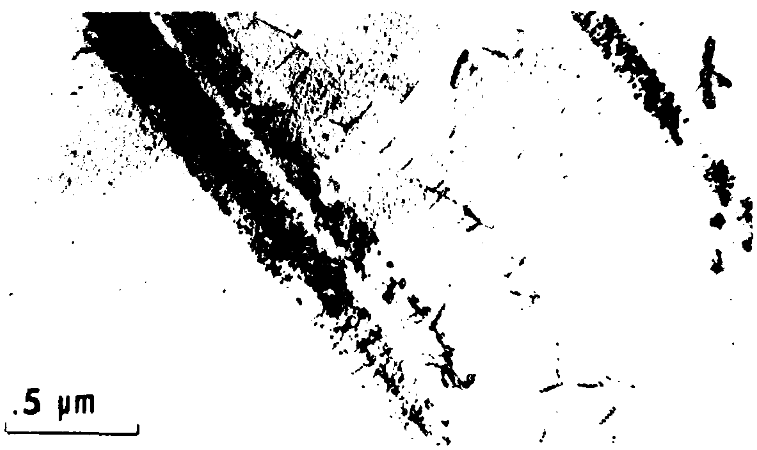

b. Planar Dislocations

Figure 39. TEM Micrograph of Fatigued Specimens with Planar Dislocations

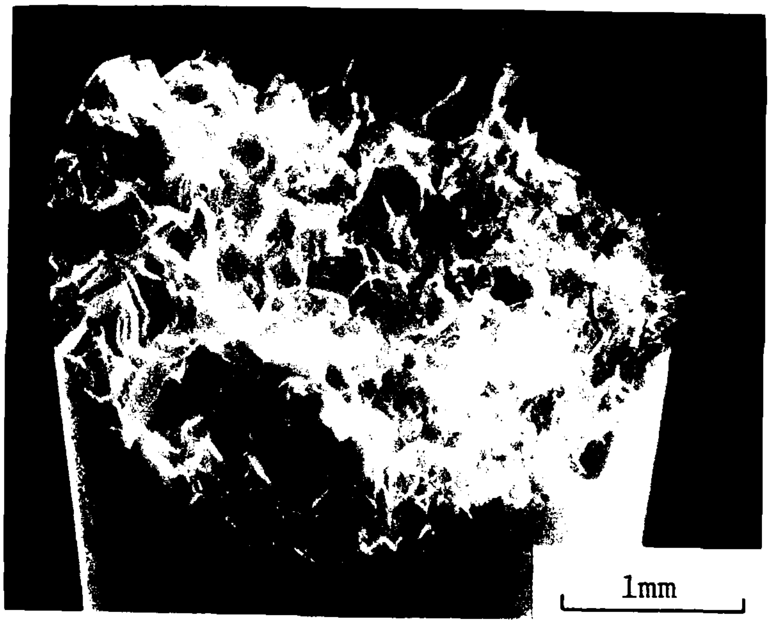

Figure 40. SEM Fractograph - LCF Specimen 33

Figure 41. SEM Fractograph, Initiation Site - LCF Specimen 33

Figure 42. SEM Fractograph, Fatigue Striations - LCF Specimen 33

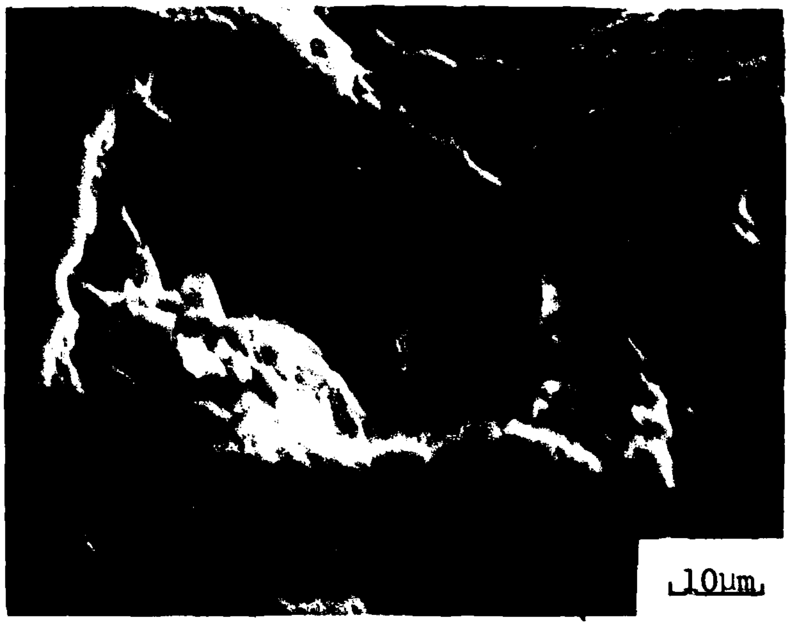

a. Cracked Titanium Carbide Particle

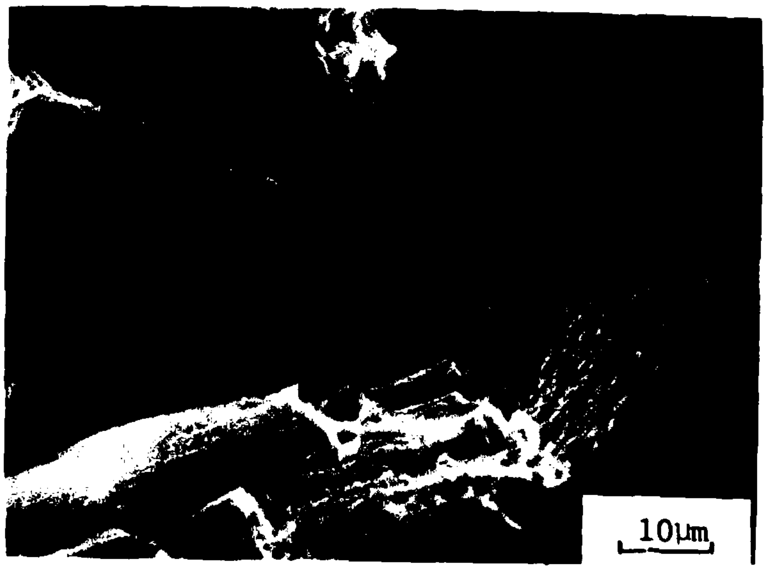

b. Cracked and Pull-Out Titanium Carbide Particles

Figure 43. SEM Fractograph, Cracked Carbides

carbide shown in Figure 43(a) suggests it may be a carbo-sulfide. The presence of these carbides may contribute to the large amount of longitudinal cracking which has been observed in this alloy (9).

D. Crack Initiation Mechanisms

i. Surface Replication

Surface replication during the course of fatigue testing was done in order to find the fraction of life at which crack initiation at 500°F occurred for total strain range of 0.75%. Two specimens, LCF Specimen 7 and LCF Specimen 8, were replicated at 500-cycle intervals. A composite of the replicas' photomicrographs are presented in Figures 44 and 46. Figure 44(a) shows the replication after 500 cycles of the area where the crack will initiate in LCF Specimen 7. At this magnification, there is no apparent crack, but persistent slip lines are evident. Figure 44(b), after 1000 cycles, still does not show a microcrack, but more intense deformation concentrated in the slip bands and grain boundaries is evident. Figure 44(c), after 1500 cycles, shows the first indication of microcracking. In Figure 44(d), after 2000 cycles, the cracking has extended into a persistent slip band. In Figure 44(e), after 2500 cycles, another microcrack becomes evident on the left-hand side. By Figure 44(f), after 3305 cycles, the two cracks have lined up and further extended. In the final series, Figure 44(g), after 3752 cycles (the last cycle), substantial crack propagation had occurred. A plot of Crack Length vs Cycles for LCF Specimen 7 is shown in Figure 45. When the crack length is extrapolated to zero length, the x-ordinate is intercepted at approximately 1500 cycles. The transition to rapid crack growth, N_i', occurred at approximately 3400 cycles.

Figure 44. Micrographs of Replicas, Cracks - LCF Specimen 7

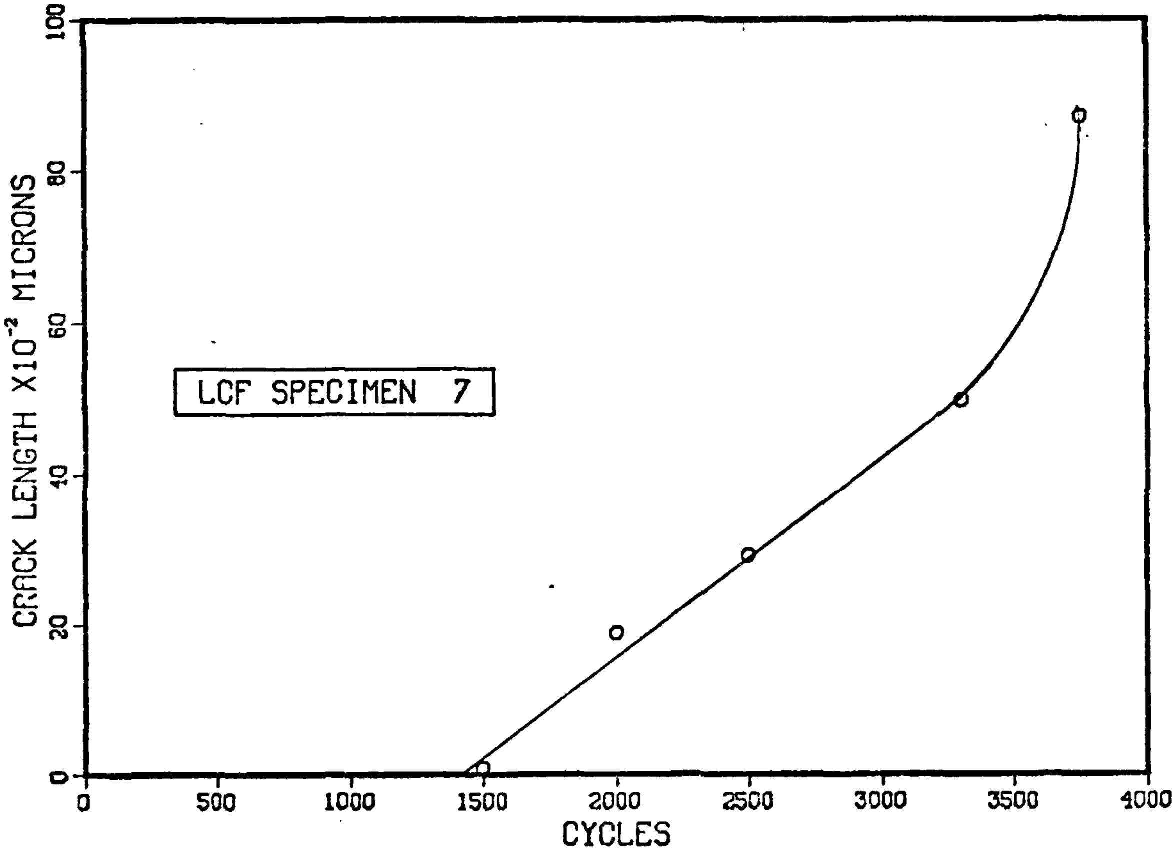

Figure 45. Plot of Crack Length vs Cycles - LCF Specimen 7

A composite of the photomicrographs of the surface replicas for LCF Specimen 8 is contained in Figure 46. In this specimen, three separate cracks form. Figure 46(a), taken after 500 cycles, shows the development of slip lines but no cracks are apparent. In Figure 46(b), after 1000 cycles, there is a persistent slip band evident in the upper right-hand portion of the collage which eventually becomes the upper crack. In Figure 46(c), after 1500 cycles, the V-shaped beginning of the middle crack is apparent. At 2000 cycles, Figure 46(d), the lower crack is evident as is a portion of the upper crack. Unfortunately, the middle crack is obscured by artifacts in the replica. In Figure 46(e), after 2500 cycles, all three cracks are clearly visible and several microcracks at either end of the middle crack are visible. By 3000 cycles, shown in Figure 46(f), the microcracks of the middle crack have linked up. Further crack extension by 3500 cycles, Figure 46(g), is readily apparent. A plot of Crack Lengths vs Cycles for LCF Specimen 8 is contained in Figure 47. The crack lengths plotted are the sum of the individual lengths. Since the measured crack lengths entailed some judgment, the scatter is not unreasonable. At the early cycles, it is especially difficult to ascertain if a crack exists and to measure its extent. Extrapolating the data back to zero crack length, it appears that crack initiation occurred at approximately 1300 cycles.

If the Stress Range vs Cycles plot for Specimens 7 and 8, contained in Figures 32 and 33, are closely examined, the asymmetric stress drop-off for LCF Specimen 7 occurs at about 1500 cycles and at about 1300 cycles for Specimen 8. These cycles correlate reasonably well with those determined from the crack length measurements. Therefore, the

Figure 46. Micrographs of Replicas, Crack - LCF Specimen 8

c

d

Figure 46 (continued)

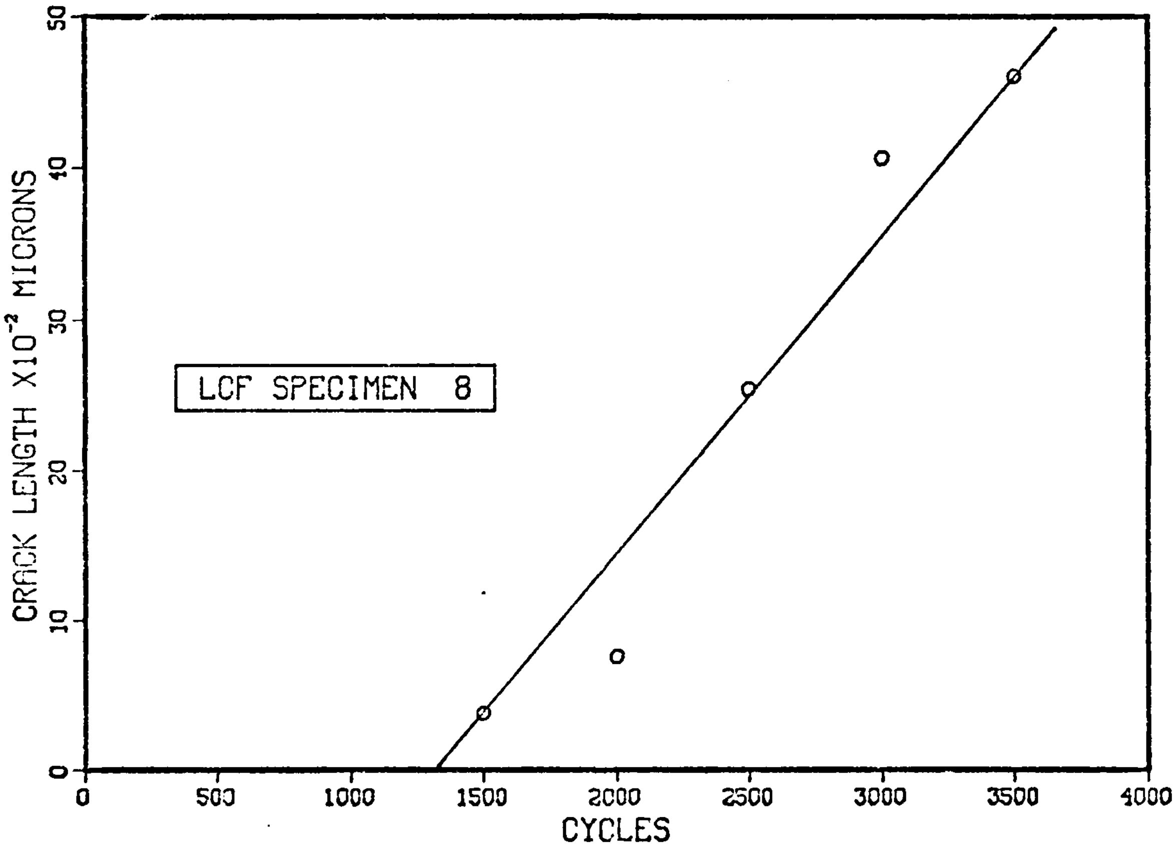

Figure 47. Plot of Crack Length vs Cycles - LCF Specimen 8

asymmetric load drop-off is used in the remainder of this dissertation as evidence that a definite crack exists. In Table 9, N_i is thus a measure of the crack initiation cycle. Furthermore, a damage level of 800 cycles was selected for rejuvenation efforts since it seemed well below the actual crack initiation point.

The slope of the lines in Figures 45 and 47 yields a crack growth rate, da/dN, of 0.27 μm/cycle or 1.07×10^{-4} in./cycle. Macha has determined crack growth rates as a function of ΔK at 400°F and 600°F (62). At 400°F he found that:

$$\frac{da}{dN} = 0.15 \times 10^{-9} \ (\Delta K)^{2.9} \tag{14}$$

where da/dN is crack growth rate in in./cycle, and ΔK is stress intensity range in ksi $\sqrt{in.}$. At 600°F, he found:

$$\frac{da}{dN} = 0.10 \times 10^{-9} \ (\Delta K)^{3.2} \tag{15}$$

Since these expressions have the form:

$$\frac{da}{dN} = C \ (\Delta K)^{m} \tag{16}$$

C and m can be estimated to be 0.125 and 3.05, respectively, at 500°F, by simple averaging. Thus, at 500°F it is estimated that:

$$\frac{da}{dN} = 0.125 \times 10^{-9} \ (\Delta K)^{3.05} \tag{17}$$

By finding ΔK for a fatigue crack in the LCF test specimen, Equation 17 can be used to verify the replication-derived crack growth rate. Irwin's methodology for a semi-elliptical crack, correcting for the plane strain plastic zone in a finite body, was used (63). It is only an approximation for the geometry of the LCF specimen. The details of the calculation are presented in Table 11. The computed value of

TABLE 11

CALCULATION OF CRACK GROWTH RATE FROM FRACTURE MECHANICS

Assumptions:

1. Initial flaw size, 2c, of 0.118 in. (3000 μm)
2. Crack aspect ratio, a/2c, of 0.30
3. Stress range, $\Delta\sigma$, of 190 ksi
4. Ratio $\sigma_{max}/\sigma_{y.s.}$ of 0.75
5. $da/dN = 0.125 \times 10^{-9} (\Delta K)^{3.05}$

Calculation: Irwin's equation of interest is

$$K_I = \frac{1.1 \sigma \sqrt{\pi a}}{\sqrt{Q}}$$

$$\text{where } Q = \int_0^{\pi/2} \left[1 - \left(\frac{c^2 - a^2}{c^2}\right) \sin^2 \right] d\phi - 0.212 \left[\frac{\sigma}{\sigma_{y.s.}}\right]^2$$

Using the above assumptions, Q = 1.4. Thus $\Delta K = 107.5$ ksi $\sqrt{\text{in.}}$

From Assumption 5,

$$\frac{da}{dN} = 1.96 \times 10^{-4}$$

da/dN = 1.96×10^{-4} in./cycle agrees reasonably well with the measured value.

Higher magnification photographs of the replicas taken for Specimens 7 and 8 revealed evidence of a concentrated deformation zone along grain boundaries. But since these specimens were not lightly etched prior to testing, these observations were inconclusive.

ii. Surface Scanning Electron Microscopy

The above replication procedure was invaluable for finding cracks during a fatigue test, but it was not suitable for defining the crack initiation mechanisms for the following reasons: (1) The sharp radius of curvature of the LCF specimen made the replication process extremely difficult to accomplish without producing artifacts in the replica; and (2) A cycle of cooling the specimen, replicating it, and reheating the specimen for further testing took 3-4 hours with the consequence that a great deal of time was consumed in the testing.

With these difficulties in mind, several different approaches were taken to better determine the crack initiation mechanism: (1) A LCF specimen was lightly etched prior to testing and a search was made for offsets in the longitudinal polishing scratches at grain boundaries; (2) A LCF specimen had two parallel flats machined longitudinally and the specimen was electropolished (one flat was lightly etched), and after 1800 cycles of testing at 500°F at a strain range of 0.75%, the flats were examined in the SEM; (3) A specimen was tested at room temperature and replicated every 300 cycles until the asymmetric load drop-off occurred and a definite microcrack could be seen; (4) A specimen, after complete testing, was placed directly in the SEM for surface observation; (5) The gauge section of a specimen was examined in the SEM after 800 cycles of testing; and (6) A longitudinal section of a gauge section was made of a specimen tested to 2103 cycles. The results of these metallographical investigations are detailed below, and a proposed mechanism for crack initiation at 500°F at $\Delta\varepsilon_t$ = 0.75% is presented.

LCF Specimen 42 was lightly etched after polishing through 4/0 emergy paper. After testing was completed, the gauge section was placed in the SEM. Using the straight polishing scratches as fiduciary marks, offsets of them along grain boundaries were observed. Figure 48(a) and (b) show typical offsets at grain boundaries. There is an apparent curvature of the scratches in the vicinity of the grain boundary indicating the existence of a band of deformation along the boundary. Also, the offsets along a boundary are not uniform. The formation of grain boundary ledges was not readily apparent, but this experimental technique may not have been sensitive enough to detect them. Figure 48 (c) shows offsets along a persistent slip band. Note that the polishing scratches which pass through a persistent slip band are relatively straight right up to the band, and that the offsets along the length of the band are reasonably uniform.

LCF Specimen F2 had two flats machined which were mechanically polished and then electropolished. One flat was lightly etched before testing. The stabilized stress range was 190.5 ksi, at total strain range of 0.75%. Crack initiation, as determined by the asymmetric load drop-off, occurred at 875 cycles. The fatigue test was halted at 1800 cycles and the flat surfaces examined in the SEM. Figure 49 shows

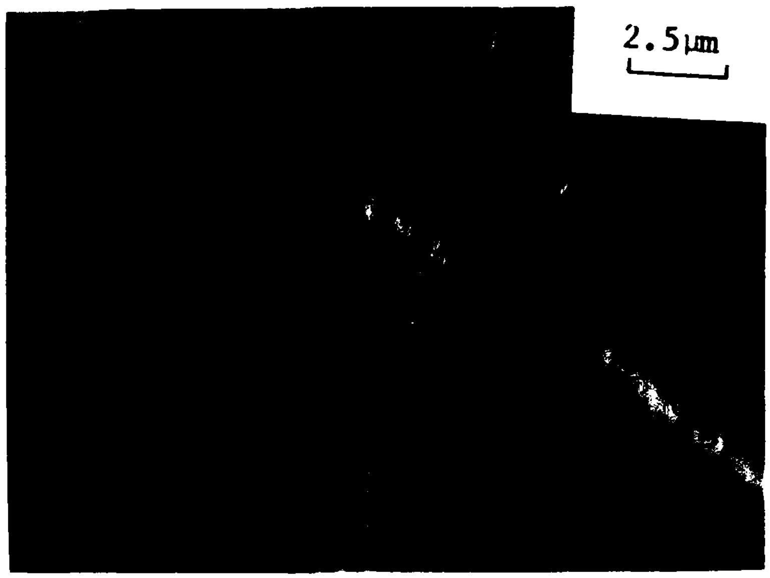

a. Offset of Polishing Scratch at a Grain Boundary

b. Offset of Polishing Scratches at a Grain Boundary

Figure 48. Electron Micrographs Depicting Grain Boundary Offsets

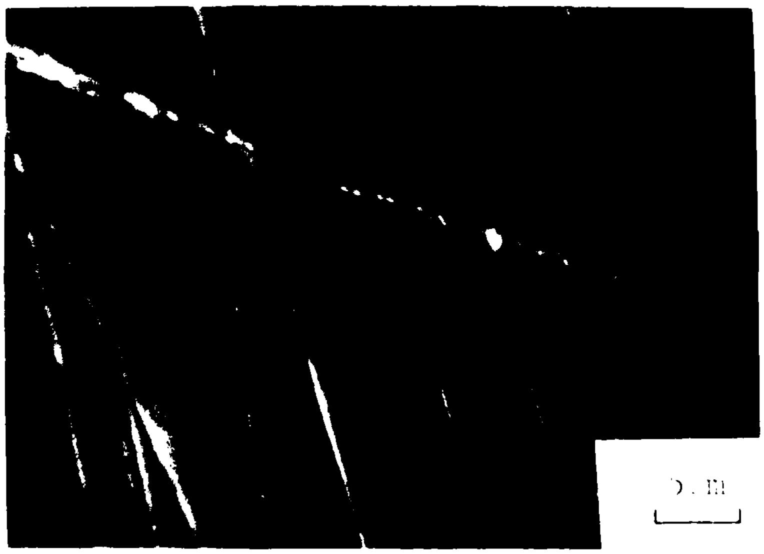

c. Offset of Polishing Scratches at a Persistent Slip Band

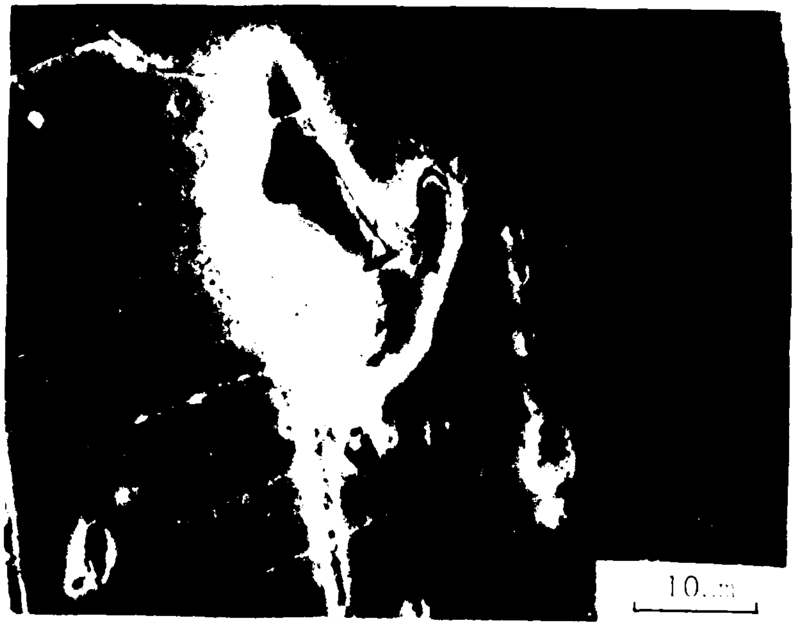

Figure 49. SEM Micrograph, Crack at Carbide - LCF Specimen F2

cracks leading away from a large carbide inclusion. Figure 50 graphically shows slip lines and cracks associated with two blocky carbides. The slip lines are at nearly a 45^{o} angle with respect to the longitudinal stress axis.

LCF Specimen 36 was tested at room temperature after light etching. The stress range, after 500 cycles, constantly decreased at the rate of 3.2 psi/cycle. The stabilized stress range was 222 ksi at a total strain range of 0.73%. The test was stopped at 3900 cycles and the specimen broken in liquid nitrogen for fractographic examination. Figure 51 is a 100× view of a replica of a typical area after 3900 cycles. The slip lines within each grain are clearly evident. As the test progressed, there appeared to be a gradual thickening of the grain boundary regions. Using the longitudinal polishing scratches as fiduciary marks, higher magnification definitely revealed offsets along the grain boundaries. Figure 52 shows a typical crack which apparently initiated at a grain boundary carbide. On the fractograph, it was difficult to differentiate the fatigue initiated fracture from the tensile overload fracture.

LCF Specimen 53, which was electropolished before testing, was placed directly in the SEM after testing at $500^{o}F$. Table 9 has a summary of its properties. Figure 53 shows a portion of the main crack. Note the grain which pulled out in the center of the photograph. This crack follows a combined transgranular and intergranular path on the surface. Figure 54 shows fatigue striations in an intergranular crack region which are obvious from looking in from the surface. Figure 55

Figure 50. SEM Micrograph, Crack at Carbide - LCF Specimen F2

Figure 51. Micrograph of Replica - LCF Specimen 36

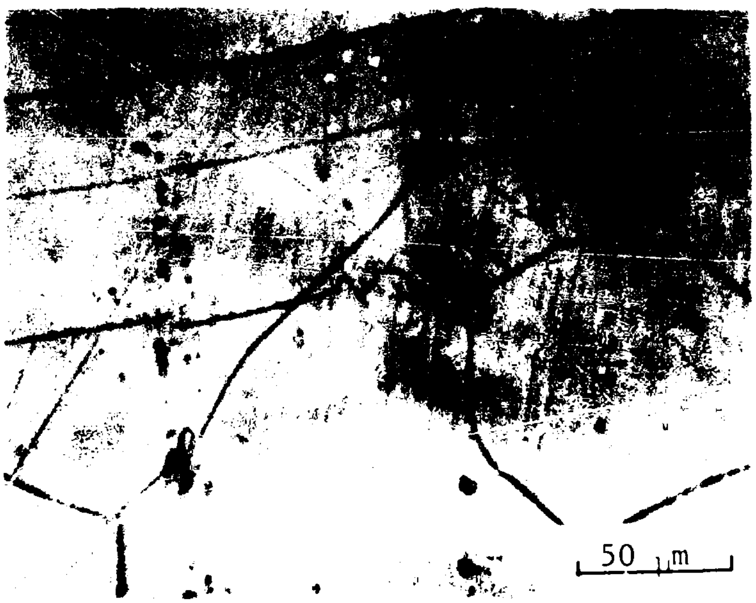

Figure 52. Micrograph of Replica, Crack at Carbide - LCF Specimen 26

Figure 53. SEM Micrograph, Main Crack - ICT Specimen 53

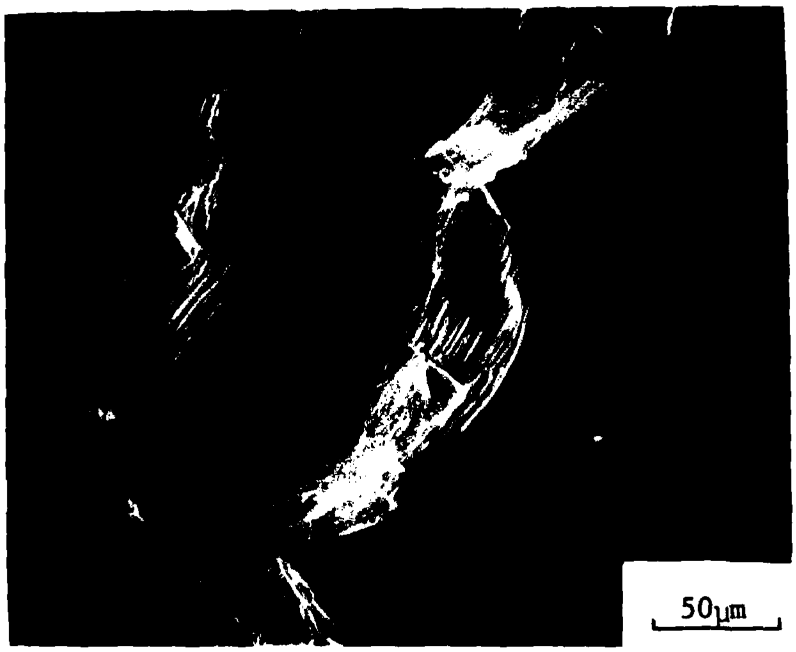

Figure 54. SEM Micrograph, Fatigue Striations - [illegible] Specimen [illegible]

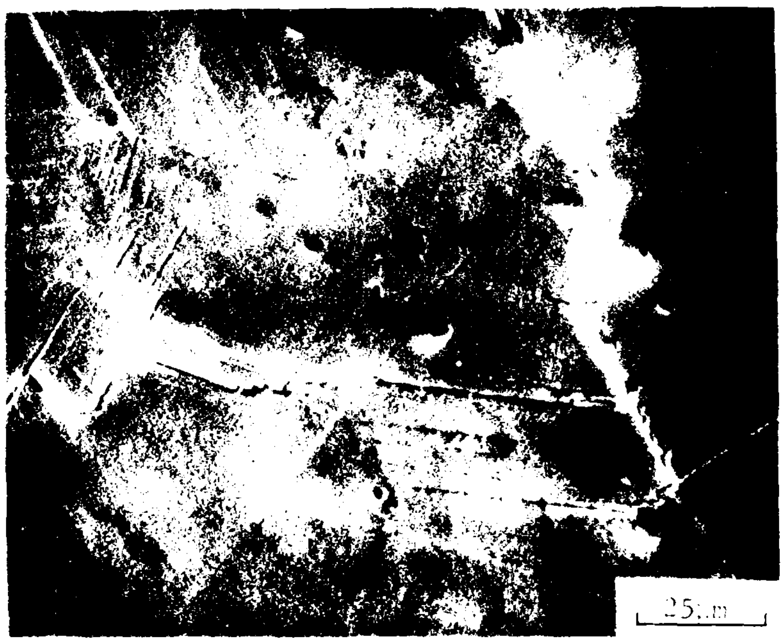

Figure 55. SEM Micrograph, Secondary Cracking - FCP Specimen 53

shows surface cracking which occurred at some distance from the main crack. The crack associated with the carbide is normal to the loading direction.

LCF Specimen 38 was removed from the Instron after 800 cycles at 500°F at a total strain range of 0.77%. It was lightly etched before testing. Figure 56(a) shows the general microstructure as viewed in the SEM. Figure 56(b) is a high magnification view of the slip line in the center of Figure 56(a). At this magnification, the slip line is seen to be an extrusion band. These extrusions were also commonly seen on other fatigue specimens examined in the SEM with greater than 800 cycles of damage. Figure 57(a) shows a blocky carbide in a grain boundary. Figure 57(b) shows that this carbide is beginning to de-cohere. The microstructural damage observed in this specimen at this stage of testing occurred well before the asymmetric load drop-off or the initiation of microcracking.

LCF Specimen 39 was tested at 500°F at a total strain range of 0.77%. The test was stopped after 2103 cycles. Crack initiation, determined by the asymmetric load drop method occurred at 1300 cycles. The specimen was sectioned longitudinally, lightly etched, gold plated, and examined in the SEM. Figure 58 shows the general microstructural appearance. The blocky carbide stringers and the grain boundary Laves phase are clearly evident, as are the small spherical precipitates. Figure 59(a) shows a crack along an apparent slip plane which is oriented 60° with respect to the applied load. Figure 59(b) is a magnified view of the edge of the crack. Figure 59(c) shows a crack running from the edge along a grain boundary oriented at 30° with respect to the applied

a. General Microstructure

b. Extrusion

Figure 56. SEM Micrograph, Extrusion after 800 Cycles - LCF Specimen 38

a. Blocky Carbide

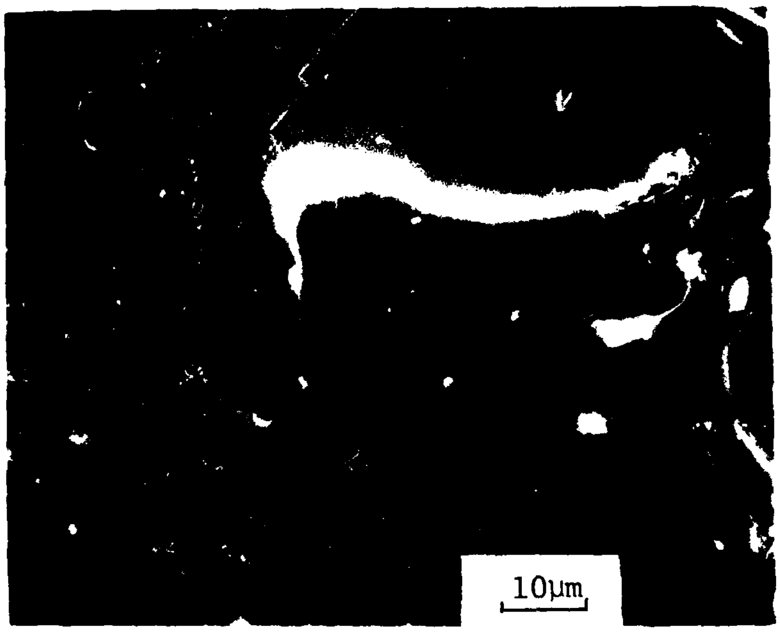

b. Magnified View of Carbide

Figure 57. SEM Micrograph, Decohering Carbide after 800 Cycles - LCF Specimen 38

Figure 58. SEM Micrograph, Longitudinal Section after 2103 Cycles - LCF Specimen 39

a. Crack 1

Figure 59. SEM Micrograph, Cracks in Longitudinal Section after 2103 Cycles - LCF Specimen 39

b. Higher Magnification View of Crack 1

Figure 59 (continued)

c. Crack 2

stress. Note that as predicted by Kim and Laird, the crack is not symmetric with respect to the boundary, but propagates primarily in one grain (48). These cracks, as they progressed into the specimen, followed a path either along another slip plane in a grain or along a grain boundary, but not deviating by more than 15^o from a 45^o angle with respect to the applied stress. Blocky carbides di... ...em to be associated with crack propagation into the thickness.

iii. Proposed Mechanism

At 500^{o}F and within the total strain range 0.7-0.8%, this material can initiate cracks at persistent slip bands or at grain boundaries, whichever is energetically favorable. Generally, cracks initiate at blocky carbide inclusions in those grain boundaries oriented between 30^o and 60^o with respect to the principle tensile direction. The combination of a deformation zone along a grain boundary, as evidenced by the offsets of polishing scratches across the boundaries, and the tendency to develop grain boundary steps, as developed by Kim and Laird (47,48), results in large compatibility strains between the carbide and the grains which are relieved by the decohering of the carbide. This marks the start of Stage I propagation and is noted by the start of the asymmetric load drop-off. Once the crack begins to propagate along a grain boundary away from the carbide, it either continues growing along the boundary both on the surface and into the material, or it turns and begins to propagate along a favorably oriented persistent slip band which had already formed a crack embryo in the form of instrusions/extrusions. Since the strain range is fairly high, these nucleation events occur at multiple locations. Once these cracks begin to link up, the crack grows more rapidly, leading to a much larger decrease in stress drop-off per cycle. The point at which this happens corresponds to N_i' in Table 9.

Thus, the carbides play a key role in the crack initiation process, but are not as important during crack propagation. Stage I cracking generally ends when the crack reaches the end of a grain or a grain boundary triple point in terms of through the thickness of the crack dimension.

The material is ductile enough so that Stage II cracking leads to the formation of fatigue striations. It is not surprising that the fracture surface shows both intergranular and transgranular cracking.

It is clear that after 800 cycles, well before the start of Stage I crack growth, substantial microstructural damage in the form of partially de-cohered carbides and persistent slip bands already exists. This information is crucial in evaluating the effects of the rejuvenation treatments.

IV. REJUVENATION EFFECTS

A. Results of HIP Treatments

i. Presentation of Data

The results of the 11 specimens, pre-damaged in LCF to a given number of cycles, hot isostatically pressed and heat treated, and then retested to failure, are summarized in Table 12. The plots of stress range vs cycles are contained in Figures 60-70. Specimen 16 was mechanically polished and electro-polished three times before retesting.

It is apparent from this data, in comparison with the baseline data of Table 9, that no rejuvenation by HIP occurred. The ceramic

TABLE 12

SUMMARY OF HIP REJUVENATION ON LCF PROPERTIES

Specimen	Prior Damage Cycles	Strain Range (%) $\Delta\varepsilon_t$	$\Delta\varepsilon_p$	$\Delta\varepsilon_e$	Stress Range (ksi)	Cycles N_i	N_i'	N_f	N_i/N_f	N_i'/N_f	Remarks
14	800	0.73	0.02	0.71	196.0	801	1750	2297	0.35	0.76	
16	800	0.73	0.03	0.70	193.0	1350	1800	2134	0.63	0.84	Electro-polished
18	800	0.72	0.03	0.69	189.0	1750	2250	2619	0.67	0.86	
19	800	0.76	0.05	0.71	195.5	1450	1650	1933	0.75	0.85	
20	800	0.73	0.02	0.71	194.8	1750	2350	3147	0.56	0.75	Coated
21	800	0.74	0.02	0.72	200.0	1150	1450	1797	0.64	0.81	Coated
22	800	0.76	0.05	0.71	197.0	1400	1700	2287	0.61	0.74	Coated
23	2100	0.76	0.05	0.71	195.0	2650	2950	3286	0.81	0.90	Coated
24	2100	0.70	0.04	0.66	186.5	801	2900	3862	0.21	0.75	
25	0	0.68	0.03	0.65	179.4	700	950	1573	0.45	0.60	Coated
29	0	0.77	0.04	0.73	202.0	900	1250	1660	0.54	0.75	

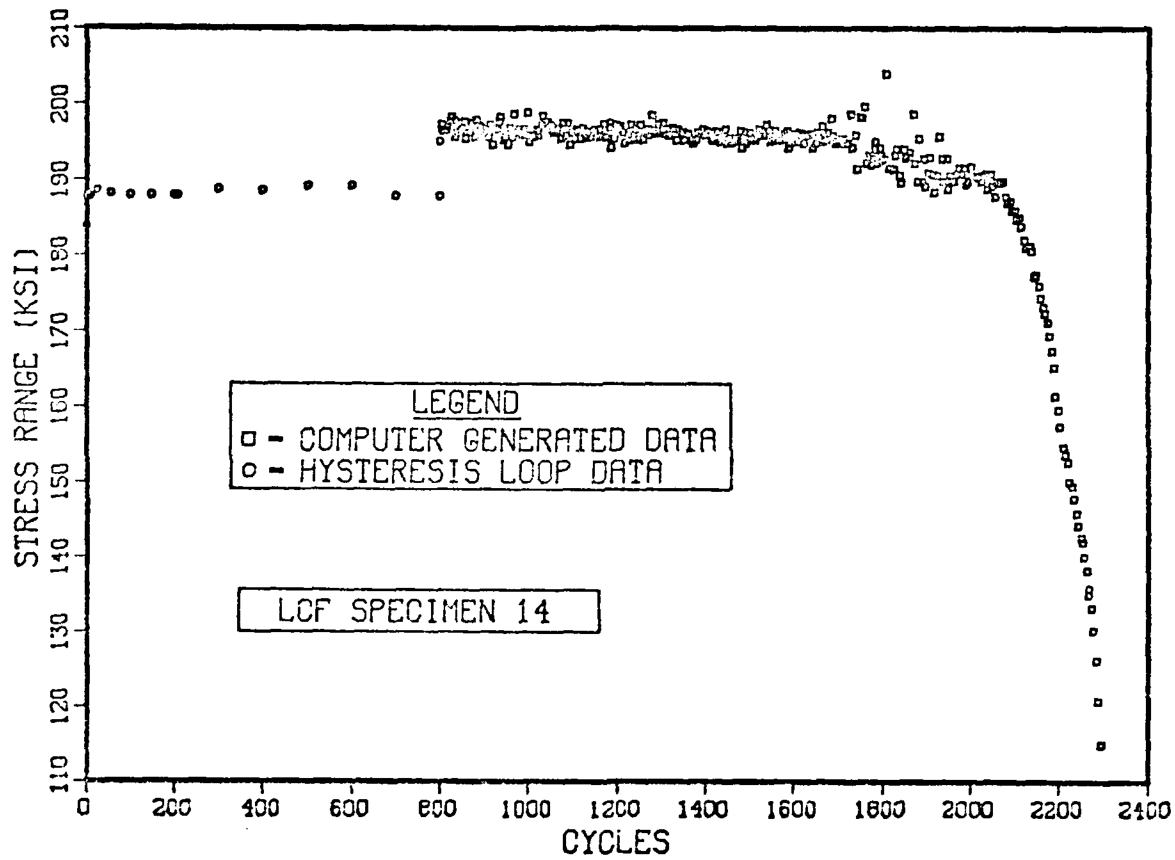

Figure 60. Plot of Stress Range vs Cycles - LCF Specimen 14

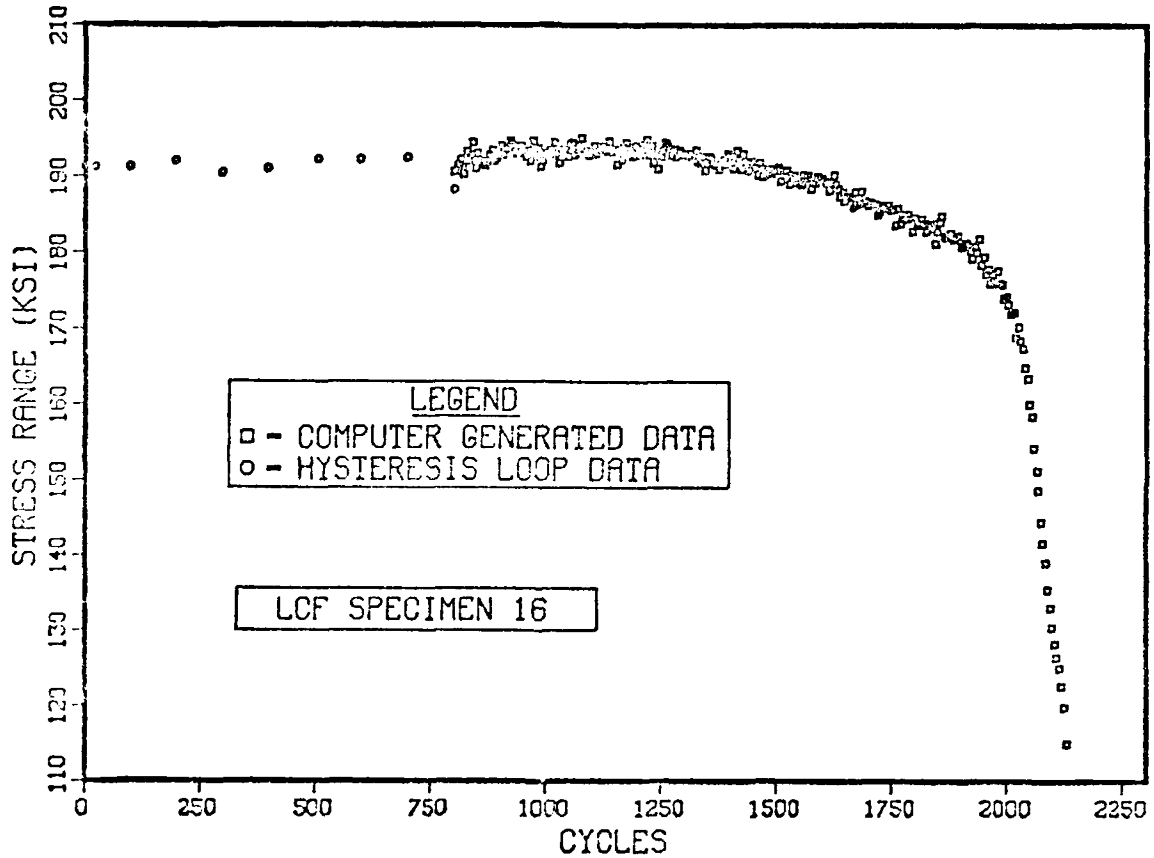

Figure 61. Plot of Stress Range vs Cycles - LCF Specimen 16

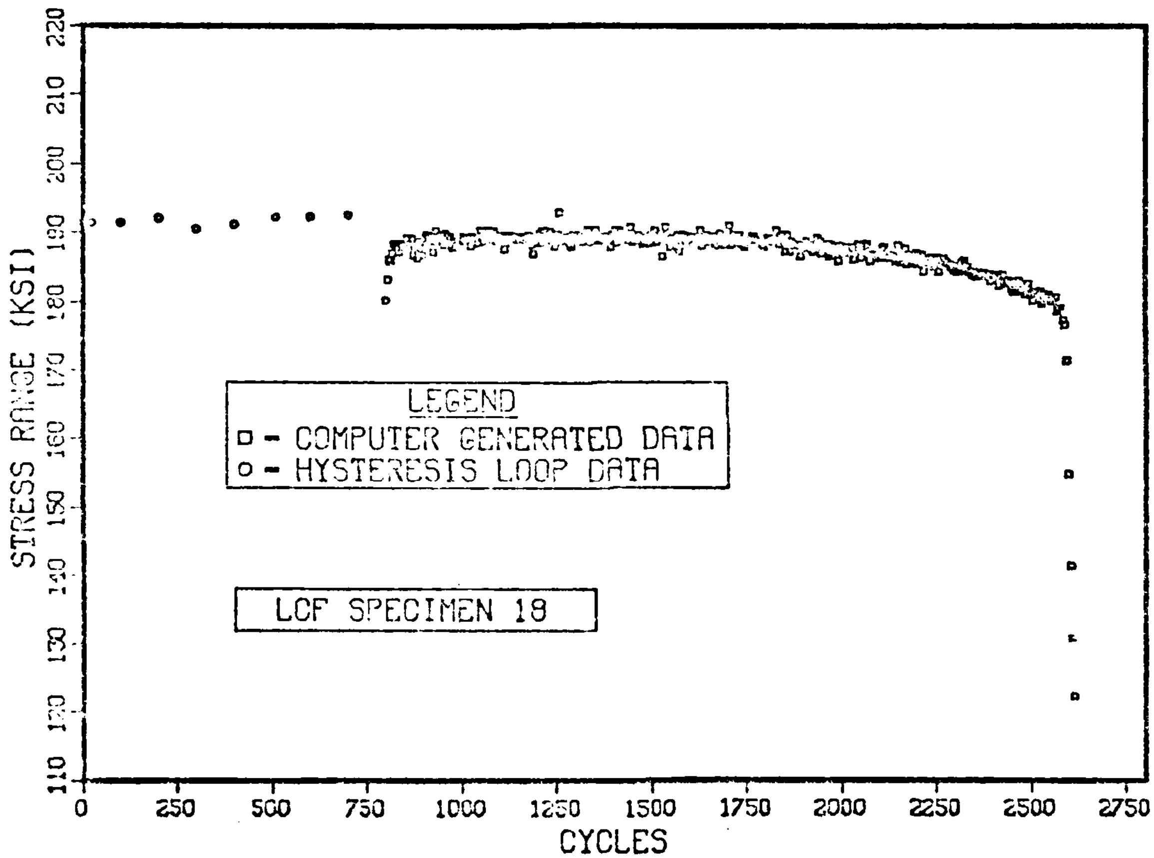

Figure 62. Plot of Stress Range vs Cycles - LCF Specimen 18

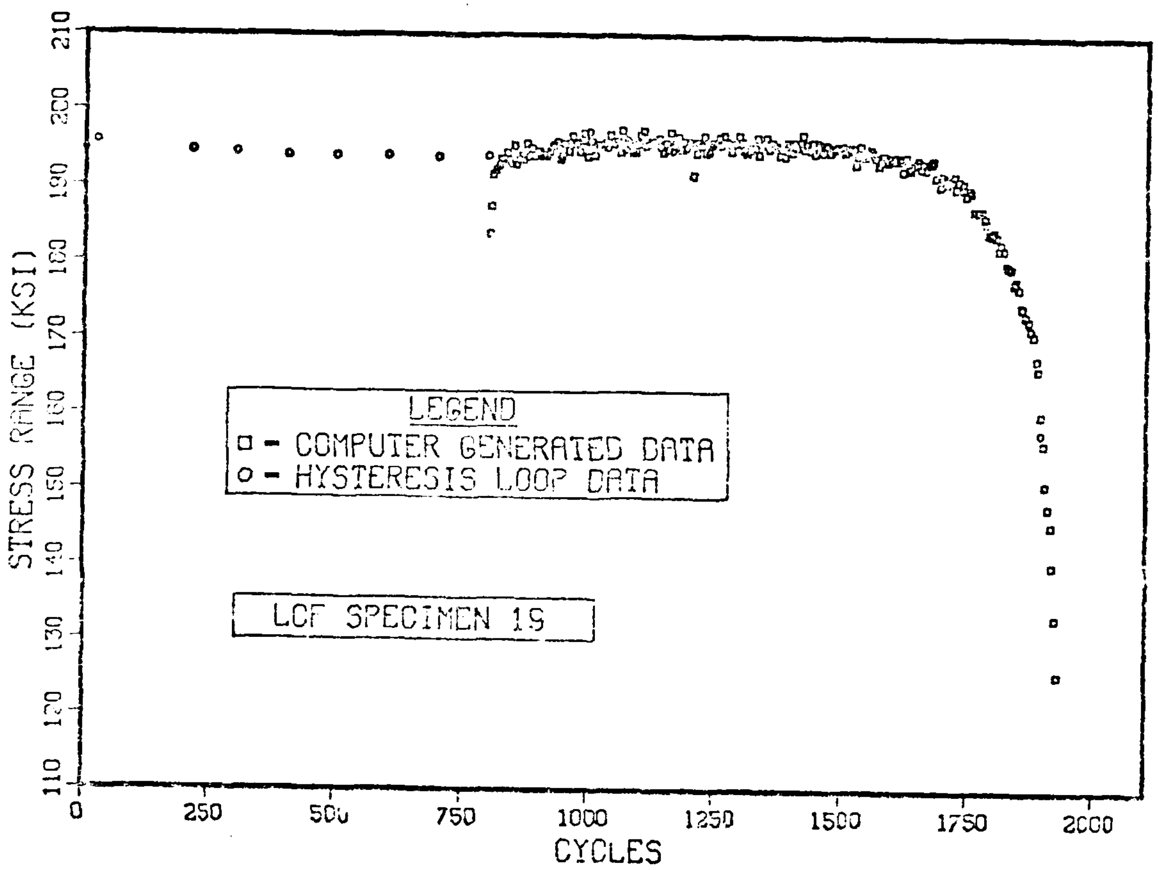

Figure 63. Plot of Stress Range vs Cycles - LCF Specimen 19

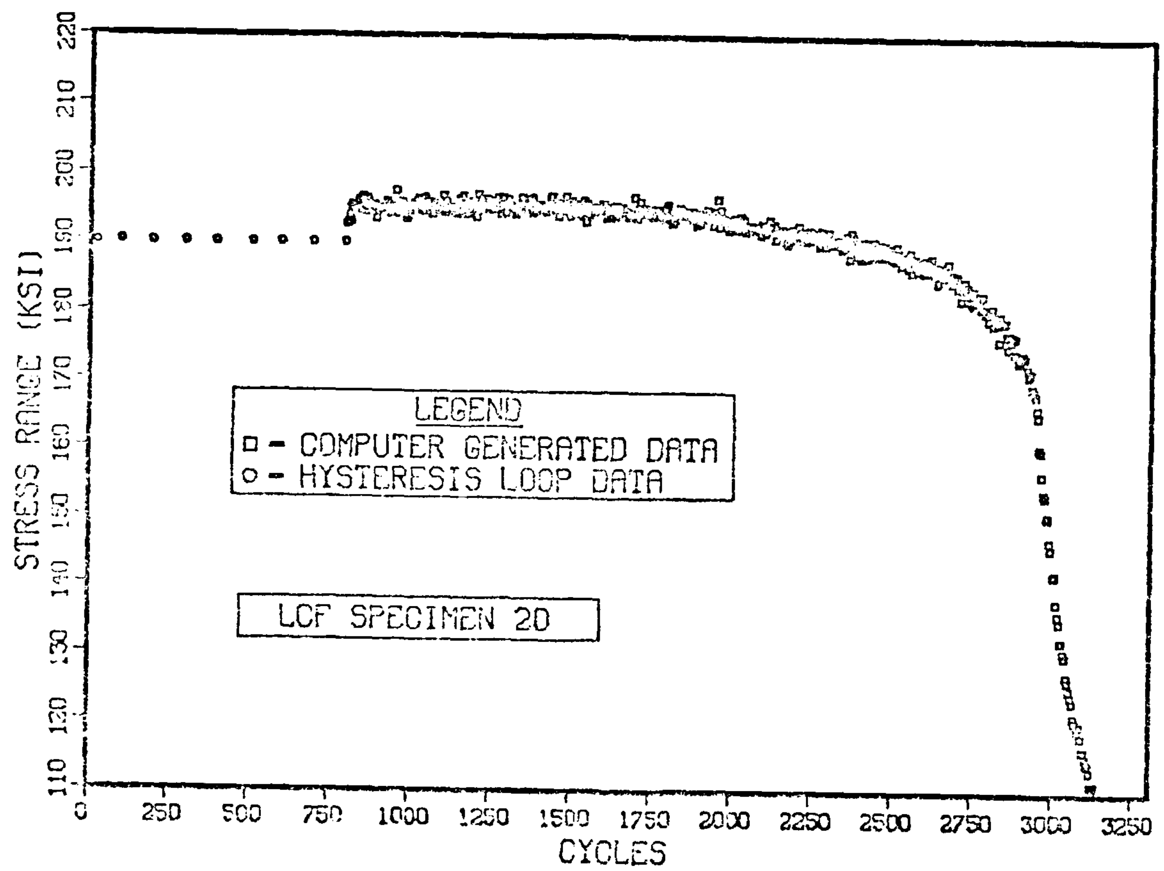

Figure 64. Plot of Stress Range vs Cycles - LCF Specimen 20

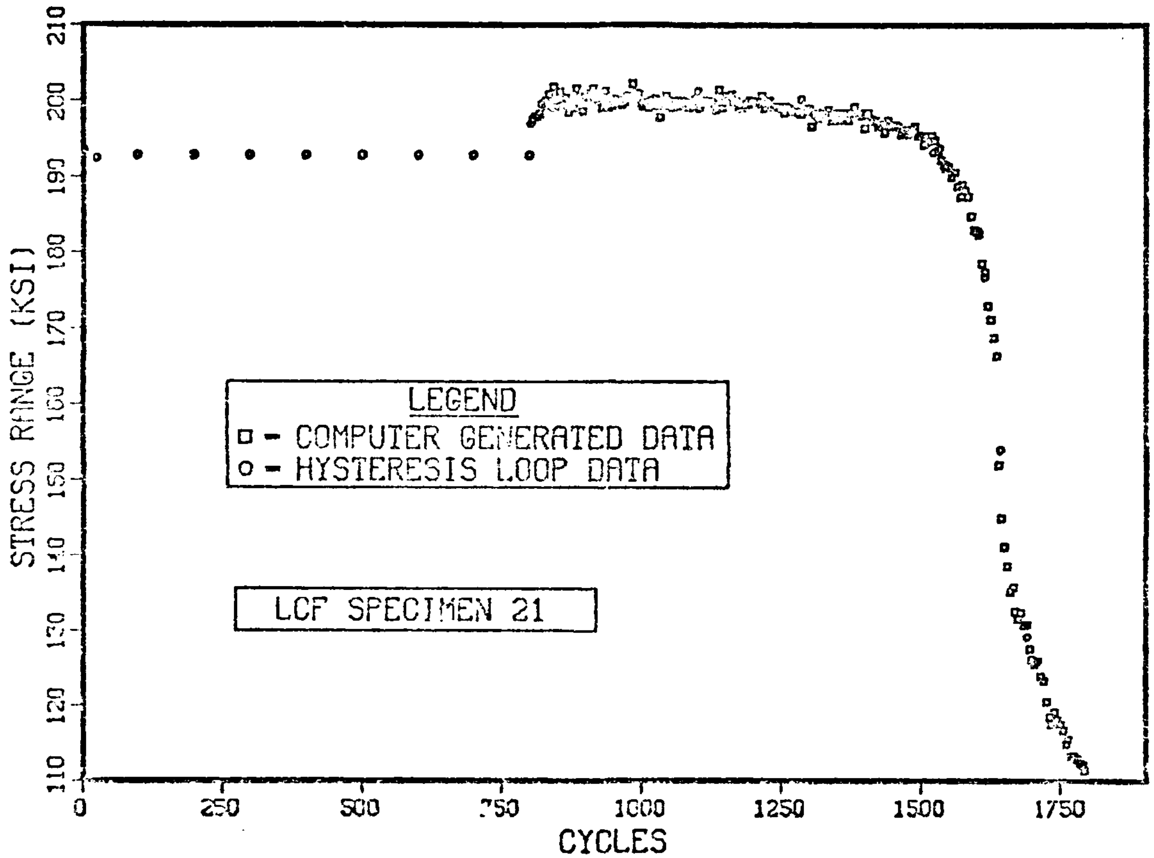

Figure 65. Plot of Stress Range vs Cycles - LCF Specimen 21

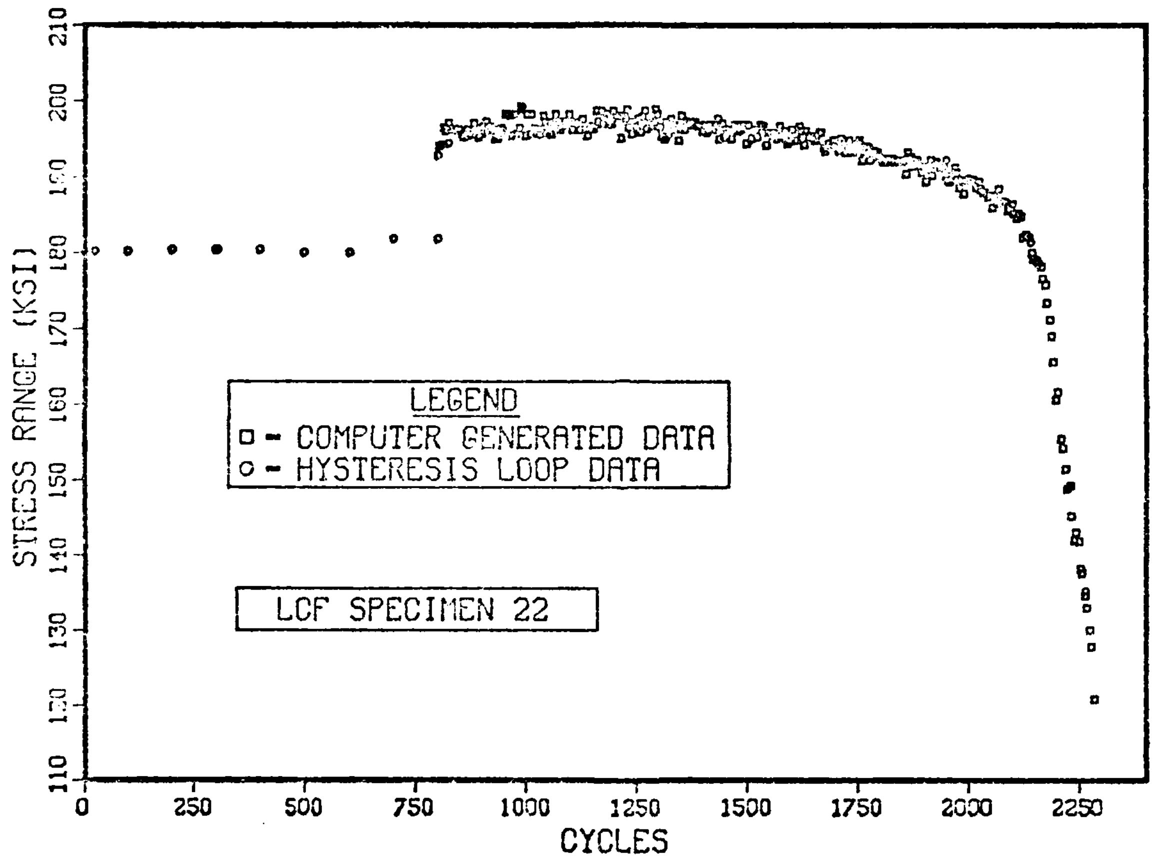

Figure 66. Plot of Stress Range vs Cycles - LCF Specimen 22

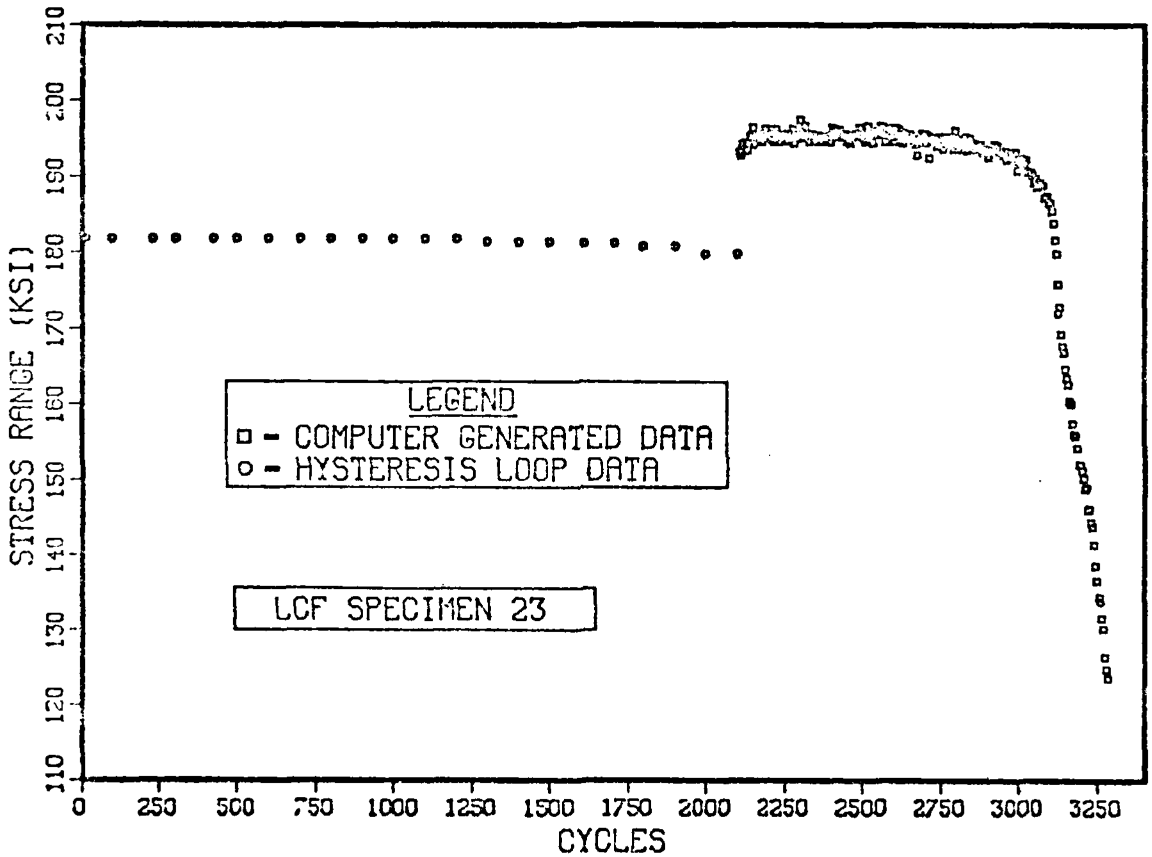

Figure 67. Plot of Stress Range vs Cycles - LCF Specimen 23

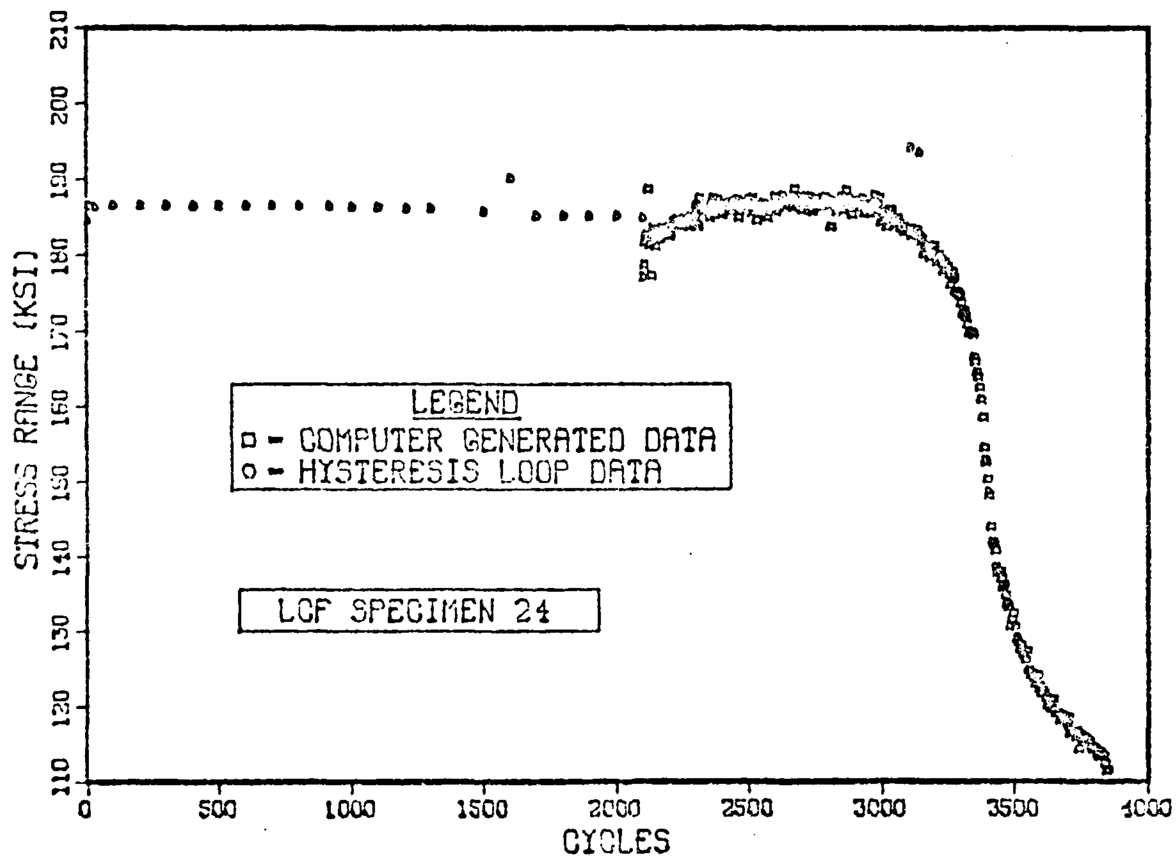

Figure 68. Plot of Stress Range vs Cycles - LCF Specimen 24

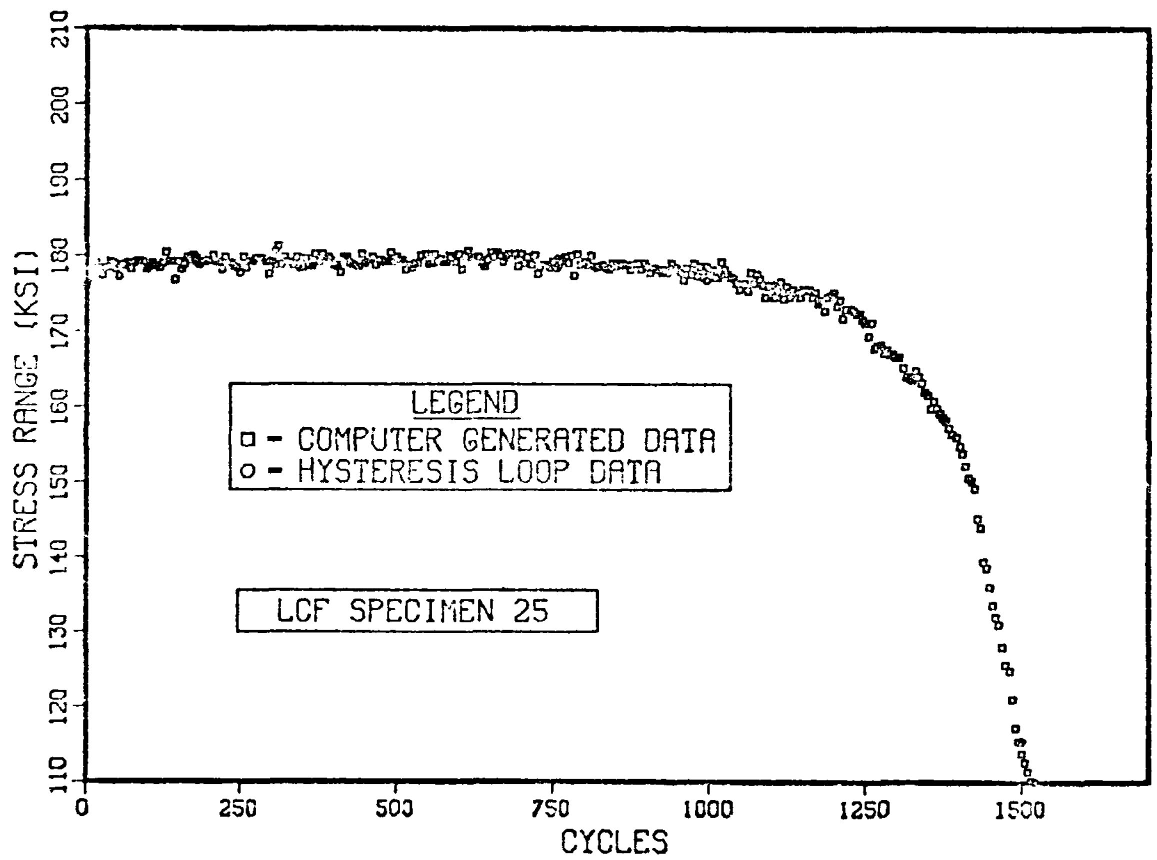

Figure 69. Plot of Stress Range vs Cycles - LCF Specimen 25

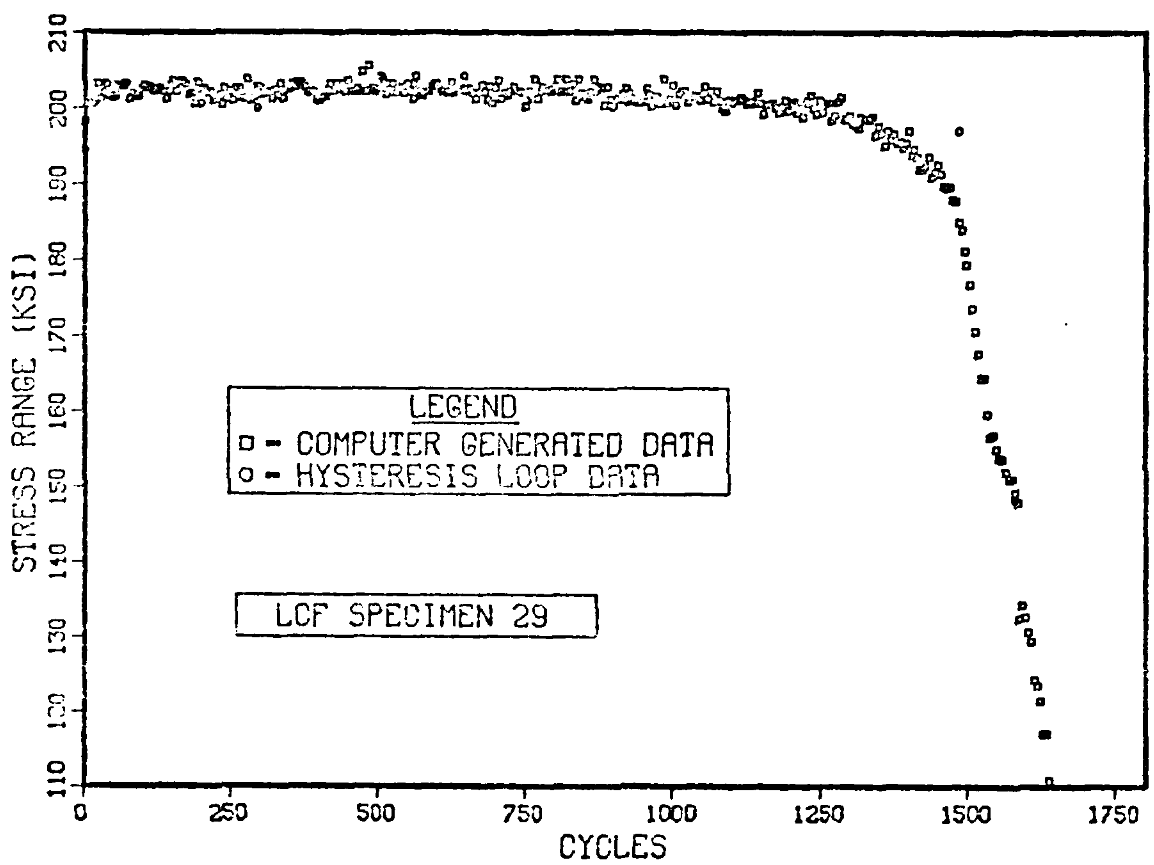

Figure 70. Plot of Stress Range vs Cycles - LCF Specimen 29

coated and the uncoated specimens performed about the same; although Specimen 20, which was coated, performed the best. On the basis of total life, these HIP specimens were clearly inferior to the baseline specimens. Specimens 25 and 29, which were HIP'd without prior damage, failed within the range of about 1600-1700 cycles. The remaining HIP'd specimens with different levels of pre-HIP damage also failed within this range of cycles after retesting commenced, regardless of the level of pre-HIP damage. This includes two specimens which were predamaged to 2100 cycles; crack initiation had already occurred in these specimens prior to the HIP treatment. This is strong evidence that the HIP processing itself adversely damaged the microstructure at the surface of the material.

Those specimens which were to be ceramic coated were first vapor honed to provide a suitable surface for the coating to adhere to. The effect of the vapor honed surface on the LCF properties was investigated. Figure 71 shows a SEM photomicrograph of the as-vapor-honed surface. The surface is fairly rumpled and some inclusions appear to have already decohered from the microstructure. The gauge section of two vapor-honed specimens was repolished and then tested at 500^{o}F. The Stress Range vs Cycles for these specimens, Specimens 27 and 28, are shown in Figures 72 and 73. Table 13 is a summary of the LCF data. It is clear that vapor honing, even after repolishing, was deleterious to the fatigue life. During repolishing, the diameter was reduced from 0.118 in. to about 0.116 in., or by 25 μ (about one-fifth of a grain diameter) along the specimen radius. Specimen 28, after testing, was placed in the SEM. In addition to the main crack, extensive cracking along the gage

TABLE 13

EFFECT OF VAPOR HONING ON LCF PROPERTIES

Specimen	Strain Range (%)			Stress Range (ksi)	Cycles			N_i/N_f	N_i'/N_f
	$\Delta\varepsilon_t$	$\Delta\varepsilon_p$	$\Delta\varepsilon_e$		N_i	N_i'	N_f		
27	0.81	0.06	0.75	205.0	900	1200	1505	0.60	0.80
28	0.76	0.04	0.72	198.0	1100	1850	1995	0.55	0.93

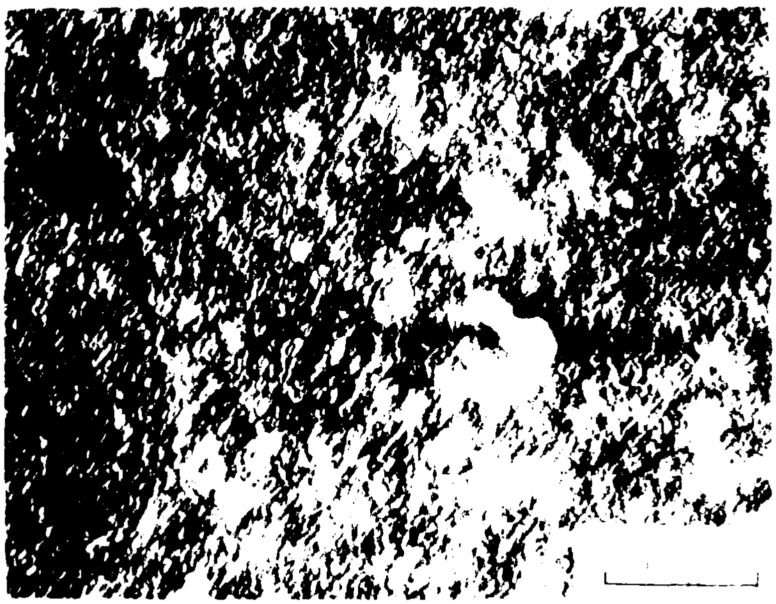

Figure 71. SEM Micrograph, As-Vapor-Honed Surface - LCF Specimen 55

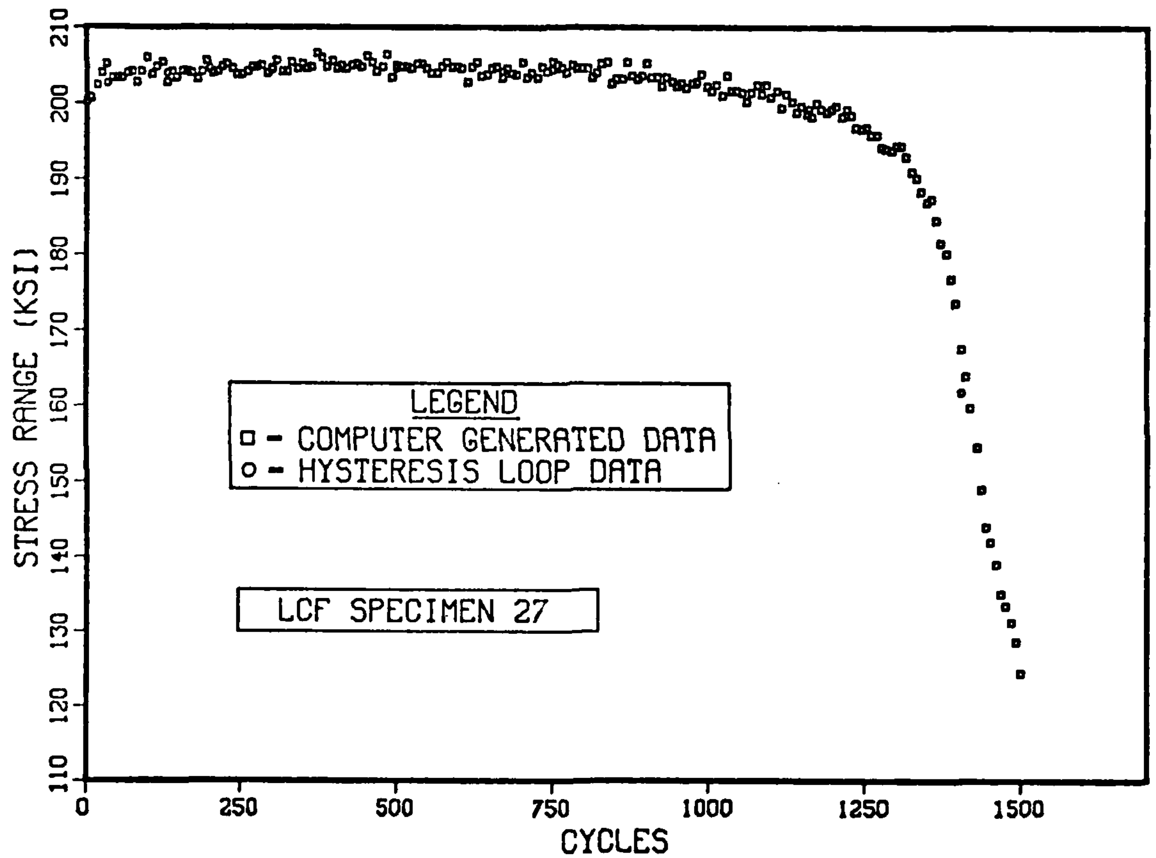

Figure 72. Plot of Stress Range vs Cycles - LCF Specimen 27

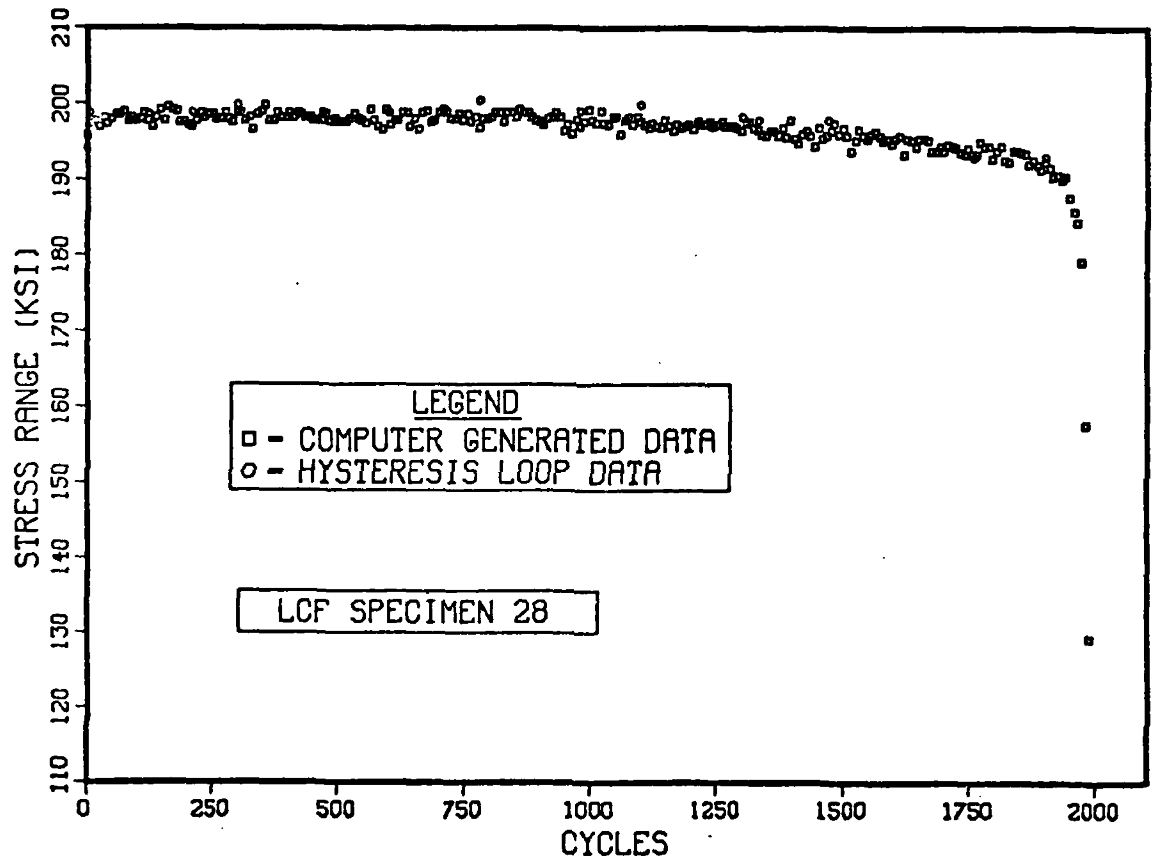

Figure 73. Plot of Stress Range vs Cycles - LCF Specimen 28

length was observed. Typical examples of secondary cracks are shown in Figures 74, 75, and 76. All three of these cracks seem to be associated with inclusions which have decohered, cracked, or failed out.

There was a reaction between the ceramic coating and the base material during HIPing. Figure 77 shows a typical reaction zone from LCF Specimen 20. This reaction was observed in the shank region, above the extensometer flange. It is assumed a similar reaction occurred in the gauge section. The apparent penetration depth of the reaction zone was at least 5 μ. This zone should have been removed during the polishing operation prior to retesting. However, the grain boundaries may have been damaged to much greater penetration depths by alloy depletion. Greater material removal than that accomplished by repolishing was deemed unwise due to the already small specimen diameter.

Figure 78 shows some fractographs taken of ceramic-coated LCF Specimen 25. The fracture appears much more intergranular in nature than for the baseline specimens.

Crack growth rate in another ceramic-coated specimen, LCF Specimen 21, was also measured by the surface replication technique. Photomicrographs of the replicas are shown in Figure 79. The plot of Crack Length vs Cycles is contained in Figure 80. Extrapolation of the crack length to zero shows that initiation occurred between 1100 and 1200 cycles. This agrees with the asymmetric load drop-off point, N_i, in Table 12 of 1150 cycles. Note that the slope of this curve is about 1.5 μm/cycle. This is 5.5 times the slope of the two baseline specimens plotted in Figures 45 and 47. Thus, the crack growth rate was greatly accelerated in the HIP rejuvenated specimen.

a. Low Magnification View of Crack

b. High Magnification View of Crack

Figure 74. SEM Micrograph, Secondary Cracking - LCF Specimen 28

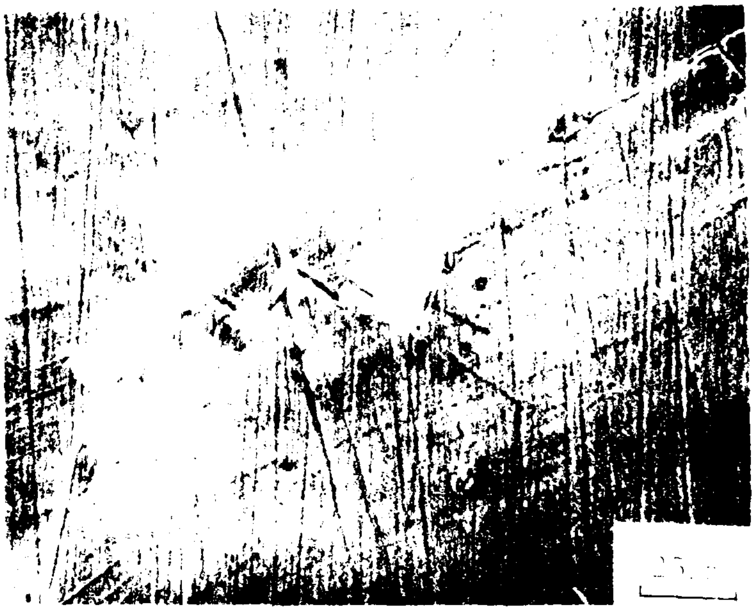

a. General Crack

b. Higher Magnification View of Crack

Figure 75. SEM Micrograph, Secondary Cracking - LCF Specimen 28

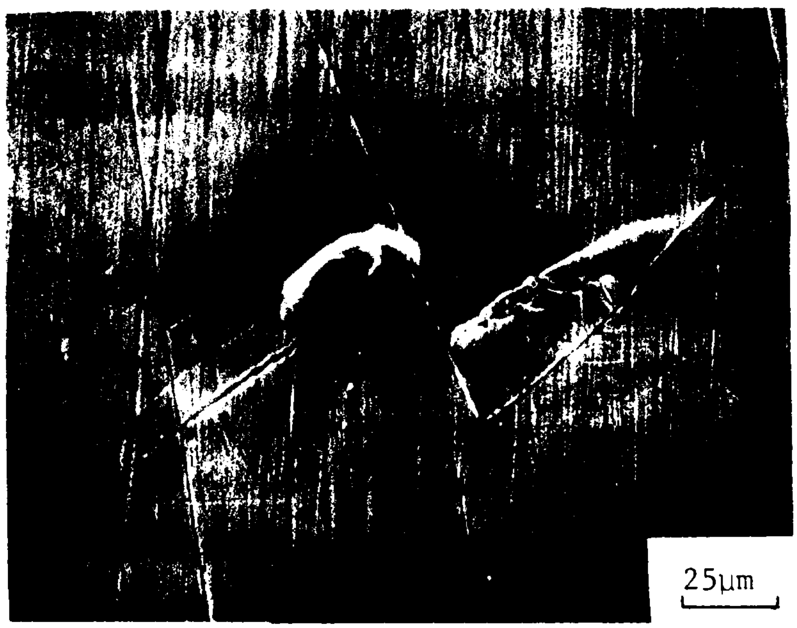

Figure 76. SEM Micrograph, Secondary Cracking - LCF Specimen 28

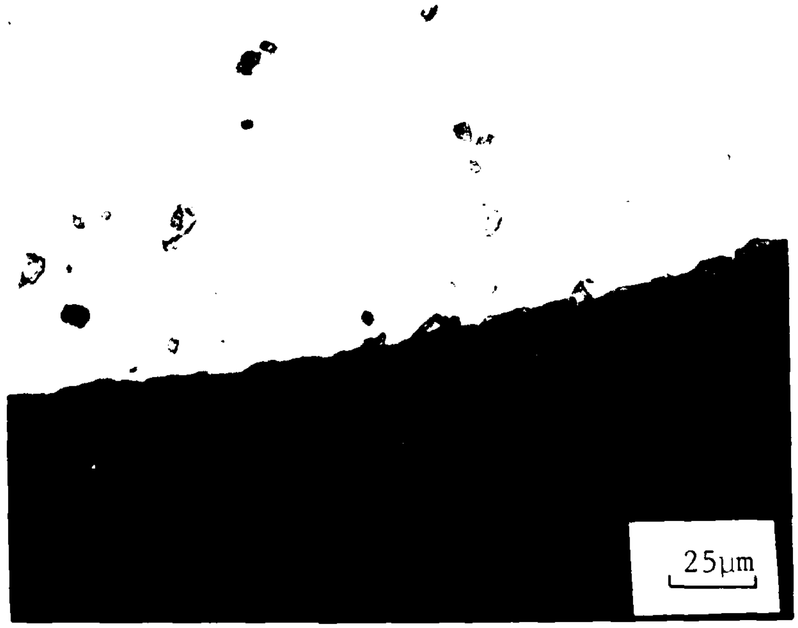

a. General Area

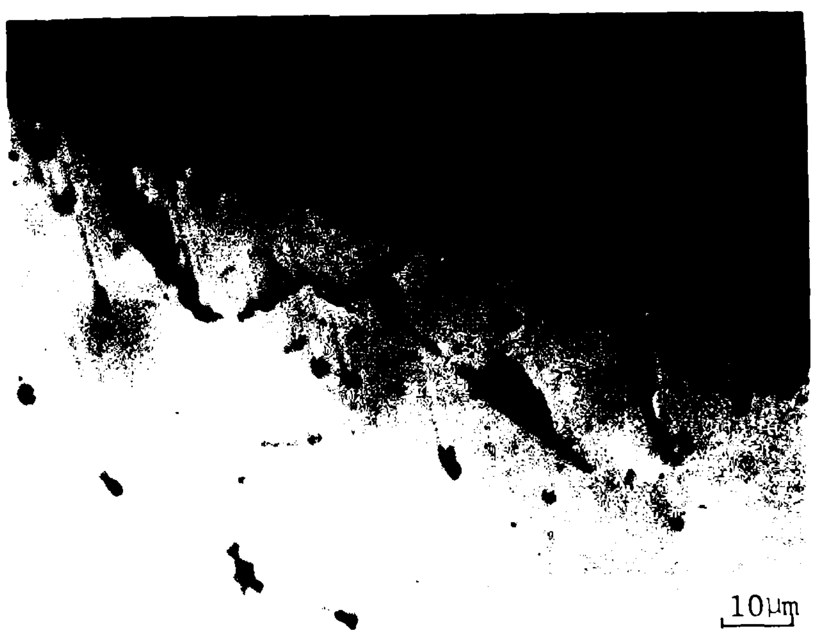

b. Higher Magnification of Reaction Zone

Figure 77. Micrograph, Coating Reaction

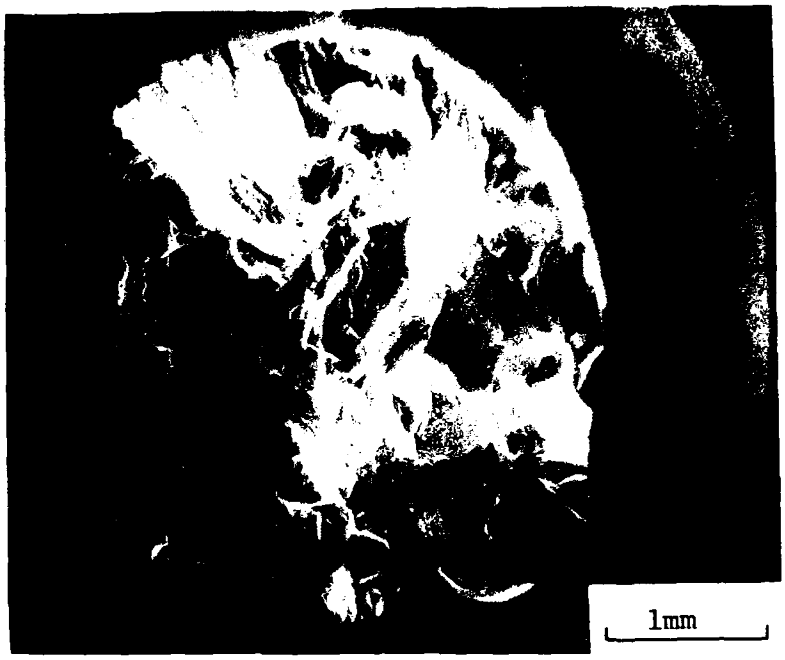

a. Fractograph

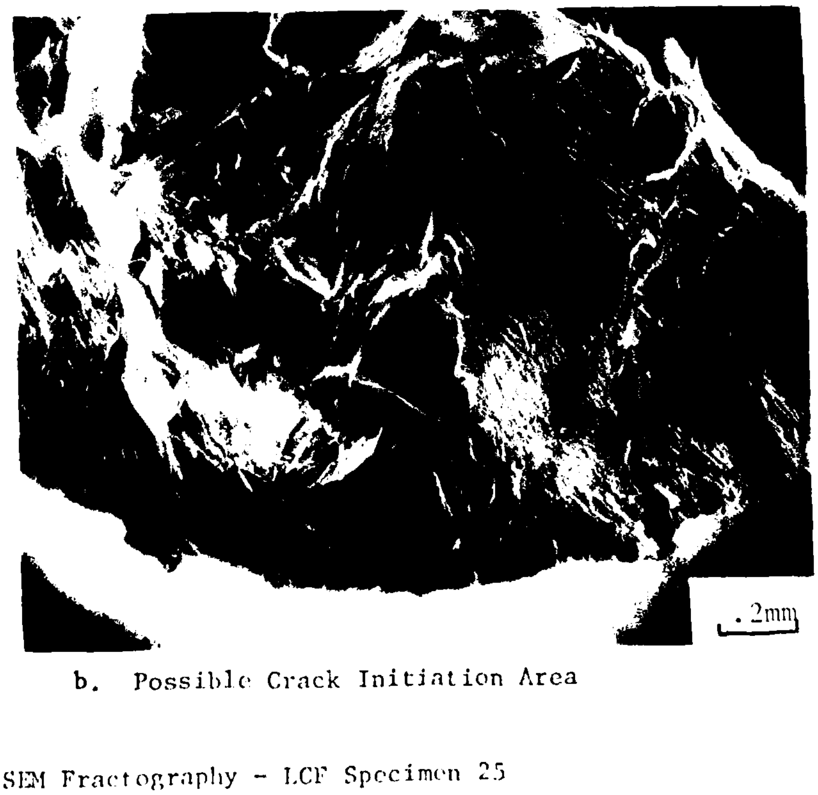

b. Possible Crack Initiation Area

Figure 78. SEM Fractography - LCF Specimen 25

Figure 79. Micrographs of Replicas, Cracks - LCF Specimen 21

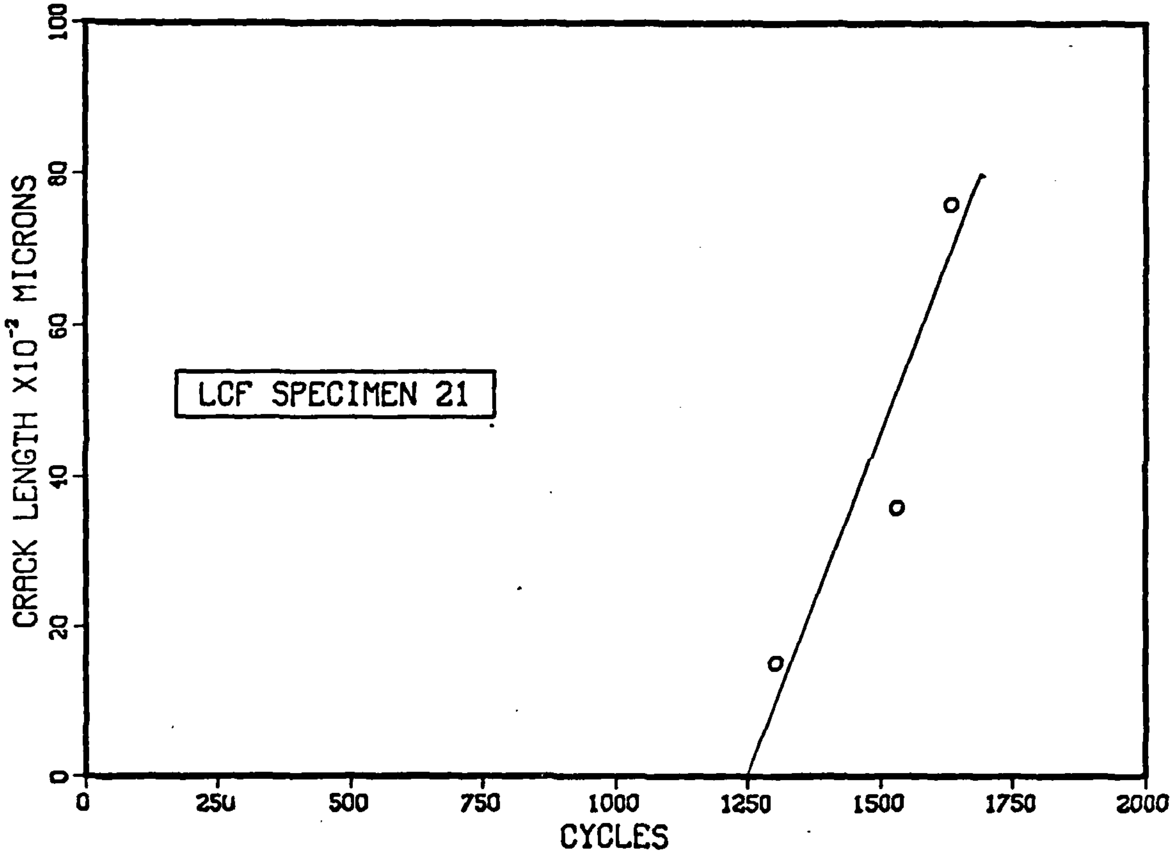

Figure 80. Plot of Crack Length vs Cycles - LCF Specimen 21

The uncoated specimens were badly contaminated after HIP processing. Figure 81 shows the reaction zone for LCF Specimen 26. The apparent reaction zone is 5-10 μ in depth. After HIP processing, alloy depletion along the grain boundaries to much greater depths has been observed in IN-713 (54). Thus, even after repolishing, the grain boundaries were still substantially weakened compared to the baseline. Figure 82 contains SEM photomicrographs of the primary crack in LCF Specimen 16. This crack had progressed completely around the circumference of the specimen. No baseline specimen had a complete circumferential crack, but it was not unusual for the HIP processed specimens (both coated and bare) to have one. Note that the crack in Figure 82(a) is both intergranular and transgranular. The role of a fractured blocky carbide in promoting cracking is graphically shown in Figures 82(b) and (c). Cracking throughout the gauge length was extensive. Figure 83 shows a typical intergranular crack located at some distance from the main crack. The fracture appearance for the uncoated specimens was very similar to that of the coated specimens.

HIP processing increased the material grain size from 120 μm to 150 μm. It is known that LCF life is usually sensitive to grain size. Merrick found an inverse relationship between grain size and fracture life for two different grain sizes at room temperature and at 1000°F (16). Handbook data at room temperature for three grain sizes also shows an inverse relationship with fracture life for stress-controlled tests (43). When this data is plotted, it is apparent that the relationship follows a Hall-Petch dependency:

$$N_f \propto \frac{1}{\sqrt{g.s.}} \qquad (18)$$

a. Surface Contamination, Area 1

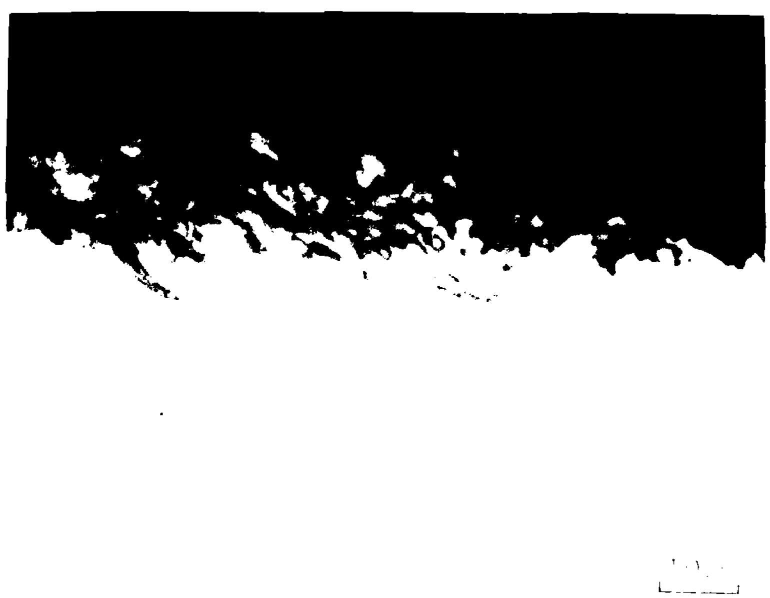

b. Surface Contamination, Area 2

Figure 81. Micrograph, Surface Oxidation - LCF Specimen 26

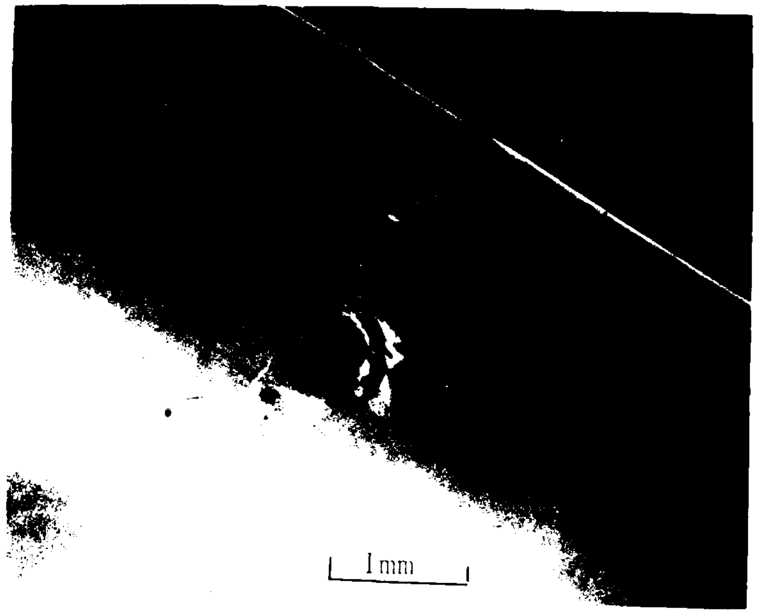

a. Main Crack

b. Magnification of Center Portion of Crack

Figure 82. SEM Micrographs, Main Crack - LCF Specimen 16

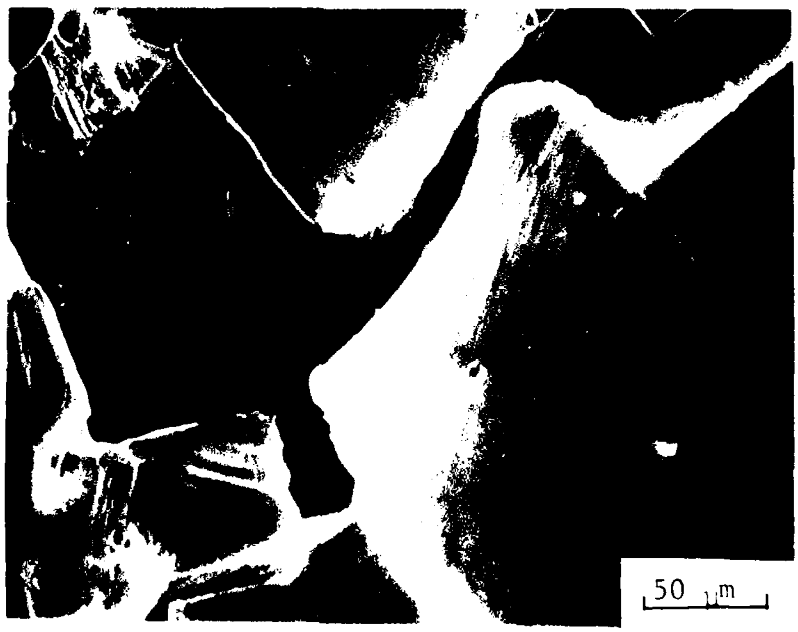

c. Possible Carbide Pullout

Figure 83. SEM Micrographs, Secondary Cracking - LCF Specimen 16

where N_f is the cycles to failure, and g.s. is the grain size. Thus, the effect of increased grain size from the rejuvenation processing on the cycles to failure can be estimated:

$$N_{f_2} = N_{f_1} \times \sqrt{\frac{g.s._1}{g.s._2}} \qquad (19)$$

Using Equation 18, a decrease in cycles to failure of 12% can be estimated to be due to the grain size changes alone.

iii. Mechanisms

Considering the data presented in Tables 12 and 13, the fatigue behavior for the HIP'd specimens (both coated and uncoated) and the vapor-honed specimens is similar. But the mechanisms of crack nucleation and growth are most likely not the same. Recall that the previous section demonstrated that the critical step for crack initiation in the baseline specimens was the decohering of a grain boundary carbide. Clearly, vapor honing, even with repolishing, can decohere or fracture carbides. This not only would greatly shorten the initiation time, but would provide many crack initiation sites. Thus, once crack growth began, it would progress very rapidly due to microcrack linkup. This is what was observed for the vapor-honed specimens.

The ceramic coating reacts with the matrix during HIP processing. Even though optical microscopy showed that the reaction depth was such that it should be removed by repolishing, localized contamination along the grain boundaries and existing persistent slip bands can be substantially greater. This would promote the early intergranular failure as was observed. This investigation is inconclusive, however, in differentiating between the damage due to vapor honing and the damage due to contamination by the ceramic coating.

The uncoated specimens had contaminated grain boundaries which were relatively weak. Thus, the carbides readily decohered and crack propagation was fairly rapid.

B. Results of Thermal Treatments

1. Presentation of Data

The results of seven thermally rejuvenated specimens are contained in Table 14. A comparison of this data with the baseline data (Table 9) and the HIP rejuvenated data (Table 12) reveals that some rejuvenation definitely occurred as a result of the thermal treatment. The plots of Stress Range vs Cycles are contained in Figures 84-90. Note that LCF Specimen 13 was heat treated in a poor vacuum and, as a result, the surface was badly oxidized. It was tested without repolishing. The remaining specimens, except for LCF Specimen 54, were all repolished after thermal treatment.

An investigation was made to determine the effect of repolishing alone on enhancing the fatigue properties. A summary of the data is contained in Table 15. The plots of Stress Range vs Cycles are shown in Figures 91 and 92. These data are essentially no different than the baseline properties. Also, since LCF Specimen 54 was not repolished after the thermal treatment and yet was clearly rejuvenated, it can be concluded that repolishing alone does not recover LCF damage for the conditions studied in this investigation.

Table 14 indicates that complete recovery of LCF damage was not accomplished. But, it was previously shown that after 800 cycles,

[illegible]

Specimen	[illegible] Cycles	Strain Range (%)			Stress Range (ksi)	Cycles				
		$\Delta\epsilon_t$	$\Delta\epsilon_p$	$\Delta\epsilon_e$		N_i	N_i'	N_f	N_i/N_f	N_i'/N_f
13*	800	0.79	0.07	0.72	198.0	1650	2100	2504	0.66	0.84
34	400	0.75	0.05	0.70	194.5	1800	2700	3333	0.54	0.81
35	800	0.74	0.03	0.71	194.0	1800	3900	5384	0.33	0.72
42	803	0.74	0.02	0.72	197.6	1800	3300	4134	0.44	0.80
43	803	0.75	0.02	0.73	200.5	2000	2650	2890	0.69	0.92
51	803	0.72	0.02	0.70	194.0	1700	3700	4475	0.38	0.83
54**	803	0.75	0.04	0.71	194.2	1900	3200	4106	0.46	0.78

*Heat treated in a poor vacuum

**Retested without repolishing

TABLE 15

SUMMARY OF REPOLISHING ON LCF PROPERTIES

Specimen	Prior Damage Cycles	Strain Range (%)			Stress Range (ksi)	Cycles			N_i/N_f	N_i'/N_f
		$\Delta\varepsilon_t$	$\Delta\varepsilon_p$	$\Delta\varepsilon_e$		N_i	N_i'	N_f		
38	803	0.76	0.05	0.71	196.0	1575	2700	3562	0.44	0.76
40	803	0.73	0.02	0.71	194.5	1300	2800	3206	0.41	0.87

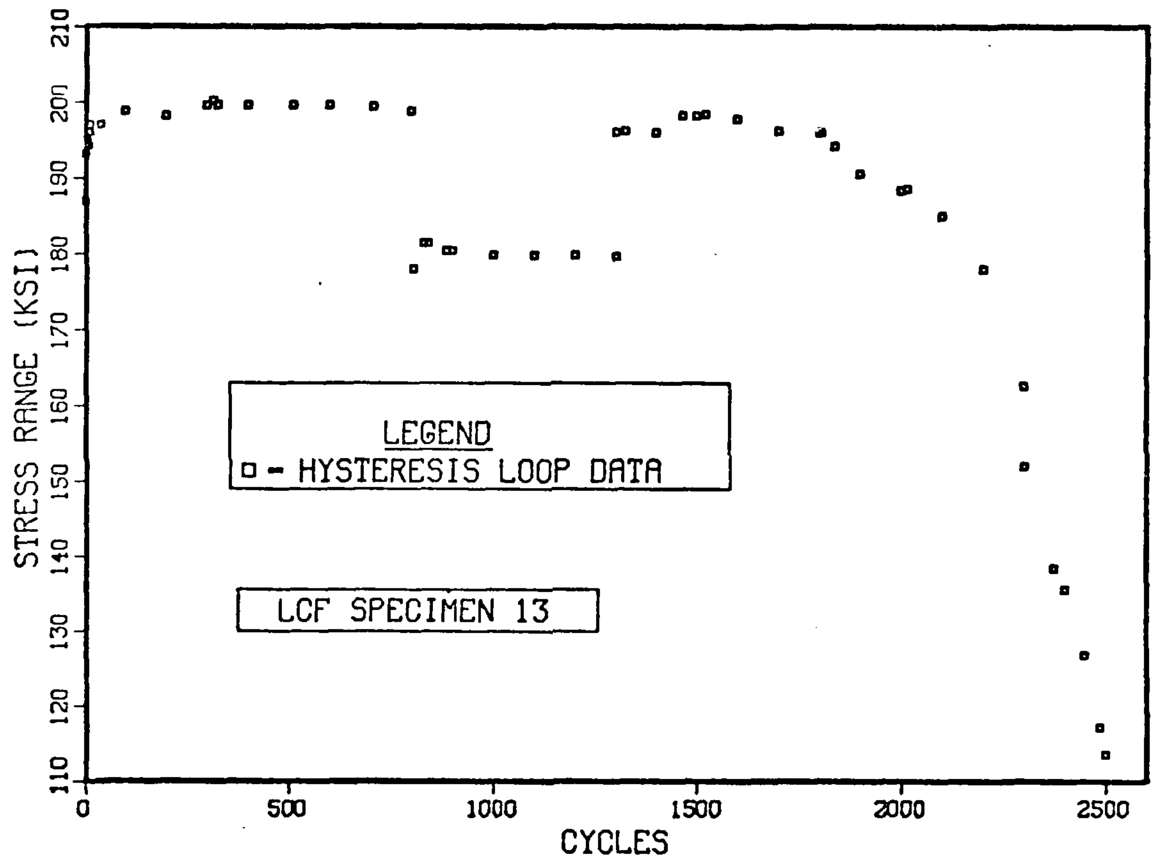

Figure 84. Plot of Stress Range vs Cycles - LCF Specimen 13

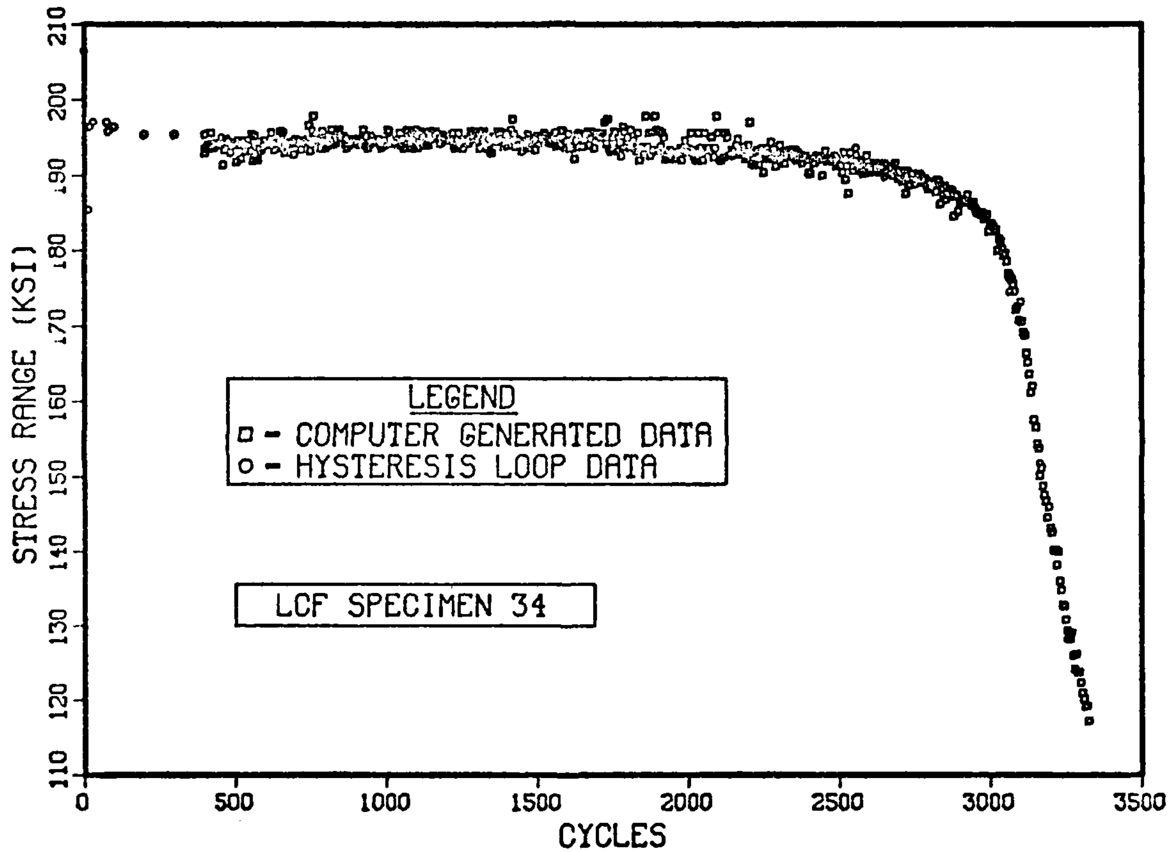

Figure 85. Plot of Stress Range vs Cycles - LCF Specimen 34

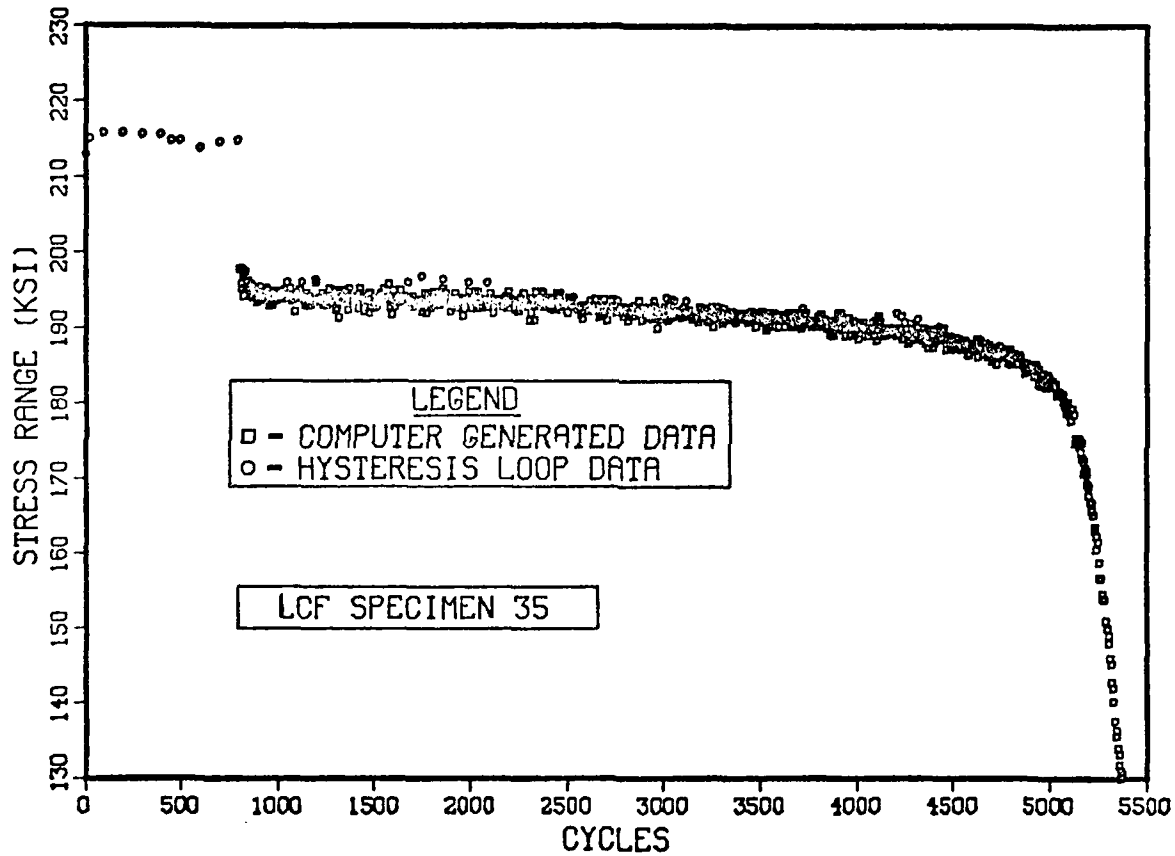

Figure 86. Plot of Stress Range vs Cycles - LCF Specimen 35

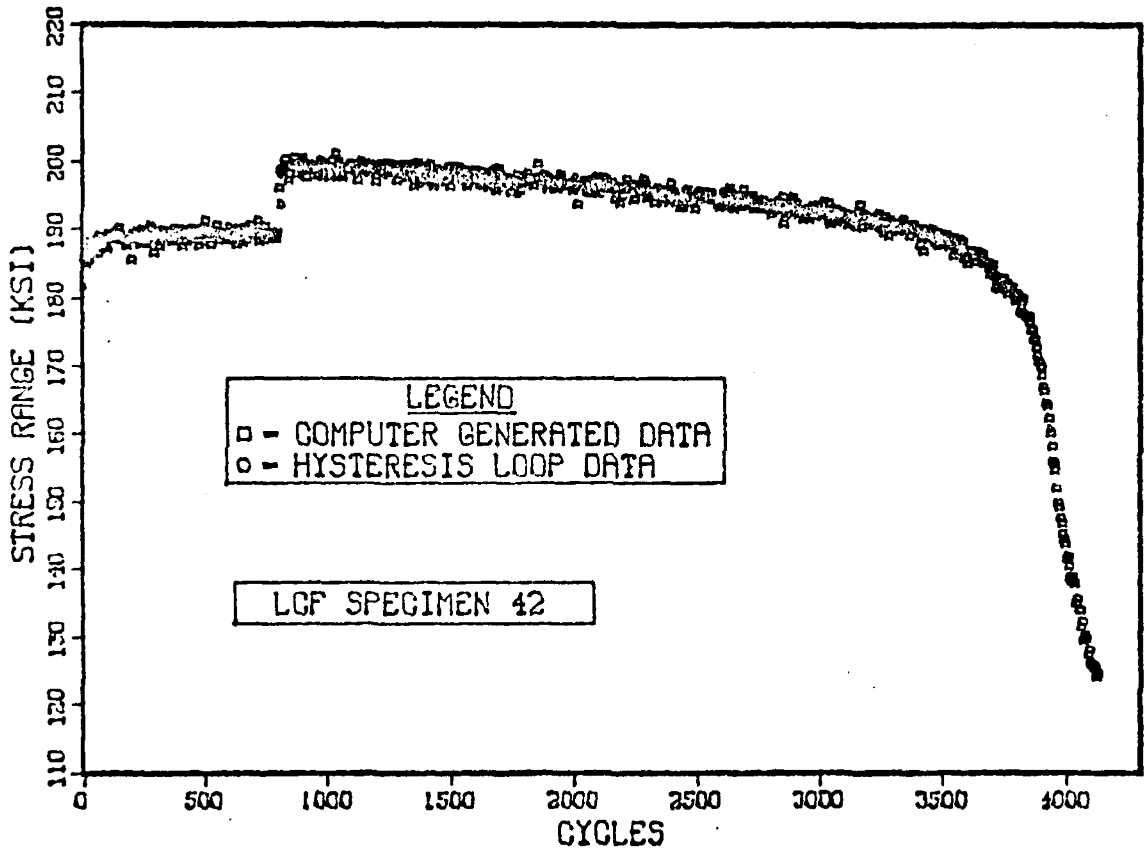

Figure 87. Plot of Stress Range vs Cycles - LCF Specimen 42

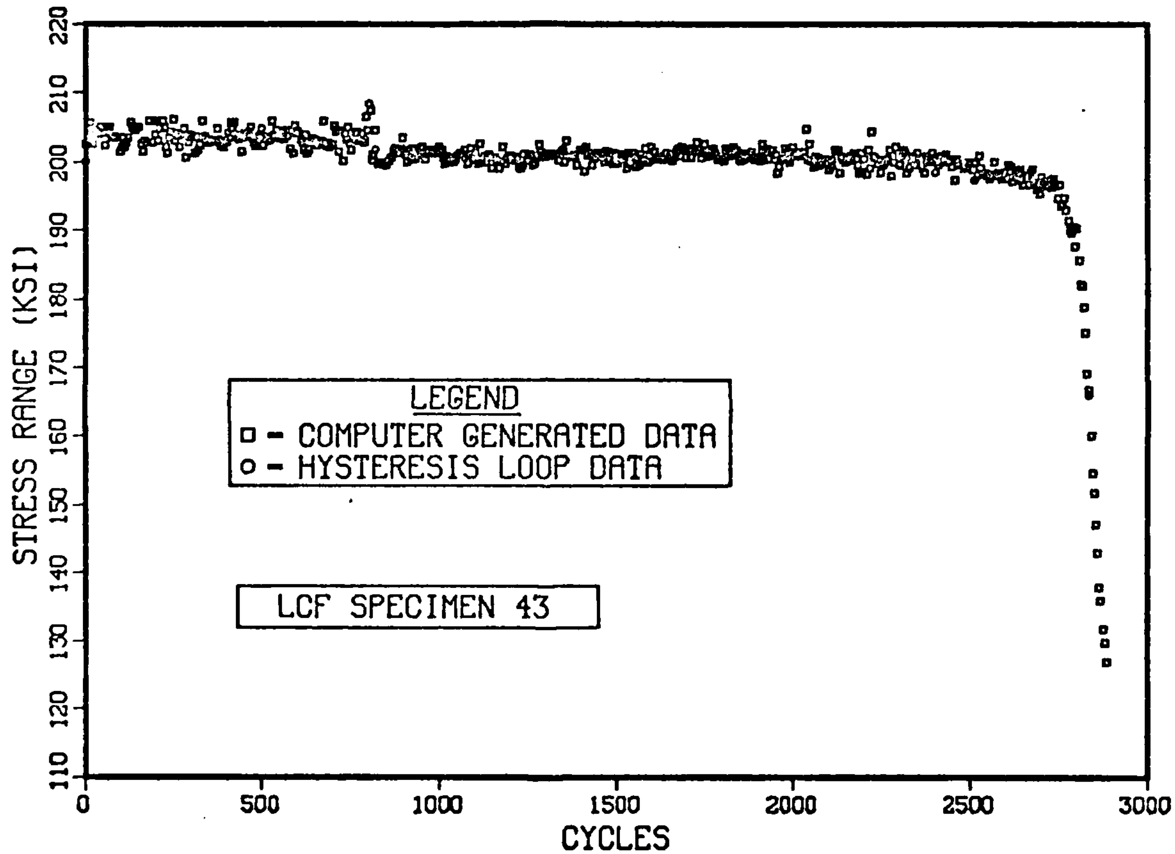

Figure 88. Plot of Stress Range vs Cycles - LCF Specimen 43

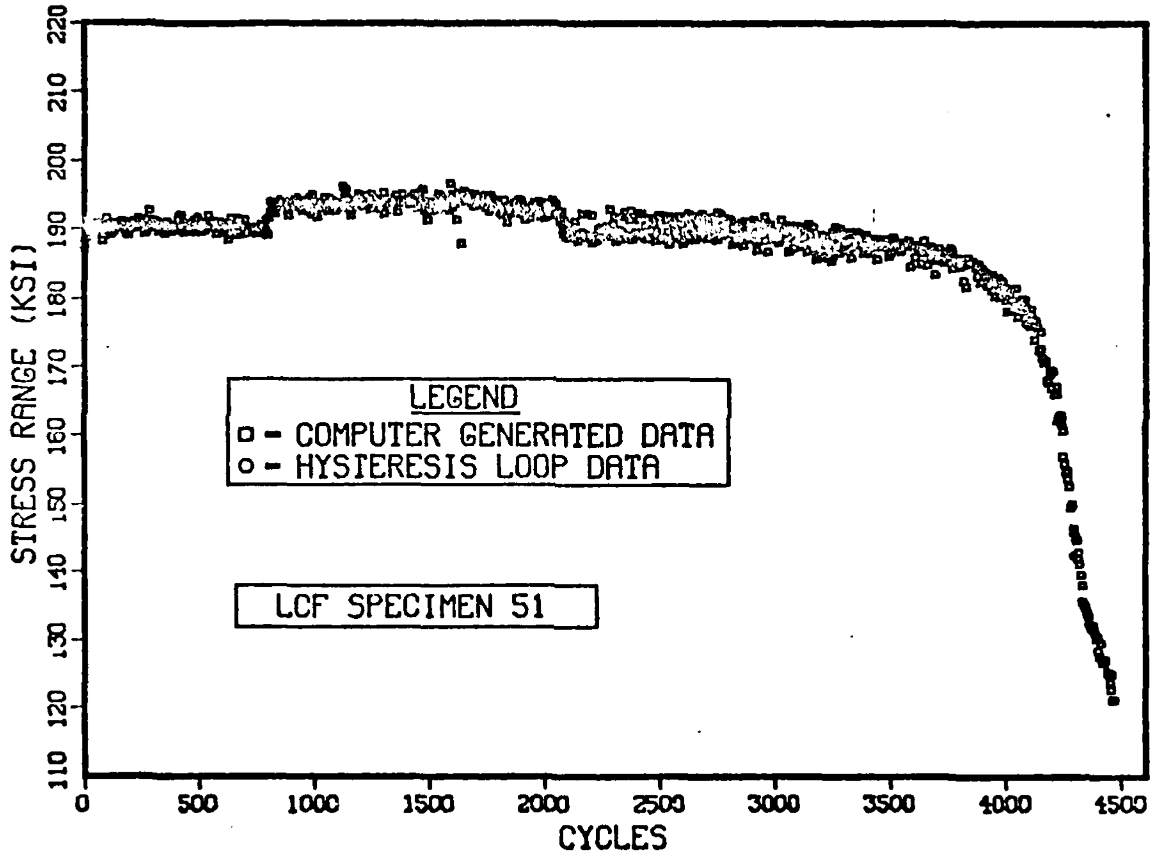

Figure 89. Plot of Stress Range vs Cycles - LCF Specimen 51

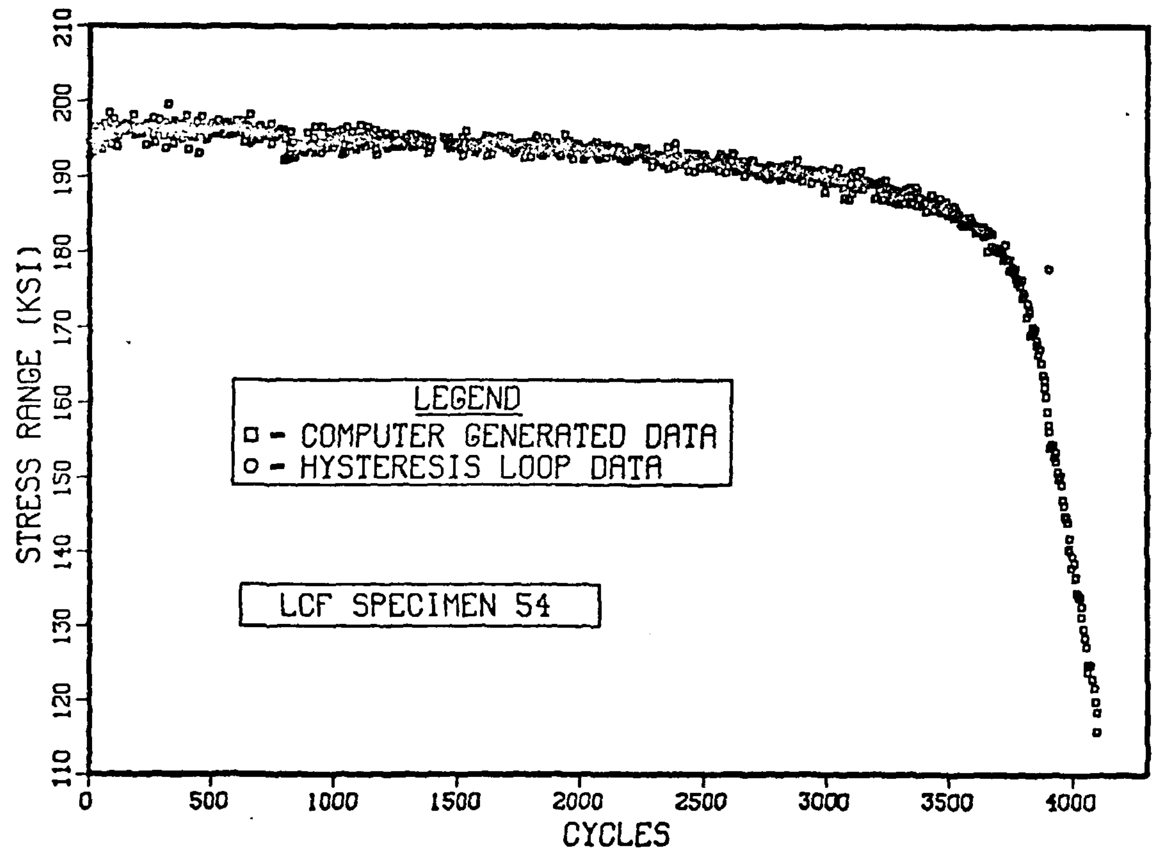

Figure 90. Plot of Stress Range vs Cycles - LCF Specimen 54

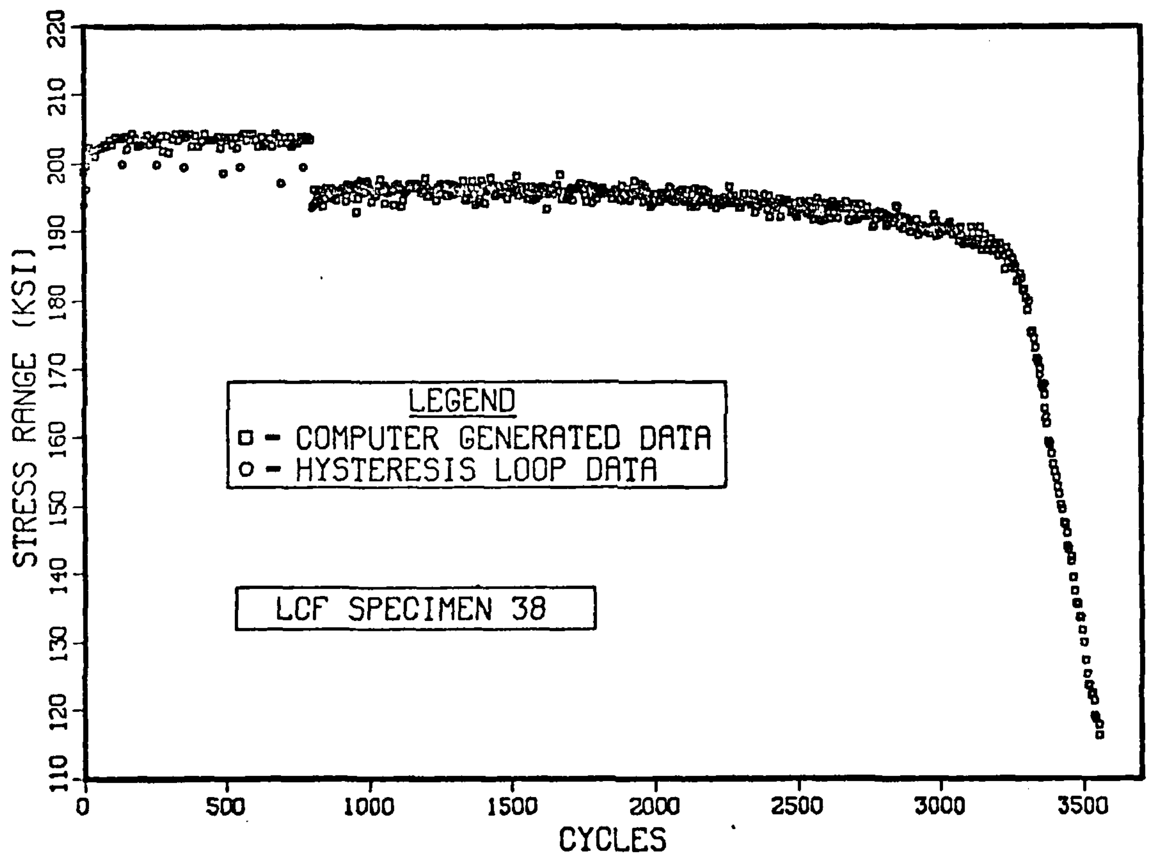

Figure 91. Plot of Stress Range vs Cycles - LCF Specimen 38

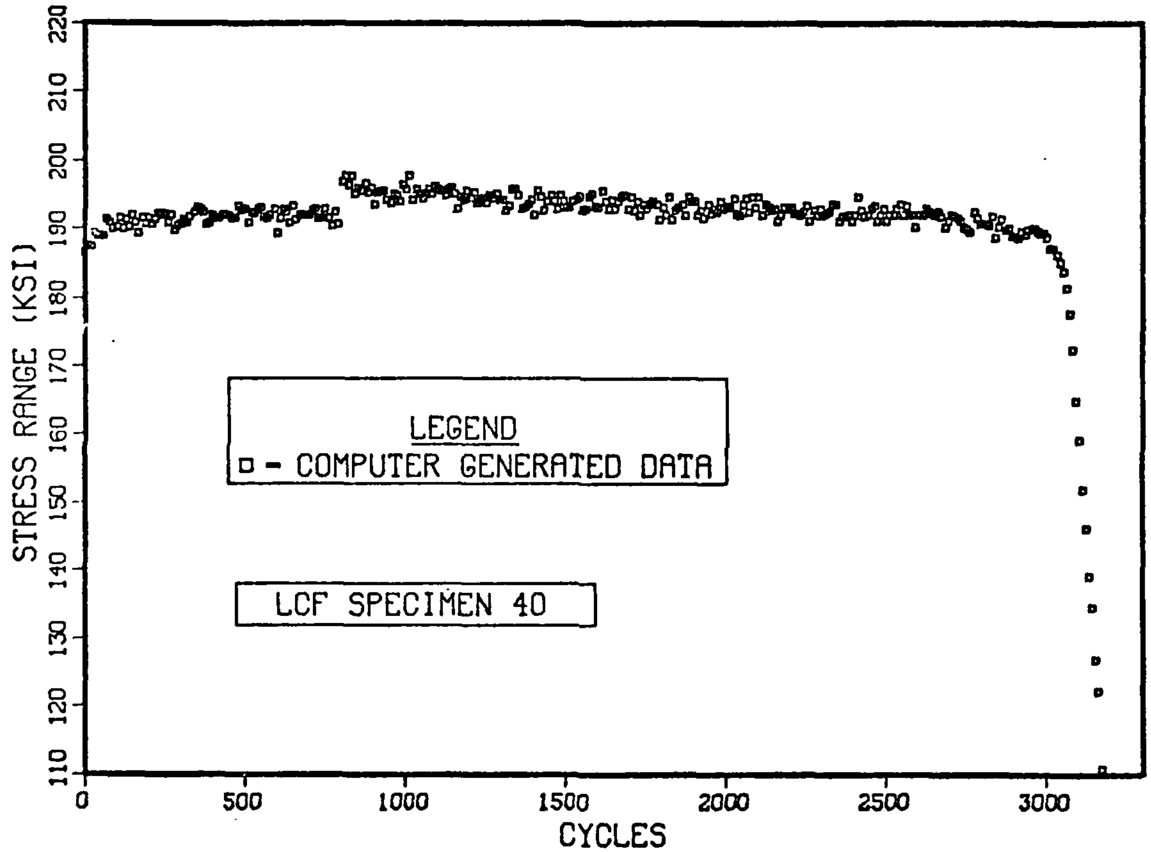

Figure 92. Plot of Stress Range vs Cycles - LCF Specimen 40

blocky carbides in the grain boundary began to decohere (Figure 51), and extrusions at persistent slip bands occurred (Figure 50). This is not the type of damage that thermal treatment can remove.

SEM photomicrographs of the gauge section of the the:mally rejuvenated specimens after N_f revealed extensive cracking and decohering of inclusions. A typical example is shown in Fig. 93 from LCF Specimen 42.

LCF Specimen 31 was damaged in LCF at 500^{o}F at a total strain range of 0.75% (stabilized stress range was 191 ksi). The gauge section was cut in two. Foils were made from one half for TEM investigation. The other half was given the thermal rejuvenation treatment, and the foils were prepared for TEM investigation. Figure 94 shows a network of dislocations beginning to form after 800 cycles. Figure 95, after the thermal treatment, shows that most of the dislocations have been annealed out.

The previous results were for a single rejuvenation treatment. In an attempt to determine the effect of multiple rejuvenations, LCF Specimen 41 was subjected to multiple blocks of 803 cycl of LCF damage plus thermal rejuvenation. The plot of Stress Range vs Cycles is contained in Figure 96. Table 16 summarizes the LCF data. Note that the thermal rejuvenation treatments seemed to have forestalled the onset of crack initiation as determined by the asymmetric load dropoff, but once the dropoff occurred, the crack progressed very rapidly. The surface of this specimen was examined in the SEM after the second block of 803 cycles (i.e., after 1606 cycles) and after failure. Figure 97 shows photomicrographs taken after 1606 cycles. Figure 97(a) shows the development of persistent slip bands

TABLE 16

SUMMARY OF LCF DATA FOR MULTIPLE THERMAL REJUVENATION - LCF SPECIMEN 41

Prior Damage Cycles	Strain Range (%)			Stress Range (ksi)	Cycles				
	$\Delta\varepsilon_t$	$\Delta\varepsilon_p$	$\Delta\varepsilon_e$		N_i	N_i'	N_f	N_i/N_f	N_i'/N_f
0	0.76	0.05	0.71	197.0	-	-	-	-	-
803	0.77	0.07	0.70	201.0	-	-	-	-	-
1606	0.77	0.06	0.71	193.0	-	-	-	-	-
2409	-	-	-	195.5	2500	2700	3134	0.80	0.86

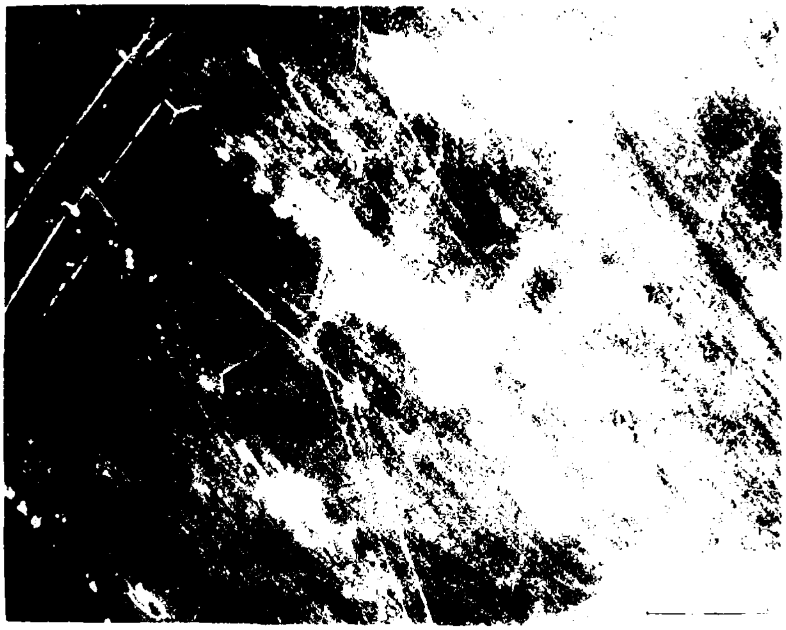

a. General Appearance of Cracking

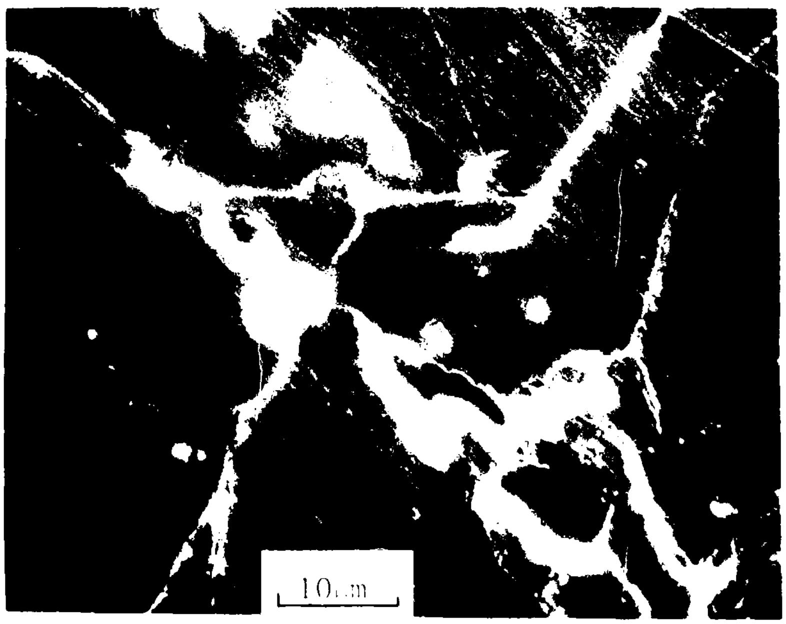

b. Decohered Inclusions and Cracking

Figure 93. SEM Micrograph, Cracking at Inclusions - LCF Specimen 42

Figure 94. TEM Micrograph, Dislocation Network after 800 Cycles - LCF Specimen 31

Figure 95. TEM Micrograph, Annealed Dislocation Network - ICF Specimen 31

AD-A107 255 AIR FORCE INST OF TECH WRIGHT-PATTERSON AFB OH F/G 11/6
MECHANISMS OF RECOVERING LOW CYCLE FATIGUE DAMAGE IN INCOLOY 90--ETC(U)
1979 R E SCHAFRIK
UNCLASSIFIED AFIT-CI-79-212D NL

3 of 3

END
DATE FILMED
12-81
DTIC

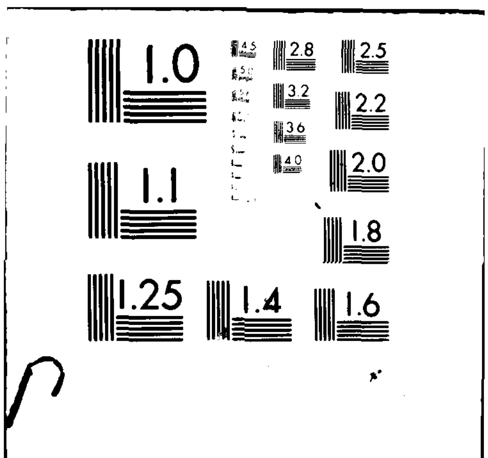

MICROCOPY RESOLUTION TEST CHART

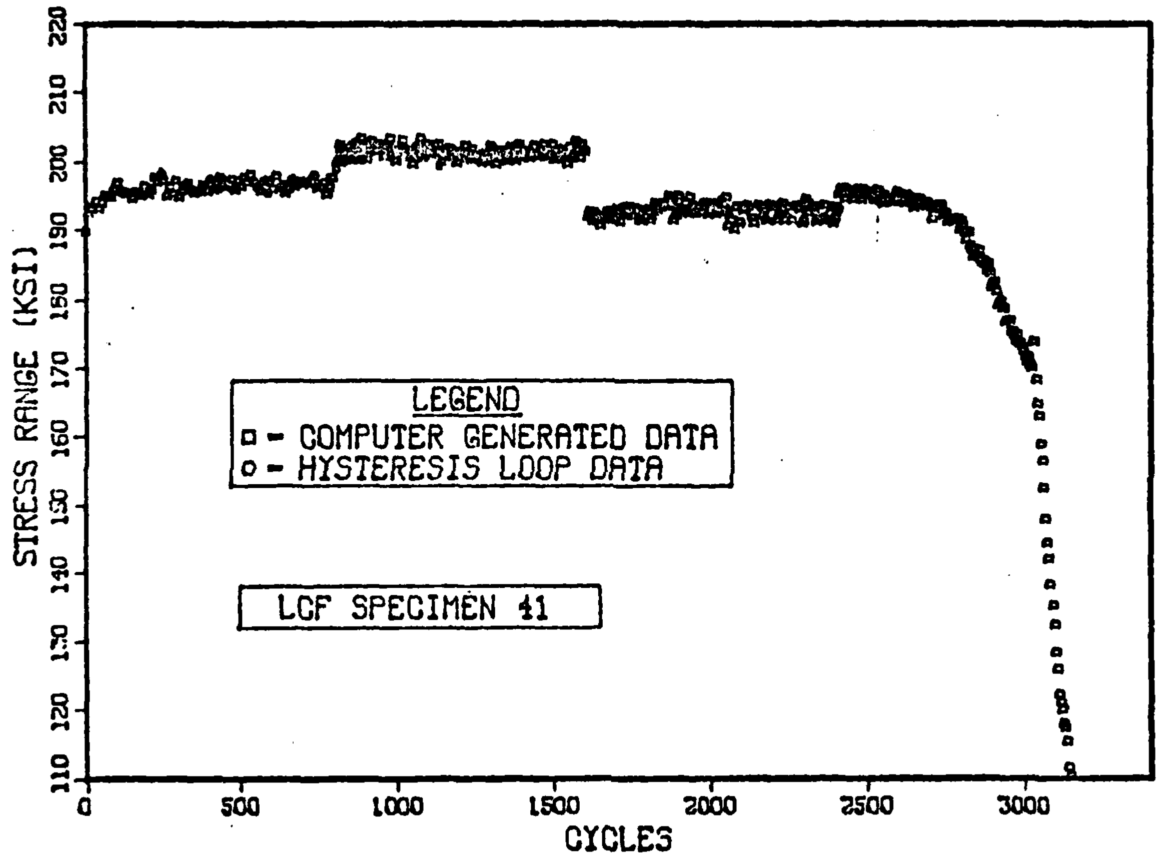

Figure 96. Plot of Stress Range vs Cycles - LCF Specimen 41

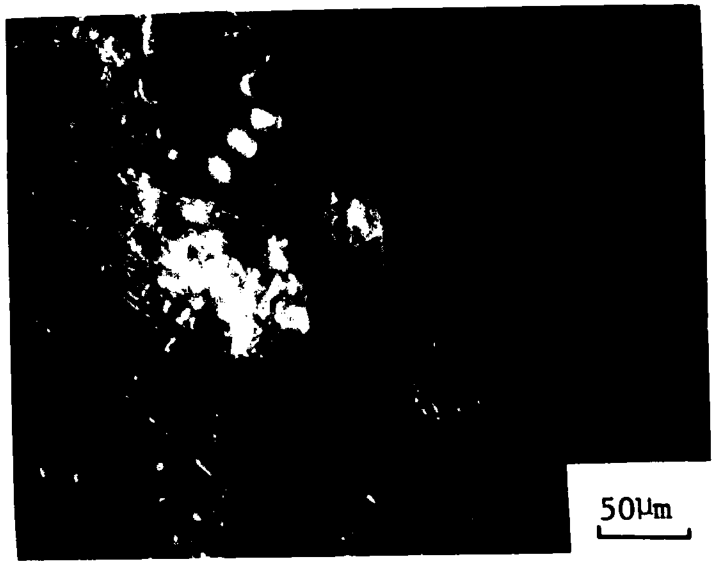

a. General Appearance of Cracking

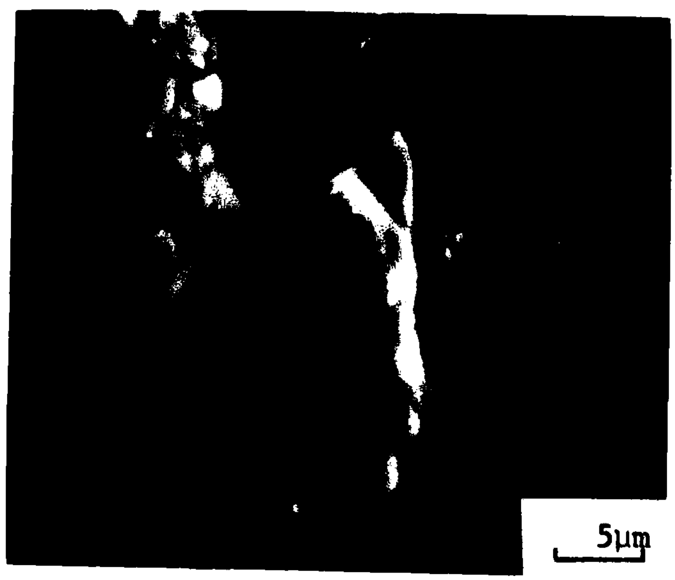

b. Decohered Inclusion

Figure 97. SEM Micrograph, Surface Cracking after 1606 Cycles - LCF Specimen 41

Figure 97 (continued)

c. Possible Cracked Grain Boundary

and the effect of polishing a group of carbides. Figure 97(b) shows a blocky grain boundary carbide in the process of decohering. Figure 97 (c) shows a grain boundary beginning to crack or form a ledge. Figure 98 are photomicrographs taken after failure. Figure 98(a) shows extensive deformation and cracking in a region near the principle crack. Figure 98(b) is a typical area located at some distance from the main crack. The grain boundary cracking and persistent slip bands are readily apparent. Note that the total life for LCF Specimen 41 was the same as could be expected for a baseline specimen. Thus, no overall rejuvenation was accomplished although the onset of gross microcracking may have been significantly retarded.

ii. Mechanisms

The rejuvenation effect of the thermal treatment was primarily due to the recovery of dislocations in the persistent slip bands and the deformation zone along the grain boundary. The fact that dislocation recovery can occur at elevated temperatures is well established, and several mechanisms have been postulated (55,56,57). Thus, after thermal rejuvenation and during subsequent testing, the planar dislocation arrays must re-form the persistent slip bands and the deformation zone along the grain boundary must be re-established. Also, the γ' precipitates which were sheared and possibly disordered are restored to their original distribution and morphology (65). The result is that the processes which lead to the decohering of the blocky grain boundary carbides are retarded. However, the decohering itself is not repaired by thermal treatment. Nor are the voids healed on the interior of a persistent slip band which developed intrusions and extrusions.

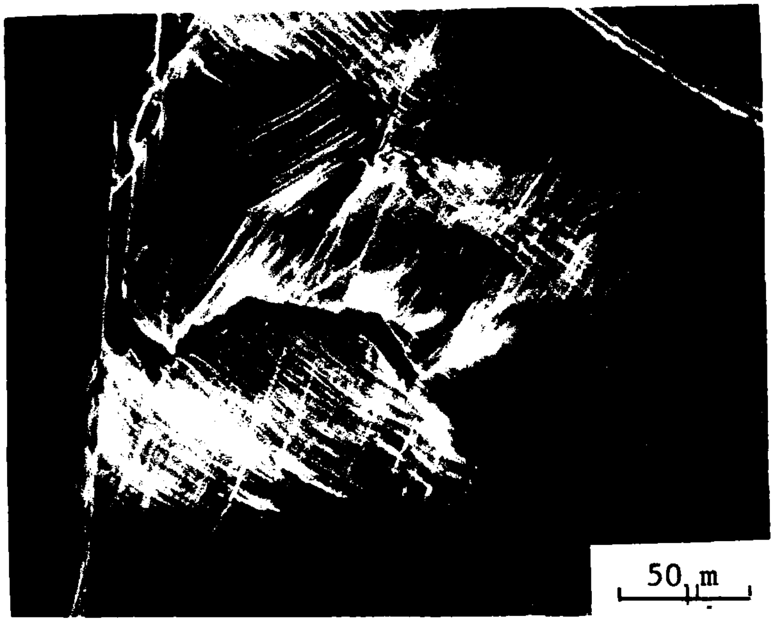

a. Surface Deformation Near Crack

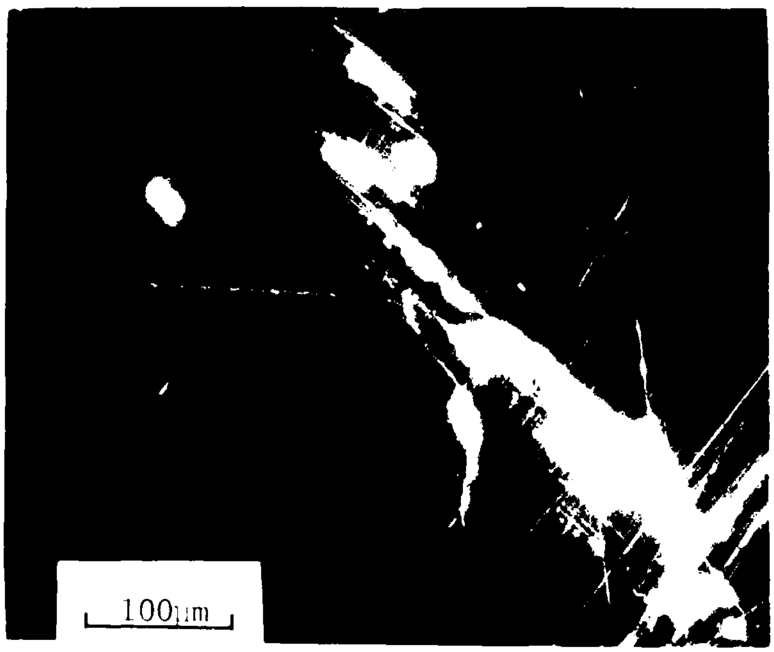

b. General Cracking

Figure 98. SEM Micrograph, Cracking after Failure - LCF Specimen 41

Also, the rejuvenation process acts to disperse slip throughout the gauge section, leading to a greater number of decohering carbides. Thus, when microcracks begin to propagate, they readily link up, leading to an accelerated crack growth rate. If the grain boundaries are simultaneously weakened during the thermal rejuvenation processing, such as by contamination from a poor vacuum, crack growth is accelerated even more.

C. Conclusions

Table 17 summarizes the cycles to crack initiation as a function of the processing, and Table 18 similarly summarizes the cycles to failure. It is evident that the data for the repolishing treatment alone belongs to the same population as the baseline data. The vapor-honed plus repolished data indicates crack initiation at about 400 cycles earlier than the baseline data, and less than half the total lifetime to failure. The HIP samples did not show any rejuvenation of LCF properties. The uncoated HIP specimens performed slightly worse than the coated HIP specimens. Crack initiation for the HIP samples (with 800 cycles of pre-HIP damage) occurred at about the same point as for the baseline specimens. But failure occurred 1300-1500 cycles earlier than the baseline data. Also, the data indicates that failure occurred within about 1600 cycles after HIP processing regardless of the level of initial damage (Table 12). The conclusion is that vapor honing and HIP processing damaged the surface of the test specimens. Vapor honing caused fracturing and decohering of blocky grain boundary carbides. Ceramic-coated plus HIP specimens not only had the deleterious effects of the vapor-honing induced damage, but also contamination due to reaction

TABLE 17

SUMMARY OF CYCLES TO CRACK INITIATION

0.70-0.80 TOTAL STRAIN RANGE

500 F TEST TEMPERATURE

		Treatment					
	Baseline	Repolish	Vapor Honed	HIP-Bare	HIP-Coated	Thermal	Thermal
Prior Damage (cycles)	0	803	0	800	800	800-803	400
No. of Data Points	8	2	2	4	3	5*	1
Mean	1388	1438	1000	1338	1433	1840	1800
Standard Deviation	448	194	141	396	301	114	-

*Excludes LCF Specimen 13

TABLE 18

SUMMARY OF CYCLES TO FAILURE

0.70-0.80 TOTAL STRAIN RANGE

500 F TEST TEMPERATURE

		Treatment					
	Baseline	Repolish	Vapor Honed	HIP-Bare	HIP-Coated	Thermal	Thermal
Prior Damage (cycles)	0	803	0	800	800	800-803	400
No. of Data Points	8	2	2	4	3	5*	1
Mean	3568	3384	1750	2246	2410	4198	3333
Standard Deviation	401	252	346	290	683	895	-

*Excludes LCF Specimen 13

between the ceramic coating and the superalloy. The uncoated HIP specimens were badly contaminated from impure argon in the HIP unit.

The thermally rejuvenated specimens definitely showed some rejuvenation. Those specimens damaged to 800 cycles before rejuvenation increased their initiation time by about 450 cycles and their total lifetime by about 630 cycles on the average (but note the high standard deviation in Table 18). The specimen predamaged 400 cycles before rejuvenation increased its initiation time by 400 cycles, but no increase in total lifetime was obtained. The experience with multiple rejuvenation (Table 16) indicates that damage accumulation in the form of decohering carbides, which are not affected by thermal treatments, leads to eventual very rapid crack extensions.

Chapter 4

SUMMARY

The mechanisms of crack initiation and growth in strain-controlled low cycle fatigue (LCF) damage were determined for the iron-nickel superalloy, Incoloy 901. Testing was done in air at a temperature of 500°F (260°C) and total strain range of 0.75%. The effect of hot isostatic pressing (HIP) and thermal treatment in reducing LCF damage was investigated.

The LCF specimens were manufactured using a low stress grinding method to maintain surface quality. Specimens were hand polished along the axial direction through 4/0 emery paper. Prior to testing, all specimens were given a standard solution treatment and double age, referred to as STA 3A (Table 4), to insure the uniform precipitate morphology and distribution from specimen to specimen. The as-received grain size was 90 μm. After STA 3A, the grain size was increased to 120 μm, but remained stable after subsequent heating to the solutioning temperature. The 0.2% offset yield stress at 500°F was 122 ksi.

Initial LCF testing was conducted over the total strain range of 0.70% to 2.44%. The Cyclic Stress-Strain Curve (Figure 24) exhibited cyclic hardening at the high strain ranges and cyclic softening at the lower ranges. A log-log plot of Total Strain Range vs Cycles (Figure 26) exhibits a linear curve with a negative slope.

Crack initiation in the baseline specimens was due to the decohering of blocky grain boundary carbides. Pre-crack initiation damage consisted of planar dislocation arrays forming persistent slip bands and an intense deformation region adjacent to favorably oriented grain boundaries. The persistent slip bands formed intrusions and extrusions at a total strain range of 0.75% by 800 cycles (about 60% of crack initiation time). Stage I crack propagation occurred along the grain boundary or along a favorably oriented persistent slip band. Substantial Stage II crack propagation occurred, as evidenced by the formation of fatigue striations. Fractography revealed a mixed fracture mode, consisting of both intergranular and transgranular fracture.

The HIP-processed specimens were subjected to a HIP cycle of 2025°F for one hour and 1975°F for two hours at 15 ksi of argon (Figures 10 and 11). Both uncoated and ceramic-coated specimens were HIP'd. Specimens had pre-HIP LCF damage of 0 cycles, 800 cycles, and 2100 cycles. The HIP processing increased the grain size by 25%. The specimens were subjected to STA 3A to restore the original morphology and distribution of the precipitates. No rejuvenation occurred. In fact, the fatigue properties were worse than the baseline properties by a substantial amount. Even correcting for the grain size change utilizing a Hall-Petch-type equation, it is clear that the HIP processing itself produced surface-related damage in the microstructure. In fact, the HIP processing caused more damage than the LCF pre-HIP damage levels.

In the case of the ceramic-coated specimens, damage resulted from at least two sources: (1) vapor honing the specimen surface to provide a matte finish for the coating to adhere to, damaged the blocky carbides by decohering and cracking them; and (2) the ceramic coating reacted with the superalloy. As a consequence, intergranular cracking was promoted, and crack growth rates were greater than five times the rate in the baseline specimens.

The uncoated HIP specimens were damaged by contamination from the HIP atmosphere. Preferential formation of oxides and nitrides along the grain boundaries led to weakening of the boundaries. This promoted intergranular cracking, accelerated crack growth rates, and early failures. Overall, there was not much apparent difference between the behavior of the coated and uncoated specimens, although the coated ones were slightly superior.

Figure 99 plots the rejuvenation data and the trend line for the baseline data on a log-log plot of Total Strain Range vs Cycles to Failure.

The thermally rejuvenated specimens were given STA 3A after 800 cycles of damage. As long as the heat treating was done in a good vacuum so that surface contamination did not occur, partial rejuvenation was accomplished. Initiation life was increased by 400 cycles and the failure cycle was increased by 600 cycles. Complete rejuvenation was not attained because the grain boundary carbides had already begun to decohere after 800 cycles and persistent slip bands had formed intrusions and extrusions. When a specimen was rejuvenated three times after blocks of 803 cycles of damage, it failed catastrophically due to rapid crack extension. Thus, the unrecovered microstructural damage can adversely affect the fatigue life.

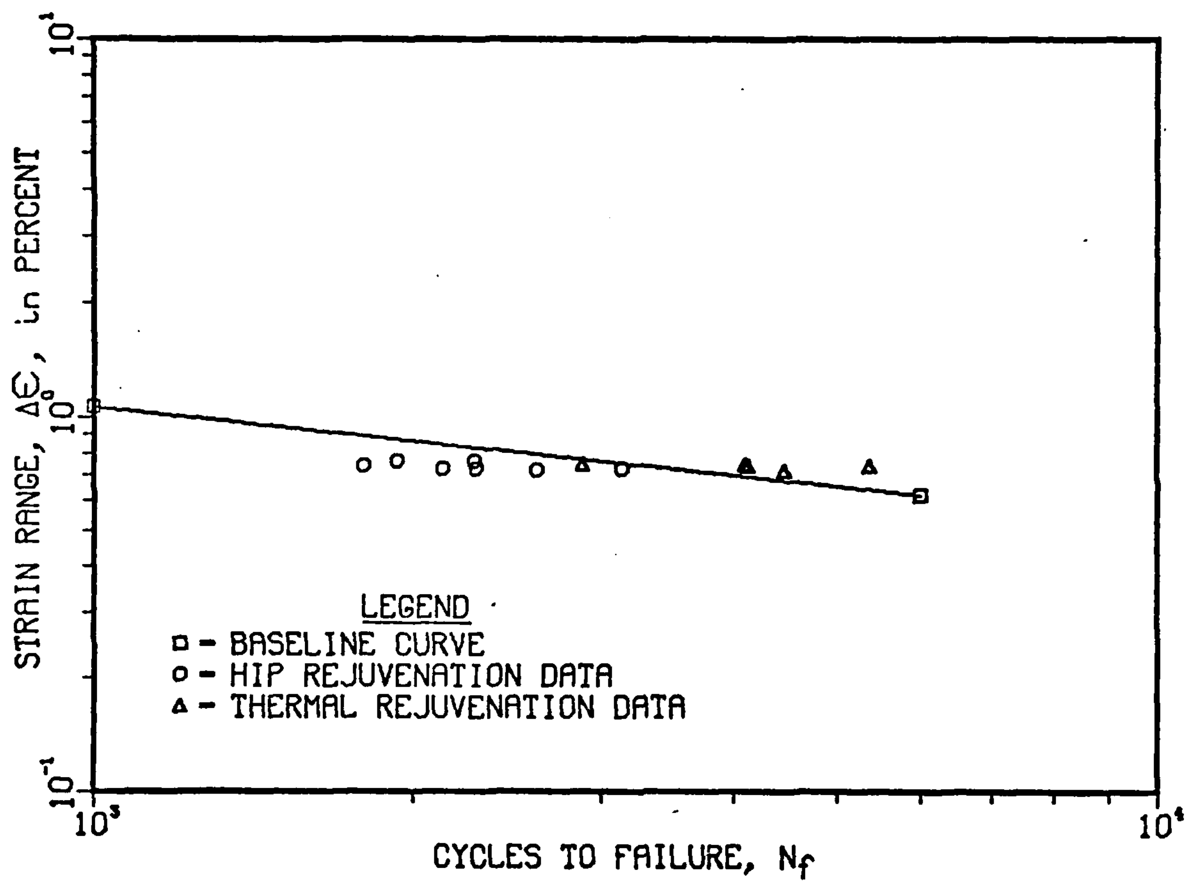

Figure 99. Plot of Strain Range vs Cycles to Failure with Baseline Trend Line and Rejuvenation Data

APPENDIX

LISTING OF COMPUTER PROGRAMS

APPENDIX I

SOURCE LISTING OF MODIFIED INSTRON LOW CYCLE FATIGUE APPLICATION PROGRAM APP-900-A3A8

PAGE 0001

```
************************************
*
*
*      LOW CYCLE FATIGUE
*
*      APP-900-A3A8+M0D2
*
*      04/04/75
*
*
************************************
*
*      COPYRIGHT INSTRON CORPORATION
*       DECEMBER  1974
*
*      MODIFIED BY STEVE LEFFLER &
*               BOB SCHAFRIK
*
*           4/13/79
*
***********************************
```

```
PAGE  0003                              LOW CYCLE FATIGUE

0039                    *
0040                    ****** BEGIN SECTION ******
0041                    *
0042  001B  F98E  BEGIN  ITBL TABLE1,33
      001C  0468
      001D  0021
0043  001E  F98E         ITBL TABLE2,33
      001F  0489
      0020  0021
0044  0021  F98E         ITBL TABLE3,23
      0022  04AA
      0023  0017
0045  0024  F98E         ITBL TABLE4,33
      0025  04C1
      0026  0021
0046  0027  F95E         INID BUFFID
      0028  053E
0047  0029  F947         FMOV F0,AUGSTN
      002A  006E
      002B  0450
0048  002C  F947         FMOV F0,DATPX AND DATPY
      002D  006E
      002E  0178
0049  002F  F997         JST  *GETSTA
0050  0030  EA8C         STX  INDEX1
0051  0031  9900         STA  INDEX     ALSO XB
            0172
0052  0032  C2B1         AXI  '1'
0053  0033  0E00         SEM
0054  0034  EB8D         STXB *CURSTP
0055  0035  0F00         SWM
0056  0036  F947         FMOV F1,FCYCLE
      0037  045E
      0038  043A
0057  0039  FA71         JST  INITCY
0058  003A  F90F         CRLF
0059  003B  F909         TYPE MAREA     ASK AREA DIMS.
      003C  04F7
0060  003D  F93D         IFLT FTHICK    GET THICKNESS
      003E  043C
0061  003F  F93D         IFLT FWIDTH    GET WIDTH
      0040  043E
0062  0041  F90F         CRLF
0063  0042  F948         FCMP FWIDTH,F0
      0043  043E
      0044  006E
0064  0045  2105         JAZ  ROUND     ZERO = ROUND
0065  0046  F943         FMPL FTHICK,FWIDTH,FAREA
      0047  043C
      0048  043E
      0049  0442
0066  004A  F20C         JMP  CLEAR1
0067  004B  F944  ROUND  FDVD FTHICK,F2,FAC1
```

```
PAGE  0002                              LOW CYCLE FATIGUE

0023  0000                   REL  0
0024                  *
0025                  ****** SSP-LINKAGE ******
0026                  *
0027  0000  0007             DATA NAME
0028  0001  001B             DATA BEGIN
0029  0002  00D6             DATA RESTRT
0030  0003  017A             DATA UPDATE
0031  0004  027A             DATA FINAL
0032  0005  0266             DATA STAT:A
0033  0006  0269             DATA STAT:B
0034                  *
0035  0007  C1D0  NAME       TEXT 'APP-900-A3'
      0008  D0AD
      0009  B9B0
      000A  B0AD
      000B  C1B3
0036  000C  C1B8             TEXT 'A8+MOD2'
      000D  ABCD
      000E  CFC4
      000F  B2A0
0037  0010  A0A0             TEXT '  LOW CYCLE FATIGUE@'
      0011  A0CC
      0012  CFD7
      0013  A0C3
      0014  D9C3
      0015  CCC5
      0016  A0C6
      0017  C1D4
      0018  C9C7
      0019  D5C5
      001A  C0A0
```

```
PAGE  0004                            LOW CYCLE FATIGUE

      004C  043C
      004D  0070
      004E  0426
0068  004F  F943          FMPL FAC:1,FAC:1,FAC:1
      0050  0426
      0051  0426
      0052  0426
0069  0053  F943          FMPL FAC:1,F:PI,FAREA
      0054  0426
      0055  007A
      0056  0442
0070  0057  F909  CLEAR1  TYPE MSTRLM    ASK STRAIN LIMITS
      0058  050D
0071  0059  F93D          IFLT MAXLIM    MAX. LIMIT
      005A  0446
0072  005B  F93D          IFLT MINLIM    MIN. LIMIT
      005C  0448
0073  005D  E100          LDX  XABC
            0170
0074  005E  F944          FDVD MAXLIM,*STVALP,HLIMIT
      005F  0446
      0060  80B4
      0061  00BE
0075  0062  F944          FDVD MINLIM,*STVALP,LLIMIT
      0063  0448
      0064  80B4
      0065  00C0
0076              ***
0077  0066  F90F          CRLF
0078  0067  F909          TYPE RNDMES    RANDOM LIMITS?
      0068  0518
0079  0069  F90B          IKB
0080  006A  C0AC          CAI  ','       LEAVE AS IS?
0081  006B  F20A          JMP  CLEAR2    YES
0082  006C  C0D9          CAI  'Y'
0083  006D  F202          JMP  RNDMLT
0084  006E  0110          ZAR            RQSTD/ASSMD NO
0085  006F  F201          JMP  $+2
0086  0070  0350  RNDMLT  ARP            SET RANDOM FLAG
0087  0071  9900          STA  RNDFLG    -
            0175
0088  0072  F90B  WTCLR   IKB            TERMINATION CHAR?
0089  0073  C0AC          CAI  ','
0090  0074  F201          JMP  CLEAR2
0091  0075  F603          JMP  WTCLR     NO
0092              ***
0093  0076  B2FE  CLEAR2  LDA  RNDFLG
0094  0077  3105          JAN  CLR2
0095  0078  F90F          CRLF
0096  0079  F909          TYPE MNSTRS    ASK MIN. STRESS
      007A  0503
0097  007B  F93D          IFLT STRSLM    GET STRESS LIMIT
      007C  0444
```

```
0098  007D  F944  CLR2   FDVD HLIMIT,F32767,HRNGE
      007E  00BE
      007F  0074
      0080  0452
0099  0081  F944         FDVD LLIMIT,F32767,LRNGE
      0082  00C0
      0083  0074
      0084  0454
0100  0085  F945         FIX  HLIMIT,HLIMIT
      0086  00BE
      0087  00BE
0101  0088  F945         FIX  LLIMIT,LLIMIT
      0089  00C0
      008A  00C0
0102  008B  F947         FMOV F1,NN
      008C  045E
      008D  0458
0103  008E  F947         FMOV F0,XX      CALC. MD AFTER
      008F  006E
      0090  045A
0104               * GET CYCLE #'S & INCREMENTS
0105  0091  F90F         CRLF
0106  0092  F909         TYPE NMMESS
      0093  00CC
0107  0094  F93D         IFLT FNM1
      0095  00C4
0108  0096  F93D         IFLT FNM2
      0097  00C6
0109  0098  F93D         IFLT FNM3
      0099  00C8
0110  009A  F90F         CRLF
0111  009B  0010         ARM             1 PASS INITIALLY
0112  009C  9ADA         STA  CNT
0113  009D  9AD5         STA  XC         NEEDED FOR FINAL
0114  009E  C70A         LAM  10
0115  009F  9AC9         STA  CNTN1      INITIALIZE
0116  00A0  B2CA         LDA  NUM1       SLOPE ROUTINE
0117  00A1  9ACA         STA  NUM
0118  00A2  9A95         STA  DLTLD
0119  00A3  8A97         ADD  I300
0120  00A4  9A97         STA  LOAD2
0121  00A5  0110         ZAR
0122  00A6  9900         STA  BRANCH
            01C7
0123  00A7  9AD0         STA  DATPX
0124  00A8  9AD0         STA  DATPY
0125  00A9  9AC3         STA  MDFLG
0126  00AA  F22B         JMP  RESTRT
```

```
PAGE  0006                          LOW CYCLE FATIGUE

0128  00AB  0000  INITCY ENT
0129  00AC  0350         ARP
0130  00AD  9AC3         STA  XBPT      OR XA
0131  00AE  F947         FMOV F1,CMPTBL
      00AF  045E
      00B0  058A
0132  00B1  F947         FMOV F2,CMPTBL+2
      00B2  0070
      00B3  058C
0133  00B4  F941         FADD F1,F2,F3
      00B5  045E
      00B6  0070
      00B7  00CA
0134  00B8  F947         FMOV F3,CMPTBL+4
      00B9  00CA
      00BA  058E
0135  00BB  DABC         IMS  DATPX     PRINT FIRST CYCLE
0136  00BC  F711         RTN  INITCY
0137              *
0138              *
0139              *
0140  00BD  0000  INDEX1 DATA 0
0141  00BE  0000  HLIMIT RES  2,0
0142  00C0  0000  LLIMIT RES  2,0
0143  00C2  0000  CURSTP BAC  STANUM+9
0144  00C3  00D9  ANDM   DATA 'Y'
0145  00C4  0000  FNM1   RES  2,0      CUT-OFF CYCLE 1 INC
0146  00C6  0000  FNM2   RES  2,0      INCREMENT TWO
0147  00C8  0000  FNM3   RES  2,0      LAST CYCLE
0148  00CA  0000  F3     RES  2,0
0149  00CC  C5CE  NMMESS TEXT 'ENTER NM1,NM2,NM3:@'
      00CD  D4C5
      00CE  D2A0
      00CF  CECD
      00D0  B1AC
      00D1  CECD
      00D2  B2AC
      00D3  CECD
      00D4  B3BA
      00D5  C0A0
```

```
                    *
                    ****** RESTART SECTION ******
                    *
00D6  F93D  RESTPT  STOP
00D7  B29D          LDA  RNDFLG    RANDOM LIMITS
00D8  2114          JAZ  RSTEX     NO
00D9  F90F          CRLF
00DA  F909          TYPE RESETM    RESET RANDOM SEQUENCE
00DB  0531
00DC  F90B          IKB
00DD  0048          TAX
00DE  C0AC          CAI  ','       DO THE SAME AS LAST TIME?
00DF  F20B          JMP  SAME2     YES
00E0  EE1D          STX  RNDM
00E1  C0CE  RESET1  CAI  'N'       RESET SEQUENCE?
00E2  F202          JMP  RSTRT0    NO
00E3  C603          LAP  3         YES
00E4  9B3F          STA  *RN1PTR
00E5  C1AC  RSTRT0  CXI  ','       SAME AS LAST TIME?
00E6  F206          JMP  RSTEX     YES
00E7  F90B          IKB            INPUT TERMINATION?
00E8  C0AC          CAI  ','
00E9  F203          JMP  RSTEX
00EA  F605          JMP  RSTRT0    NO, KEEP WAITING
00EB  B628  SAME2   LDA  RNDM
00EC  F60B          JMP  RESET1
                    *
00ED  F90F  RSTEX   CRLF
00EE  F909          TYPE MRATE
00EF  0522
00F0  F93D          IFLT SRRATE
00F1  044A
00F2  F90F          CRLF
00F3  E27C          LDX  XABC
00F4  F944          FDVD SRRATE,*STVALP,CLKRT
00F5  044A
00F6  80B4
00F7  044C
00F8  F90F          CRLF
00F9  F913          RATE CLKRT     SET TIME VALUE
00FA  044C
00FB  E274          LDX  XABC      FORCE INDEX IN XA
00FC  0128          IXR
00FD  F944          FDVD *LDVALP,FAREA,STRESV
00FE  80A0
00FF  0442
0100  044E
0101  F944          FDVD STRSLM,STRESV,STRESS
0102  0444
0103  044E
0104  0272
0105  F945          FIX  STRESS,STRESS
0106  0272
```

PAGE 0008 LOW CYCLE FATIGUE

```
0107  0272
0108  F912          MODE STROKE
0109  0001
010A  F90F          CRLF
010B  F909          TYPE MEXEC     PRINT EXECUTE
010C  052D
010D  F90F          CRLF
010E  F909          TYPE MHEAD
010F  0558
0110  F90F          CRLF
0111  F951          CLOS
                *
0112  0800  SETTBL ENT
0113  DA64          IMS  DATPX     PRINT ALL TRIGGER CYCLES
                * STORE CURRENT CYCLE - END OF TEST?
0114  F947          FMOV FCYCLE,FTCYC
0115  043A
0116  013F
0117  F948          FCMP FNM3,F0  SEE IF DEFAULT
0118  00C8
0119  006E
011A  2104          JAZ  SETTB2
011B  F948          FCMP FTCYC,FNM3 LAST CYCLE?
011C  013F
011D  00C8
011E  3095          JAP  INCDNE
011F  B251  SETTB2 LDA  XBPT
0120  0150          IAR
0121  C004          CAI  4
0122  F202          JMP  INCTBL
0123  9A4D          STA  XBPT
0124  F712          RTN  SETTBL
0125  0350  INCTBL ARP
0126  9A4A          STA  XBPT
0127  FA19  INCTB2 JST  CYADJ
0128  F947          FMOV FTCYC,CMPTBL
0129  013F
012A  058A
012B  FA15          JST  CYADJ
012C  F947          FMOV FTCYC,CMPTBL+2
012D  013F
012E  058C
012F  FA11          JST  CYADJ
0130  F947          FMOV FTCYC,CMPTBL+4
0131  013F
0132  058E
0133  F721          RTN  SETTBL
0134  0010  INCDNE ARM
0135  9A91          STA  BRANCH   FINI
0136  F956          EXIT
                *
0137  0000  OLDLD  DATA 0
0138  0000  DLTLD  DATA 0
```

```
PAGE  ØØØ9                          LOW CYCLE FATIGUE

Ø227  Ø139  ØØØØ  DLTSTN DATA Ø,Ø
      Ø13A  ØØØØ
Ø228  Ø13B  Ø12C  I3ØØ   DATA 3ØØ
Ø229  Ø13C  ØØØØ  LOAD2  DATA Ø
Ø23Ø  Ø13D  ØØØØ  CUPLD  DATA Ø
Ø231  Ø13E  ØØØØ  CUPSTN DATA Ø
Ø232  Ø13F  ØØØØ  FTCYC  RES  2,Ø       CYCLE VALUE
Ø233              *
Ø234              * ADJUST CYCLE TRIGGER VALUE
Ø235  Ø141  Ø8ØØ  CYADJ  ENT
Ø236  Ø142  F948         FCMP FTCYC,FNM1 SEE IF INC BY 1
      Ø143  Ø13F
      Ø144  ØØC4
Ø237  Ø145  3Ø85         JAP  CYAD2     INC BY MORE
Ø238  Ø146  F941         FADD F1,FTCYC,FTCYC
      Ø147  Ø45E
      Ø148  Ø13F
      Ø149  Ø13F
Ø239  Ø14A  F2Ø4         JMP  CYAD3
Ø24Ø  Ø14B  F941  CYAD2  FADD FNM2,FTCYC,FTCYC INC BY FNM2
      Ø14C  ØØC6
      Ø14D  Ø13F
      Ø14E  Ø13F
Ø241  Ø14F  F7ØE  CYAD3  RTN  CYADJ
Ø242              *
Ø243              *
```

```
PAGE 0010                         LOW CYCLE FATIGUE

                  *
0150  B218  N1      LDA  CNTN1
0151  2103          JAZ  N1X
0152  B219          LDA  NUM
0153  9616          SUB  CURLD     SAVE POINTS
0154  2031          JAM  DATN1
0155  F236  N1X     JMP  NOT1
0156  B214  DATN1   LDA  NUM1      OF LOAD
0157  8A14          ADD  NUM
0158  9A13          STA  NUM       AND STRAIN
0159  B61C          LDA  CURLD
015A  F991          GIVE TABLE3
015B  04AA
015C  F206          JMP  FULLN1
015D  B61F          LDA  CURSTN    IN 5%
015E  F991          GIVE TABLE3
015F  04AA
0160  F202          JMP  FULLN1
0161  DA07          IMS  CNTN1
0162  F279          JMP  NOT1
0163  0110  FULLN1  ZAR
0164  9A04          STA  CNTN1     SLOPE
0165  F957          CUE  SLOPE:,1000
0166  03B9
0167  03E8
0168  F273          JMP  NOT1
                  *
0169  0000  CNTN1   DATA 0         CALCULATION
016A  0190  BPEAK   DATA 400       20% FS
016B  0064  NUM1    DATA 100
016C  0000  NUM     DATA 0
016D  0000  MDFLG   DATA 0
016E  0000  UTEMP1  DATA 0
016F  0000  UTEMP2  DATA 0
0170  0171  XABC    DATA $+1
0171  0000  XBPT    DATA 0         OR XA
0172  0000  INDEX   DATA 0         OR XB
0173  0000  XC      DATA 0
      0004  VALPTR  EQU  :4
0174  0385  PN1PTR  DATA PN1
0175  0000  PNDFLG  DATA 0
0176  0368  GETNUM  DATA RANDOM
0177  0000  CNT     DATA 0
0178  0000  DATPX   DATA 0
0179  0000  DATPY   DATA 0
```

```
                        *

PAUSE
                        *
                        ****** UPDATE SECTION ******
                        *
       017A  F910   UPDATE READ LOAD,CURLD
       017B  0000
       017C  013D
       017D  F910          READ STROKE,CURSTN
       017E  0001
       017F  013E
       0180  B246          LDA  BRANCH
       0181  3081          JAP  $+2        IF < 0 THEN
       0182  F95F          DONE            REQUESTED DONE
       0183  3181          JAG  $+2
       0184  F243          JMP  UP:
       0185  E6C8          LDX  INDEX1
       0186  B648          LDA  CURSTN
       0187  9504          SUB  @*VALPTR
       0188  D61E          CMS  BREAK
       0189  F202          JMP  $+3
       018A  0000          NOP
       018B  F95F          DONE
       018C  B64E          LDA  CURSTN
       018D  D6CD          CMS  LLIMIT
       018E  F206          JMP  REVUP
       018F  0000          NOP
       0190  B653          LDA  CURLD
       0191  9E5A          STA  OLDLD
       0192  F911          RAMP DOWN
       0193  8000
       0194  F956          EXIT
                        *
       0195  B61C   REVUP  LDA  DATRY
       0196  210A          JAZ  XX3
       0197  B659          LDA  CURSTN
       0198  BE29          EMA  UTEMP2
       0199  0048          TAX
       019A  B65D          LDA  CURLD
       019B  BE2D          EMA  UTEMP1
       019C  F957          CUE  PRINT,2900
       019D  02F6
       019E  0B54
       019F  0110          ZAR
       01A0  9E27          STA  DATRY
       01A1  E631   XX3    LDX  XABC
       01A2  F948          FCMP *CMPTBL,FCYCLE
       01A3  858A
       01A4  C43A
       01A5  3189          JAG  DATA01     FILL TABLE UNLESS CYCLE <
       01A6  B669          LDA  CURLD      VALUE SOUGHT
       01A7  0000          NOP
       01A8  0000          NOP
       01A9  0000          NOP
```

```
PAGE  0012                            LOW CYCLE FATIGUE

0331  01AA  B66C          LDA   CURSTN
0332  01AB  0000          NOP
0333  01AC  0000          NOP
0334  01AD  0000          NOP
0335  01AE  FE9C          JST   SETTBL
0336  01AF  F941  DATA01  FADD  FI,FCYCLE,FCYCLE
      01B0  045E
      01B1  043A
      01B2  043A
0337  01B3  B67C          LDA   OLDLD
0338  01B4  8E49          ADD   NUM1
0339  01B5  9E7D          STA   DLTLD
0340  01B6  8E7B          ADD   I302
0341  01B7  9E7B          STA   LOAD2
0342  01B8  F911          RAMP  UP
      01B9  0000
0343  01BA  B645          LDA   RNDFLG
0344  01BB  2108          JAZ   RMPUP
0345  01BC  FF46          JST   *GETNUM
0346  01BD  F943          FMPL  HRNGE,RNDTMP,HLIMIT
      01BE  0452
      01BF  0456
      01C0  00BE
0347  01C1  F945          FIX   HLIMIT,HLIMIT
      01C2  00BE
      01C3  00BE
0348  01C4  0110  RMPUP   ZAR
0349  01C5  9A01          STA   BRANCH
0350  01C6  F956          EXIT
0351              *
0352  01C7  0000  BRANCH  DATA  0
0353              *
0354  01C8  E100  UP:     LDX   INDEX1
            00BD
0355  01C9  B504          LDA   @*VALPTR
0356  01CA  968C          SUB   CURSTN
0357  01CB  D661          CMS   BREAK
0358  01CC  F202          JMP   $+3
0359  01CD  0000          NOP
0360  01CE  F95F          DONE
0361  01CF  B100          LDA   HLIMIT
            00BE
0362  01D0  D692          CMS   CURSTN
0363  01D1  F24C          JMP   REVDUN
0364  01D2  0000          NOP
0365  01D3  B696          LDA   CURLD
0366  01D4  9E9D          STA   OLDLD
0367  01D5  F911          RAMP  UP
      01D6  0000
0368  01D7  F948          FCMP  FCYCLE,FI
      01D8  043A
      01D9  045E
0369  01DA  3101          JAN   NOT1
```

```
PAGE  0013                               LOW CYCLE FATIGUE

0370  01DB  F63B          JMP  N1         RETURNS TO NOT1
0371  01DC  B66F   NOT1   LDA  MDFLG
0372  01DD  200F          JAM  UPEXIT
0373  01DE  3189          JAG  MD2ND
0374  01DF  B6A2          LDA  CUPLD      AT 1ST SMPL PT?
0375  01E0  D6A8          CMS  DLTLD
0376  01E1  F23B          JMP  UPEXIT     NO
0377  01E2  0000          NOP
0378  01E3  9EAB          STA  DLTLD      YES, STORE DATA
0379  01E4  B6A6          LDA  CURSTN
0380  01E5  9EAC          STA  DLTSTN
0381  01E6  DE79          IMS  MDFLG
0382  01E7  F235          JMP  UPEXIT
0383  01E8  B6AB   MD2ND  LDA  CUPLD      AT 2ND SMPL PT?
0384  01E9  D6AD          CMS  LOAD2
0385  01EA  F232          JMP  UPEXIT
0386  01EB  0000          NOP
0387  01EC  B6AF          LDA  CUPLD      YES, CALC. MD
0388  01ED  96B5          SUB  DLTLD
0389  01EE  9EB6          STA  DLTLD
0390  01EF  B6B1          LDA  CURSTN
0391  01F0  96B7          SUB  DLTSTN
0392  01F1  9EB3          STA  DLTSTN
0393  01F2  F946          FLT  DLTLD,MOD
      01F3  0138
      01F4  045C
0394  01F5  F943          FMPL MOD,STPESV,MOD
      01F6  045C
      01F7  044E
      01F8  045C
0395  01F9  F946          FLT  DLTSTN,DLTSTN
      01FA  0139
      01FB  0139
0396  01FC  E68C          LDX  XABC       XB=INDEX
0397  01FD  F943          FMPL DLTSTN,*STVALP,DLTSTN
      01FE  0139
      01FF  80B4
      0200  0139
0398  0201  F944          FDVD MOD,DLTSTN,MOD
      0202  045C
      0203  0139
      0204  045C
0399  0205  F943          FMPL MOD,F1000,MOD
      0206  045C
      0207  0466
      0208  045C
0400  0209  F941          FADD MOD,XX,XX CALC. NEW
      020A  045C
      020B  045A
      020C  045A
0401  020D  DE96          IMS  CNT        MODULUS
0402  020E  F20C          JMP  XIT        EVERY 4TH
0403  020F  F944          FDVD XX,NN,MD CYCLE
```

```
PAGE  0014                              LOW CYCLE FATIGUE

      0210  045A
      0211  0458
      0212  0274
0404  0213  C704          LAM  4          AVERAGE OVER
0405  0214  9E9D          STA  CNT        4 CYCLES
0406  0215  F947          FMOV F0,XX
      0216  006E
      0217  045A
0407  0218  F947          FMOV F4,NN
      0219  0460
      021A  0458
0408  021B  0010   XIT    ARM             RESET FLAG
0409  021C  9EAF          STA  MDFLG
0410  021D  F956   UPEXIT EXIT
0411               *
0412  021E  B6A9   REVDWN LDA  RNDFLG     NO STRESS TEST
0413  021F  3104          JAN  RVDN       WITH RANDOM OPTION
0414  0220  B251          LDA  STRESS
0415  0221  96E4          SUB  CURLD
0416  0222  2031          JAM  $+2
0417  0223  F95F          DONE            END OF TEST
0418  0224  B6AC   RVDN   LDA  DATPX
0419  0225  210D          JAZ  XX2
0420  0226  B6E9          LDA  CURLD
0421  0227  9EB9          STA  UTEMP1
0422  0228  B6EA          LDA  CURSTN
0423  0229  9EBA          STA  UTEMP2
0424  022A  F947          FMOV FCYCLE,FAC:3
      022B  043A
      022C  0278
0425  022D  F947          FMOV MD,FAC:4
      022E  0274
      022F  02F4
0426  0230  0110          ZAR
0427  0231  9EB9          STA  DATPX
0428  0232  DEB9          IMS  DATPY
0429  0233  F946   XX2    FLT  CURSTN,TEMPAV
      0234  013E
      0235  0438
0430  0236  F941          FADD TEMPAV,AUGSTN,AUGSTN
      0237  0438
      0238  0450
      0239  0450
0431  023A  E6CA          LDX  XABC
0432  023B  F948          FCMP *CMPTBL,FCYCLE
      023C  858A
      023D  043A
0433  023E  3190          JAG  DATA02
0434  023F  B100          LDA  CURLD
            013D
0435  0240  0000          NOP
0436  0241  0000          NOP
0437  0242  0000          NOP
```

PAGE 0015 LOW CYCLE FATIGUE

```
0243  B100           LDA  CURSTN
      013E
0244  0000           NOP
0245  0000           NOP
0246  0000           NOP
0247  B22C           LDA  MD
0248  0000           NOP
0249  0000           NOP
024A  0000           NOP
024B  B229           LDA  MD+1
024C  0000           NOP
024D  0000           NOP
024E  0000           NOP
024F  F911   DATA02  RAMP DOWN
0250  8000
0251  0110           ZAR
0252  9EE5           STA  MDFLG
0253  B6DE           LDA  RNDFLG
0254  2108           JAZ  RMPDN
0255  FFDF           JST  *GETNUM
0256  F943           FMPL LRNGE,RNDTMP,LLIMIT
0257  0454
0258  0456
0259  00C2
025A  F945           FIX  LLIMIT,LLIMIT
025B  00C0
025C  00C0
025D  0350   RMPDN   ARP
025E  9E97           STA  BRANCH
025F  F956           EXIT
             *
0260  F957   FULL    CUE  WINKER,1005 FLASH STATUS 1
0261  026D
0262  03ED
0263  0010           ARM            REQUEST A DONE
0264  9E9D           STA  BRANCH    IN UPDATE
0265  F956           EXIT
             *
0266  0010   STAT:A  ARM            REQUEST A DONE
0267  9EA0           STA  BRANCH    IN UPDATE
0268  F951           CLOS
             *
0269  DEF1   STAT:B  IMS  DATPX
026A  F958           WINK 2
026B  0002
026C  F951           CLOS
             *
026D  F958   WINKER  WINK 1
026E  0001
026F  F951           CLOS
             *
0270  00AB   INITCY  DATA INITCY
0271  0112   SETPTR  DATA SETTBL
```

```
PAGE  0016                        LOW CYCLE FATIGUE

0272  0000  STRESS RES   2,0
0274  0000  MD     RES   2,0
0276  0000  FAC:2  RES   2,0
0278  0000  FAC:3  RES   2,0
            *
PAUSE
            ****** FINAL SECTION ******
            *
027A  0110  FINAL  ZAR
027B  9EB4         STA  BRANCH
027C  F90F         CRLF
027D  F90F         CRLF
            * TYPE TRAILER
027E  F909         TYPE NULL
027F  04E2
0280  F909         TYPE NULL
0281  04E2
0282  0000         NOP
0283  F993         DATE
0284  F90F         CRLF
0285  F909         TYPE BUFFID
0286  053E
0287  F90F         CRLF
0288  F90F         CRLF
0289  F900         JST  SWAP       SAVE CYCLE
      0398
028A  B400         LDA  00         DATA IN CASE OF
028B  3181         JAG  LOOP3      START
028C  FF1C         JST  *INITCX
028D  E265  LOOP3  LDX  XABCP
028E  F947         FMOV *CMPTBL,FAC:1
028F  853A
0290  0426
0291  F992         GET  TABLE1
0292  0468
0293  F242         JMP  EMPTY
0294  9E1C         STA  FAC:3
0295  F992         GET  TABLE4
0296  04C1
0297  F23E         JMP  EMPTY
0298  9E22         STA  FAC:2
0299  F992         GET  TABLE4
029A  04C1
029B  F23A         JMP  EMPTY
029C  9E25         STA  FAC:2+1
            *      TAB 2
            *      VDEC FAC:1,9,0 CYCLE #
029D  F94D         VFLT FAC:1
029E  0426
            *      TAB 5
            *      VDEC FAC:2,10,0 MODULUS
029F  F94D         VFLT FAC:2
02A0  0276
            *      TAB 6
```

```
02A1  FA0C           JST  PRINTV
02A2  C6A0           LAP  ' '
               *     LXP 31
02A3  C41C           LXP  28
02A4  F92E           OTT
02A5  00A8           DXR
02A6  3842           JXN. $-2
02A7  F992           GET  TABLE1
02A8  0468
02A9  F22C           JMP  EMPTY
02AA  9E32           STA  FAC:3
02AB  FA02           JST  PRINTV
02AC  FF3B           JST  *SETPTR
02AD  F620           JMP  LOOP3
               *
02AE  0300    PRINTV ENT
02AF  F946           FLT  FAC:3,FAC:3
02B0  0278
02B1  0278
02B2  F943           FMPL FAC:3,STRESV,FAC:3
02B3  0278
02B4  044E
02B5  0278
               *     VDEC FAC:3,8,3 STRESS
02B6  F94D           VFLT FAC:3
02B7  0278
               *     TAB 6
02B8  E23A           LDX  XABCP
02B9  F992           GET  TABLE2
02BA  0489
02BB  F21A           JMP  EMPTY
02BC  9A37           STA  FAC:4
02BD  F946           FLT  FAC:4,FAC:4
02BE  02F4
02BF  02F4
02C0  F943           FMPL FAC:4,*STVALP,FAC:4
02C1  02F4
02C2  80F4
02C3  02F4
               *     VDEC FAC:4,7,4 STRAIN
02C4  F94D           VFLT FAC:4
02C5  02F4
               *     TAB 7
02C6  F944           FDVD FAC:3,FAC:2,FAC:3
02C7  0278
02C8  0276
02C9  0278
02CA  F943           FMPL FAC:3,F1000,FAC:3
02CB  0278
02CC  0466
02CD  0278
02CE  F942           FSUB FAC:4,FAC:3,FAC:3
02CF  02F4
```

```
PAGE  0018                           LOW CYCLE FATIGUE

      02D0  0278
      02D1  0278
0554              *      WDEC FAC:3,9,7 PLASTIC STRAIN
0555  02D2  F94D         WFLT FAC:3
      02D3  0278
0556  02D4  F90F         CRLF
0557  02D5  F727         RTN  PRINTV
0558              *
0559  02D6  F90F  EMPTY  CRLF
0560  02D7  F90F         CRLF
0561  02D8  F909         TYPE MLAST
      02D9  0575
0562              *      WDEC FCYCLE,9,0 FINAL CYCLE #
0563  02DA  F94D         WFLT FCYCLE
      02DB  043A
0564  02DC  F90F         CRLF
0565  02DD  F909         TYPE MAVGS
      02DE  057A
0566  02DF  F944         FDVD AVGSTN,FCYCLE,AVGSTN
      02E0  0450
      02E1  043A
      02E2  0450
0567  02E3  E20F         LDX  XABCP
0568  02E4  F943         FMPL AVGSTN,*STVALP,FAC:3
      02E5  0450
      02E6  80B4
      02E7  0278
0569              *      WDEC FAC:3,7,4 PEAK STRAIN
0570  02E8  F94D         WFLT FAC:3
      02E9  0278
0571  02EA  F90F         CRLF
0572  02EB  F909         TYPE MSLOPE
      02EC  0583
0573              *      WDEC RESULT,10,0 SLOPE
0574  02ED  F94D         WFLT RESULT
      02EE  0436
0575  02EF  FAA8         JST  SWAP
0576  02F0  F90F         CRLF
0577  02F1  F90F         CRLF
0578  02F2  F951         CLOS
0579              *
0580  02F3  0171  XABCP  DATA XBPT
0581  02F4  0000  FAC:4  RES  2,0
0582              *
0583  02F6  9900  PRINT  STA  FAC:1
            0426
0584  02F7  EE31         STX  FAC:2
0585  02F8  F946         FLT  FAC:1,FAC:1
      02F9  0426
      02FA  0426
0586  02FB  F946         FLT  FAC:2,FAC:2
      02FC  0276
      02FD  0276
```

```
PAGE  0019                                  LOW CYCLE FATIGUE

0587  02FE  F943          FMPL  FAC:1,STRESV,FAC:1
      02FF  0426
      0300  044E
      0301  0426
0588  0302  E60F          LDX   XABCP
0589  0303  F943          FMPL  FAC:2,*STVALP,FAC:2
      0304  0276
      0305  80B4
      0306  0276
0590  0307  C606          LAP   6
0591  0308  9900          STA   OUFLEN    FIELD LENGTH = 6
            05EE
0592  0309  FAA5          JST   CPLF2
0593                *     TAB 2
0594                *     WDEC FAC:3,9,0 CYCLE #
0595                * OUTPUT CYCLE #
0596  030A  F947          FMOV F1,OUFLZ / 1.
      030B  045E
      030C  05F2
0597  030D  F947          FMOV FAC:3,OUFLX
      030E  0278
      030F  05F0
0598  0310  F941          FADD F1E14,OUFLX,OUFLX ELIM 13.99
      0311  05F8
      0312  05F0
      0313  05F0
0599  0314  F900          JST   OUFLFX
            0596
0600  0315  FA95          JST   SPACE
0601                * OUTPUT MODULUS
0602  0316  F947          FMOV F1E6,OUFLZ / 1.E6
      0317  05F4
      0318  05F2
0603  0319  F947          FMOV FAC:4,OUFLX
      031A  02F4
      031B  05F0
0604  031C  F900          JST   OUFLFX
            0596
0605  031D  FA8D          JST   SPACE
0606                * OUTPUT MAX STRESS
0607  031E  F947          FMOV FAC:1,OUFLX
      031F  0426
      0320  05F0
0608  0321  F947          FMOV F1,OUFLZ / 1.
      0322  045E
      0323  05F2
0609  0324  F900          JST   OUFLFX    PRINT NUM
            0596
0610  0325  FA85          JST   SPACE
0611                * STORE STRAIN
0612  0326  F947          FMOV FAC:2,OUTMP1
      0327  0276
      0328  03B5
```

PAGE 0020 LOW CYCLE FATIGUE

```
                   *       TAB 7
0329   FA5D                JST   PRNTSB
032A   F946                FLT   UTEMP1,FAC:1
032B   016E
032C   0426
032D   F946                FLT   UTEMP2,FAC:2
032E   016F
032F   0276
0330   F943                FMPL  FAC:1,STRESV,FAC:1
0331   0426
0332   044E
0333   0426
0334   E641                LDX   XABCP
0335   F943                FMPL  FAC:2,*STVALP,FAC:2
0336   0276
0337   80B4
0338   0276
                   * OUTPUT MIN STRESS
0339   F947                FMOV  FAC:1,OUFLX
033A   0426
033B   05F0
033C   F947                FMOV  F1,OUFLZ / 1.0
033D   045E
033E   05F2
033F   F900                JST   OUFLFX
       0596
0340   FA6A                JST   SPACE
                   * OUTPUT MAX STRAIN
0341   F947                FMOV  F1E13,OUFLZ / 1.E-3
0342   05F6
0343   05F2
0344   F947                FMOV  OUTMP1,OUFLX
0345   03B5
0346   05F0
0347   F900                JST   OUFLFX
       0596
0348   FA62                JST   SPACE
                   * OUTPUT MIN. STRAIN
0349   F947                FMOV  F1E13,OUFLZ / 1.E-3
034A   05F6
034B   05F2
034C   F947                FMOV  FAC:2,OUFLX
034D   0276
034E   05F0
034F   F900                JST   OUFLFX
       0596
0350   FA5A                JST   SPACE
                   *       TAB 7
                   * OUTPUT PLASTIC STRAIN MAX.
0351   F947                FMOV  F1E14,OUFLZ / 1.E-4
0352   05F8
0353   05F2
0354   F947                FMOV  OUTMP2,OUFLX
```

```
0355  03B7
0356  05F0
0357  F900            JST  OUFLFX
      0596
0358  FA52            JST  SPACE
0359  FA2D            JST  PRNTSB
                * OUTPUT MIN RSTRAIN
035A  F947            FMOV F1E14,OUFLZ / 1.E-4
035B  05F8
035C  05F2
035D  F947            FMOV OUTMP2,OUFLX
035E  03D7
035F  05F0
0360  F900            JST  OUFLFX
      0596
0361  FA49            JST  SPACE
0362  FA4C            JST  CRLF2
0363  F95A            DIM  2
0364  0002
0365  F95A            DIM  1
0366  0001
0367  F951            CLOS
                *
                *
0368  0800      RANDOM ENT
0369  5804            DATA :5804    ICA, GET CONSOLE STATUS
036A  9AEB            STA  RNDTMP   SAVE IT
036B  C6AA            LAP  :AA      IS THIS AN LSI OR ALPHA?
036C  4404            DATA :4404    OCA
036D  5804            DATA :5804    ICA
036E  3107            JAN  LSI      IT'S AN LSI IF NON-ZERO RESPON
036F  E215            LDX  RN1      ELSE, IT'S AN ALPHA
0370  11A3            RRX  1
0371  6903            SIN  2
0372  B213            LDA  RN2
0373  0110            ZAR
0374  19AE            DATA :19AE    MPS 15
0375  F204            JMP  RNDFIN
0376  0110      LSI   ZAR
0377  E20E            LDX  RN2      ASSURE X-REG POSITIVE FOR LSI
0378  1960            DATA :1960,RN1 MPY RN1
0379  0385
037A  B2DB      RNDFIN LDA RNDTMP
037B  4404            DATA :4404    OCA, RESTORE CONSOLE STATUS
037C  13A3            LRX  1
037D  3801            JXN  $+2
037E  C403            LXP  3
037F  EA05            STX  RN1
0380  EAD5            STX  RNDTMP
0381  F946            FLT  RNDTMP,RNDTMP
0382  0456
0383  0456
0384  F71C            RTN  RANDOM
```

```
0385  0003  FN1     DATA 3
0386  00FD  FN2     DATA 253
                    *
0387  0800  PRNTSB  ENT
0388  F944          FDVD FAC:1,FAC:4,FAC:1
0389  0426
038A  02F4
038B  0426
038C  F943          FMPL FAC:1,F1000,FAC:1
038D  0426
038E  0466
038F  0426
0390  F942          FSUB FAC:2,FAC:1,FAC:1
0391  0276
0392  0426
0393  0426
                    *       WDEC FAC:1,9,7 PLASTIC STRAIN
                    * STORE MAX. PLASTIC STRAIN
0394  F947          FMOV FAC:1,OUTMP2
0395  0426
0396  03B7
0397  F710          RTN  PRNTSB
                    *
0398  0800  SWAP    ENT
0399  E23B          LDX  ACMPTB    SWAP THE CONTENTS OF
039A  EA97          STX  TEMP1     CMPTBL & TMPTBL
039B  C206          AXI  6
039C  EA97          STX  TEMP2
039D  C706          LAM  6
039E  9AB7          STA  RNDTMP
039F  E6AC          LDX  XABCP
03A0  B402          LDA  @2
03A1  BC00          EMA  @0
03A2  9C02          STA  @2
03A3  B33E  SWLOOP  LDA  *TEMP1
03A4  BB3F          EMA  *TEMP2
03A5  9B3C          STA  *TEMP1
03A6  DA3B          IMS  TEMP1
03A7  DA3C          IMS  TEMP2
03A8  DAAD          IMS  RNDTMP
03A9  F606          JMP  SWLOOP
03AA  F712          RTN  SWAP
                    * PRINT SPACE
03AB  0800  SPACE   ENT
03AC  C620          LAP  :20
03AD  F90E          OTT
03AE  F703          RTN  SPACE
                    * DO CRLF - NO PARITY BIT
03AF  0800  CRLF2   ENT
03B0  C60D          LAP  :0D       CR
03B1  F90E          OTT
03B2  C60A          LAP  :0A       LF
03B3  F90E          OTT
```

```
PAGE  0023                              LOW CYCLE FATIGUE

0721  03B4  F725          RTN  CRLF2
0722  03B5  0000  OUTMP1  RES  2,0
0723  03B7  0000  OUTMP2  RES  2,0
```

```
PAGE  0024                              LOW CYCLE FATIGUE

                     *
                     ****** CALCULATE SLOPE ******
                     *
03B9   F947   SLOPE:  FMOV F0,NMBPTS
03BA   006E
03BB   0428
03BC   F947           FMOV F0,XSUM
03BD   006E
03BE   042A
03BF   F947           FMOV F0,YSUM
03C0   006E
03C1   042C
03C2   F947           FMOV F0,XXSUM
03C3   006E
03C4   042E
03C5   F947           FMOV F0,XYSUM
03C6   006E
03C7   0430
03C8   F992   SLOPE1  GET  TABLE3
03C9   04AA
03CA   F228           JMP  LAST
03CB   9A66           STA  TEMP1
03CC   F946           FLT  TEMP1,TEMP2
03CD   0432
03CE   0434
03CF   F941           FADD TEMP2,YSUM,YSUM
03D0   0434
03D1   042C
03D2   042C
03D3   F992           GET  TABLE3
03D4   04AA
03D5   F21D           JMP  LAST
03D6   9A5B           STA  TEMP1
03D7   F946           FLT  TEMP1,TEMP1
03D8   0432
03D9   0432
03DA   F943           FMPL TEMP1,TEMP2,TEMP2
03DB   0432
03DC   0434
03DD   0434
03DE   F941           FADD TEMP2,XYSUM,XYSUM
03DF   0434
03E0   0430
03E1   0430
03E2   F941           FADD TEMP1,XSUM,XSUM
03E3   0432
03E4   042A
03E5   042A
03E6   F943           FMPL TEMP1,TEMP1,TEMP1
03E7   0432
03E8   0432
03E9   0432
03EA   F941           FADD TEMP1,XXSUM,XXSUM
```

```
        03EB  0432
        03EC  042E
        03ED  042E
0747    03EE  F941          FADD F1,NMBPTS,NMBPTS
        03EF  045E
        03F0  0428
        03F1  0428
0748    03F2  F62A          JMP  SLOPE1
0749                  *
0750    03F3  F943  LAST    FMPL XSUM,YSUM,TEMP1
        03F4  042A
        03F5  042C
        03F6  0432
0751    03F7  F943          FMPL NMBPTS,XYSUM,TEMP2
        03F8  0428
        03F9  0430
        03FA  0434
0752    03FB  F942          FSUB TEMP2,TEMP1,TEMP2
        03FC  0434
        03FD  0432
        03FE  0434
0753    03FF  F943          FMPL XSUM,XSUM,TEMP1
        0400  042A
        0401  042A
        0402  0432
0754    0403  F943          FMPL NMBPTS,XXSUM,XXSUM
        0404  0428
        0405  042E
        0406  042E
0755    0407  F942          FSUB XXSUM,TEMP1,TEMP1
        0408  042E
        0409  0432
        040A  0432
0756    040B  F944          FDVD TEMP1,TEMP2,RESULT
        040C  0432
        040D  0434
        040E  0436
0757    040F  E100          LDX  XABCP
              02F3
0758    0410  F944          FDVD F1,RESULT,RESULT
        0411  045E
        0412  0436
        0413  0436
0759    0414  F943          FMPL RESULT,*LDVALP,RESULT
        0415  0436
        0416  80A0
        0417  0436
0760    0418  F944          FDVD RESULT,*STVALP,RESULT
        0419  0436
        041A  80D4
        041B  0436
0761    041C  F944          FDVD RESULT,FAREA,RESULT
        041D  0436
```

```
PAGE  0026                              LOW CYCLE FATIGUE

      041E  0442
      041F  0436
0762  0420  F943         FMPL RESULT,F1000,RESULT
      0421  0436
      0422  0466
      0423  0436
0763  0424  F951         CLOS
0764               *

PAUSE
0765               *
0766               *
0767  0425  058A   ACMPTB DATA CMPTBL
0768  0426  0000   FAC:1  RES  2,0
0769  0428  0000   NMBPTS RES  2,0
0770  042A  0000   XSUM   RES  2,0
0771  042C  0000   YSUM   RES  2,0
0772  042E  0000   XXSUM  RES  2,0
0773  0430  0000   XYSUM  RES  2,0
0774  0432  0000   TEMP1  RES  2,0
0775  0434  0000   TEMP2  RES  2,0
0776  0436  0000   RESULT RES  2,0
0777  0438  0000   TEMPAV RES  2,0
0778  043A  0000   FCYCLE RES  2,0
0779  043C  0000   FTHICK RES  2,0
0780  043E  0000   FWIDTH RES  2,0
0781  0440  0000   WIDTH  RES  2,0
0782  0442  0000   FAREA  RES  2,0
0783  0444  0000   STRSUM RES  2,0
0784  0446  0000   MAXLIM RES  2,0
0785  0448  0000   MINLIM RES  2,0
0786  044A  0000   SRRATE RES  2,0
0787  044C  0000   CLKPT  RES  2,0
0788  044E  0000   STRESM RES  2,0
0789  0450  0000   AVGSTN RES  2,0
0790  0452  0000   HRNGE  RES  2,0
0791  0454  0000   LRNGE  RES  2,0
0792  0456  0000   PNDTMP RES  2,0
0793  0458  0000   NN     RES  2,0
0794  045A  0000   XX     RES  2,0
0795  045C  0000   MOD    RES  2,0
0796  045E  4080   F1     DATA :4080,0
      045F  0000
0797  0460  4180   F4     DATA :4180,0
      0461  0000
0798  0462  41A0   F5     DATA :41A0,0
      0463  0000
0799  0464  4220   F10    DATA :4220,0
      0465  0000
0800  0466  457A   F1000  DATA :457A,0
      0467  0000
0801               *
0802               *
0803               *
0804               *
```

PAGE 0027 LOW CYCLE FATIGUE

```
0805        0000  LOAD    EQU   0
0806        0001  STROKE  EQU   1
0807        0002  STRAIN  EQU   2
0808              *
0809        0000  UP      EQU   0
0810        8000  DOWN    EQU   :8000
0811              *
0812              *
0813        0074  F32767  EQU   :74
0814        007A  F:PI    EQU   :7A
0815        006E  F0      EQU   :6E
0816        0070  F2      EQU   :70
0817        0097  GETSTA  EQU   :97
0818              *
0819              *
0820        00A0  LDVALP  EQU   :A0
0821        00B4  STVALP  EQU   :B4
0822              *
0823  0468  0000  TABLE1  RES   33,0
0824  0489  0000  TABLE2  RES   33,0
0825  04AA  0000  TABLE3  RES   23,0
0826  04C1  0000  TABLE4  RES   33,0
0827              *
0828  04E2  0000  NULL    RES   20,0
0829  04F6  C0C0          TEXT  '@@'
0830              *
0831  04F7  C4C9  MAREA   TEXT  'DIMS. (THICK,WIDTH):: @'
      04F8  CDD3
      04F9  AEA0
      04FA  A8D4
      04FB  C8C9
      04FC  C3CB
      04FD  ACD7
      04FE  C9C4
      04FF  D4C8
      0500  A9BA
      0501  BAA0
      0502  C0A0
0832  0503  CDC9  MMSTPS  TEXT  'MIN. STRESS (KSI): @'
      0504  CEAE
      0505  A0D3
      0506  D4D2
      0507  C5D3
      0508  D3A0
      0509  A8CB
      050A  D3C9
      050B  A9BA
      050C  A0C0
0833  050D  D3D4  MSTRLM  TEXT  'STRAIN LMTS (+,-):: @'
      050E  D2C1
      050F  C9CE
      0510  A0CC
      0511  CDD4
```

```
      0512  D3A0
      0513  A8AB
      0514  ACAD
      0515  A9BA
      0516  BAA0
      0517  C0A0
0834  0518  D2C1  RNDMES TEXT 'RANDOM LMTS (Y,N): @'
      0519  CEC4
      051A  CFCD
      051B  A0CC
      051C  CDD4
      051D  D3A0
      051E  A8D9
      051F  ACCE
      0520  A9BA
      0521  A0C0
0835  0522  D3D4  MRATE  TEXT 'STRAIN RATE (1/SEC): @'
      0523  D2C1
      0524  C9CE
      0525  A0D2
      0526  C1D4
      0527  C5A0
      0528  A8B1
      0529  AFD3
      052A  C5C3
      052B  A9BA
      052C  A0C0
0836  052D  C5D8  MEXEC  TEXT 'EXECUTE@'
      052E  C5C3
      052F  D5D4
      0530  C5C0
0837  0531  D2C5  RESETM TEXT 'RESET RANDOM NOS. (Y,N): @'
      0532  D3C5
      0533  D4A0
      0534  D2C1
      0535  CEC4
      0536  CFCD
      0537  A0CE
      0538  CFD3
      0539  AEA0
      053A  A8D9
      053B  ACCE
      053C  A9BA
      053D  A0C0
0838              *
0839  053E  C0C0  BUFFID RES  26,:C0C0
0840              *
0841  0558  C3D9  MHEAD  TEXT 'CYCLES MODULUS (+)STRESS(-)'
      0559  C3CC
      055A  C5D3
      055B  A0CD
      055C  CFC4
      055D  D5CC
```

```
PAGE  0029                              LOU CYCLE FATIGUE

      055E  D5D3
      055F  A0A3
      0560  ABA9
      0561  D3D4
      0562  D2C5
      0563  D3D3
      0564  A8AD
      0565  A9A0
0842  0566  A0A8          TEXT ' (+)T.DISPL.(-) '
      0567  ABA9
      0568  D4AE
      0569  C4C9
      056A  D3D0
      056B  CCAE
      056C  A8AD
      056D  A9A0
0843  056E  A8AB          TEXT '(+)PLASTIC(-)@'
      056F  A9D0
      0570  CCC1
      0571  D3D4
      0572  C9C3
      0573  A8AD
      0574  A9C0
0844  0575  C3D9   MLAST  TEXT 'CYCLES= @'
      0576  C3CC
      0577  C5D3
      0578  BDA0
      0579  C0A0
0845  057A  C1D6   MAVGS  TEXT 'AVG PEAK STRAIN= @'
      057B  C7A0
      057C  D0C5
      057D  C1CB
      057E  A0D3
      057F  D4D2
      0580  C1C9
      0581  CEBD
      0582  A0C0
0846  0583  D3CC   MSLOPE TEXT 'SLOPE(PSI)= @'
      0584  CFD0
      0585  C5A8
      0586  D0D3
      0587  C9A9
      0588  BDA0
      0589  C0A0
0847  058A  0000   CMPTBL RES  6,0
0848  0590  0000   TMPTBL RES  6,0
0849               *
0850               *
0851               * SUBROUTINE TO CONVERT FLOAT TO FIX POINT.
0852  0596  0300   OUFLFX ENT
0853               *
0854               * OUTPUT FIX POINT NUMBERS
0855               * AT CALL:  OUFLEN - CONTAINS (INT) FIELD LENGTH
```

PAGE 0030 LOW CYCLE FATIGUE

```
                  *         OUFLX  - X (F.P.) # TO BE OUTPUT (LOST)
                  *        OUFLZ - Z(F.P.) NUM TO DIVIDE BY: Z=Z/10
                  *
0597  B256              LDA  OUFLEN    SAVE LENGTH
0598  9A56              STA  OUFLN2
0599  BA53              STX  OUSAVX    SAVE X-REG
059A  0000              NOP
059B  0000              NOP
059C  0000              NOP
059D  0000              NOP
059E  0000              NOP
059F  0000              NOP
05A0  F944              FDVD OUFLX,OUFLZ,OUFLZ Z=X/Z (RIGHT UNITS)
05A1  05F0
05A2  05F2
05A3  05F2
05A4  0110              ZAR
05A5  9A46              STA  OUPK      K=0
05A6  C701              LAM  1
05A7  3A47              ADD  OUFLN2    L=L-1
05A8  2095              JAM  A         RETURN
05A9  9A45              STA  OUFLN2
                  *
                  * PRINT SIGN (+ OR -)
                  *
05AA  F948              FCMP OUFLZ,F0 SEE IF Z<0 OR >0,A=-1,OR +1
05AB  05F2
05AC  006E
05AD  3086              JAP  OU2       Z>0
05AE  0048              TAX            (SAVE A)
05AF  F942              FSUB F0,OUFLZ,OUFLZ Z=ABS(Z)
05B0  006E
05B1  05F2
05B2  05F2
05B3  0030              TXA            (RESTORE A)
05B4  3101  OU2         JAN  $+2
05B5  C601              LAP  1         A=1,IF Z=0
05B6  0308              NAX            X=-A
05B7  C22C              AXI  :2C       X=:2C -(A)
05B8  0030              TXA            A=X = "+" OR "-"
05B9  F90E              OTT            PRINT "+" OR "-"
05BA  C601              LAP  1         A=1
05BB  9A2F  OU1         STA  OUPJ      J=1
05BC  C701  OULOOP      LAM  1         A=-1
05BD  3A31              ADD  OUFLN2    L=L-1
05BE  20AA  A           JAM  OURET     RETURN
05BF  9A2F              STA  OUFLN2
05C0  F948  OU3         FCMP OUFLZ,F1
05C1  05F2
05C2  045E
05C3  2088              JAM  OU3B      Z<1
05C4  F944              FDVD OUFLZ,F10,OUFLZ Z=Z/10
05C5  05F2
```

```
05C6  0464
05C7  05F2
05C8  C601        LAP  1
05C9  8A21        ADD  OUPJ      J=J+1
05CA  9A20        STA  OUPJ
05CB  F60B        JMP  OU3
05CC  C601  OU3B  LAP  1
05CD  8A1E        ADD  OUPK      K=K+1
05CE  9A1D        STA  OUPK      STORE K
05CF  921B        SUB  OUPJ      A=K-J
05D0  3103        JAN  OU4
            * PRINT DECIMAL POINT
05D1  C62E        LAP  :2E
05D2  F90E        OTT
05D3  F617        JMP  OULOOP
05D4  F943  OU4   FMPL OUFLZ,F10,OUFLZ Z=Z*10
05D5  05F2
05D6  0464
05D7  05F2
05D8  F945        FIX  OUFLZ,OUFLX X=INT(Z)
05D9  05F2
05DA  05F0
05DB  F946        FLT  OUFLX,OUFLX BACK TO F.P.
05DC  05F0
05DD  05F0
05DE  F942        FSUB OUFLZ,OUFLX,OUFLZ Z=10*Z-INT(10*Z)
05DF  05F2
05E0  05F0
05E1  05F2
05E2  F945        FIX  OUFLX,OUFLX BACK TO FIX
05E3  05F0
05E4  05F0
            * PRINT DIGIT
05E5  C630        LAP  :30
05E6  8A09        ADD  OUFLX
05E7  F90E        OTT
05E8  F62C        JMP  OULOOP
            * RETURN
05E9  E203  OURET LDX  OUSAVX    RESTORE X
05EA  F754        RTN  OUFLFX
            *   DATA
            *
05EB  0000  OUPJ   DATA 0        DECIMAL POINT LOCATOR
05EC  0000  OUPK   DATA 0        CHARACTER POINTER
05ED  0000  OUSAVX DATA 0        XREG
05EE  0000  OUFLEN DATA 0        FIELD LEN.
05EF  0000  OUFLN2 DATA 0        TEMP
05F0  0000  OUFLX  RES  2,0      (F.P.) X
05F2  0000  OUFLZ  RES  2,0      (F.P) Z
05F4  4A74  F1E6   DATA :4A74,:2400 1.E6
05F5  2400
05F6  3B83  F1EM3  DATA :3B83,:126F 1.E-3
05F7  126F
```

```
PAGE  0032                               LOW CYCLE FATIGUE

0935  05F8  39D1  F1EM4  DATA :39D1,:B717 1.E-4
      05F9  B717
0936              *
0937                     END
```

PAGE 0033 LOW CYCLE FATIGUE

ACMPTB	0425	AUGSTN	0450	A	05BE	BEGIN	001B
BRANCH	01C7	BREAK	016A	BUFFID	053E	CLEAR1	0057
CLEAR2	0076	CLKRT	044C	CLR2	007D	CMPTBL	058A
CNTN1	0169	CNT	0177	CPLF2	03AF	CUPLD	013D
CURSTN	013E	CURSTP	00C2	CYADJ	0141	CYAD2	014B
CYAD3	014F	DATA01	01AF	DATA02	024F	DATN1	0156
DATPX	0178	DATPY	0179	DLTLD	0138	DLTSTN	0139
DOWN	8000	EMPTY	02D6	FAC:1	0426	FAC:2	0276
FAC:3	0278	FAC:4	02F4	FAREA	0442	FCYCLE	043A
FINAL	027A	FNM1	00C4	FNM2	00C6	FNM3	00C8
FTCYC	013F	FTHICK	043C	FULLN1	0163	FULL	0260
FWIDTH	043E	F0	006E	F1E3	05F6	F1E4	05F8
F1E6	05F4	F1	045E	F10	0464	F1000	0466
F2	0070	F3	00CA	F32767	0274	F4	0460
F5	0462	F:PI	007A	GETNUM	0176	GETSTA	0097
HLIMIT	00BE	HRNGE	0452	INCDNE	0134	INCTBL	0125
INCTB2	0127	INDEX	0172	INDEX1	00BD	INITCX	0270
INITCY	00AB	I300	0133	LAST	03F3	LDVALP	00A0
LLIMIT	00C0	LOAD	0000	LOAD2	013C	LOOP3	028D
LRNGE	0454	LSI	0376	MAREA	04F7	MAVGS	057A
MAXLIM	0446	MDFLG	016D	MD	0274	MD2ND	01E8
MEXEC	052D	MHEAD	0558	MINLIM	0448	MLAST	0575
MMSTRS	0503	MOD	045C	MRATE	0522	MSLOPE	0583
MSTRLM	050D	NAME	0007	NMBPTS	0428	NMMESS	00CC
NN	0458	NOT1	01DC	NULL	04E2	NUM	016C
NUM1	016B	NIX	0155	N1	0150	OLDLD	0137
OUFLEN	05EE	OUFLFX	0596	OUFLN2	05EF	OUFLX	05F0
OUFLZ	05F2	OULOOP	05BC	OUPJ	05EB	OUPK	05EC
OURET	05E9	OUSAVX	05ED	OUTMP1	03B5	OUTMP2	03B7
OU1	05EB	OU2	05B4	OU3B	05CC	OU3	05C0
OU4	05D4	PRINTV	02AE	PRINT	02F6	PRNTSB	0387
RANDOM	0368	RESETM	0531	RESET1	00E1	RESTRT	00D6
RESULT	0436	REVDWN	021E	REVUP	0195	RMPDN	025D
RMPUP	01C4	RNDFIN	037A	RNDFLG	0175	RNDMES	0518
RNDMLT	0070	RNDM	00C3	RNDTMP	0456	RN1PTR	0174
RN1	0385	RN2	0386	ROUND	004B	RSTEX	00ED
RSTRT0	00E5	RVDN	0224	SAME2	00EB	SETPTR	0271
SETTBL	0112	SETTB2	011F	SLOPE1	03C8	SLOPE:	03B9
SPACE	03AB	SPRATE	044A	STAT:A	0266	STAT:B	0269
STRAIN	0002	STRESS	0272	STRESV	044E	STROKE	0001
STRSLM	0444	STVALP	00B4	SWAP	0398	SWLOOP	03A3
TABLE1	0468	TABLE2	0489	TABLE3	04AA	TABLE4	04C1
TEMPAV	0438	TEMP1	0432	TEMP2	0434	TMPTBL	0590
UPDATE	017A	UPEXIT	021D	UP	0000	UP:	01C8
UTEMP1	016E	UTEMP2	016F	VALPTR	0004	WIDTH	0440
WINKER	026D	WTCLR	0072	XABCP	02F3	XABC	0170
XBPT	0171	XC	0173	XIT	021B	XSUM	042A
XXSUM	042E	XX	045A	XX2	0233	XX3	01A1
XYSUM	0430	YSUM	042C				

APPENDIX II

SOURCE LISTING OF FORTRAN PROGRAM FOR STRESS AND STRAIN COMPUTATIONS AND PLOTTING

```
      PROGRAM DATA (OUTPUT,TAPE1,TAPE2,TAPE3,TAPE4,
     1 TAPE5,TAPE6,INPUT=/7.)
C
C         ************************
C         THIS PROGRAM DEVELOPED BY
C            CAPT ROBERT SCHAFRIK
C                  MAY,1979
C         ************************
C
      COMMON /A/ N(1500),E(1500),SIGMA1(1500),SIGMA2(1500),ELONG1(1500),
     AELONG2(1500),PLST1(1500),PLST2(1500),TITL(60),R1(1500),
     BDELTEP(1500)
      REAL N
C
C     IFLAG = YES       FOR COMPUTER DATA
C     IFLAG = NO    FOR NO COMPUTER DATA
C     IFLAG1 = YES FOR COMPUTER DATA PRINT-OUT (DATA ON P.F.)
C     IUNIT IS THE TAPE NUMBER
C
      READ 4,IFLAG,IUNIT,IFLAG1
    4 FORMAT ( / A1,4X,I1,4X,A1)
C
      IF (IUNIT.LE.0.OR.IUNIT.GT.6) IUNIT=1
      PRINT  8,IFLAG,IUNIT,IFLAG1
    8 FORMAT (1H1,T2,*FROM DATA :    COMPUTER DATA = *,A1,
     A/T3,*TAPE UNIT IS *,I1  /
     BT4,*COMPUTER DATA FLAG IS *,A1//)
      IF (IFLAG.NE.1HY) GO TO 50
C
      READ (IUNIT,9) (TITL(JT),JT=1,60)
    9 FORMAT(60A1)
C
      IMAX=1500
      I=0
    1 CONTINUE
      I=I+1
      IF (I.GT.IMAX) GO TO 1000
C
      READ (IUNIT,10) N(I),E(I),SIGMA1(I),SIGMA2(I),ELONG1(I),ELONG2(I),
     1PLST1(I),PLST2(I)
   10 FORMAT (8(F7.0,1X))
C
      IF(N(I).LT.0.9)  GO TO 3
      IF (EOF(IUNIT))2,1
    3 CONTINUE
      PRINT 30
   30 FORMAT (T2,*READ TERMINATED BY ZERO VALUE*)
      I=I-1
      GO TO 40
 1000 CONTINUE
      I=IMAX
      PRINT 1001,I
 1001 FORMAT(T2,4H**** ,2X,*IMAX = *,I5,2X,
     1 *DATA PTS EXCEED ARRAY DIMENSIONS*,//)
      GO TO 40
    2 CONTINUE
      PRINT 31
   31 FORMAT (T2,*READ TERMINATED BY EOF*)
      I=I-1
   40 CONTINUE
      PRINT 16,(TITL(JA),JA=1,60)
   16 FORMAT (// T2,60A1, /T2,60(1H*)//)
      PRINT 11,I
```

```
 11   FORMAT(                             /T2,*NUMBER OF DATA PTS = *,I5
     1, //)
      IF (I.EQ.0) STOP
      DO 20 J=1,I
      IF (IFLAG1.NE.1HY)  GO TO 45
      PRINT 21,    N(J),E(J),SIGMA1(J),SIGMA2(J),ELONG1(J),
     1ELONG2(J),PLST1(J),PLST2(J)
 21   FORMAT (T2,F7.0, 3(1X,F7.2), 4(1X,F7.3))
 45   CONTINUE
      E(J)=E(J)*1.E6
      ELONG1(J)=ELONG1(J)*1.E-3
      ELONG2(J)=ELONG2(J)*1.E-3
      PLST1(J)=PLST1(J)*1.E-3
      PLST2(J)=PLST2(J)*1.E-3
 20   CONTINUE
      CALL LCF(I)
      GO TO 51
 50   CONTINUE
      I=0
      PRINT 55
 55   FORMAT (// T2,*NO COMPUTER DATA*, ///)
C
      READ 9,TITL
C
      PRINT 18, (TITL(JA),JA=1,50)
      CALL LCF(I)
 51   CONTINUE
      CALL DATA1
      CALL SUBPLOT(I)
      STOP
      END
C
C****************************************************************
C
      SUBROUTINE LCF(I)
      COMMON /A/ N(1500),E(1500),SIGMA1(1500),SIGMA2(1500),ELONG1(1500),
     AELONG2(1500),PLST1(1500),PLST2(1500),TITL(60),R1(1500),
     BDELTEP(1500)
      COMMON /D/ LPLST,LELST
      REAL LPLST,LELST,N
      DIMENSION MSIG(1500)
      DIMENSION DELTSIG(1500),DELTEL(1500),DELTPL(1500),DELTEE(1500),
     ADELTSTN(1500)
      EQUIVALENCE (E(1),DELTSIG(1)) , (ELONG1(1),DELTEL(1)) ,
     A(ELONG2(1),DELTPL(1)) ,(PLST1(1),DELTEE(1)) ,
     B(PLST2(1),DELTSTN(1))
C
      DATA MSIG /1500*(1H )/
      DATA IFLG /0/
C
C
      READ *,EACT,LELST,LPLST,SFACTOR,DFACTOR,IFLG
C
C     EACT IS ACTUAL ELASTIC MODULUS IN E6 PSI
C     LELST IS AN ASSUMED ELASTIC EFFECTIVE GAGE LENGTH
C     LPLST IS EFFECTIVE PLASTIC GAGE LENGTH
C     SFACTOR - COMPUTER STRESS CORRECTION FACTOR
C     DFACTOR - DISPL CORRECTION FACTOR, COMPUTER
C     IFLG IS USED TO SPECIFY DATA PRINT-OUT
C      FOR PRINT-OUT, USE 1
C
C
      PRINT 23,EACT,LELST,LPLST,SFACTOR,DFACTOR,IFLG
 23   FORMAT (T2,*FROM LCF* / T2,*EACT = *,E12.5,*, LELST = *, E12.5,
     Z*  LPLST = *, E12.5 / T3,3H***,
     1*, SFACTOR = *, E12.5, *, DFACTOR = *, E12.5 / ,
```

```
 AT3,*COMPUTER DATA PRINT-OUT FLAG IS = *,I1 //)
C
      IF (I.EQ.0) RETURN
C
      EACT=EACT*1.E+6
      DELTEET=0.0
C
      DO 9  J=1,I
      DELTEET=DELTEET+E(J)
 9    CONTINUE
C     ASSUME MINI-COMPUTER INTERNAL ARITHMETIC IS OK
      DELTEET=DELTEET/I*(1.00/1.00)
      LELST=EACT/DELTEET
C
      DO 10  J=1,I
      SIGMA1(J)=SIGMA1(J)*SFACTOR
      SIGMA2(J)=SIGMA2(J)*SFACTOR
      ELONG1(J)=ELONG1(J)*DFACTOR
      ELONG2(J)=ELONG2(J)*DFACTOR
      DELTSIF=SIGMA1(J)-SIGMA2(J)
      DELTEK=ELONG1(J)-ELONG2(J)
C     ELASTIC STRAIN = SIGMA/E = (UT-UP)/LELST
C
      PL1=PLST1(J)
      PLST1(J)=ELONG1(J)-(LELST*SIGMA1(J)*1.E+3/EACT)
      PL2=PLST2(J)
      PLST2(J)=ELONG2(J)-(LELST*SIGMA2(J)*1.E+3/EACT)
      DELTPK=PLST1(J)-PLST2(J)
      IF (DELTPK.LE.1.E-6)  GO TO 11
 12   CONTINUE
      DELTED=(DELTEK-DELTPK)/LELST
      DELTEP(J)=(DELTPK/LPLST)
      DELTSTM=DELTED+DELTEP(J)
      R1(J)=ABS(SIGMA1(J)/SIGMA2(J))
      GO TO 8
 11   CONTINUE
      PLST1(J)=PL1*LELST
      PLST2(J)=PL2*LELST
      MSIG(J)=1H*
      DELTPK=PLST1(J)-PLST2(J)
      RPL=DELTSIF/DELTEET
      DISPDIF=RPL/DELTEK
      DRATIO=DISPDIF*DFACTOR*1.E3
      PRINT 101, N(J),DRATIO
 101  FORMAT(T3,*CORRECTION FACTOR FOR DISPLACEMENTS: N = *,
     AF6.1,3X,*SUGGESTED DFACTOR = *,F6.4)
      IF (DELTPK.GT.1.E-6)  GO TO 12
      MSIG(J)=1HX
      DELTPK=1.E-5
      GO TO 12
 8    CONTINUE
      E(J)=DELTSIF
      ELONG1(J)=DELTEK
      ELONG2(J)=DELTPK
      PLST1(J)=DELTED
      PLST2(J)=DELTSTM
 10   CONTINUE
C
      PRINT 20,(TITL(JA),JA=1,31)
 20   FORMAT(1H1,T40,*INSTRON COMPUTER*/ T28,
     Z*DATA FOR *, 31A1 / T28,40(1H*), 3(/),
     XT59, *RATIO*, /  T56, *MAX STRESS*,/
     1T11,*TOTAL*, T20,*PLASTIC*, T30 ,
     2*STRESS*, T40,*MAX*, T49, *MIN*,T60, *TO*, T68, *ELASTIC*,
     3T79, *PLASTIC*, T89,*STRAIN*  /
     4 T2,*CYCLES*,                T11, *ELONG*,  T21, *ELONG*,  T30,
```

```
     5        *RANGE*,  T40,*STRESS*,
     6  T48,  *STRESS*,  T56,  *MIN STRESS*,  T68,  *STRAIN*,
     7 T79,  *STRAIN*,  T89,  *RANGE*/,
     8              T10,*(INCHES)*,  T20,  *(INCHES)*,  T30,
     9       *(KSI)*,  T4_,  *(KSI)*,  T48,
     A *(KSI)*, T68, *(PCNT)*,  T79, *(PCNT)*,  T89, *(PCNT)* /)
C
      DO 30  K=1,I
      DELTEP(K)=DELTEP(K)*100.
      DELTEE(K)=DELTEE(K)*100.
      DELTSTN(K)=DELTSTN(K)*100.
      NT=N(K)
C
C USE TO ELIMINATE PRINTING
C
      IF (IFLG.NE.1)  GO TO 99
C
      PRINT 22,NT,     DELTEL(K),DELTPL(K),
     1DELTSIG(K),SIGMA1(K),SIGMA2(K),R1(K),DELTEE(K),
     3DELTEP(K),DELTSTN(K),MSIG(K)
 22   FORMAT (T2, I5,              T11,  F6.5,  T21,  F6.5, T30,
     1    F7.2, T40,  F5.1, T48,  F6.1, T56,  F7.3,
     3  T68,F5.3,T79,F6.4,  T89,  F5.3,T120,A1)
C
 99   CONTINUE
C
 30   CONTINUE
      PRINT 40
 40   FORMAT(///  )
      PRINT 31,DELTEET,LELST
 31   FORMAT (1H1,
     1           T ,*THE AVERAGE MODULUS FOR THIS DATA WAS*,E12.5,*   PSI*,
     2 / T2,*EFFECTIVE ELASTIC GAGE LENGTH IS *,E12.5,* INCHES*/)
      RETURN
      END
C
C**********************************************************
C
      SUBROUTINE DATA1
      COMMON /A/ BA(12000),TITL(60),BB(3000)
      COMMON /C/ SIGC(70) ,STRT(70) ,STRP(70) ,STRNC(70) ,NC(70) ,KI,
     ZDELTELC(70),DELTPLC(70)
      INTEGER UNITS,DATASTS
      REAL NC
C
      READ 11,DATASTS
 11   FORMAT(I1)
C
      IF (DATASTS.LE.0)  GO TO 50
C
      KA=0
      DO 15 M=1,DATASTS
C
C     FOR CHART DIMENS IN MM,USE  M
C     FOR CHART DIMENSIONS IN INCHES, USE  I
C
      READ 2,UNITS,FCTR
 2    FORMAT (A1,4X,F5.0)
C
      PRINT 9,TITL
 9    FORMAT(/ T2,80(1H5)/ T2,60A1)
      PRINT 6,UNITS,FCTR
 6    FORMAT (/T2,*FROM DATA1, UNITS = *,A1 ,/,
     AT2,*ADD THESE NUMBER OF CYCLES TO DATA 1*,1X,F5.0/)
      IF (UNITS.EQ.1HI.OR.UNITS.EQ.1HM) GO TO 51
      GO TO 50
```

```
 51   CONTINUE
C
C     CALSIG IS CALIBRATION FACTOR FOR LOAD SCALE ON H-P CHART
C     CALDIS1 IS EXTENSOMETER CALIB FACTOR
C     CALDIS2 IS CALIBRATION FACTOR FOR H-P CHART
C     SPECA IS SPECIMEN AREA
      READ *,CALSIG,CALDIS1,CALDIS2,SPECA
C
      PRINT 10,CALSIG,CALDIS1,CALDIS2,SPECA
 10   FORMAT (// T2,*FROM DATA1*/ T2,*H-P CHART LOAD SCALE CALIBRATION
     1IS *, F7.5,
     2 / T2,*EXTENSOMENTER CALIBRATION FACTOR IS *, F7.5,
     4 / T2, *H-P CHART DISPLACEMENT SCALE CALIBRATION IS *,F7.5,
     5 / T2,*SPECIMEN AREA = *,F7.5 /)
      PRINT 29,UNITS
 29   FORMAT (T2,* UNITS DESIG IS *, A2/)
      CALDIS=CALDIS1*CALDIS2
C
      KT=KA
 100  CONTINUE
      KA=KA+1
      IF (KA.GT.70)  GO TO 70
C
      READ *,NC(KA),STRT(KA),STRP(KA),SIGC(KA)
C     USE -1. TO TERMINATE READING DATA STRING
C     PRINT *,NC(KA),STRT(KA),STRP(KA),SIGC(KA)
      IF(NC(KA).LT.0.9) GO TO 103
      NC(KA)=NC(KA)+FCTR
      GO TO 100
 70   CONTINUE
      PRINT 71
 71   FORMAT (4(/)  T3,*EXCEEDED ARRAY DIMENSIONS IN DATA1*,3(/))
 103  CONTINUE
      PRINT 4
 4    FORMAT(// T2,*CYCLES*, T10,*T.DISP*, T18,*PL.DISP*,T28,
     1*STRESS*/)
      KA=KA-1
      KI=KA
      KS=KT+1
C
      DO 1 J=KS,KI
      PRINT 5,NC(J),STRT(J),STRP(J),SIGC(J)
 5    FORMAT (T2,F5.0,T10,F5.2,T18,F5.2,T28,F5.2)
 1    CONTINUE
      CALL DATA2 (CALSIG,CALDIS,SPECA,UNITS,KS)
 15   CONTINUE
C
      PRINT 9
      PRINT 21,(TITL(JA),JA=1,31)
 21   FORMAT (1H1,T28,*HYSTERESIS LOOP*,/
     AT16,*DATA FOR *, 31A1/
     BT16,40(1H*),  3(/)
     CT10,*TOTAL*,  T20,*PLASTIC*,T31,
     D*STRESS*,  T42,*ELASTIC*,  T53,
     E*PLASTIC*,  T65,*STRAIN*  /  T2
     F,*CYCLES*,  T11,*ELONG*,  T21, *ELONG*,
     GT31, *RANGE*,  T42, *STRAIN*,  T53,
     H*STRAIN*,  T65,*RANGE*  ,  /   T10,
     I*(INCHES)*,  T20,  *(INCHES)*,  T31,
     J*(KSI)*, T42,  *(PCNT)*,  T53,*(PCNT)*,
     KT65, *(PCNT)* /)
C
      DO 28  MC=1,KI
      NT=NC(MC)
      PRINT 22,NT,DELTELC(MC),DELTPLC(MC),SIGC(MC),
     ASTRT(MC),STRP(MC),STRNC(MC)
```

```
 22   FORMAT(T2,I5,T11,F6.5,T21,F6.5,T30,F7.2,T42,F5.3
     AT53,F6.4,T65,F5.3)
 26   CONTINUE
      PRINT 27
 27   FORMAT (1H1)
C
      RETURN
 50   CONTINUE
      PRINT 7
 7    FORMAT (/ T2,*NO HYSTERESIS LOOP DATA* ,/)
      KI=0
      RETURN
      END
C
C**********************************************************
C
      SUBROUTINE DATA2(CALSIG,CALDIS,SPECA,UNITS,KS)
      COMMON /C/ SIGC(70) ,STRT(70) ,STRP(70) ,STRNC(70) ,NC(70) ,KI
     A,DELTELC(70),DELTPLC(70)
      COMMON /D/ LP,LE
      INTEGER UNITS
      REAL NC
C  LE IS EFF ELAST GAGE LGTH,LP IS PL EFF GAGE LENGTH,
      REAL LE,LP
C
      SIG( C,CAL,A,F)=C/F*CAL*500./A
      E(C,CAL,F)=C/F*CAL
      STNE(UTOT,UPL,EE)=(UTOT-UPL)/EE
      STNP(UPL,EP)=UPL/EP
C
      PRINT 8,LE,LP,CALSIG,CALDIS
 8    FORMAT (T2,* LE,LP,CALSIG,CALDIS  ARE = *, 4F9.5, //)
      PRINT 6
 6    FORMAT (3(/), T2,*CYCLES*,  T9,*ELAST STN*, T22, *PL STRN*,
     1 T35, *TOT STRN*,T48,*STRESS*,T57,*TOT DISPL* ,T70,*PL DISPL* /)
      IF (UNITS.EQ.1HI)  FACTOR=1.00
      IF (UNITS.EQ.1HM)  FACTOR=2.54
C
      DO 5 K=KS,KI
      SIGC(K)=SIG(SIGC(K),CALSIG,SPECA,FACTOR)*1.E-3
      UT=E(STRT(K),CALDIS,FACTOR)
      UP=E(STRP(K),CALDIS,FACTOR)
      STNEL=STNE(UT,UP,LE)*1.E2
      STNPL=STNP(UP,LP)*1.E2
      STRNC(K)=STNEL+STNPL
C     STORE ELAS & PLAST STRAIN
      STRT(K)=STNEL
      STRP(K)=STNPL
      DELTELC(K)=UT
      DELTPLC(K)=UP
      UT=UT*1.E3
      UP=UP*1.E3
      PRINT 7,NC(K),STRT(K),STRP(K),STRNC(K),SIGC(K),UT,UP
 7    FORMAT (T2,F5.0,T9,F4.3,T22,F4.3   ,T35,F5.3,  T48,F5.1,T57,
     1 F4.2,T70,F4.3)
 5    CONTINUE
      RETURN
      END
C
C**********************************************************
C
      SUBROUTINE SUBPLOT(I)
      COMMON /A/ N(1500),DELTSIG(1500),X(1500),Y(1500),DELTEL(1500),
     ADELTPL(1500),DELTEE(1500),DELTSTN(1500),TITL(60),
     BR1(1500),DELTEP(1500)
      COMMON /C/ SIGC(70),STRT(70),STRP(70),STRNC(70),NC(70),KI
```

```
     A,DELTELC(70),DELTPLC(70)
      REAL N,U(50),NC
      REAL XA(70),YA(70)
      DIMENSION IPAK(50),MPLOT(10)
      LOGICAL HYPLOT,COMPLOT,DUALPT
C
      PRINT 10,I,KI
 10   FORMAT (1H1//T2,*FROM SUBPLOT : NO. OF COMPUTER DATA PTS IS = *,
     AI5 / T17,*NO. OF HYSTERESIS LOOP DATA PTS IS = *, I5/)
      CALL COMPRS
C
      COMPLOT=.T.
      HYPLOT=.T.
      DUALPT=.F.
      IF (I.LE.0) COMPLOT=.F.
      IF (KI.LE.0) HYPLOT=.F.
      IF (HYPLOT.AND.COMPLOT) DUALPT=.T.
C
      PRINT 6, COMPLOT,HYPLOT,DUALPT
 6    FORMAT ( / *  COMPLOT = *, L3, 5X, *,HYPLOT = *, L3/,
     AT3,*DUALPT = *,L3 /)
C
      IF (.NOT.COMPLOT.AND..NOT.HYPLOT) RETURN
C
      LN2=1
      IF (DUALPT) LN2=2
C
C  DEFINE MESSAG LTR HEIGHT & BLNK1 SIZE
      HT=0.14
C   ASSUMES 15 PLOTTED CHARACTERS
C
      XLNGTH=15.*HT+2.*HT
      YLNGTH=2.*HT
      XORGIN=1.0
      YORGIN=1.0
C    ESTABLISH LENGTHS FOR BLANKING
      XF=XORGIN+XLNGTH
      YF=YORGIN+YLNGTH
C    ESTABLISH MESSAG PRINT POSITIONS
      XO=XORGIN+HT*2.
      YO=YORGIN+HT/2.
C
C
C     FOR PLOTS 1-10   USE  Y
C
      READ 1, (MPLOT(L),L=1,10)
 1    FORMAT(10A1)
C
      PRINT 9, (MPLOT(L),L=1,10)
 9    FORMAT (T2, *MPLOT IS : *, 10(A1,1X) /)
C
C     ASSUMES 15 CHARACTERS + $
      ENCODE (16,20,U)  (TITL(KL),KL=1,15)
 20   FORMAT (15A1, "$")
C
C     YMIN2,YMAX2 - STRESS RANGE FOR PLOT 2
C     YMIN3,YMAX3 - STRAIN RANGE FOR PLOT 3
C     YMIN4,YMAX4 - STRESS RANGE FOR PLOT 4
C     YMIN5,YMAX5 - STRESS RANGE FOR PLOT 5
C     XMAX1 - DEFINED MAX NUMBER OF CYCLES FOR 2ND PLOT GROUP
C
      READ *,YMIN2,YINC2,YMAX2
      READ *,YMIN3,YINC3,YMAX3
      READ *,YMIN4,YINC4,YMAX4
      READ *,YMIN5,YINC5,YMAX5
      READ *,X5ORGN,XCYCLE
```

```
      READ *,XINC1,XMAX2
C
      PRINT 8,YMIN2,YINC2,YMAX2,YMIN3,YINC3,YMAX3,YMIN4,YINC4,YMAX4,
     AYMIN5,YINC5,YMAX5,X5ORGN,XCYCLE,XINC1,XMAX2
  8   FORMAT (/T3,*YMIN2,YINC2,YMAX2 = *,3F10.2/
     AT3,*YMIN3,YINC3,YMAX3 = *,3F10.2/
     BT3,*YMIN4,YINC4,YMAX4 = *,3F10.2 /
     CT3,*YMIN5,YINC5,YMAX5 = *,3F10.2/
     ET3,*X5ORGN,XCYCLE = *,2F10.2/
     DT3,*XINC1,XMAX2 = *,2F10.2/)
C
      JTEST=0
      DO 607  JRS=1,10
      IF (MPLOT(JRS).EQ.1HY) JTST=1
      JTEST=JTEST+JTST
 607  CONTINUE
      IF (JTEST.EQ.0)   GO TO 1001
      CALL BGNPL(-1)
      DO 1000  MINDEX=1,2
      IF (MINDEX.EQ.1.AND.COMPLOT) GO TO 400
      IF (MINDEX.EQ.1.AND..NOT.COMPLOT) GO TO 410
      IF (MINDEX.EQ.2.AND.COMPLOT) GO TO 405
      IF (MINDEX.EQ.2.AND..NOT.COMPLOT) GO TO 405
 400  CONTINUE
C     FIND XMAX
      XMAX=N(1)
      DO 30  M=2,I
      IF (N(M).GT.XMAX)  XMAX=N(M)
  30  CONTINUE
      XMAX=XMAX/100.
      IXMAX=XMAX
      XMAX=(IXMAX+1)*100.
      IF (DUALPT)  GO TO 402
      GO TO 401
 402  CONTINUE
      DO 32  M=1,KI
      IF (NC(M).GT. XMAX)  XMAX=NC(M)
  32  CONTINUE
      XMAX=XMAX/100.
      IXMAX=XMAX
      XMAX=(IXMAX+1)*100.
      GO TO 401
C
 410  CONTINUE
C     FIND NC-MAX
      XMAX=NC(1)
      DO 31  M=2,KI
      IF (NC(M).GT.XMAX)  XMAX=NC(M)
  31  CONTINUE
      XMAX=XMAX/100.
      IXMAX=XMAX
      XMAX=(IXMAX+1)*100.
      GO TO 401
C
 405  CONTINUE
 415  CONTINUE
      XMAX=XMAX2
      GO TO 401
C
 401  CONTINUE
      PRINT 3, MINDEX,XMAX
  3   FORMAT (T2,*MINDEX= *, I3, 4X,*XMAX = *,F7.1 /)
C
      IF (MPLOT(MINDEX*5-4).NE.1HY)  GO TO 502
 501  CONTINUE
C
```

```
C PLOT S-MAX/S-MIN VS CYCLES            PLOT #1
C$$$$$$$$$$$$$$$$$$$$$$$$$$$$$$$$$$$$$$$$$$$$$$$$$$$$$$$$
C
      IF (.NOT.COMPLOT) GO TO 120
      PRINT 7,I
 7    FORMAT(///* SUBPLOT *//,T2,* I= *,I5/)
C     DO 10 J=1,I
C     PRINT 1,J, N(J), R1(J)
C1    FORMAT (T2,  *J= *,I5,3X,* N= *,F7.1,3X,* R1= *,F5.3)
C10   CONTINUE
C
      XLTH=7.0
      YLTH=5.0
      XMIN=0.0
      XINC=500.
      YINC=.1
      YMIN=.4
      YMAX=1.3
C     ELIM OUT OF RANGE PTS
      IT=0
      DO 210  IJ=1,I
      IF (R1(IJ).LT.YMIN.OR.R1(IJ).GT.YMAX) GO TO 211
      IF (N(IJ).LT.XMIN.OR.N(IJ).GT.XMAX) GO TO 211
      IT=IT+1
      X(IT)=N(IJ)
      Y(IT)=R1(IJ)
      GO TO 210
 211  CONTINUE
 210  CONTINUE
C
      CALL BASALF("STANDARD")
      CALL MIXALF ("INSTRUCTION")
      CALL MX3ALF ("L/CSGREEK" ,1H*)
      CALL TITLE(1H ,-1,"CYCLES$",100,"RATIO (H2.)*S)(LH.5)MAX(LXHX) TO
     1(H2.)*S)(LH.5)MIN(LXHX)$", 100, XLTH  ,YLTH)
      CALL HEADIN ("RATIO OF (H2.)*S)(LH.5)MAX(LXHX) TO (H2.)*S(LH.5)MIN
     1(LXHX)$",   100,3,2)
      CALL HEADIN ("VERSUS CYCLES$", +100, 3,2)
      CALL BLNK1(XORGIN,XF,YORGIN,YF,+1)
      CALL INTAXS
      CALL FRAME
      CALL GRAF(XMIN,XINC,XMAX,YMIN,YINC,YMAX)
      CALL SCLPIC(0.5)
      CALL CURVE (X,Y,IT,-1)
      CALL RESET("BLNK1")
      CALL HEIGHT (HT)
      CALL MESSAG(U,100,XO,YO)
      CALL ENDPL(MINDEX*5-4)
      CALL RESET ("HEIGHT")
C
C
 502  CONTINUE
      IF (MPLOT(MINDEX*5-3).NE.1HY)  GO TO 503
C
C
C     PLOT STRESS RANGE VS CYCLES       PLOT #2
C$$$$$$$$$$$$$$$$$$$$$$$$$$$$$$$$$$$$$$$$$$$$$$$$$$$$$$$$
C
C     DO 11 J=1,I
C     PRINT 2, J, N(J),DELTSIG(J)
C2    FORMAT(T2,*J= *,I5,3X,*N= *,F7.1,3X,*DELTSIG= *, F6.1)
C11   CONTINUE
C
      XLTH=7.0
      YLTH=5.0
      YMIN=YMIN
```

```
      YINC=YINC2
      YMAX=YMAX2
      XMIN=0.0
      XINC=500.
      IF (MINDEX.EQ.1) XINC=XINC1
C
      IF (.NOT.COMPLOT)  GO TO 120
      IT=0
      DO 220  IJ=1,I
      IF (DELTSIG(IJ).LT.YMIN.OR.DELTSIG(IJ).GT.YMAX) GO TO 221
      IF (N(IJ).LT.XMIN.OR.N(IJ).GT.XMAX) GO TO 221
      IT=IT+1
      X(IT)=N(IJ)
      Y(IT)=DELTSIG(IJ)
      GO TO 220
 221  CONTINUE
 220  CONTINUE
C
 120  CONTINUE
      IF (.NOT.HYPLOT) GO TO 227
      JT=0
      DO 225 IJ=1,KI
      IF (SIGC(IJ).LT.YMIN.OR.SIGC(IJ).GT.YMAX) GO TO 226
      IF (NC(IJ).LT.XMIN.OR.NC(IJ).GT.XMAX)  GO TO 226
      JT=JT+1
      XA(JT)=NC(IJ)
      YA(JT)=SIGC(IJ)
      GO TO 225
 226  CONTINUE
 225  CONTINUE
 227  CONTINUE
C
C
      CALL SCLPIC(1.0)
      CALL RESET ("MXALFS")
      CALL BASALF("STANDARD")
      CALL TITLE(1H  ,-1,  "CYCLES$",  100,  "STRESS RANGE (KSI)$",
     1  100,XLTH, YLTH)
      CALL HEADIN ("STRESS RANGE  VS  CYCLES$", -100,3,1)
      CALL BLNK1(XORGIN,XF,YORGIN,YF,+1)
      CALL BLNK2(0.35,4.25,1.95,2.65,+1)
      CALL INTAXS
      CALL FRAME
      CALL GRAF (XMIN,XINC,XMAX,YMIN,YINC,YMAX)
      CALL SCLPIC(0.5)
      IF (COMPLOT) CALL CURVE (X,Y,IT,-1)
      IF (HYPLOT)  CALL CURVE(XA,YA,JT,-1)
      CALL RESET("BLNK1")
      CALL RESET("BLNK2")
      CALL HEIGHT (HT)
      CALL MESSAG(U,100,XO,YO)
      CALL SCLPIC(1.00)
      IF (COMPLOT) CALL LINES("COMPUTER GENERATED DATA$",IPAK,1)
      IF (HYPLOT) CALL LINES ("HYSTERESIS LOOP DATA$",IPAK,LN2)
      CALL LEGEND(IPAK,LN2,1.0,2.0)
      CALL ENDPL(MINDEX*5-3)
      CALL RESET ("HEIGHT")
C
 503  CONTINUE
      IF (MPLOT(MINDEX*5-2).NE.1HY)  GO TO 504
C
C
C     PLOT STRAIN RANGE VS CYCLES       PLOT #3
C$$$$$$$$$$$$$$$$$$$$$$$$$$$$$$$$$$$$$$$$$$$$$$$$$$$$$
C
C     DO 12 J=1,I
```

```
C     PRINT 3, J,N(J),DELTSTN(J)
C3    FORMAT(T2,*J= *,I5,3X,*N= *,F7.1,3X,*DELTSTN= *,F6.4)
C12   CONTINUE
C
      XLTH=7.0
      YLTH=5.0
      YMIN=YMIN3
      YINC=YINC3
      YMAX=YMAX3
      XMIN=0.0
      XINC=500.
      IF (MINDEX.EQ.1) XINC=XINC1
C
      IF (.NOT.COMPLOT) GO TO 130
      IT=0
      DO 230  IJ=1,I
      IF (DELTSTN(IJ).LT.YMIN.OR.DELTSTN(IJ).GT.YMAX) GO TO 231
      IF (N(IJ).LT.XMIN.OR.N(IJ).GT.XMAX) GO TO 231
      IT=IT+1
      X(IT)=N(IJ)
      Y(IT)=DELTSTN(IJ)
      GO TO 230
 231  CONTINUE
 230  CONTINUE
 130  CONTINUE
C
      IF (.NOT.HYPLOT)  GO TO 237
      JT=0
      DO 235 IJ=1,KI
      IF (STRNC(IJ).LT.YMIN.OR.STRNC(IJ).GT.YMAX) GO TO 236
      IF (NC(IJ).LT.XMIN.OR.NC(IJ).GT.XMAX) GO TO 236
      JT=JT+1
      XA(JT)=NC(IJ)
      YA(JT)=STRNC(IJ)
      GO TO 235
 236  CONTINUE
 235  CONTINUE
 237  CONTINUE
C
      CALL SCLPIC(1.0)
      CALL TITLE (1H , -1,"CYCLES$",  100, "STRAIN RANGE (PERCENT)$",
     1 100,XLTH, YLTH)
      CALL HEADIN ("STRAIN RANGE  VS  CYCLES$",   -100, 3,1)
      CALL FRAME
      CALL BLNK1(XORGIN,XF,YORGIN,YF,+1)
      CALL BLNK1(0.95,4.25,1.95,2.65,+1)
      CALL XINTAX
      CALL GRAF (XMIN,XINC,XMAX,YMIN,YINC,YMAX)
      CALL SCLPIC(0.5)
      IF (COMPLOT) CALL CURVE (X,Y,IT,-1)
      IF (HYPLOT)  CALL CURVE(XA,YA,JT,-1)
      CALL RESET("BLNK1")
      CALL RESET ("BLNK2")
      CALL HEIGHT (HT)
      CALL MESSAG(U,100,XO,YO)
      CALL SCLPIC(1.0)
      IF (COMPLOT) CALL LINES("COMPUTER GENERATED DATA$",IPAK,1)
      IF (HYPLOT) CALL LINES ("HYSTERESIS LOOP DATA$",IPAK,LN2)
      CALL LEGEND (IPAK,LN2,1.0,2.0)
      CALL ENDPL(MINDEX*5-2)
      CALL RESET ("HEIGHT")
C
 504  CONTINUE
      IF (MPLOT(MINDEX*5-1).NE.1HY)  GO TO 505
C
C ... PLOT EXPLODED STRESS RANGE VS CYCLES  PLOT #4
```

```
C$$$$$$$$$$$$$$$$$$$$$$$$$$$$$$$$$$$$$$$$$$$$$$$$$$$$$$$$$$$$$$$
C
      XLTH=7.0
      YLTH=5.0
      YMIN=YMIN4
      YINC=YINC4
      YMAX=YMAX4
      XMIN=0.0
      XINC=500.
      IF (MINDEX.EQ.1) XINC=XINC1
C
      IF (.NOT.COMPLOT) GO TO 140
      IT=0
      DO 240  IJ=1,I
      IF (DELTSIG(IJ).LT.YMIN.OR.DELTSIG(IJ).GT.YMAX ) GO TO 241
      IF (N(IJ).LT.XMIN.OR.N(IJ).GT.XMAX) GO TO 241
      IT=IT+1
      X(IT)=N(IJ)
      Y(IT)=DELTSIG(IJ)
      GO TO 240
 241  CONTINUE
 240  CONTINUE
 140  CONTINUE
C
      IF (.NOT.HYPLOT) GO TO 247
      JT=0
      DO 245 IJ=1,KI
      IF (SIGC(IJ).LT.YMIN.OR.SIGC(IJ).GT.YMAX) GO TO 246
      IF (NC(IJ).LT.XMIN.OR.NC(IJ).GT.XMAX) GO TO  246
      JT=JT+1
      XA(JT)=NC(IJ)
      YA(JT)=SIGC(IJ)
      GO TO 245
 246  CONTINUE
 245  CONTINUE
 247  CONTINUE
C
      CALL SCLPIC(1.0)
      CALL TITLE(1H  ,-1,  "CYCLES$",  100,  "STRESS RANGE (KSI)$",
     1  100,XLTH, YLTH)
      CALL HEADIN ("STRESS RANGE  VS  CYCLES$", -100,3,1)
      CALL FRAME
      CALL BLNK1(XORGIN,XF,.30 ,.60 ,+1)
      CALL BLNK2(0.60,3.90,3.90,1.6,+1)
      CALL INTAXS
      CALL GRAF (XMIN,XINC,XMAX,YMIN,YINC,YMAX)
      CALL GRID (5,5)
      CALL SCLPIC(0.5)
      IF (COMPLOT) CALL CURVE (X,Y,IT,-1)
      IF (HYPLOT)   CALL CURVE(XA,YA,JT,-1)
      CALL RESET("BLNK1")
      CALL RESET ("BLNK2")
      CALL HEIGHT (HT)
      CALL MESSAG(U,100,XO,.38)
      CALL SCLPIC(1.0)
      IF (COMPLOT) CALL LINES("COMPUTER GENERATED DATA$",IPAK,1)
      IF (HYPLOT) CALL LINES ("HYSTERESIS LOOP DATA$",IPAK,LN2)
      CALL LEGEND (IPAK,LN2,.65,.95)
      CALL ENDPL (MINDEX*5-1)
      CALL RESET ("HEIGHT")
C
C
 505  CONTINUE
      IF (MPLOT(MINDEX*5).NE.1HY)  GO TO 99
C
C     PLOT STRESS RANGE VS LOG CYCLES  PLOT #5
```

```
C$$$$$$$$$$$$$$$$$$$$$$$$$$$$$$$$$$$$$$$$$$$$$$$$$$$$$$$$$$$$
C
      YMIN=YMIN5
      YMAX=YMAX5
      YLTH=5.
      XLTH=7.
      YSTEP=YINC5
      XMIN=0.0
      IF ((YMIN5+YLTH*YINC5).LT.YMAX5) YSTEP=(YMAX5-YMIN5)/YLTH
C
      IF (.NOT.COMPLOT) GO TO 150
      IT=0
      DO 250 IJ=1,I
      IF (DELTSIG(IJ).LT.YMIN.OR.DELTSIG(IJ).GT.YMAX)  GO TO 251
      IF (N(IJ).LT.XMIN.OR.N(IJ).GT.XMAX) GO TO 251
      IT=IT+1
      X(IT)=N(IJ)
      Y(IT)=DELTSIG(IJ)
      GO TO 250
  251 CONTINUE
  250 CONTINUE
      IF (IT.EQ.0) GO TO 260
  150 CONTINUE
C
      IF (.NOT.HYPLOT)  GO TO 257
      JT=0
      DO 255  IJ=1,KI
      IF (SIGC(IJ).LT.YMIN.OR.SIGC(IJ).GT.YMAX) GO TO 256
      IF (NC(IJ).LT.XMIN.OR.NC(IJ).GT.XMAX)  GO TO 256
      JT=JT+1
      XA(JT)=NC(IJ)
      YA(JT)=SIGC(IJ)
      GO TO 255
  256 CONTINUE
  255 CONTINUE
      IF (JT.EQ.0) GO TO 260
  257 CONTINUE
C
      PRINT 280,YMIN,YMAX,YLTH,XLTH,YSTEP
  280 FORMAT (T2 ,*YMIN5,YMAX5,YLTH,XLTH,YSTEP = *,5F7.1 /)
C
      CALL MIXALF ("L/CSTD")
      CALL TITLE  ("STRESS RANGE  VS  L(OG) CYCLES$", -100,
     1 "CYCLES$", 100,  "STRESS RANGE (()KSI())$",  100,
     2  XLTH,YLTH)
      CALL YINTAX
      CALL FRAME
      CALL BLNK1(XORGIN,XF,YORGIN,YF,+1)
      XINC5=XLTH/XCYCLE
      PRINT 281,X5ORGN,XINC5,YMIN,YSTEP
  281 FORMAT (T2,*X5ORGN,XINC5,YMIN,YSTEP = *,4F7.1/)
C
      CALL XLOG(X5ORGN,XINC5,YMIN,YSTEP)
      CALL SCLPIC(0.5)
      IF (COMPLOT) CALL CURVE (X,Y,IT,-1)
      IF (HYPLOT)   CALL CURVE(XA,YA,JT,-1)
      CALL RESET("BLNK1")
      CALL HEIGHT (HT)
      CALL MESSAG(U,100,XO,YO)
      CALL SCLPIC(1.0)
      IF (COMPLOT) CALL LINES("COMPUTER GENERATED DATA$",IPAK,1)
      IF (HYPLOT) CALL LINES ("HYSTERESIS LOOP DATA$",IPAK,LN2)
      CALL LEGEND (IPAK,LN2,1.,2.)
      CALL ENDPL (MINDEX*5)
C
      GO TO 99
```

```
 260  CONTINUE
      PRINT 264,IT,JT
 264  FORMAT (T3, 3H*** , *NO DATA PTS WITH RANGE OF PLOT 5*/
     AT4,*IT = * I5, 3X, *,JT = *, I5/)
C
 99   CONTINUE
C
C$$$$$$$$$$$$$$$$$$$$$$$$$$$$$$$$$$$$$$$$$$$$$$$$$
 1000 CONTINUE
      CALL DONEPL
 1001 CONTINUE
      RETURN
      END
```

BIBLIOGRAPHY

1. M. N. Menon and W. H. Reimann, "Low Cycle Fatigue Crack Initiation Study in René 95," J. Mater. Sci. 10, 1571-1581 (1975).

2. B. Leis and A. Clauer, Investigation of Rejuvenation of Fatigue Damage in IN-718. Air Force Materials Laboratory Technical Report, AFML-TR-78-90, AF Contract F33615-76-C-5100 (Air Force Materials Laboratory, Wright-Patterson Air Force Base, Ohio, 1978).

3. S. S. Manson, Thermal Stress and Low Cycle Fatigue, McGraw-Hill (1966).

4. M. Gill, G. R. Leverant, and C. H. Wells, "The Fatigue Strength of Nickel-Base Superalloys," Achievement of High Fatigue Resistance in Superalloys, ASTM STP 467, American Society of Testing and Materials, 53-76 (1970).

5. C. H. Wells and C. P. Sullivan, "Low Cycle Fatigue of Udimet 700 at 1700 F," Trans. ASM 61, 149-155 (1968).

6. C. H. Wells and C. P. Sullivan, "The Effect of Temperature on the Low Cycle Fatigue Behavior of Udimet 700," Trans. ASM 60, 217-222 (1967).

7. C. H. Wells and C. P. Sullivan, "The Low Cycle Fatigue Characteristics of a Nickel-Base Superalloy at Room Temperature," Trans. ASM 57, 841-855 (1964).

8. M. Gell and G. R. Leverant, "The Fatigue of the Nickel-Base Superalloy MAR-M-200 in Single Crystal and Columnam Grain Forms at Room Temperature," Trans. AIME 242, 1869-1879 (1968).

9. P. Gauthier, H. DeRandy, and J. Auvinet, "Secondary Cracking Process During Fatigue Crack Propagation," Eng. Fract. Mech. 5, 977-981 (1973).

10. W. H. Vaughan, R. J. Sanford, J. M. Krofft, W. H. Cullen, and J. W. Dolly, Failure Studies of a Third Stage Fan Disk from a TF-30 Turbine Engine, NRL Memorandum Report 3874, Naval Research Laboratories (1978).

11. A. H. Cottrell, "Fracture," Proc. Roy. Soc. London A 276, 1-18 (1963).

12. A. W. Funkenbusch and L. F. Coffin, "Low Cycle Fatigue Crack Nucleation and Early Growth in Ti-17," Met. Trans. 9A, 1159-1167 (1978).

13. J. C. Grosskrentz, Phys. Stat. Solidi (B) 47, 359-396 (1971).

14. G. E. Dieter, Mechanical Metallurgy, McGraw-Hill, 403-450 (1976).

15. C. H. Wells and C. P. Sullivan, "The Low Cycle Fatigue Characteristics of a Nickel-Base Superalloy at Room Temperature," Trans. ASM 57, 841-847 (1964).

16. H. F. Merrick, "The Low Cycle Fatigue of Three Wrought Nickel-Base Alloys," Met. Trans. 5, 891-897 (1974).

17. D. R. Muzyka, "The Metallurgy of Iron Nickel Alloys," The Superalloys (C. T. Sims and W. C. Hagel, eds.), John Wiley and Sons, New York (1972).

18. R. F. Decker and S. Floreen, "Precipitation from Substitutional Iron-Base Austenitic and Martensitic Solid Solutions," Precipitation from Iron Base Alloys (G. R. Speich and J. B. Clark, eds.), Gordon and Breach Scientific Publishers, New York (1965).

19. E. F. Bradley and M. J. Donachie, "Forgings for Jet Engines: More Quality at Less Cost," Metals Prog. 106/2, 80-82 (July 1974).

20. D. Raynor and J. M. Silcock, "Strengthening Mechanisms in Gamma-Prime Precipitating Alloys," Metal Sci. J. 4, 121-130 (1970).

21. D. R. Muzyka, "Controlling Microstructure and Properties of Superalloys Via Use of Precipitated Phases," Metals Eng. Qtrly 11/4, 12-20 (1971).

22. G. R. Speich, "Cellular Precipitation in an Austenitic Fe-30Ni-6Ti Alloy," Trans. AIME 227, 754-762 (1963).

23. C. C. Clark and J. S. Iwanski, "Phase Changes in Precipitation Hardening Nickel-Chromium-Iron Alloys during Prolonged Heating," Trans. AIME 215, 648-651 (1959).

24. H. J. Beattie and W. C. Hagel, "Intragranular Precipitation of Intermetallic Compounds in Complex Austenitic Alloys," Trans. AIME 221, 28-35 (1961).

25. E. E. Brown, R. C. Boettner, and D. L. Ruckle, Minigrain Processing of Nickel-Base Alloys, presented at the Metallurgical Society of AIME Fall Meeting, Cleveland, 1970.

26. R. F. Decker and C. T. Sims, "The Metallurgy of Nickel-Based Superalloys," The Superalloys (C. T. Sims and W. C. Hagel, eds.) John Wiley and Sons, New York (1972).

27. C. T. Sims, "The Occurrence of Topologically Close-Packed Phases," The Superalloys (C. T. Sims and W. C. Hagel, eds.), John Wiley and Sons, New York (1972).

28. J. P. Dennison and B. Wilshire, "Mechanisms of Improving Creep Rupture Lives by Re-Heat Treatments," Fracture 2, 635-639 (1977).

29. J. P. Dennison, P. D. Holmes, and B. Wilshire, "The Creep and Fracture Behavior of the Cast Nickel-Based Superalloy IN-100," Mater. Sci. & Eng. 33, 35-47 (1978).

30. K. C. Anthony and J. F. Rodavitch, The Effects of HIP Rejuvenation of Turbine Blades, presented at the AIME Annual Meeting, Atlanta, Georgia.

31. Summary Report on the Powder Metallurgy Seminar, Air Force Materials Laboratory Technical Report AFML-TM-LT-74-4 (Air Force Materials Laboratory, Wright-Patterson Air Force Base, Ohio, 1974).

32. ASTM Standard E407-70, "Standard Methods for Microetching Metals and Alloys," Annual Book of ASTM Standards, American Society of Testing and Materials, Philadelphia (1974).

33. M. F. Henry, A Technique for Monitoring Time Dependent Surface Damage, General Electric Report No. 71-C-338, Schenectady, New York (1971).

34. Pratt and Whitney Aircraft Specification 1003H, East Hartford, Conn. (November 1973).

35. W. P. Koster and J. B. Kohls, Relationship of Surface Integrity to Cost and Reliability of Structural Components, SME Technical Paper IQ72-207 (1972).

36. R. L. Ketter and S. P. Prawel, Modern Methods of Engineering Computation, McGraw-Hill (1969).

37. L. G. Heroux and C. P. Sullivan, "Metallographic Replication of Curved Surfaces," Trans. ASM 56, 861-863 (1963).

38. L. K. Singhal and M. L. Vaidya, "Precipitation of Sigma Phase in a Duplex Fe-Cr-Ni-Ti Alloy," Trans. ASM Qtrly 62, 879-885 (1969).

39. W. H. Hill, K. D. Shimmin, and B. A. Wilcox, "Elevated Temperature Dynamic Moduli of Metallic Materials," ASTM Proc. 61, 890-906 (1961).

40. S. Spinner and W. F. Tefft, "A Method for Determining Mechanical Resonance Frequencies and for Calculating Elastic Moduli from These Frequencies," ASTM Proc. 61, 1221-1238 (1961).

41. W. E. Tefft, "Numerical Solution of the Frequency Equations for the Flexural Vibration of Cylindrical Rods," J. Research NBS 64B, 237-242 (1960).

42. ASTM Standard E112-61, "Standard Methods for Estimating the Average Grain Size of Metals," Annual Book of ASTM Standards, American Society of Testing and Materials, Philadelphia (1974).

43. Aerospace Structural Metals Handbook, Code 4107, Mechanical Properties Data Center, Traverse City, Michigan (December 1973).

44. A. Green, H. Sieber, D. Wells, and T. Wolfe, Research Investigation to Determine Mechanical Properties of Nickel and Cobalt-Base Alloys for Inclusion in Military Handbook 5, Air Force Materials Laboratory Technical Report ML-TDR-64-116, DDC AD-608813, V1, 500-508 (1964).

45. SEM/TEM Fractography Handbook, MCIC-HB-06, compiled by McDonnell Douglas Astronautics Co., published by Metals and Ceramics Information Center, Battelle-Columbus Laboratories, Columbus, Ohio (1975).

46. C. Laird, Mechanisms and Theories of Fatigue, presented at the Materials Science Seminar, American Society for Metals, St. Louis, Missouri (1978).

47. W. H. Kim and C. Laird, "Crack Nucleation and Stage I Propagation in High Strain Fatigue - I. Microscopic and Interferometric Observations," Acta Met. 26, 777-787 (1978).

48. W. H. Kim and C. Laird, "Crack Nucleation and Stage I Propagation in High Strain Fatigue - II. Mechanism," Acta Met. 26, 789-799 (1978).

49. D. Kuhlmann-Wilsdorf and C. Laird, "Dislocation Behavior in Fatigue," Mater. Sci. and Eng. 31, 137-156 (1977).

50. W. A. Wood, Fatigue in Aircraft Structures, Academic Press, New York (1956).

51. C. Laird, Fatigue Crack Propagation, ASTM 415, American Society for Testing and Materials, Philadelphia (1967).

52. A. S. Tetelman and A. J. McEvily, Fracture of Structural Materials, 347-400 (1967).

53. American Society for Metals, Failure Analysis and Prevention, vol. 10, Metals Handbook (8th ed.), Metals Park, Ohio (1975).

54. F. Petit, Personal Communication, Materials Research Laboratory, Pratt and Whitney Aircraft, Commercial Products Division, East Hartford, Conn. (June 1979).

55. R. Sandström, "Subgrain Growth Occurring by Boundary Migration," Acta Met. 25, 905-911 (1977).

56. R. Sandström, "On Recovery of Dislocations in Subgrains and Subgrain Coalescence," Acta Met. 25, 897-904 (1977).

57. J. P. Hirth and J. Lothe, Theory of Dislocations, McGraw-Hill, New York (1968).

58. M. R. James and A. W. Sleeswyk, "Influence of Intrinsic Stacking Fault Energy on Cyclic Hardening," Acta Met. 26, 1721-1726 (1978).

59. R. W. Landgraf, "The Resistance of Metals to Cyclic Deformation," Achievement of High Fatigue Resistance in Metals and Alloys, ASTM STP 467, American Society of Testing and Materials, 3-36 (1970).

60. R. W. Smith, M. H. Hirschberg, and S. S. Manson, Fatigue Behavior of Materials under Strain Cycling in Low and Intermediate Life Range, NASA Technical Note D-1574, Lewis Research Center, Cleveland, Ohio (1963).

61. T. J. Dolan, "Designing Structures to Resist Low-Cycle Fatigue," Metals Eng. Qtrly 10, 18-25 (November 1970).

62. D. Macha, Unpublished Research, Air Force Materials Laboratory, Metals Behavior Branch (AFML/LLN), Wright-Patterson Air Force Base, Ohio 45433 (1977).

63. G. R. Irwin, Plastic Zone Near a Crack and Fracture Toughness, Seventh Sagamore Ordinance Materials Research Conference (August 1960).

64. C. Calabrese and C. Laird, "High Strain Fatigue Fracture Mechanics in Two Phase Alloys," Met. Trans. 5, 1785-1793 (1974).

65. C. Calabrese and C. Laird, "Cyclic Stress-Strain Response of Two-Phase Alloys; Part I. Microstructures Containing Particles Penetrable by Dislocations," Mater. Sci. and Eng. 13, 141-157 (1974).

66. C. Calabrese and C. Laird, "Cyclic Stress-Strain Response of Two-Phase Alloys; Part II. Particles Not Penetrated by Dislocations," Mater. Sci. and Eng. 13, 159-174 (1974).

67. W. H. Kim and C. Laird, "The Role of Cyclic Hardening in Crack Nucleation at High Strain Amplitude," Mater. Sci. and Eng. 33, 225-231 (1978).

68. C. Laird, V. J. Langelo, M. Hallrah, N. C. Yang, and R. DeLaVeaux, "The Cyclic Stress-Strain Response of Precipitation Hardened Al-15 wt% Ag Alloy," Mater. Sci. and Eng. 32, 137-160 (1978).

69. H. J. Beattie, Jr., "The Crystal Structure of a M_3B_2-Type Double Boride," Acta Cryst. 11, 607-609 (1958).

70. M. J. Fleetwood and C. A. P. Horton, "The Use of the Microprobe Analyzer and the Electron Microscope for the Identification of Precipitate Particles in a Nickel-Chromium-Iron Alloy," J. Roy. Microsc. Soc. 83, 245-250 (1964).

DA
FILM